Morphogenetic Mechanisms of Blood Vessel Fusion in the Zebrafish Embryo

Inauguraldissertation

zur
Erlangung der Würde eines Doktors der Philosophie
vorgelegt der
Philosophisch-Naturwissenschaftlichen Fakultät
der Universität Basel

von

Lukas Walter Herwig

aus Basel, Schweiz

Basel, 2012

creative commons

Namensnennung-Keine kommerzielle Nutzung-Keine Bearbeitung 2.5 Schweiz

---

Sie dürfen:

das Werk vervielfältigen, verbreiten und öffentlich zugänglich machen

Zu den folgenden Bedingungen:

Namensnennung. Sie müssen den Namen des Autors/Rechteinhabers in der von ihm festgelegten Weise nennen (wodurch aber nicht der Eindruck entstehen darf, Sie oder die Nutzung des Werkes durch Sie würden entlohnt).

Keine kommerzielle Nutzung. Dieses Werk darf nicht für kommerzielle Zwecke verwendet werden.

Keine Bearbeitung. Dieses Werk darf nicht bearbeitet oder in anderer Weise verändert werden.

- Im Falle einer Verbreitung müssen Sie anderen die Lizenzbedingungen, unter welche dieses Werk fällt, mitteilen. Am Einfachsten ist es, einen Link auf diese Seite einzubinden.
- Jede der vorgenannten Bedingungen kann aufgehoben werden, sofern Sie die Einwilligung des Rechteinhabers dazu erhalten.
- Diese Lizenz lässt die Urheberpersönlichkeitsrechte unberührt.

Quelle: http://creativecommons.org/licenses/by-nc-nd/2.5/ch/ Datum: 3.4.2009

Genehmigt von der Philosophisch-Naturwissenschaftlichen Fakultät
auf Antrag von

Prof. Dr. Markus Affolter

Prof. Dr. Rolf Zeller

Basel, den 21.02.2012

Prof. Dr. Martin Spiess

Dekan

TABLE OF CONTENT

1 List of Abbreviations

aa	Amino acid(s)
AJs	Adherens junctions
aPKC	atypical proteinkinase C
AMIS	apical membrane initiation sides
bp	base pairs
CBP	CREB (cAMP Responsive Element) Binding Protein
Cdc42	cell division control protein 42 homologue
COUP-TFII	chicken ovalbumin upstream promoter transcription factor 2
DA	Dorsal aorta
ddH_2O	double deionized water (Quarz-Water)
DNMTs	DNA methyltransferases
DLAV	Dorsal longitudinal anastomotic vessel
DLL4	Delta-like-4
DNA	Deoxyribonucleic acid
dpc	Days post coitum
dpf	Days post fertilization
E. coli	Escherichia coli
ECs	Endothelial cells
EGFP	Enhanced GFP
ephrinB2	Ephrin receptor B2
ESAMs	Endothelial Cell Selective Adhesion Molecules
E1b	originally: weak minimal adenoviral promoter; later a synthetic oligonucleotide of 45 bp (Eurogentec) was inserted so that a transcriptional start site from a fish promoter (carp b-actin) is located 25 bp downstream of the TATA box.
ETS	transcription factors with E-twenty-six conserved DNA binding domain
Etsrp	ets1-related protein
fli-1	Friend leukemia integration 1
flk-1 (kdr)	Fetal liver kinase 1 (VEGFR2)
flt4	fms related tyrosin kinase 4 (VEGFR3)
GATA	transcription factors with aility to bind a GATA-DNA sequence
Gal4VP16	DNA binding domain of Gal4 fused to transcriptional activation domain of herpes simplex virus gene 16
GFP	Green florescent protein
hpf	Hours post fertilization
HEY1/HEY2	hairy- and enhancer of split-related with YRPW motif
ICM	Intermediate cell mass
ISV	Intersegemental vessel
JAM	Junctional adhesion molecule
kdr (flk-1)	Kinase insert domain receptor
LCS	Leica confocal software
LM	Lateral mesoderm
MAGUK	membrane-associated guanylate kinase
MCS	Multiple cloning site

MDCK	Madin-Darby canine kidney (cells)
NEB	New England Biolab
NRARP	Notch regulated ankyrin repeat protein
obd	out of bounds
PAPs	pre-apical patches
PAR	Polarization complex including CDC42, PAR3, PAR6 and aPKC
PAR3	Partitioning defective 3 homolog
PAR6	Partitioning defective 6 homolog
PBS	Phosphate-buffered saline
PBST	Phosphate-buffered saline-Tween 20
PBSTX	Phosphate-buffered saline-Tween 20- Triton-X 100
PCR	Polymerase chain reaction
PCV	Posterior cardinal vein
PDZ	specific domain (Postsynaptic-density protein 95 (PSD95), Drosophila disc large tumor suppressor (DlgA), and Zonula occuldens-1 protein (ZO1)
PFA	Paraformaldehyde
plcg1	Phospholipase C γ
PM	Plasma membrane
PMT	Photomultiplier
polyA	polyadenylation signal (SV40)
PTEN	Phosphatase and tensin homologe ten
PTU	Propylthiouracil
p120	prototypic member of a growing subfamily of Armadillo-domain proteins
RhoA	GTPase: Ras homolog gene family member A
RAC1	GTPase: Ras-related C3 botulinum substrate 1
Shh	sonic hedgehog
SAP	Shrimp Alkaline Phosphatase
SV40	Simian virus 40 (polyA signal)
TFs	Transcription factors
TJs	Tight junctions
UAS	Upstream activating sequence/site
VE-cadherin	Vascular endothelial cadherin
VEGF	Vascular endothelial growth factor
VEGFR	Vascular endothelial growth factor receptor
VPF	Vascular permeability factor
VP16	herplex simplex virion protein 16
Wnt	*W, Wingless; nt, Int-1*
ZO1	Zonula occuldens-1 protein

2 Abstract

The formation of a vascular network requires the connection and formation of a lumen between individual endothelial sprouts, a process called vessel fusion or anastomosis. In the vertebrate trunk of the zebrafish (*Danio rerio)*, the intersegmental vessels (ISVs) develop by angiogenesis, i.e. the formation of new vessels by pre-existing vessels, in a conserved metameric manner, which allows the analysis of morphogenetic mechanisms of blood vessel development. From the dorsal aorta (DA) individual endothelial sprouts, led by tip cells and trailing stalk cells, grow between the somite boundaries dorsally towards the roof of the neural tube where they extend anterior and posterior. Neighboring extensions of sprouts fuse to each other and eventually form a continuous lumen, which results in the formation of a new vessel, the dorsal longitudinal anastomotic vessel (DLAV). In the past, many molecular key players of blood vessel formation have been identified and a number of studies described endothelial lumen formation *in vivo*. However, how individual cellular behaviors contribute to the process of vessel fusion have not yet been described. Thus, I engineered a transgenic zebrafish reporter system labeling endothelial cell-cell junctions by an EGFP-hZO1 (human Zonula Occludens-1 protein fused to enhanced green fluorescent protein) fusion protein. This reporter system allowed analysis of the dynamics of endothelial tight junctions during intersegmental vessel fusion *in vivo* and thus, the relative behavior of individual endothelial cells (ECs). We previously proposed that neighboring ISVs make contact to each other by filopodial extensions. This behavior is reflected by the *de novo* formation of point-like junctional complexes (i.e. Vascular endothelial cadherin (VE-cadherin) and ZO1) which elaborate into ring-like structures as the contacting sprout extensions enlarge their mutual surface, suggesting the formation of new apical membrane compartments. Following individual cell-cell junctions in the fusing ISVs and analyzing a novel apical marker, podocalyxin2 (Pdxl2), we confirmed the formation of apical membrane compartments during the initial phase of vessel fusion and deciphered two distinct cellular mechanisms of blood vessel fusion, a cord hollowing and membrane invagination mechanism, that result in the formation of different types of biological tubes. In cord hollowing, cell rearrangements of ECs in fusing neighboring sprouts result in the formation of a multicellular tube. Here, a tip cell forms two apical membrane compartments, one with a stalk cell and another one with a neighboring tip cell. These are then brought together by cell rearrangements and coalesce into one larger membrane compartment that eventually integrates into a continuous lumen within the ISV/DLAV. During membrane invagination, the membrane of a tip cell, adjacent to a preexisting lumen, undergoes apicobasal polarization and invaginates through its own cell body and coalesces with one of the previously formed apical membrane compartments at the sites of contact between neighboring tip cells, which results in the formation of a seamless tube.

3 Introduction

The development of multicellular organisms reaching a critical size, requires a system for the efficient transportation of liquids, gases, hormones, nutrients and immunogenic compounds (Chung et al., 2011). In vertebrates, this task is performed by the vascular system, a hierarchically branched tubular network of blood- and lymphatic vessels, which are formed by endothelial cells (ECs) that are organized into an epithelial structure, the endothelium. Aberrant regulation of its embryonic development results in malformations or even lethality of the growing embryo. Furthermore, it has essential roles during homeostasis in the adult organism, during wound healing and when miss-regulated, it contributes to many pathological processes, for instance during tumorigenesis. Thus, the vascular system is indispensable for proper development of a vertebrate embryo and not surprisingly, it is the first organ to be built and expands its capacity significantly during embryonic and postnatal growth (Chung et al., 2011; Alitalo et al., 2005).

3.1 Biological tubes and their formation

Polarized epithelia separate distinct body parts from each other and can form a huge variety of structures including biological tubes, which can be organized into hierarchically ramified tubular networks such as the lung, respiratory system of insects, the transport system of plants or the vascular system. Such tubular organs are often shaped and formed by branching morphogenesis which involves the remodeling of polarized epithelia into tubes (tubulogenesis) and their reiterative branching (Affolter et al., 2009, 2003; Datta et al., 2011).

3.1.1 Epithelial and endothelial organization

In epithelia, the plasma membrane of cells is polarized into specific domains which are differentially organized regarding their lipid and protein composition and exert distinct functions. The apical domain faces the lumen, whereas the basolateral surface contacts neighboring cells and the extracellular matrix (ECM). Further, cell-cell junctions connect individual cells to each other, form a barrier and maintain polarization by preventing diffusion between apical and basolateral proteins and lipids (Martin-Belmonte et al., 2008). In mammalian epithelia, for instance tubes, tight junctions (TJs) are located at the apical site whereas adherens junctions (AJs) are found basal to the TJs. (Figure 1) (Andrew et al., 2010).

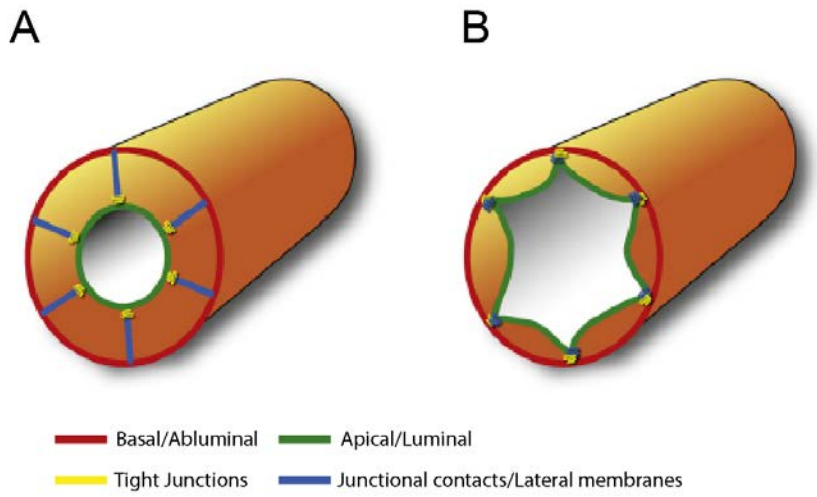

Figure 1 The organization of epithelial and endothelial cells. (A) Epithelial cells forming a tube: Cells have a cuboidal shape, a basal membrane, a lateral membrane and an apical domain facing the luminal space. Tight junctions are sub-apical whereas adherens junctions seal individual cells together at the lateral side. (B) Endothelial cells forming a tube. Cells have a flat and more elongated shape. The apical domain faces the lumen whereas the basal membrane connects to the extracellular matrix. The lateral membrane is extremely small since endothelial cells are extremely thin, thus tight and adherens junctions are thought to be intermingled. Figure adapted from Xu and Ondine Cleaver, 2011.

However, in the endothelium the TJs are intermingled with AJs all along the contact area of two cells since ECs display a very thin and elongated shape with the lateral side reduced to a minimum, which is in contrast to other epithelial cells that have a more cuboidal shape with larger lateral sides (Figure 1). In the endothelium (Figure 2), TJs are circumferential rings containing Claudins, Occludins, members of Junctional Adhesion Molecules (JAMs) and members of Endothelial Cell Selective Adhesion Molecules (ESAMs), at the apex of epithelial cells that seal adjacent cells to one another. In addition, there are many intracellular TJ proteins such as Zonula Occludens-1 and 2 proteins, which belong to the membrane-associated guanylate kinases (MAGUK) family. ZO1 acts as a scaffold protein, providing an interface for many protein interactions through its distinct domains, for instance its three PDZ domains. AJs are cell-cell adhesion complexes, containing Cadherins, for instance Vascular Endothelial Cadherin (see below) and Catenins, attached to cytoplasmic actin filaments (Dejana, 2004). Vascular endothelial cadherin (VE-cadherin) is a type-II endothelial-restricted classical cadherin localized to the adherens junction complex. VE-cadherin has essential roles regarding endothelial integrity and barrier function by regulating the permeability of blood vessel walls for molecules. Further, VE-cadherin plays a key role during blood vessel formation. Mice, deficient for VE-cadherin, are lethal as a result of defects during remodeling processes of the endothelium (Vestweber, 2008; Harris et al., 2010). In the zebrafish, knockdown of VE-cadherin causes strong defects during the fusion of vessels; vessels do not form connections or a lumen and eventually collapse (Montero-Balaguer et al., 2009).

The basic structure of VE-cadherin consist of 5 extracellular domains (EC1-EC5, with Ca^{2+} binding sites between the repeats), which mediate homophilic Ca^{2+}-dependent interactions, a transmembrane domain and a cytoplasmic domain specified into the “juxtamembrane domain”, binding to p120-catenin and the “catenin-binding domain” which binds β-catenin and plakoglobin. It is thought that the catenins couple VE-cadherin to the actin cytoskeleton. However, p120-catenin as well as β-catenin can translocate to the nucleus where they regulate the expression of genes (Harris et al., 2010).

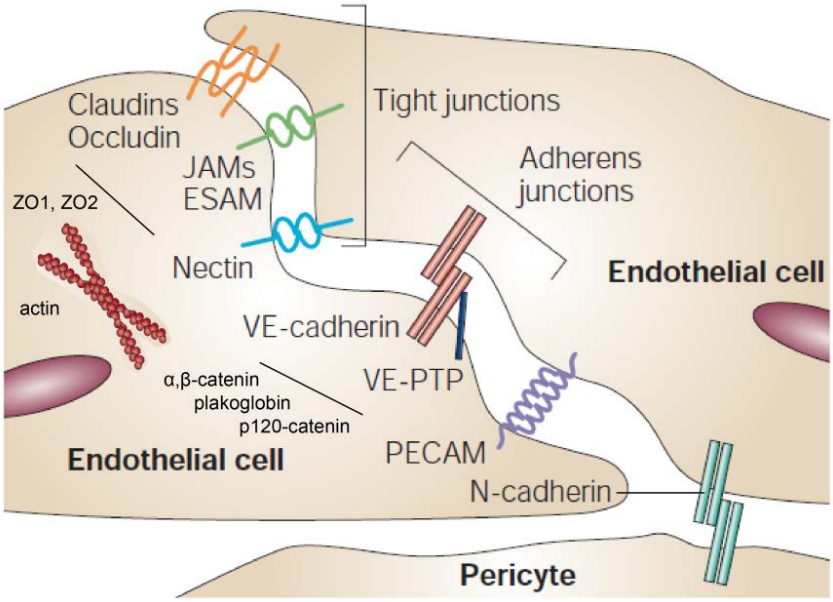

Figure 2 The organization of endothelial cell-cell junctions. Many different transmembrane adhesion proteins and intracellular binding proteins are found at endothelial cell-cell junctions. At tight junctions, adhesion is mediated by members of the claudin family, occluding, junctional adhesion molecules (JAMs) and the endothelial cell selective adhesion molecule (ESAM). At the TJs, many intracellular proteins, including zonula occuldens-1 and 2 protein (ZO1, ZO2), contain PDZ domains, which interact with other proteins. ZO1 can interact with the claudins, occluding or JAMs and indirectly with the cytoskeleton by binding α-catenin via one of its PDZ domains and directly by an F-actin binding domain. PECAM (platelet endothelial cell adhesion molecule) contributes to adhesion between ECs. However, at the adherens junctions, the main adhesion molecule is Vascular Endothelial Cadherin (VE-cadherin). Vascular Endothelial Protein Tyrosine phosphatase (VE-PTP), which can modulate cadherin and catenin phosphorylation and vascular permeability, associates with VE-cadherin via its extracellular domain. The intracellular domain of VE-cadherin is thought to interact with p120-catenin, α,β-catenin and plakoglobin. These intracellular proteins interact direct or indirectly with the actin cytoskeleton of the cells. In addition, N-cadherin is expressed in ECs and promotes the binding to supporting cells such as pericytes which are essential for blood vessel maturation, whereas Nectin contributes to both, the AJs and TJs. Figure adapted from Dejana, 2004.

3.1.2 Different types of biological tubes

In every biological tube the apical side faces the luminal space whereas the basal side faces the outside of the tube. Based on their cellular architecture biological tubes can be divided into three different types of tubes which vary in their size and shape (Figure 3). In multicellular tubes many polarized cells contribute to tube formation and accordingly, in cross sections, more than one cell is found to constitute the tube circumference. Here, a mesh-like

distribution of junctions constitutes the connections between individual cells making the tube. In unicellular tubes the luminal surface is lined out by a single cell that closes the tube by auto-cellular junctions along its own axis. It is also possible that a lumen passes through a single cell. This type of tube is called a seamless tube since it does not display junctions along its tubular axis (Baer et al., 2009; Lubarsky and Krasnow, 2003).

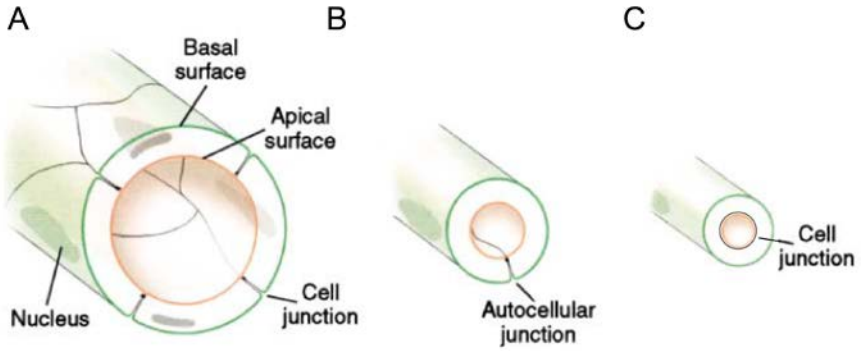

Figure 3 Different biological tubes: (A) Multicellular tube consisting of many epithelial or endothelial cells. Cells are connected to each other by cell-junctions. (B) Unicellular tube with auto-cellular junctions along the cell axis sealing the tube. (C) Unicellular, seamless tube where the lumen passes through the cell. Ring-like junctions are found at the end of each cell connecting it to the next unicellular, seamless cell. (black lines indicate cell(-cell) junctions). Figure adapted from Lubarsky and Krasnow, 2003.

3.1.3 Different morphogenetic mechanisms of tube formation

During tubulogenesis, cells of an epithelium/endothelium follow three common principles. *First*, cells need to know about their position and orientation compared to other cells in the environment. Thus, cells need to communicate with neighboring cells and the ECM to gain positional information. *Second*, when orientation has been specified, cells need to establish polarization. This means they will define apical, lateral and basal identity with the apical side at the future luminal site, whereas the basolateral site contacts the ECM and neighboring cells. *Third*, cells need to form (local) lumens at the apical side. Their expansion or coalescence eventually results in the formation of a tube (Datta et al., 2011). Despite these general principles, different morphogenetic mechanisms have been described of how a biological tube can be formed. Depending on the state of tissue polarity at the beginning of tubulogenesis, there are mechanisms where a pre-polarized epithelial structure is remodeled into a tube – *wrapping* and *budding* - or where polarization is generated simultaneously with and part of the tube formation process – *cavitation*, *cord hollowing* and *cell hollowing* (Figure 4) (Baer et al., 2009; Andrew and Ewald, 2010; Lubarsky and Krasnow, 2003).

3.1.3.1 Tubulogenesis by pre-polarized tissues

The invagination and “rolling up” of selected cells from an epithelial sheet until the edges of the invaginating cell area connect to each other and thereby close the forming tube, is called *wrapping* (Baer et al., 2009; Lubarsky and Krasnow, 2003) (Figure 4). For example in the chicken embryo, the invagination of the neural plate into a neural groove, which is then

closed at the edges, results in the formation of the neural tube, a hollow nerve cord containing the rudiments of the adult nervous system (Colas and Schoenwolf, 2001). The shrinking of one side of a cell, is thought to cause the bending or invagination of an epithelial sheet (Rhumbler, 1902). Indeed, apical constriction has been shown to be an essential driving force during gastrulation and tubulogenesis, (reviewed in Sawyer et al., 2010) and is thought to be primarily driven by the contraction of an actomyosin network (Martin et al., 2009; Hildebrand, 2005; Karfunkel, 1972).

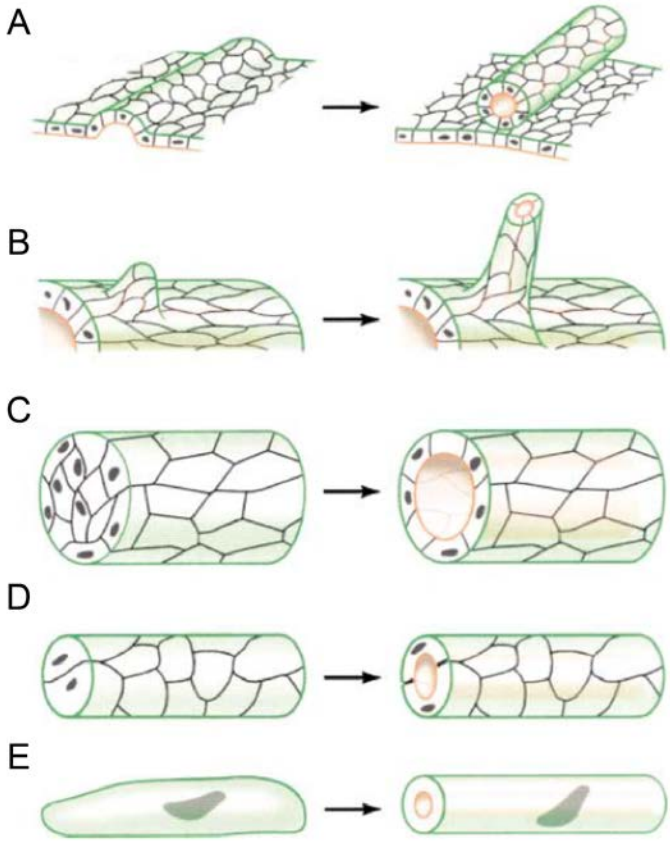

Figure 4 Different morphogenetic mechanisms of tubulogenesis: (A) Wrapping: A polarized sheet of connected cells undergoes coordinated bending along an axis until the edges of the bending region meet and seal, forming a tube running in parallel to the original sheet. (B) Budding: a budlike structure grows out from a tube (or a sheet) and extends as a direct extension of the original tube. (C) Cavitation: cell in the center of a solid multicellular cord are eliminated to convert it into a tube. (D) Cord hollowing: in a cylindrical multicellular cord a lumen is generated de novo between neighboring cells. (E) Cell hollowing: A single cell gets hollowed out and a lumen gets formed along the length of the cell. Figure adapted from Lubarsky and Krasnow, 2003.

In *budding*, selected cells grow out from a pre-existing polarized tissue, and extend into the surrounding tissue to form a branch which is then transformed into a tube. Here, the new tube is thought to be a direct extension of the original tube (Baer et al., 2009; Lubarsky and Krasnow, 2003) (Figure 4). Budding events have been described in several organisms and tissues such as the kidney (Costantini and Shakya, 2006), the lung (Metzger et al., 2008), mammary gland (Cowin and Wysolmerski, 2010) and during tracheal development of *Drosophila melanogaster* (Samakovlis et al., 1996).

3.1.3.2 Tubulogenesis from non-polarized tissues

In *cavitation*, inner cells of a cord, the cells that do not contact the ECM but only neighboring cells, are removed and thereby hollow out the original cord (Baer et al., 2009; Lubarsky Krasnow, 2003) (Figure 4). This mechanism has been shown to take place for instance during mammary gland (Cowin and Wysolmerski, 2010; Mailleux et al., 2007) and mammalian salivary gland (Tucker, 2007) formation. Apoptosis, the caspase-dependent programmed death of cells, (Guimarães and Linden, 2004; Elmore, 2007) is a critical process during cavitation since mice, deficient for a pro-apoptotic factor of the BCL2 family (Huang and Strasser, 2000), show a delay in lumen formation of the developing mammary gland. However, since cells of the mammary gland undergo a caspase-independent cell death in this mutant, other mechanisms than apoptosis that lead to the removal of cells might be at work. For example Autophagy (Greek for *auto:*self-*phagy:*eating), which is an alternative death style that has been described in 1963 for the first time at the CIBA Foundation Symposium on Lysosomes in London by Christian de Duve (Mailleux et al., 2007; Klionsky, 2007), in which the cytoplasmic components are degraded in membrane vesicles after their fusion with lysosomal compartments (Kundu and Thompson, 2008).

During *cord hollowing*, a solid cord is hollowed out by the generation of extracellular spaces between the apical membranes of neighboring cells that face the future luminal side (Baer et al., 2009; Lubarsky and Krasnow, 2003) (Figure 4). In the intestine of the developing zebrafish embryo, multiple small local lumens at different positions extend and coalesce and thereby form a continuous lumen (Bagnat et al., 2007) whereas in the dorsal aorta of the embryonic mouse, a central lumen is formed between contacting ECs (Strilic et al., 2009 and see also 5.1.2, p.53 and 6.1.3, p.80).

Cell hollowing generates a seamless tube, which is different from the two other mechanisms described above, during which multicellular tubes are generated. Here, a lumen forms within a single cell, resulting in unicellular tube (Figure 4) (Baer et al., 2009; Lubarsky and Krasnow, 2003). This mechanism has been described in the excretory cell of *C. elegans* (Buechner, 2002) and special tracheal fusion cells in *Drosophila melanogaster* (Lee and Kolodziej, 2002; Kakihara et al., 2007) and the intersegmental vessels (ISVs) of the zebrafish (Kamei et al., 2006). In the endothelium vacuolar or vesicular intracellular fusion events have been described *in vitro* as well as *in vivo* and were suggested to be involved into this process (Iruela-Arispe and Davis, 2009; Lubarsky and Krasnow, 2003).

Two rather new mechanisms of how a biological tube can be formed have been observed in heart tube development of *Drosophila melanogaster* and the digestive tract of *C. elegans*. The connecting part between the pharynx and the intestine in *C. elegans* is formed by single cells that wrap around the future luminal side and then undergo a *self-fusion* mechanism resulting in seamless cells arranged in a rod like fashion (Rasmussen 2008).

In the fly heart, cardioblast cells have evolved a mechanism, which is based on the establishment of specialized adhesion sites and active repulsion of the future apical membranes between contacting cells. In this scenario, dorsal and ventral specific “foci” establish contact to neighboring cells, whereas the region between these contact sites undergo an active repulsion mechanism to generate a lumen (Santiago-Martínez et al., 2008).

3.1.4 Molecular regulation of lumen formation

3.1.4.1 Finding cell orientation and position

As mentioned earlier, cells need to communicate with their environment during tubulogenesis (i.e. other cells and the ECM). Knowing their orientation and position then allows proper orientation of polarity, with apical at the future luminal site (Datta et al., 2011). Cells interact with neighboring cells via different adhesion receptors that include cadherins and nectins (Harris and Tepass, 2010). Such interactions give cells instructive cues where to start the polarization (see also 6.1.1, p.77). However, in a tissue, cells are also surrounded by the ECM, which provides them with further positional/instructive information. Integrin-ECM interactions are thought to have crucial roles during blood vessel morphogenesis including the control of lumen formation (Rupp and Little, 2001; Avraamides et al., 2008) and *β*1-integrin containing complexes have been shown to be essential key players in sensing the ECM (Datta et al., 2011). Furthermore, integrin signaling activates Rho GTPases, which controls the endothelial cytoskeleton and tube “morphogenetic responses” (Iruela-Arispe and Davis, 2009). For instance, the Rho GTPase Cdc42 (cell division control protein 42 homologue) and Rac1 have recently been shown to be involved in EC lumen formation (Bayless and Davis, 2002) and are thought to be activated by integrin signaling **(**Davis and Bayless, 2003). Here, Cdc42 and Rac1 are essential for the process of intracellular vacuole formation and coalescence, which is thought to regulate endothelial lumen formation in three-dimensional extracellular matrices (see also 3.2.4.2.7, p.25). In Madin-Darby Canine Kidney (MDCK) cells (cells that do form cyst when cultured in three-dimensional collagen gels), orientation of apical-basal polarity is regulated by a *β*1-integrin dependent pathway that requires Rac1, a Rho GTPase. Blocking this pathway with an antibody against *β*1-integrin results in the inversion of polarity, which can be rescued by activated Rac1 expression (Yu et al., 2005). Further, blocking *β*1-integrin in the chicken results in the total absence of lumens in the aorta (Drake et al., 1992) which demonstrates the importance of cell-(integrin)-ECM communication regarding endothelial polarization and lumen formation.

After cells have determined the directionality of lumenogenesis, they need to generate an apical side at the future luminal site, thus they need to polarize.

3.1.4.2 Polarization of cells

Endothelial cell polarization is essential for the process of lumen formation, but how EC polarization contributes to lumen formation is only at the beginning to be well understood. It is also thought that polarization of epithelial cells is different in several aspects than polarization of the endothelium (Iruela-Arispe and Davis, 2009). In general, polarization of epithelial cells is controlled and maintained by three conserved “core protein complexes”, the PAR (CDC42-PAR3-PAR6-aPKC), Crumbs (Crb-PALS-PATI) and Scribble (Scrib-Dlg-Lgl) complexes. In epithelial cells, the PAR and Crumbs complexes regulate formation of the apical side whereas the Scribble complex promotes basolateral identity. At least one of the three polarity complexes, the PAR complex, is involved in endothelial cell polarization and lumen formation (see below). However, at this moment, there is little information whether or how the Crumbs and Scribble complexes are involved in EC polarization and lumen formation (Iruela-Arispe and Davis, 2009). In general, during PAR complex activation, which is essential regarding apical polarization, PAR3 gets recruited to sites of contact between neighboring cells. A pre-formed PAR6-aPKC unit is then bound by active Cdc42 which results in the activation of the PAR3-PAR6-aPKC complex at the future apical surface and marks the separation between the basolateral and apical domains and site of TJ formation (Willenborg and Prekeris, 2011). CDC42 has been shown to interact with the PAR complex by directly binding to PAR6 (Garrard et al., 2003). In *C. elegans*, the deletion of a specific GAP controlling CDC42, results in polarity defects as well as ectopic localization of polarity complexes (Anderson et al., 2008). In endothelial cells, it was shown that a PAR complex lacking aPKC, localizes and interacts with VE-cadherin at the adherens junctions, which is different to vertebrate epithelial cells, where the PAR complex is thought to be localized at the tight junctions (Iden et al., 2006). However, a more recent study showed that lumen formation of ECs in three-dimensional collagen matrices is controlled by a Cdc42-Par3-Par6-PKCζ complex (PKCζ = isoform of aPKC). Disruption of any member within this complex lead to impaired lumen formation, which demonstrates the importance of apical polarization regarding lumenogenesis (Koh et al., 2008). Further, in the aorta of the mouse, *β*1-integrin acts upstream of Par3, as part of a signaling cascade, during EC polarization and lumen formation (Zovein et al., 2010).

The differential distribution of phosphatidylinositol-phosphates (PIPs) to distinct membrane domains is important regarding polarization since PIPs function as “apical and basolateral determinants”, recruiting proteins important for epithelial morphogenesis (Willenborg and Prekeris, 2011). However, there is less evidence for apical and basolateral protein sorting in ECs (Iruela-Arispe and Davis, 2009). PAR3 is thought to localize lipid phosphatase PTEN (phosphatase and tensin homologue deleted on chromosome 10) to tight junctions where it converts PIP3 into PIP2 (von Stein et al., 2005; Feng et al., 2008). In mammalian epithelial

cells, PIP2 is found at the apical surface, whereas PIP3 is localized at the basolateral site. Further, PIP2 is thought to recruit Cdc42 to the apical surface and PTEN depletion in MDCK cells results in reduced PIP2 levels and the generation of an apical lumen is inhibited. The action of PTEN at the tight junctions probably prevents PIP3 from entering apical areas by its phosphatase activity (Gassama-Diagne et al., 2006; Martin-Belmonte et al., 2007; Martin-Belmonte and Mostov, 2007). In the endothelium, chemical inhibition of PTEN results in reduced formation of the dorsal aorta in the mouse whereas genetic disruption of PTEN results in rather normal formation of the dorsal aortae (Suzuki et al., 2007; Strilic et al., 2009).

Rab11, a small monomeric GTPase, is thought to be a key regulator of the polarized endocytotic transportation and sorting in epithelial cells (Prekeris, 2003). For instance, the AREs (apical recycling endosomes, distinct apical domain-specific organelles from the AEE = apical early endosomes (Willenborg and Prekeris, 2011)) transport cargo to the apical domain and are marked by the monomeric GTPase Rab11a/b (Brown et al., 2000). In addition to the specificity that is given by the Rab proteins, the so-called exocyst complex (Wu et al., 2008), plays a crucial role in the tethering and fusion of vesicles with the PM and thus, is essential for epithelial cell polarization. Localization and function of this complex are regulated by different binding proteins including members from the Rab family (Willenborg and Prekeris, 2011). Another set of proteins, which is essential for the fusion of vesicles with their target membrane, are the SNARE proteins (soluble N-ethylmaleimide-sensitive fusion protein-attachment protein receptors (Jahn and Scheller, 2006)). They are thought to act specifically at apical and basolateral sites. For instance, the snare protein syntaxin 3 is found at apical sites whereas syntaxin 4 is found at basolateral sites (Low et al., 1996). How a polarization complex is linked to the membrane traffic machinery has recently been reported by Bryant and colleagues who describe a Rab11 regulated molecular mechanism for the *de novo* formation of an apical surface and a lumen in mammalian MDCK cells. In this mechanism, Rab11 recruits Par3 and activated CDC42 to the apical membrane, which demonstrates the link between members of polarization complexes and the trafficking machinery during polarization and lumen formation (Bryant et al., 2010).

3.1.4.3 Lumen expansion

Expansion of small lumens is thought to happen to a certain extend by hydrostatic pressure, which is regulated by the activation of pumps and ionic channels (Datta et al., 2011). It has been shown that smaller lumens may expand and coalesce to form a single continuous lumen. Proteins of the Claudin family and the Na-K-ATPase play key roles during the expansion and coalescence of smaller lumens; for instance, multiple lumens are formed in

zebrafish gut lumenogenesis when Claudin 15 and Na-K-ATPase are down-regulated by the loss of the transcription factor *Tcf2* (Bagnat et al., 2007; Gutzman and Sive, 2010).

3.2 The vascular system and its formation

The vertebrate vasculature is formed by two fundamental distinct processes - vasculogenesis and angiogenesis (Figure 5): The first extra- and intra-embryonic blood vessels are formed by vasculogenesis, the *de novo* formation of blood vessels. This is the differentiation of angioblasts, endothelial precursor cells (EPCs) derived from the mesoderm, their migration and subsequent aggregation into vessels (Risau and Flamme, 1995). These vessels will later undergo strong remodeling and eventually new vessels will be formed by these pre-existing vessels, a process called angiogenesis. Angiogenesis can occur in distinct ways: (i) non-sprouting angiogenesis or intussusception and (ii) sprouting angiogenesis (Risau, 1997). During sprouting angiogenesis, individual sprouts or vessels need to connect to each other, a process called vessel fusion or anastomosis (Herbert and Stainier, 2011; Blum et al., 2008; Hogan and Kolodziej, 2002).

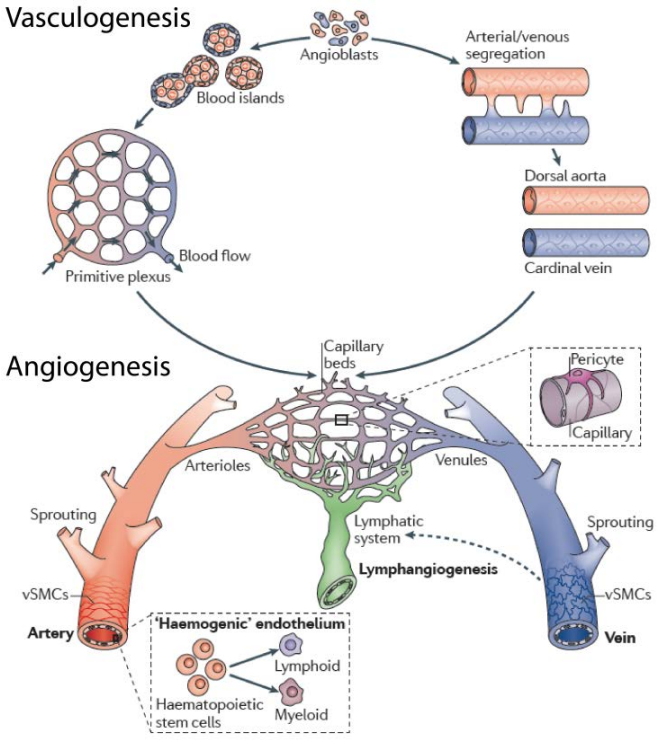

Figure 5 Overview of vascular development. Vasculogenesis (formation of blood vessels *de novo*): Mesodermal derived angioblast migrate to distinct sites within the embryo, acquire arterial or venous fates and coalesce to form the first blood vessels, the dorsal aorta and the cardinal vein. In the zebrafish, the sorting of arterial and venous angioblasts and ventral venous angioblast sprouting, results in the formation of the distinct dorsal aorta and cardinal vein. Angioblasts also form so called blood islands, which will fuse and form capillary plexi. Angiogenesis (formation of blood vessels from pre-existing vessels): Angiogenic remodeling creates a highly branched vascular network of arteries, arterioles, capillary beds, venules and veins. During vessel maturation mural cells support and stabilize the nascent vessels. Additionally, sprouting of lymphatic cells from venous vessels generates the lymphatic system. Further, hematopoietic stem cells originating from arterial hemogenic endothelium give rise to myeloid and lymphoid blood cell lineages. Figure adapted from Herbert and Stainier, 2011.

3.2.1 Vascular anatomy of vertebrates

In vertebrates, the early embryonic vasculature in the trunk is conserved regarding its body plan, which is later further branched and remodeled according species-specific developmental programs. However, at the early stage, vertebrates possess two axial main vessels, the dorsal aorta (DA) and posterior cardinal vein (PCV), which run along the anterior-posterior body axis. From these main vessels, smaller intersegmental vessels (ISVs) run dorso-ventrally between the somites, notochord and neural tube whereas the so called parachordal chain runs longitudinal on each side of the notochord and contributes to the lymphatic system (Figure 6) (Isogai et al., 2001; Isogai et al., 2003; Yaniv et al., 2006; Lim et al., 2011).

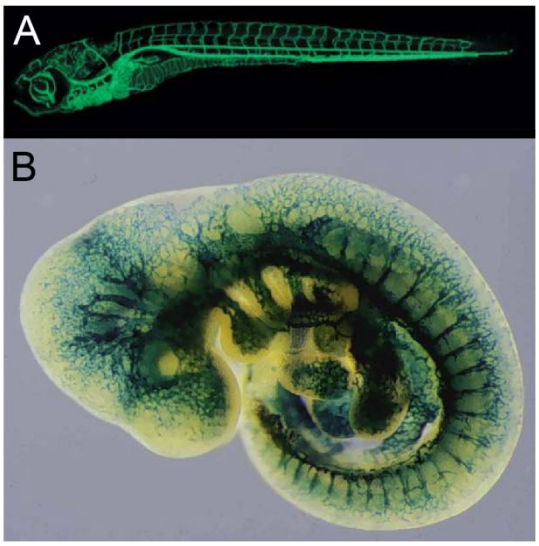

Figure 6 A conserved vascular body plan in the early developing vertebrate embryo. (A) Vascular system in the zebrafish embryo at 6 dpf. (B) Vascular system in a mouse embryo at 9.5 dpc. In both organisms, the intersegmental vessels (ISVs), dorsal aorta (DA) and posterior cardinal vein (PCV) are conserved and established early in development. (A) adapted from Isogai et al., 2001 and (B) courtesy of V. Bautch, UNC (University of North Carolina).

Later, in the adult, blood proceeds from the heart through tubes or vessels of different size, shape and characteristics (Figure 5). First, blood is pumped into arteries, later into arterioles and then into the peripheral parts of the body, which are nerved by very small vessels called capillaries, providing the connection of the circulatory loop between arteries and veins. From the capillaries, the blood is transported back to the heart via venules and veins. Intercellular protein-rich fluid, excreted from the blood vessels, is collected by “blind-ended”, unidirectional vessels of the lymphatic system draining it back through collecting vessels, lymph nodes, lymphatic trunks and ducts to the venous circulation (Alitalo et al., 2005; Adams and Alitalo, 2007).

3.2.2 Vascular development

3.2.2.1 Vascular endothelial growth factors and its receptors

Discovered in 1983, vascular permeability factor (VPA), later called vascular endothelial growth factor A (VEGF-A), was shown to be a strong angiogenic mitogen (Leung et al., 1989; Henzel and Press, 1989; Senger et al., 1983) and is key player during vascular development and growth (Chung, 2011; Ferrara, 2009). VEGF has mitogenic activities, it triggers vascular outgrowth and branching, it is involved in chemotaxis of monocytes, it regulates vascular permeability and it has been shown to act as a survival factor for ECs. VEGF is also involved in pathological angiogenesis (Ferrara et al., 2003), for instance during tumorigenesis where VEGF mRNA is shown to be up-regulated in human tumor cells (Factor et al., 1995). Mice deficient for only one single VEGF-A allele are embryonic lethal and show strong vascular abnormalities. These mutant mice display a delay in EC differentiation, have disorganized vessels, impaired blood-island formation and show a disturbed formation of hematopoietic cells (Carmeliet et al., 1996; Ferrara et al., 1996). VEGF is thought to be expressed under hypoxic conditions and recent findings suggest a VEGF-inducible role for sonic hedgehog (Shh) (Fraisl et al., 2009; Pola et al., 2001; Lawson et al., 2002).

VEGF-A is a homodimeric glycoprotein and belongs to a bigger family of receptor-binding growth factors displaying a cysteine-knot like structure. This family, beside VEGF-A, includes VEGF-B, VEGF-C, VEGF-D as well as placental growth factor (PlGF) (Holmes and Zachary, 2005; Neufeld et al., 1999; Lohela et al., 2009). In addition to these VEGFs, viral VEGF homologs (collectively called VEGF-E) and snake VEGFs (called VEGF-F) have been identified (Yla-Herttuala et al., 2007). VEGFs signal through different endothelial tyrosine kinase receptors (RTKs), the so called vascular endothelial growth receptors (VEGFRs) of which VEGFR-1/Flt1, VEGFR2/Flk1 and VEGFR3/Flt4 have attracted much attention in the last years (Figure 7).

Among all the different VEGF forms, VEGF-A and its binding partners VEGFR1 and VEGFR2 are the best described signaling pathways during vascular development. Vegfr2 null mice die during embryonic development displaying severe defects regarding hematopoietic and endothelial cells (Shalaby et al., 1995) similar to what has been described in *vegf*$^{-/-}$ mice (Carmeliet et al., 1996; Ferrara et al., 1996). VEGFR-2 signaling induces angiogenesis by triggering proliferation, sprouting and migration as well as the survival of ECs (Lohela et al., 2009; Masabumi and Claesson-Welsh, 2006). VEGFR3, as mentioned above, is thought to regulate blood vessel development, vein specification, as well as lymphangiogenic processes (Koch et al., 2011). During development VEGFR3 is expressed in the endothelium and later, in the adult stage, its expression gets restricted to the lymphatic system. In the postnatal mouse retina, it is predominately expressed at the front of growing

endothelial sprouts and its blocking results in impaired angiogenic sprouting and formation of a vascular network (Tammela et al., 2008) (Figure 7).

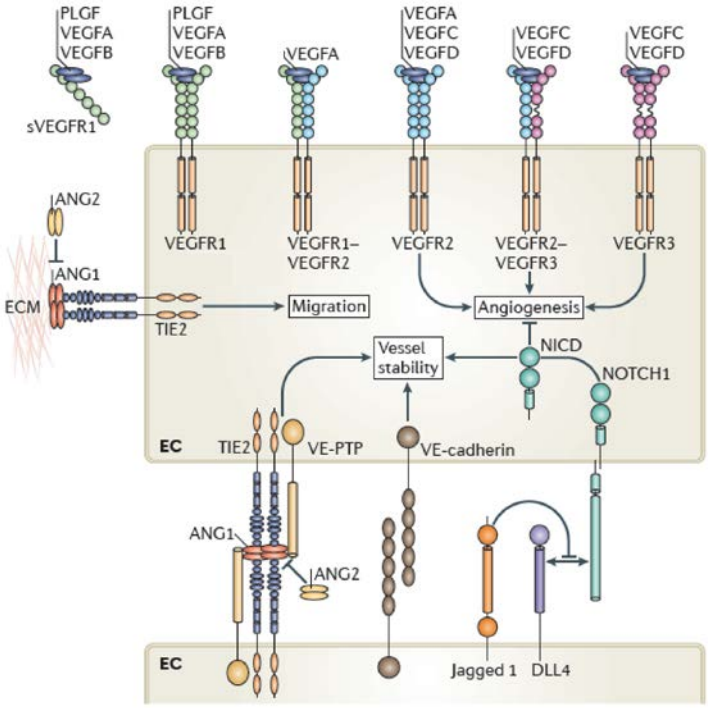

Figure 7 Overview of different VEGFs and VEGFRs. Vascular endothelial growth factors (VEGFs) bind different homodimers and heterodimers of VEGF receptors (VEGFRs). Their signaling via VEGFR2, VEGFR3 or VEGFR2– VEGFR3 heterodimers is pro-angiogenic. PlGF (not shown in this figure) Maglione, D., Guerriero, V., Viglietto, G., Delli-Bovi, P. and Persico, M. G. (1991) and VEGF-B can signal through VEGFR-1, whereas VEGF-B was shown to be regulating lipid metabolism in the heart (Olofsson et al., 1998; Tarallo et al., 2011; Lohela et al., 2009)(Olofsson et al. 1998, Park et al. 1994) and is commonly seen as an angiogenic modifier. VEGF-C and VEGF-D bind to VEGFR-3 and are important first of all during the formation of the lymphatic system (Achen et al., 1998; Joukov et al., 1996; Lohela et al., 2009). VEGFR-2 signaling induces angiogenesis by triggering proliferation, sprouting and migration as well as the survival of ECs (Lohela et al., 2009; Masabumi Shibuya and Claesson-Welsh, 2006).The binding of VEGFA to VEGFR1 and its secreted version sVEGFR1, the extracellular domain of VEGFR1 are thought to function as a sink for VEGFA thereby decreasing VEGFR2 activity. The interaction of TIE2 receptor interaction with the matrix-bound form of angiopoietin 1 (ANG1) induces EC cell-migration. In contrast ANG1 localized in the membrane of ECs binding to TIE2 at cell-cell junctions by trans-complex formation with TIE2 on adjacent cells, promotes angiogenic quiescence. Such complexes involve vascular endothelial protein Tyr phosphatase (VE-PTP). ANG2 antagonizing the activity of ANG1 on TIE2 leads to vessels destabilization and supports angiogenic remodeling. Homophilic VE-cadherin interactions maintain the adherens junctional complex and are important for endothelial integrity and barrier function by the regulation of blood vessel permeability (3.1.1, p.4). DLL4-mediated Notch signaling upon the proteolytic release of the intracellular domain of Notch (NICD) represses angiogenic cell behavior. Jagged 1 interaction with Notch receptor can antagonize Notch signaling. Figure adapted from Herbert and Stainier, 2011.

VEGF-A exists as different isoforms that have distinct binding affinities on heparin and heparan sulphates (HS), linear polysaccharides present on the surface of a cell or in the extracellular matrix (ECM), that can bind a large variety of proteins including growth factors to regulate biological processes (Herbert and Stainier, 2011). HS is found on syndecans and glypicans, two families of proteoglycans that are membrane-bound. The binding of a secreted molecule to heparin or HSPGs, glycoproteins that are bound to heparan sulphates (Bernfield et al., 1999), amplifies the capacity to be deposited in the ECM (Esko and Lindahl,

2001). VEGF isoforms that lack the presence of domains responsible for heparin or HSPG binding are thought to distribute differentially in the environment of cells secreting VEGFs (Houck et al., 1992). For instance the matrix binding isoform VEGF165 directs formation of filopodia, branching of vessels as well as the migratory behavior of ECs. Conversely, VEGF120, a freely diffusible isoform unable to bind heparan sulphate, results in impaired extension of filopodia at the tips of growing vessels, decreased branch points in capillary networks but a larger diameter of vessels. VEGF188, a solely binding isoform of heparin sulfate, displays the opposite phenotype, ectopic filopodial extensions, an excess of branching and thin vessels (Ruhrberg et al., 2002). Taken together, the different VEGF isoforms localized in the ECM provide spatially restricted information for the various EC behaviors that are required to establish vascular branching patterns (Ruhrberg et al., 2002; Stalmans et al., 2002; Carmeliet and Tessier-Lavigne, 2005). In addition, heparin-binding isoforms of VEGF-A also bind neuropilins (NP1/2), co-receptors which potentiate signaling via VEGFR2 or can signal independently of VEGFR2. It was found that VEGF165 stimulated migration of ECs in the presence of NP1 is enhanced in cells expressing a recombinant form of VEGFR2 (Prahst et al., 2008; Soker et al., 1998).

3.2.3 Vasculogenesis

3.2.3.1 ECs differentiation and formation of the first vessels

As mentioned above, mesodermal cells differentiate into endothelial cells that later surface the inner wall of the vessels. During early somatogenesis, cells from the lateral plate mesoderm are specified by the expression of conserved families of transcription factors, such as members of the ETS or GATA family, into hematopoietic cells and endothelial precursor cells, so called angioblasts, which migrate to distinct places within the embryo where they will coalesce and form the first blood vessels (Simon, 1995; Risau and Flamme, 1995; Weiss and Orkin, 1995; Brown et al., 2000). Fli1 (friend leukemia integration 1), an ETS family member, is thought to act at the top of the transcriptional network which regulates blood cell and endothelial cell development and a constitutively active form of this transcription factor is able to induce expression of key genes, that drive the differentiation of the hematopoietic and endothelial cell lineage. These genes include *scl/tal1, lmo2, gata2, etsrp,* and *flk-1*, the receptor for VEGF-A (Liu et al., 2008). However, the expression of Fli1 becomes continuously restricted to the endothelium in the trunk as shown during zebrafish and Xenopus development (Meyer et al., 1995; Brown et al., 2000). In the yolk sac, but also the embryo itself, migrating angioblasts coalesce and contribute to the so called blood islands which will fuse and thereby form honey-comb like capillary plexi. Later theses capillary plexi are remodeled into a network of hierarchically organized arterioles, arteries,

capillaries, venules and veins by the process of angiogenesis (Figure 5) (Risau and Flamme, 1995; Adams and Alitalo, 2007). The dorsal aorta and cardinal vein are thought to be formed directly by the aggregation of angioblasts at the midline of the embryo (Coultas et al., 2005; Coffin and Poole, 1988) and it has been shown that the notochord is an essential structure during DA formation and patterning (Fouquet et al., 1997; Sumoy et al., 1997; Cleaver and Krieg, 1998). VEGF is thought to be expressed at the midline (Cleaver and Krieg, 1998) as well as in the underlying notochord (Coultas et al., 2005) which attracts migrating angioblasts expressing VEGFR-2. Recently, chemokine signaling has been identified to be an essential pathway in patterning the first embryonic artery in the zebrafish (Siekmann et al., 2009). Here, missing Cxcl12b (chemokine C-X-C motif ligand 12b), a Cxcr4a ligand, in the underlying notochord phenocopies the deficiency effects of Cxcr4a which is an incomplete formation of the lateral dorsal aortae. In the zebrafish, live observations using endothelial specific transgenic reporter lines, particularly a fluorescence marker under the control of the ETS transcription factor fli1a (see above), have shown that angioblasts first appear at 12 hpf in the lateral plate mesoderm (LPM). Guided by stimuli from the endoderm they then migrate as individual cells in two waves to the midline of the embryo where they coalesce (Figure 8) (Lawson, 2002; Roman and Weinstein, 2000; Jin et al., 2005). Cells of the first wave at around 14 hpf are thought to form the dorsal aorta (DA), whereas cells of the second wave at around 16 hpf will generate the posterior cardinal vein (PCV). Initially, these cells form a structure called vascular cord, a simple cluster of angioblasts, which then at 17 hpf start to establish cell-cell junctions as shown with immunostainings using an antibody against the tight junctional protein Zonula Occludens-1 (ZO1) (Jin et al., 2005, see also Eriksson and Löfberg, 2000; Fouquet et al., 1997). At 17 hpf, angioblasts start to differentiate into arterial and venous ECs (Jin et al., 2005). EphrinB2, a member of the Eph ligand family, is detectable in future arterial cells (Zhong et al., 2001; Lawson et al., 2001) whereas Flt4 becomes visible in venous cells (Thompson et al., 2008). At around 18 hpf the vascular cord is lumenized by cord hollowing to form the DA as suggested by live imaging and the analysis of polarity- and junctional proteins (Jin et al., 2005; Herbert et al., 2009). Alternatively, as shown by high-resolution live imaging of the embryonic zebrafish trunk, the PCV is formed by a ventral sprouting mechanism from a common precursor vessel with a mixed population of arterial and venous ECs (Figure 5 and Figure 8). Here, selected ECs sprout ventrally and separate from that common precursor vessel resulting in the formation of the DA and PCV. This observation is further supported by the fact that this ventral sprouting mechanism is disrupted when arterio-venous differentiation is blocked (Herbert et al., 2009).

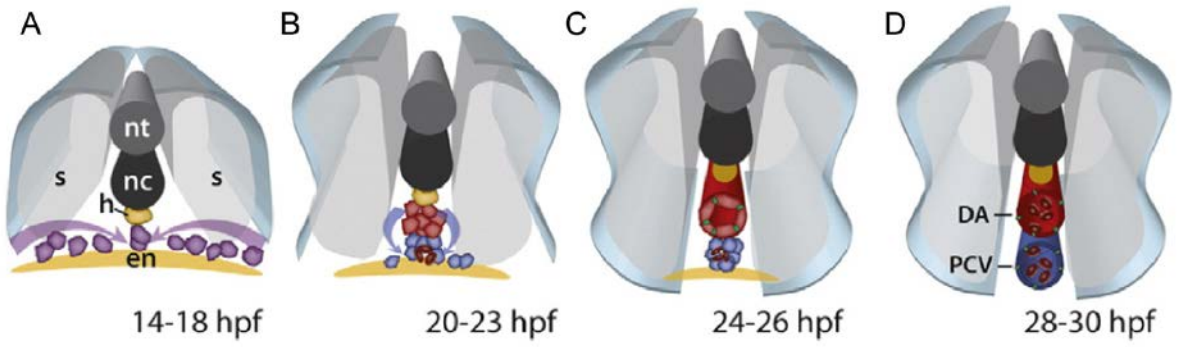

Figure 8 Vasculogenesis in the zebrafish embryo. (A-D) Schematic cross-sections of the trunk region during different stages of development. (A) At around 14 hpf, angioblasts, originating from the lateral plate mesoderm migrate over the endoderm towards the midline where thy form a vascular cord below the hypochord. At around 17 hpf, angioblasts start expressing markers of arterio-venous differentiation, such ephrin-B2a in more dorsally located arterial cells (marked in red). (B) These ephrin-B2a positive cells will give rise to the DA, whereas ephb4a positive cells are located more ventrally and will contribute to the PCV most-likely by a ventral directed sprouting process from the DA at around 21 hpf. (C) Cord hollowing lumenizes the DA which happens in the absence of blood cells and prior to the lumenization of the PCV and. Venous angioblasts aggregate and coalesce around the blood cells to ultimately form a tube.(D) At 30 hpf, both vessels are fully formed and carry blood flow. Endothelial cell junctions are indicated in green. Figure adapted from Ellertsdottir et al., 2009.

3.2.3.2 Arterio-venous differentiation of endothelial cells

For a long time it was believed that arterial venous differentiation is primarily driven by hemodynamic forces as recently shown for extraembryonic vessels in the chick embryo yolk sac (le Noble et al., 2004). However, differential expression of the arterial marker ephrin-B2 and its receptor EphB4 which is expressed in veins in developing vessels already before the onset of circulation, changed this common idea of predominant extrinsic factors that regulate the differentiation process and intrinsic, i.e. genetic factors became more and more prominent (Wang et al., 1998; Rocha and Adams, 2009). Ephs are RTKs that bind to their ligands ephrins and are involved in embryonic development where they regulate patterning, neuronal targeting, vascular development and neovascularization (Cheng et al., 2002). After angioblasts have aggregated, they will undergo further differentiation to form either arterial or venous endothelium. Arterial differentiation has been shown to be driven by Notch dependent signaling. The expression of a non DNA-binding form of “Suppressor of hairless”, which acts as an inhibitor of Notch signaling, results in reduced ephrin-B2 expression but enhanced EphB4 expression in the zebrafish aorta, causing reduced size of the latter (Lawson et al., 2001). In addition the basic helix-loop-helix transcription factor genes *Hey1* and *Hey2* (hairy- and enhancer of split-related with YRPW motif) are direct Notch target genes and mice deficient for *Notch1* or *Hey1/Hey2* fail to express the arterial specific marker ephrin-B2 and the paired dorsal aortae are strongly reduced or even missing (Fischer et al., 2004). In addition, the gene *Gridlock*, a HEY family member, was shown to influence vessel specific cell fate decision since *Gridlock* mutants display disturbed formation of the aorta (Zhong, 2000). Furthermore, gradual reduction of the gene by morpholino knockdown leads

to a decrease in artery development but an expansion of the vein accompanied by increased expression of EphB4 and ephrinB2 reduction, respectively (Zhong et al., 2001). In contrast the orphan nuclear receptor COUP-TFII (chicken ovalbumin upstream promoter transcription factor 2), specifically expressed in venous ECs, was shown to repress Notch signaling thereby promoting vein identity (You et al., 2005). Altogether, Notch signaling seems to suppress venous differentiation during normal vascular development whereas COUP-TFII counteracts the Notch pathway to allow venous identity (Coultas et al., 2005).

3.2.4 Angiogenesis

Angiogenesis, the formation of new vessels from pre-existing vessels (Risau, 1991), occurs in different ways: **(i)** through non-sprouting angiogenesis which includes intussusception and **(ii)** through sprouting-angiogenesis (Risau, 1997).

3.2.4.1 Non-sprouting angiogenesis

During non-sprouting angiogenesis or intussusceptive angiogenesis (IA), first described by Caduff and colleagues in 1986, existing vessels are split by the local insertion of tissue pillars from surrounding tissues, i.e. transluminal tissue pillar formation. Such tissue pillars subsequently expand and fuse to each other resulting in new vessels or vessel branching (Makanya et al., 2009; Adams and Alitalo, 2007). Blood flow has been shown to directly influence IA whereas the molecular control remains still poorly described. There are three phases of IA which have been described: intussusceptive growth (IMG), intussusceptive arborization (IAR) and intussusceptive branching remodeling (IBR). IMG will increase the inner surface of vessels by expansion of tissue pillars. IAR demarcates future vessels by the insertion of vertical serial tissue pillars giving the vasculature a tree-like shape and IBR optimizes the geometry of vessel branching by intussusception pillars at bifurcations (points where a vessel splits into two) of vessels that will fuse with the connective tissue at the bifurcation site (Makanya et al., 2009; Djonov et al., 2002)

3.2.4.2 Sprouting Angiogenesis

3.2.4.2.1 Principles of sprouting angiogenesis

In order to produce an angiogenic sprout that will become a stable vessel integrated into a vascular network, ECs exert a number of distinct cellular behaviors. VEGF-A acts upstream of a so called “angiogenic cascade”, a sequential series of events forming new blood vessels, which includes proteolysis of the ECM, migration, proliferation and finally the fusion of sprouts to form a (capillary) network (Augustin et al., 2009).

In fact, resting ECs have to overcome quiescence, they will have to loosen their cell-cell contacts, and form a bipolar sprout with a front and a connecting part linking the sprout to the parental vessel. The extracellular basement membrane needs to be degraded to allow migration of ECs towards angiogenic stimuli. Along their way, angiogenic sprouts need to elongate which is mainly achieved by cell proliferation and cell shape changes. The newly developed vessels will be stabilized by supporting cells and eventually fusion of individual sprouts occurs to allow blood circulation (Figure 5) (Herbert and Stainier, 2011; Ausprunk and Folkman, 1977; Carmeliet and Jain, 2011).

3.2.4.2.2 Breaking angiogenic quiescence

The vascular specific tyrosine kinase receptors, including Tyr kinase with Ig and EGF homology domains receptor 1 and 2 (Tie1/2) and their ligands angiopoietin1 and 2 (ANG1/2) have been shown to be essential during vessel assembly and maturation in the embryonic tissue. Further, this signaling system seems to be crucial during adult vascular homeostasis. The quiescent phenotype of ECs in parental vessels, maintained by ANG1/Tie2 signaling, can be antagonized by ANG2, leading to vessel destabilization and is thought to support the angiogenic remodeling (Augustin et al., 2009; Herbert and Stainier, 2011). Interestingly, the interaction of TIE2 receptor with ANG1 bound in the ECM induces migration of ECs (Saharinen et al., 2008). However, VEGF is the key pro-angiogenic stimuli and induces single ECs from a larger vessel to become more angiogenic than their neighboring cells. These cells will modify their cell-cell junctions, become more motile and start to express and secret proteases that will degrade the basement membrane (Adams and Alitalo, 2007).
In order to effectively invade avascular territories to form vascular patterns according to local demands, ECs of angiogenic sprouts need to form a “bi-polar” sprout. This means ECs have to adopt “functional specialization” that allows navigation and elongation of the growing sprout towards angiogenic stimuli (Gerhardt 2005).

3.2.4.2.3 Tip cell selection

As mentioned above, upon VEGF-A signaling, some ECs will become more angiogenic than others and will leave the vessel wall first and thus, will be at the front of growing sprouts. Such leading cells called “tip cells” (TCs) (Gerhardt et al., 2003) scan the environment by filopodial extensions for attractive and repulsive signals. These extensions are induced by VEGF-A/VEGFR2 signaling too. Gerhardt and colleagues showed that perturbation of the normal VEGF-A gradient inhibits filopodial extension and the peripheral outgrowth of ECs in the mouse retina, suggesting that directed tip cell migration depends on the ability of the tip cell to distinguish signaling information at the tips of filopodia from other information provided at the cell body. Thus, the tip cells respond to VEGF-A by guided migration, whereas

neighboring less angiogenic ECs, so-called stalk cells (SCs), trail the leading tip cells (Gerhardt et al., 2003). Shown *in vitro* as well as *in vivo*, specific Notch receptors and delta-like ligands are expressed in the endothelium (Phng and Gerhardt, 2009; Gridley, 2010). It turned out that hypoxia or VEGF-A can induce Dll4 expression and that haploinsufficient mice for *dll4* are embryonic lethal due to severe arterial defects (Williams et al., 2006; Nicholas et al., 2004; Liu et al., 2003; Mailhos et al., 2001). Furthermore, VEGF induces dynamic expression of *dll4* in the mouse retina, predominantly in the leading cells of growing vessels (Lobov et al., 2007). Recent studies have shown that VEGF-A mediated Notch signaling is a key signaling pathway to select tip cells in angiogenic sprouts (Figure 9) (Lawson et al., 2002).

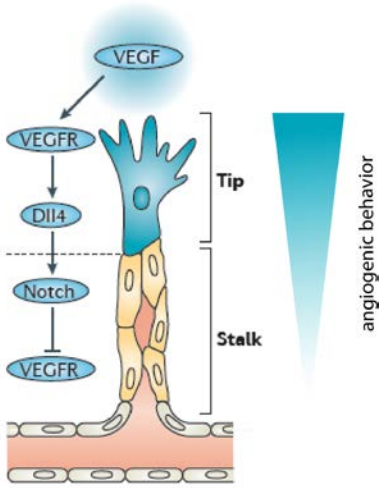

Figure 9 Selection of the tip cell. The tip cell behavior is induced by VEGF signaling, whereas the Dll4-mediated Notch signaling represses VEGF receptor signaling in adjacent cells and thus represses their angiogenic behavior. The tip cell is high in VEGFR signaling but low in Notch signaling. It forms multiple filopodial extensions, is highly motile and leads and guides a sprout through the avascular territory towards pro-angiogenic stimuli. The stalks cells in contrast are low in VEGFR signaling but high in Notch signaling. They maintain their junctions and connect to the parent vessel. Further they are trailing the tip cells and less motile and lumen morphogenesis starts in the region of the stalk. Figure adapted from Herbert and Stainier 2011.

In the mouse retina, treatment with γ-secretase inhibitors block Notch cleavage and signaling or genetic disruption of the pathway leads to an increase in tip cell number (Hellström et al., 2007). Local VEGF-A sources induce the expression of Dll4 in endothelial cells. Dll4 binds to Notch1 in adjacent ECs leading to the activation of specific target genes. In cells with high Notch signaling, VEGFR3 is down-regulated restricting angiogenic cell behavior to the tip cell (Siekmann and Lawson, 2007). Second, Notch signaling in the SCs leads to an up-regulated expression of the soluble- and membrane bound form of vascular endothelial growth factor receptor 1 ((s)flt1/(s)VEGFR1), and the soluble form is thought to function as a VEGF-A sink. This in counteracts pro-angiogenic VEGFR2/3 signaling in cells with high Notch signaling (Funahashi et al., 2010). Third, the Notch intracellular domain (NICD) activates *dll4* itself leading to further pro-angiogenic suppression in neighboring stalk cells (i.e. lateral inhibition). A Notch Regulated Ankyrin Repeat-containing Protein (NRARP) up-regulates Wnt signaling,

which is important for cell proliferation and maintaining of cell-cell junctions. It also antagonizes NICD directly and thus has negative feedback control functions on Notch signaling (Phng et al., 2009).

Taken together, VEGF-A induced Dll4-mediated Notch signaling is negatively controlling tip cell behavior in stalk cells. The tip cell, high in Dll4 expression, inhibits tip cell specific behavior in following, neighboring stalk cells via Notch signaling. However, this expression pattern is dynamic and can change during sprouting angiogenesis causing shuffling between tip and stalk cell fate and position (Jakobsson et al., 2010).

3.2.4.2.4 Hypoxia and VEGF regulate the outgrowth of sprouts

ECs are equipped with mechanisms sensing oxygen, as demonstrated by the constriction of the ductus arteriosus upon breathing after birth (Fraisl et al., 2009; Weir et al., 2002, 2005). Hypoxia, the lack of oxygen, can up-regulate VEGF expression (Forsythe et al., 1996), and mice deficient for the Hif-1α subunit (hypoxia-inducible-factor 1α, a molecular interface that allows the expression of many target genes including genes regulating angiogenesis (Semenza, 2003)) display a complete loss of the cephalic vasculature. The activity of HIF-1α is regulated by oxygen sensing enzymes including PHDs (prolyl hydroxylase domain proteins) and FIHs (factor inhibiting HIFs) (Kaelin and Ratcliffe, 2008). Under normal conditions, when enough oxygen is available, HIF-1α is degraded, whereas under hypoxic conditions, PHDs/FIHs become inactive and HIF-1α is stabilized and can activate target genes which will lead to the expression of pro-angiogenic genes such as VEGF-A (Fraisl et al., 2009; Forsythe et al., 1996) and the outgrowth of angiogenic sprouts into hypoxic regions.

3.2.4.2.5 Guidance of angiogenic sprouts

In a vertebrate organism nerves and blood vessels are often found alongside each other and share many similarities regarding morphology and behavior. For instance, the filopodia rich, invasive and very motile tip cells of vascular sprouts are similar to the growth cones of axons, a highly specialized structure at the tip of an axon, which guides it towards a target according to positive or repulsive stimuli (Eichmann et al., 2005; Carmeliet and Tessier-Lavigne, 2005; Gerhardt et al., 2003). Beside their similarity in structure and behavior, it is now clear that growing axons and growing vascular sprouts share many common molecules guiding them to their target tissues.

One of these common molecules is Netrin which, for example, has either attractive or repulsive functions during axon guidance depending on which receptor it binds to in the axon. The family members of the Uncoordinated 5 Receptors (UNC5) have been shown to promote axon repulsion, whereas receptors of the Deleted on Colorectal Cancer (DCC)

family reveal attractive guidance on axons (Dickson and Keleman, Carmeliet et al., 2005, 2002, Adams and Eichmann 2010). UNC5B was found to be expressed specifically in arterial sprouting capillaries and tip cells (Lu et al., 2004; Suchting et al., 2007). Mice deficient for *Unc5b* or zebrafish morphants lacking both UNC5B and Netrin1a show an excessive branched vasculature, as well as uncontrolled filopodial extensions in tip cells (Lu et al., 2004). Supporting evidence comes from the chick model where Netrin-1 repels UNC5B expressing blood vessels (Bouvrée et al., 2008). This suggests that UNC5B is an evolutionary conserved repulsive receptor that is also used during blood vessel morphogenesis. However, it might be that Netrin has also pro-angiogenic effects, since UNC5B provokes apoptosis in the absence of its ligand Netrin (Castets et al., 2009).

Other common signaling molecules are found within the semaphoring/plexin ligand-receptor family. Semaphorins are either membrane bound and bind directly to plexin receptors thereby influencing cell motility, whereas the secreted semaphorin class III members need neuropilins as co-receptors for plexin signaling. In the vasculature, secreted Sema3e signals independently of a neuropilin co-receptor directly to PlexinD1 receptor, which is expressed in ECs (van der Zwaag et al., 2002; Gu et al., 2005). In mice, interruption of the PlexinD1 pathway leads to patterning defects, increased endothelial sprouting and neolethality (Gitler et al., 2004). In zebrafish a mutant form of the receptor PlexinD1 (*obd*: out of bounds) (Childs et al., 2002; Torres-Vázquez et al., 2004) causes enhanced ISV sprouting and abnormal ISV patterning in the trunk of the embryo. Normally ISVs grow between intersomitic boundaries in the trunk, in *obd* mutants the ISVs do not grow between somites but rather form interconnecting patterns and sprout ectopically along the trunk. Here, a possible binding partner might be Sema3a since knockdown experiments reveal similar phenotypes to those found in the *obd*-mutant background (Torres-Vázquez et al., 2004). These studies show that Semaphorin/Plexin signaling plays an important role in vascular path finding.

3.2.4.2.6 Vessel maturation

Developing vessels need to undergo maturation which is essential for their survival and proper perfusion of the surrounding tissues. During vessel maturation, vessels are stabilized by the attraction of mesenchymal derived mural cells and the generation of ECM. The supporting mural cells, pericytes and vascular smooth muscle cells (vSMC), are embedded within the basement membrane at the outer surface of the vessel walls protecting developing vessels from disturbing signals (Jain, 2003). It has been shown that TGFβ signaling is involved in the differentiation of mesenchymal cells into mural cells as well as ECM deposition (Pepper, 1997; Chambers et al., 2003). The expression of platelet derived growth factor B (PDGF-B) by ECs attracts mural cells, which express the PDGFR-β receptor on their surface, and stimulates their proliferation and migration (Hellström et al., 2001). Mural cells

themselves express Angiopoietin 1 (Ang1) thereby activating Tie2 receptor in endothelial cells (Suri et al., 1996), which promotes vessels stabilization by the facilitation of interactions between ECs and mural cells as well as the ECM and ECs. Furthermore, Tie2 activation is thought to suppress apoptosis of ECs (Jain, 2003).

3.2.4.2.7 Formation of the intersegmental vessels and their fusion

To form a fully functional network of vessels that allows blood circulation, growing angiogenic sprouts have to fuse to each other, i.e. establish a stable contact and subsequently form a continuous lumen, which interconnects the former individual sprouts. In the zebrafish embryonic trunk vasculature, the formation of the intersegmental vessels (ISVs) serves as an *in vivo* model to study angiogenesis. In general, during ISV development, endothelial sprouts leave the epithelium of the dorsal aorta (DA), grow dorsally towards the roof of the neural tube, where they make contact with neighboring intersomitic sprouts, and subsequently establish a lumenized tube, the dorsal longitudinal anastomotic vessel (DLAV) (Isogai et al., 2003). In more detail, in a "primary sprouting" process, beginning at about 20 hpf, endothelial tip cells grow out from the DA adjacent to intersomitic boundaries in a stereotyped manner, whereas following ECs, the stalk cells, trail these leading cells. Such bi-polar sprouts then grow towards the dorsal side between the somite boundaries and the notochord until they have passed the horizontal myoseptum. From here, they leave the somitic boundaries and growth dorsally between the neural tube and the somites. When reaching the dorsolateral roof of the neural tube, the tip cells extend anterior and posterior into two branches that will fuse with the branches of neighboring sprouts to form the dorsal longitudinal anastomotic vessel(s) (DLAV(s)) on either side of the neural tube (Figure 10).

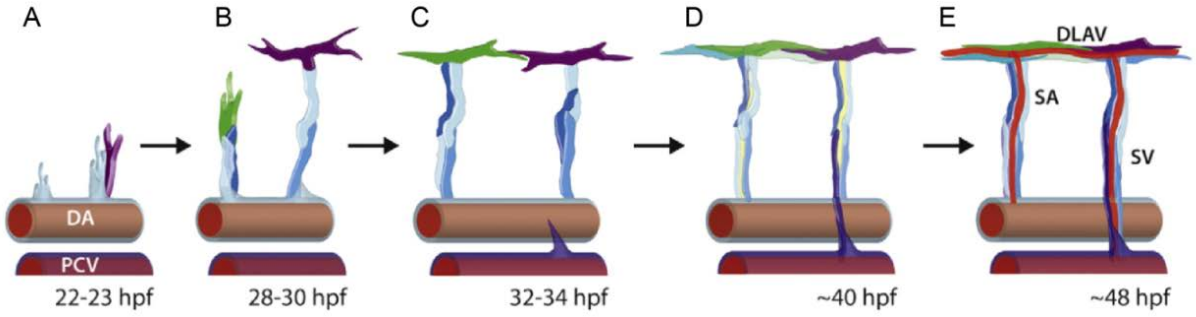

Figure 10 Model of the morphogenetic events that lead to the formation of ISV and DLAV. At 22 hpf ECs of the DA form sprouts (A) that grow along the somite boundaries up to the dorsal roof of the neural tube (B). Here, at the dorsal side of the embryo, anterior and posterior filopodial extensions between the tip cells establish contacts. During this phase, the ECs establish a scaffold consisting of a vascular cord that is not yet lumenized (B, C). A continuous apical surface is built which results in the formation of a lumen (yellow) (D). At around 32 hpf, a secondary wave of angiogenic sprouts emerges from the PCV. These sprouts either generate a group of lymphatic cells, called parachordal lymphangioblasts (chain) (not shown), or connect with the adjacent primary vessel (D, on the right), which will become a segmental vein. Blood flow in ISVs commences after SA, SV and DLAV have been established (E). Figure adapted from Ellertsdottir et al., 2009.

At about 1.5 dpf, secondary sprouts arise from the PCV. These new sprouts grow bilaterally in every myotomal segment, like primary sprouts do, but less synchronously. About half of these sprouts eventually connect to adjacent primary ISVs and link the PCV to the primary network. The other half will build up so called lymphatic parachordal chain (Lim et al., 2011), lying horizontally along the myoseptas, and a few sprouts simply disappear. By this "secondary sprouting" process, the DA and PCV are connected to each other and blood flow through the ISVs and DLAVs can occur (Figure 10). At 3 days of development, the zebrafish embryo has a closed circulation of a complex blood system in the head and all organs, such as gut, liver, kidney and pancreas and in the trunk region and strong closed blood flow can be observed within DA, ISVs and DLAVs (Isogai et al., 2003; Torres-Vázquez et al., 2004; Childs et al., 2002; Roman and Weinstein, 2000). During such vessel fusion, a lumen has to be built between anastomosing sprouts. In three-dimensional extracellular matrices the GTPases Cdc42 and Rac1 target vesicles to vacuolar membranes and are required during lumen formation in ECs since the expression of dominant-negative forms impairs the formation of vacuoles and a proper lumen (Bayless and Davis, 2002). Live imaging using a fli:EGFP-cdc42 transgenic zebrafish reporter line labelling vacuolar membranes *in vivo* suggested that vacuolar fusion events to hollow out single cells in the intersegmental vessels (Kamei et al., 2006). In this scenario, three ECs are arranged in a rod-like fashion, as described by (Childs et al., 2002). These live observations suggested that vacuoles fused to large intracellular compartments in SAs, which then later fused with neighbouring intracellular vacuoles to generate an intercellular continuous lumen. This behaviour of ECs during ISV tubulogenesis results in the generation of a seamless, unicellular SA.

A recent study from our lab analyzing ISV/SA architecture during their development and the initial steps of fusion, i.e. contact formation (see below), in greater detail found SAs to be of multicellular architecture, where ECs overlap to a large extend all along their stalks. This finding suggests an alternative mechanism of lumen formation where the lumen is formed by a cord hollowing mechanism after neighboring SAs have established contact by filopodial extensions (Blum et al., 2008). Recently, Essner and colleagues defined such a novel cord hollowing mechanism during the initial phases of ISV tubulogenesis where integration of intracellular vacuolar structures into the luminal membrane is driving the expansion of a primary lumen (Wang et al., 2010). In polarized endothelial cells, both Actin and Myosin are localized apically and at the adherens junctions (Bretscher et al., 2002; Strilic et al., 2009). Using a Moesin1-EGFP endothelial specific transgenic zebrafish reporter line, they found intracellular vacuoles fusing with the apical, luminal membrane (as defined by adherens junctions) between at least two ECs. These fusion events lead to an expansion of the primary lumen between endothelial cells in ISVs all along their cell-cell junctions (Wang et al., 2010). Both studies mentioned (i.e. (Kamei et al., 2006; Wang et al., 2010)), provide

insight into endothelial tubulogenesis, suggesting stepwise luminal expansion by the involvement of intracellular vacuolar structures that either undergo intracellular and later intercellular fusion events (Kamei et al., 2006) or fuse with the luminal membrane between ECs (Wang et al., 2010). Both studies suggest *de novo* formation of luminal spaces that are reached and integrated by an expanding lumen. However, both studies lack detailed cellular resolution and are limited in temporal description. First of all, both a proper junctional marker as well as an apical marker labeling the (future) luminal side, for *in vivo* analysis are missing. Furthermore, none of the studies addressed the question of vessel fusion – how the lumen is formed and connected between neighboring endothelial tip cells which is part of the process of anastomosis or vessel fusion. Recently, we and others (Armer et al., 2009) have shown that during vessel fusion, endothelial tip cells of individual growing sprouts make contact to neighboring tip cells via filopodial extensions. We found that those tip cells subsequently increase their mutual surface. This behavior is reflected by a dynamic deployment of junctional components (i.e. ZO1 and VE-cadherin) at the sites of cell contacts at the onset of the fusion process. Based on immunostainings using antibodies against ZO1 and VE-cadherin at different time points, we proposed a model (Figure 11) where after filopodial contact formation dot-like junctional structures appear, and that these, as the fusion process proceeds, subsequently enlarge into ring-like structures suggesting the formation of new apical membrane compartments within the junctional rings between these cells. However, how individual cell behaviors contribute to the fusion process of neighboring SAs/ISVs remained somewhat unclear and is the main focus of this thesis.

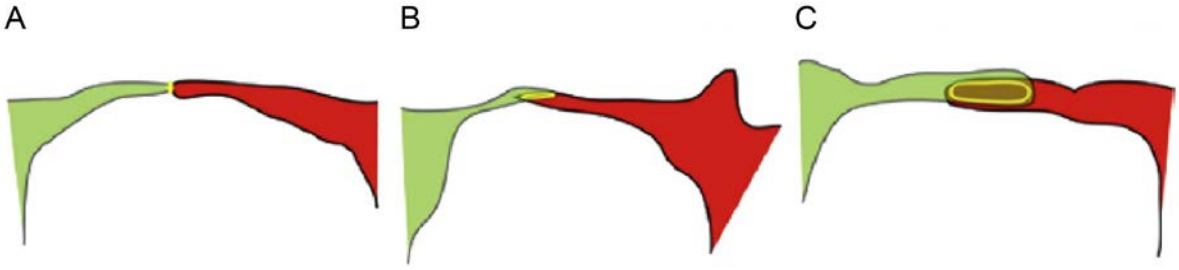

Figure 11 (A–C) Schematic representation of immunostaining based junctional protein (ZO-1) patterns during contact formation between fusing vessels. Junctional proteins accumulate at the contact site of two tip cells, which then increase their mutual surface which leads to the formation of a junctional ring suggesting the formation of a new apical membrane compartment between the cell extensions within this ring. Figure adapted from Blum et al., 2008.

3.3 Goal of thesis

The goal of this thesis was to resolve morphogenetic mechanisms of intersegmental blood vessel fusion at the single cell level in an in vivo system, the zebrafish embryo.

Blood vessel fusion or anastomosis, which is the inter-connection of dead-ended vascular sprouts, creates a network of vessels where blood flow is allowed away from and towards the heart. The temporal and spatial coordination of cellular events, such as cell migration, cell rearrangements, cell division or cell shape changes during the fusion of individual vessels had been ill described. In the zebrafish, the metameric arrangement and relative anatomical simplicity of the intersegmental vessels (ISVs) makes them an ideal paradigm to study morphogenetic cellular mechanisms during their fusion. Cell-cell junctions are located between individual cells, demarcating the outline of a cell. Thus, tracking the dynamics of individual cell-cell junctions allows analysis of single cell behaviors such as relative cell movements and cell shape changes during morphogenetic processes. Therefore, tagging endothelial cell-cell junctions with a fluorescent marker provides the necessary information to investigate cellular behaviours during blood vessel fusion. The UAS/Gal4 system offers an excellent opportunity to label and investigate junctional proteins during morphogenetic processes such as the formation of tracheal branches (Ribeiro et al., 2004; Brand and Perrimon, 1993). Thus, the goal of this thesis was, to label endothelial cell-cell junctions and analyze and better understand the cellular behaviors during intersegmental vessel fusion *in vivo* using the Gal4/UAS system.

4 Materials and Methods

4.1 Materials

4.1.1 Materials used for molecular cloning

For all (biochemical) reactions ddH_20 provided from the local kitchen was used.

4.1.1.1 Pipettes and tips

- Gilson PIPETMAN 1000 µl
- Gilson PIPETMAN 200 µl
- Gilson PIPETMAN 20 µl
- Gilson PIPETMAN 2 µl
- 1000 µl blue tips (Treff Lab)
- 200 µl yellow tips (Greiner bio-one)
- 20 µl white tips (Treff Lab)

4.1.1.2 Tubes

- Eppendorf tubes 1.5 ml (eppendorf)
- Eppendorf tubes 2.0 ml (eppendorf)
- Falcon tubes 50 ml (BD)

4.1.1.3 Machines

- BioPhotometer (eppendorf)
- NanoDrop (Thermo Fischer Scientific)
- ULTROSPEC II (Ukb Biochrom)
- Centrifuge 5415 D
- HiCen 21 C (Herolab)
- Megafuge 1.0 R (Hereaus)
- T3 Thermocycler (PCR machine) (Biometra)
- Thermocycler (eppendorf)

4.1.1.4 Reagents for DNA restriction digestion (enzymes/buffers)

- NEB or Roche restriction enzymes and their corresponding buffers from NEB or Roche were used.

4.1.1.5 Reagents for PCR

- DNA Pfu Polymerase (Promega)
- Pfu 10x buffer (Promega)
- Taq Polymerase (Promega)
- ThermoPol buffer 10x (Promega)
- Phusion® Enzyme (Finnzymes)
- Phusion® Enzyme buffer 5x (Finnzymes)
- Individual Primers: Corresponding PCR primers (Sigma-Aldrich), 100µM 1^{st},tock→5 µM 2^{nd} stock

4.1.1.6 Reagents for DNA ligation

- T4 DNA ligase (NEB)
- Ligase 10x buffer (NEB)

4.1.1.7 Reagents for DNA blunting

- T4 DNA Polymerase (NEB) → removal of 3' overhangs
- 10x restriction digestion buffer 2 (NEB)
- Klenow enzyme (Roche) → refilling of 5' overhangs
- Klenow buffer 10x (Roche)
- 1mM dNTPs for blunting with T4 DNA Polymerase
- 10mM dNTPs for blunting with Klenow enzyme

4.1.1.8 Reagents for DNA dephosphorylation

- Shrimp Alkaline Phosphatase (Roche)
- 10x SAP buffer (Roche)

4.1.1.9 Reagents for agarose gels

- Ethidiumbromide
- Agarose (Eurogentec)
- 50x TAE-buffer (242 g Trizma, 57.1 ml Aceticacid, 100ml 0.5 M EDTA, fill up with ddH_20 to 1000ml; 1x TAE: 20 ml 50x TAE in 980ml ddH_20)
- running chambers (Amersham Bioscience ®)
- 10x orange standard loading buffer
- 1kb plus ladder (Promega)

4.1.1.10 Reagents for blue-white selection

- X-Gal (100mg dissolved in 2ml N,N'-dimethylformamide, wrapped in aluminium folia)
- 1.5ml aliquoted IPTG (stock: 1.2 g in 50 ml ddH_20)
  Individual primers (rev/fwd) ordered from Sigma Aldrich
- Individual DNA templates

4.1.1.11 Cells and plates

- Top10 cells (electrocompetent)
- Plates Amp (10 µg/µl) and Kan (50 µg/µl)

4.1.1.12 Kits

- QIAGEN Gel extraction Kit (QIAGEN)
- QIAGEN Plasmid Midi Kit (QIAGEN)
- QIAGEN PCR purification Kit (QIAGEN)
- SIGMA GenElute™ Plasmid Miniprep Kit
- pENTR™/D-TOPO® Cloning Kit (Invitrogen)

4.1.1.13 Filters

- 0.025 µm membrane filter paper (Millipore®)
- Folted filters (Schleicher and Schuell)

4.1.1.14 Cloning software

- Ape v2.0.37 (A plasmid-editor, open source)

4.1.1.15 Solutions to transform electrocompetent cells

SOC medium (filter-sterilized, protocol from Promega!)

- 2.0g Bacto®-tryptone
- 0.5g Bacto®-yeast extract
- 1ml 1M NaCl
- 0.25ml 1M KCl
- 1ml Mg2+ stock
- (1M MgCl2 . 6H2O,
- 1M MgSO4 . 7H2O),
- filter-sterilized
- 1ml 2M glucose,
- Bring to 100ml with distilled water. Add Bacto®-tryptone, Bacto®-yeast extract, NaCl and KCl to 97ml distilled water. Stir to dissolve. Autoclave and cool to room temperature. Add 2M Mg2+ stock and 2M glucose stock, each to a final concentration 20mM. Filter the complete medium through a 0.2µm filter unit. Adjust the pH to 7.0.
- LB medium (standard protocol from local kitchen!)
- LB medium with ampicilin (10 µg/µl) or Kanamycin (50 µg/µl)

4.1.1.16 Sequencing

All DNA samples have been sequenced by Microsynth (Economy Bar Service), Switzerland

4.1.2 Materials used for Fish protocols

4.1.2.1 Materials used for injections

- eppendorf FemtoJet ® or free hand modules (tritech research)
- eppendorf Microloader tips
- Glass needles: GB100F-10 (with and without filament) Science Products
- 1.5% agarose filled petri dishes (microinjection chambers)

4.1.2.2 Materials for Immunostainings

primary antibodies:

- mouse anti human ZO1, 1:200 (Zymed)
- rabbit anti-zf-CDH5 1:1000

secondary antibodies:

- Alexa-568 goat anti-rabbit IgG, 1:1000
- Alexa-568 goat anti-mouse IgG, 1:1000
- Alexa-633 goat anti-mouse IgG, 1:1000
- (All secondary antibodies were purchased from Invitrogen)

4.1.2.3 Solutions / mounting media

- Egg water: 0.3 g sea salt in 1 l of ddH_2O with 1ml methylen-blue
- 50x PTU (10mM) stock: Sigma P7629, dissolved in water
- PBST: 1 x PBS with 0.1 % Tween-20 (Fluka)
- PBSTX: 1 x PBS with 0.1% Tween-20 (Fluka) and 0.1% TritonX-100 (Fluka)
- PFA: 4% Paraformaldehyde (Polyscience) in PBS
- 10% BSA (Bovine Albumin Serum, Sigma Aldrich)
- 1% NGS (Normal Goat Serum, Sigma Aldrich)
- Methylcellulose 2% in egg water
- Pronase 10mg/ml in Danieau's
- Vectashield ® (Vector Laboratories, Inc. Burlingame)

4.1.2.4 Materials used for genomic DNA extraction

- 99.9 % ethanol
- 70 % ethanol
- 99.9% Isopropanol
- Na-Acetat (3 M, pH 4.6)
- DNA extraction buffer (filter-sterilized)
- 10mM Tris-HCl (pH 8.2)
- 10mM EDTA
- 200mM NaCk
- 0.5% SDS
- + 200ng/µl Proteinase K

4.1.3 Material used for live Imaging

4.1.3.1 Microscopes and imaging software

- Leica SP5 MP confocal microscope
- Leica SP5-II-Matrix
- Leica confocal microscope DME-7
- Leica confocal software (LCS)
- Leica MZFLIII binocular
- Leica M205 FA stereo binocular
- Leica DM6000B laser cutting microscope
- Zeiss Stani SV 11 binocular (Zeiss)

4.1.3.2 Imaging software

- ImageJ 1.44p (open source: Rasband, W.S., ImageJ, U. S. National Institutes of Health, Bethesda, Maryland, USA, http://imagej.nih.gov/ij/, 1997-2011. *and* (M. D. Abràmoff et al.))
- (Imaris 4.15)
- Adobe Illustrater CS5 and Adobe Photshop, Microsoft Powerpoint

4.1.3.3 Mounting materials

- MatTek Glass bottom culture dishes P35G-1.5-10-C
- 0.7% low-melting agarose (Sigma Aldrich)

4.1.4 Fish strains

4.1.4.1 Fish strains

wild type strains:

- AB/EK and EK/TL (W. Driever, Freiburg)

transgenic zebrafish lines:

- Tg(fli1:EGFP)^{y1}(N. Lawson, 2002)
- Tg(UAS:RFP) (Asakawa et al., 2008)
- Tg(UAS:KAEDE)^{rk8} (Hatta et al., 2006)
- Tg*(kdrl:EGFP)*^{S843} (S.-W. Jin et al., 2005)
- Tg(fli1ep:GAL4FF)^{Ubs2,Ubs3,Ubs4} (this thesis)
- Tg(UAS:EGFP-ZO1-cmlc2:EGFP)$^{Ubs5,\ Ubs6,Ubs7}$ (this thesis)

4.2 Methods

4.2.1 Standard cloning protocol

4.2.1.1 Polymerase Chain Reaction (PCR)

For all PCRs done in this work the following mix was set up:

Template DNA	100-200 ng
Primers (5µM)	1 µl each
DNA polymerase buffer 10x/5x5 or	10 µl
DNA polymerase (Tag, Phusion or Pfu)	1 µl
dNTPs (2 mM each dNTP)	5 µl
ddH_2O up to	50 µl

4.2.1.2 DNA restriction digestion

Commercial restriction enzymes and 10x buffers (NEB, Roche) were used for double and single digestions.

DNA	0.5-2 µg
10x buffer	2µl
enzyme(s)	1µl
ddH_2O up to	20µl

Depending on enzymes, the reaction mixture was put at 30°C, 37°C or 50°C for 1-2h or o/n in a heating block.

4.2.1.3 Pouring of standard 1% agarose gels

Digested backbones, inserts and PCR fragments were separated via a 1% agarose (Eurogentec) gels.

1xTAE buffer	50 ml
Agarose	0.5 g

were heated up in an Erlenmeyer flask in the microwave until boiling was observed and the whole agarose was melted and solved in the 1x TAE-buffer. 5 µl of Ethidiumbromide were added and the solution was filled into a gel chamber with a desired comb (depending on the type of gel: 8 lanes to extract DNA, 12-16 lanes for analytical gels (minipreps!)). After polymerization occurred, the comb was removed and the gel chamber was placed in a running chamber (Amersham Bioscience ®), filled with 1x TAE buffer. DNA, mixed with orange loading buffer (1x) was loaded and the gel was run at 100 V for 30min-1h. As a reference a single lane with 1kb plus ladder (marker) was run in parallel.

4.2.1.4 DNA isolation

In order to isolate PCR products, linearized plasmids, or inserts, DNA was run on standard agarose gel (1-2 %) and extracted.

4.2.1.5 DNA gel extraction

To cut out specific DNA bands, gels were placed on an UV-table at 75% for as short as possible to prevent mutations in the DNA. At 75% UV power, the desired DNA bands were cut out with a razor blade and put into a 1.5 ml eppendorf tube. For safety reasons (to prevent nasty mutations and burnings by the UV light) a helmet consisting of plexiglas and gloves were used. For analytical gels, pictures were taken at 100% UV light.
The extraction was made following the QIAGEN Gel Extraction protocol. DNA was eluted in 30 µl ddH_2O.

4.2.1.6 DNA ligation

For efficient ligation, 1 µl of the digested DNA fragments were measured with a NanoDrop (Thermo Fischer Scientific)
Using http://www.insilico.uni-duesseldorf.de/Lig_Input.html or the following calculation, optimal ligation concentration was calculated:

$$\frac{\text{ng of vector} \times \text{kb size of insert}}{\text{kb size of vector}} \times \text{molar ratio of insert/vector} = \text{ng of insert}$$

In almost all cases, a molecular vector insert ratio of 1:3 was used.

vector	x µl
insert	y µl
10x ligase buffer	1 µl
T4 DNA Ligase	1 µl
ddH_2O up to 10µl$_{\text{reaction volume}}$	z µl

Ligation reaction was mixed and put on 18°C o/n or at 4°C for 2 days.

4.2.1.7 Transformation of electrocompetent cells

Electrocompetent E. coli bacteria TOP-10 were used for transformation. Upon electroporation, ligation-mixture was dialysed against ddH_2O on a 0.025 µm membrane filter paper (Millipore ®) o/n to lower the salt concentration and thus, increase transformation efficacy. The whole transformation procedure was performed on ice. Frozen E. coli (50 µl in eppendorf tubes) from the -80°C freezer were thawed on ice. 1-3 µl of the DNA ligation was added and mixed by pippeting gently up and down. Then the bacteria were transferred to a 1 mm electroporation cuvette (Bio Rad). The bacteria were electroporated (Bio Rad 1.8 mV, 200 ohm, 25 µF) and then transferred with 0.5 ml preheated (37°C) LB or SOC medium !without! antibiotica to a 1.5 ml eppendorf tube. Bacteria were grown at 37°C on a shaker or rotator for 1 hour and then centrifuged down at 1500 rpm, resuspended in 200 µl and plated on an agar plate with the appropriate antibiotic by the use of glass beads. Colonies were grown over night, upside-down in the 37°C breeding incubator.

4.2.1.8 Minipreps

Clones were picked from agar plates and grown in 3 ml LB medium, in test-tubes with the appropriate antibiotic on a shaker at 37°C o/n. Then minipreps were performed following the SIGMA GenElute^{TM} Plasmid Miniprep Kit. DNA was eluted in 90 µl ddH_2O.

4.2.1.9 Midipreps

50 ml LB medium with appropriate antibiotics were inoculated by positive clones. Culture was grown over night and then centrifuged for 15 min in a Heraeus centrifuge at 4°C. Then the QIAGEN Plasmid Midi Kit was followed. DNA was eluted in 90µl ddH_2O. Purity and amount were measured with NanoDrop (Thermo Fischer Scientific).

4.2.2 Fish protocols

4.2.2.1 Fish maintenance and stocks, breeding and collection of eggs

Zebrafish were maintained at standard conditions (Westerfield, 2000). Embryos were staged by hours post-fertilization (hpf) at 28.5 °C (C. B. Kimmel et al., 1995).

4.2.2.2 Dechorionation of eggs

Dechorionation was done by hand with watch maker forceps (Dumont #5F).

4.2.2.3 Inhibition of pigmentation

When working with fixed embryos older than 36 hpf, pigmentation of embryos was inhibited, since at around 28 hpf, pigmentation of embryos starts. To inhibit pigmentation PTU (propylthiouracil) was used. Egg water of 24 hpf old embryos was exchanged with PTU egg

water. PTU egg water was produced by adding 10 ml of a 50x PTU stock solution to 490 ml of egg water. As usual methylen blue was included in the egg water.

4.2.2.4 Fixing of embryos

Dechorionated embryos in a 2 ml eppendorf tube were anesthetized on ice for 5 min. Then egg water was exchanged by 1 ml pre-chilled 4% PFA. After 5 min PFA was replaced by fresh pre-chilled 4% PFA. The eppendorf tube was wrapped in aluminium folia to prevent bleaching of the fluorescent proteins and put on the shaker in the 4°C room o/n.

4.2.2.5 Microinjections

Capillaries were pulled to produce very thin glass needles. Microinjection chamber plates were made by pouring 1% agarose (solved in egg water) into a petridish and putting a mold (template) on the agarose. The mold was removed after polymerization of the agarose. The plate were stored at 4°C and covered with egg water. Freshly laid eggs (one cell stage) were oriented so that they had the cells looking up and then gently pressed into the rills of the injection plate. Needles were filled with the DNA solution using Eppendorf Microloader. Needles were mounted on the eppendorf FemtoJet injector ® or the or free hand modules (tritech research) and broken by forceps, plunged into the eggwater and tested for outflow. Needle was filled with DNA solution and pressure was adjusted (ca. 300 kPa). For best results whenever possible the cell and not the yolk was injected. Drop sizes were as small as possible (~4nl / embryo). For all injections Tol2 transgeneis RNA was used.

4.2.2.6 Immunofluorescence

4.2.2.6.1 Immunostaining protocol

Embryos from 22–48 hpf were fixed in 4% paraformaldehyde for 2 h at room temperature. Embryos were then washed 4×5 min in PBST (PBS+0.1% Tween20) and once in PBSTX (PBS+0.1% Tween20+0.1% Triton ×100). Embryos were then blocked in PBSTX+10% BSA+1% NGS for 2 h. Embryos were incubated with primary antibodies (in PBSTX+1% BSA+0.1% NGS) overnight at 4 °C. Embryos were then washed 6×1 h in PBSTX+1% BSA+ 0.1% NGS and then incubated with the secondary antibody (in PBSTX+1% BSA+0.1% NGS) overnight at 4 °C. Embryos were finally washed several times in PBST. All steps were performed at RT except for antibody incubations. The following antibodies were used: mouse anti human ZO1, 1:200 (Zymed); rabbit anti-zf-CDH5 (Blum et al., 2008), 1:1000; Alexa-568 goat anti-rabbit IgG, 1:1000; Alexa- 568 goat anti-mouse IgG, 1:1000; Alexa-633 goat anti-mouse IgG, 1:1000 (All secondary antibodies were purchased from Invitrogen.).

After fixation, PFA was replaced by PBST and embryos were incubated for at least 30 min at RT on a shaker in the dark. As the trunk vasculature was the object of interest, the embryos

were transferred into a Petri dish containing PBST and the head and yolk were cut off at the yolk / yolk extension boundary. This made the specimen way thinner and scanning with the objectives more agreeable. The tails were mounted in 0.7% low-melting agarose placed in Matek 0.17 mm bottom petri dishes.

4.2.3 Imaging

All confocal pictures within this thesis (collaborations excluded) have been taken using either a Leica SP5 or SP1 confocal microscope.

4.2.3.1 Principles of confocal microscopy

The optical system of a confocal microscope focuses a spot of light onto a single point at a specific depth within a sample, whereas widefield epi-fluorescence microscopes focus a wide cone of illumination onto a large volume of a sample. This whole region is then uniformly and simultaneously illuminated (Figure 12).

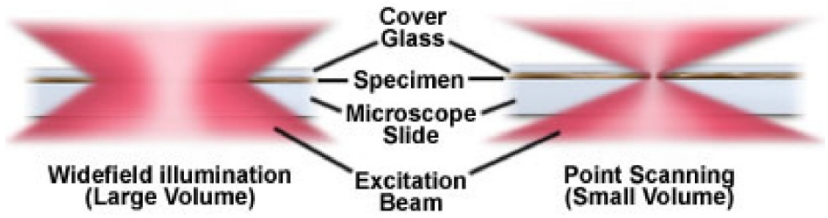

Figure 12 Widefield illumination versus confocal illumination

In confocal microscopes, strong laser light from a pinpoint illumination passes through a pinhole onto a single point in the sample. The emitted light from this point is collected by a detector. Here, a pinhole aperture is placed in front of the detector which is at a position that is *confocal* with the illuminated point in the sample. *Confocal* means, it is positioned precisely where the rays, which are emitted from the illuminated point in the sample, come to a focus (*confocal point*). Thus, the significant amount of fluorescence emission occurring at points above and below the objective focal points are not confocal with the pinhole and excluded (Figure 13). This is different in a normal fluorescent microscope setup, where the pinhole aperture in front of the detector is missing and thus, also “out-of-focus-rays” are allowed to pass. Since by this method only single points of a plane of interest are illuminated, such a plane needs to be illuminated sequentially point by point to generate an image. This reiterative illumination of other points of the same and other planes (scanning) allows 3D reconstruction of the original sample by computer software. (http://micro.magnet.fsu.edu/primer/index.html and Alberts et al., 2008)

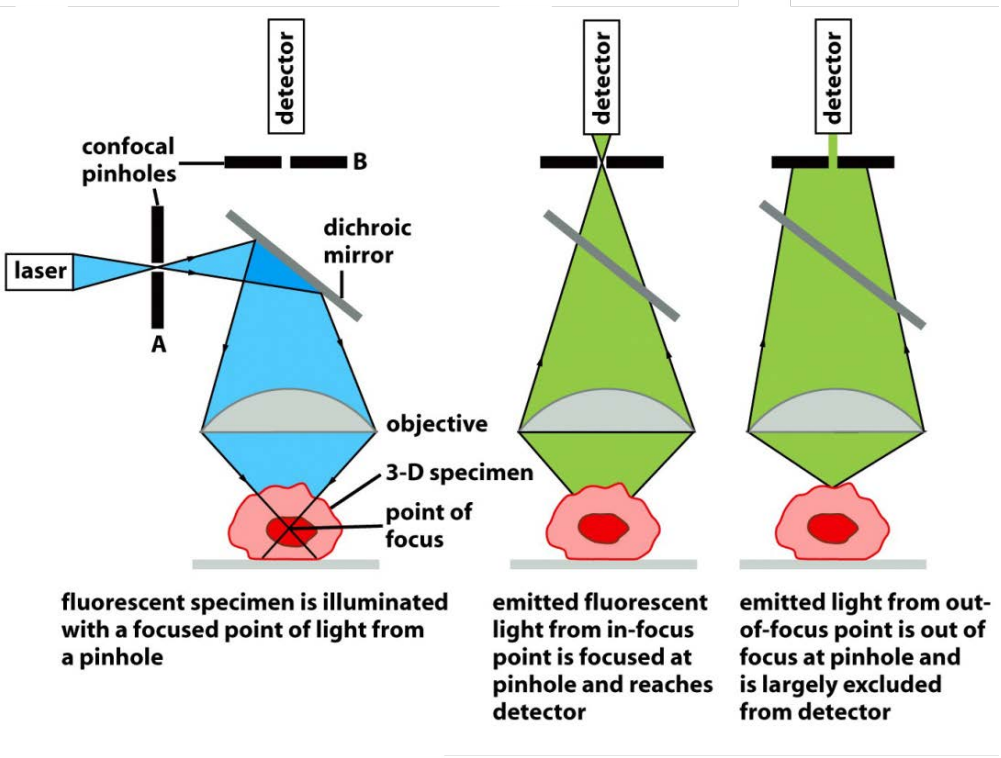

Figure 13 Overview of confocal microscopy

4.2.3.2 Live imaging and embryonic manipulations

4.2.3.2.1 Selection of Tg(fli1ep:Gal4FF^{ubs3};UAS:RFP;UAS:EGFP-ZO1^{ubs5}) embryos

Triple transgenic embryos Tg(fli1ep:Gal4FF^{ubs3};UAS:RFP;UAS:EGFP-ZO1^{ubs5}) were selected using a Leica MZ FLIII fluorescent stereomicroscope. Embryos were selected for RFP ensuring the presence of the fli1ep:Gal4FF and UAS:RFP transgene and for the presence of the heart marker *cmlc2*:EGFP. Selected embryos were anaesthetized using tricaine and mounted in a 35 mm glass bottom petri dish (0.17 mm, MatTek), using 0.7% low melting agarose (Sigma) containing 0.01% tricaine and 0,003% PTU. All movies have an initial frame size of 512x512 pixels. Routinely, z-stack consisted of 50-80 slices with a step size of 0.8-1.0 µm. Stacks were taken every 5 minutes, unless noted differently.

4.2.4 Photoconversion

To label individual ECs, KAEDE photoconversion was done on a Leica SP5 fluorescence microscope by 20-second exposures using a solid-state laser (405nm). At 2 dpf, when nuclei of individual ECs are easily discernible in ISVs having an inflated lumen, fli1ep:GAL4FF;UAS:KAEDE transgenic embryos were anaesthetized with tricaine, mounted in 0.7% low melting agarose and a defined region of interest (ROI) within individual nuclei was exposed to the violet light. Subsequently high resolution x,y,z stacks were acquired with

a 63x glycerol immersion objective using the suggested slice thickness by the confocal software. Slice numbers ranged from 80 to 200 slices per stack.

4.2.5 Quantum Dot-injection

705 nm Quantum Dot (Invitrogen) were injected into the sinus venosus of mounted embryos at a concentration of 1:2. Special manufactured glass needles (Biomedical Instruments, Jena, Germany) with tip opening of 10 µm and beveled tip were utilized to reduce damage to the embryo.

4.2.6 *In vivo* time-lapse analysis

Embryos were imaged overnight on a Leica SP5 confocal microscope using a 63x glycerol immersion objective with a numerical aperture of 1.2 with additional zoom of 1-1.3x. In some cases resonance scanning with an optical zoom of 1.7 was used. All movies have an initial frame size of 512x512 pixels. Routinely, z-stack consisted of 50-80 slices with a step size of 0.8-1.0 µm. Stacks were taken every 5 minutes, unless noted differently.

4.2.7 Image processing

All stacks were processed with ImageJ (or occasionally Imaris). All images were further processed with a standard deviation and an edge preserving filter to sharpen the image and get rid of background. All images have the anterior to the left and dorsal to the top.

4.3 Gal4/UAS System

In 1993 A. Brand and N. Perrimon designed an indirect gene expression system, the Gal4/UAS system, which allows *in vivo* expression of a gene of interest in a spatiotemporal way (Brand and Perrimon, 1993). Under the control of the regulatory sequence of a given gene H, which provides temporal and spatial specificity, the yeast transcriptional factor Gal4 binds to 5 repeated Upstream Activation Sites (UAS elements from yeast) located upstream of a minimal promoter from heat shock gene *hsp70.* These two regulatory units precede the open reading frame (ORF) of a gene of interest, which will be expressed upon Gal4 binding (Figure 14).

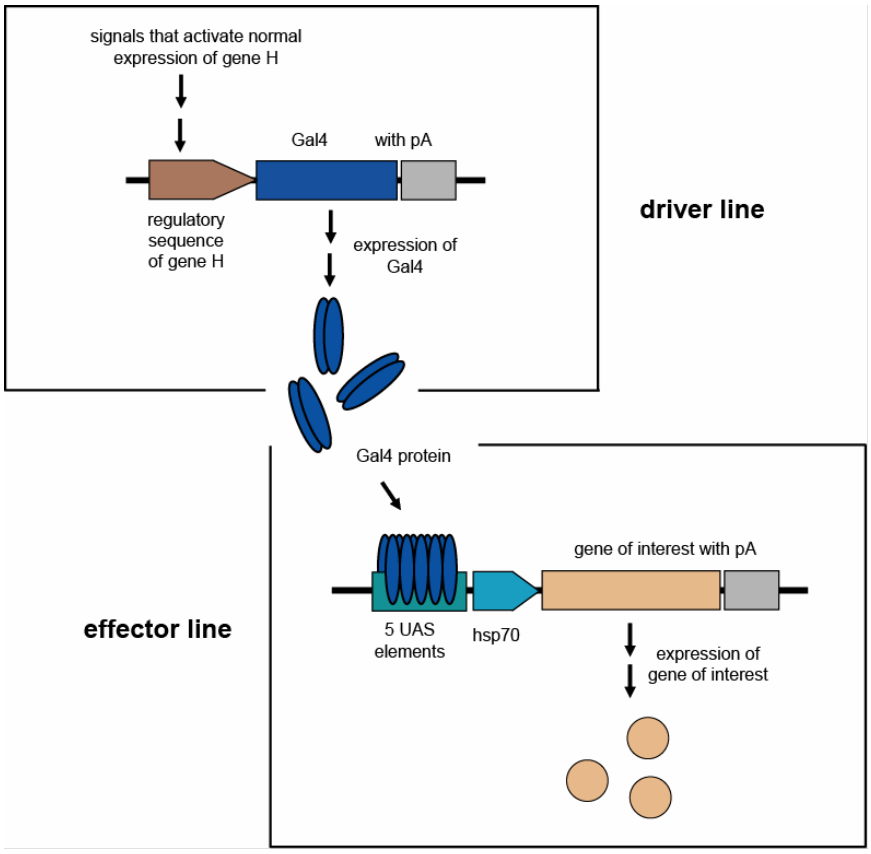

Figure 14 General genetic setup of the inducible Gal4/UAS system. The UAS/Gal4 system is an *in vivo* system consisting of two transgenic organisms (black boxes in figure) allowing the expression of a given gene of interest in a spatial and temporal restricted manner: a driver line expressing the yeast transcriptional activator (Gal4) under the control of a specific regulatory sequence of a gene H, is crossed to an effector line encoding upstream activating sites as well as a minimal promoter element, here *hsp70*. After crossing, Gal4 binds as a dimer to these UAS elements (here 5 elements) and induces the expression of a given gene of interest encoded downstream of the UAS sites. Upstream activating sequences (UAS) are 18 bp long sequences with two palindromic triplets at the 5 and 3 prime ends spaced by 11 nucleotides that are recognized by the zinkcluster elements of DNA binding domain of Gal4 homodimers i.e. CGG and CCG (Ptashne and Gann, 2002).

This system has been adapted recently to the zebrafish where several modifications (for example: number of UAS sites, enhanced Gal4 versions) have been introduced to increase its efficiency in this vertebrate model organism (Asakawa et al., 2008; Köster and Fraser, 2001; Distel et al., 2009; Akitake et al., 2011; Scheer and Campos-Ortega, 1999). The Gal4/UAS system has several advantages. *First*, the concept of indirect expression allows separation of an UAS-driven gene of interest from the transcriptional activator Gal4 in two distinct transgenic lines, a driver and effector/responder line, which, for instance, allows the expression and analysis of otherwise toxic genes or lethal mutations until the developing organism eventually dies. *Second,* ectopic target gene expression can be directed to different tissues since driver and effector lines can be crossed in any given combination. *Third*, expression of the gene of interest is enhanced; therefore, fluorescent signals are amplified and easier to detect.

4.4 Cloning of vectors and generation of transgenic zebrafish lines

General note:

All the different constructs I generated have been sequenced by Microsynth©, Switzerland. Sequences are found on the DVD in the appendix of this thesis. All transgenic lines have been generated by Tol2 transgenesis technique (Kawakami et al., 2000), thus all vectors are flanked by Tol2 transposable elements.

4.4.1 Cloning of constructs

4.4.1.1 Cloning of pT2fli1ep:Gal4FF

pT2fli1ep:Gal4FF was generated by Gateway cloning technology using a newly generated pENTER:Gal4FF entry clone and a pTolfli1epDest destination clone (Villefranc et al., 2007). To generate the pENTER:GFF entry clone, a PCR amplified Gal4FF fragment from pT2KhspGal4FF vector (Kawakami lab) was directional TOPO cloned into pENTR™/D-TOPO® (Invitrogene) using following primers (fwd pr. 5'-caccatgaagctactgtcttc-3' / rev pr. 5'-ttagttacccgggagcatatc-3'). Using Gateway technology the Gal4FF insert was cloned into pTolfli1epDest vector (Lawson lab).

4.4.1.2 Cloning of pT214xUAS:EGFP-hZO1-*cmlc2*:EGFP

A XhoI/AgeI 14xUASE1b fragment was PCR amplified using the following primers (fwd. pr. 5'-gtgacCTCGAGaagcttaggcctccaagg-3' rev.pr. 5'- gtatcACCGGTtcgagggaattcgtgtgg -3'), cut and cloned via triple ligation together with an EGFP-humanZO1 fragment isolated from pG1UAS: EGFPhZO1 (prior cloned in the Affolter lab)***** with AgeI/Asp718 into SalI/Asp718 cut vector pDestTol2CG2 (Chien lab).

Note: it is possible that due to recombination events in some of the recovered plasmids the two transgenes UAS:EGFPhZO1 and *cmlc2*:EGFP share now a single SV40 site which is readable in both orientations (for more information see sequence found on DVD in the appendix).

* A XhoI/AgeI-cut 14xUASE1b fragment, generated by PCR using the following primers, fwd. pr. 5'-gtgacCTCGAGaagcttaggcctccaagg-3' and rev. pr. 5'-gtatcACCGGTtcgagggaattcgtgtgg-3' and pBUASE1b vector (gift from Reinhard W. Köster) as a template, was cloned into the XhoI and AgeI digested pG1 flk-1:EGFP-ZO1 (cloned by HG. Belting, Affolter lab) vector.

4.4.1.3 Cloning of pT2fli1ep:Gal4FF-cmlc2:EGFP

A BglII cut and blunted *cmlc2*:EGFP insert from pDestTol2CG2 (Chien lab) was ligated into ApaI cut and blunted pT2fli1ep:Gal4FF vector (see above). *cmlc2*:EGFP inserted downstream of the Gal4FF transgene in reverted orientation.

4.4.1.4 Cloning of pT25xUAS:VEcad∆CD-EGFP

Generation of the VEcad∆CD-EGFP deletion: a pENTER:VEcadEGFP entry clone was generated and cloned into pTolfli1epDest vector using Gateway technology© (Lawson lab). To generate pENTER: VEcadEGFP entry clone, a PCR amplified VEcadEGFP fragment from pBS-VEcadEGFP vector (Essner lab) was directional TOPO cloned into pENTR™/D-TOPO® (Invitrogene) using following primers (fwd pr. 5'- caccatgatgaaacagtgtgccagg-3' / rev pr. 5'-ttacttgtacagctcg-3'). In this new construct, pT2fli1ep:VEcadEGFP, the cytoplasmic domain (CD=aa615–aa719, cytoplasmic domain determined after http://www.uniprot.org/uniprot/Q68SP4 Q68SP4; cdh5, *Danior rerio* full-length VE-cadherin 676 aa) was deleted (∆),using single primer mutation technique (single primer: gtgttgagacggcgctatcaaactagtgtgagcaagggcgag) (Makarova et al., 2000) resulting in pT2fli1ep:VEcad∆CDEGFP vector. To generate the pT25xUAS:VEcad∆CD-EGFP construct, a fwd. BglII-primer (gccgtgAGATCTatgatgaaacagtgtgcc) and rev. EcoRV-primer (gccgtgGATATCttacttgtacagctcgtc) PCR amplified VEcad∆CDeGFP fragment was cloned into BglII/EcoRV cut pT2UAS:MCS vector (gift from K. Kawakami).

4.4.1.5 Cloning of pT24XnrUAS:EGFP-hZO1

A AgeI/SpeI cut EGFP-hZO1 insert (including polyA and Tol2 arm downstream of hZO1) from pT2cmlc2:EGFP-5xUAS:EGFP-hZO1 vector (previously cloned by L. Herwig, Affolter lab*) was ligated into AgeI/SpeI cut pT24XnrUAS:FR-mKate vector (cloned previously by L. Sauteur, Affolter lab)**. *An ApaI cut cmlc2:EGFP insert was ligated into pT25xUAS:MCS (kind gift from K. Kawakami) in reverse orientation upstream of the 5xUAS cassette, resulting in vector pT2cmlc2:EGFP-5xUAS:MCS. From pEGFP-C1-hZO1 vector (vector obtained from H-G. Belting, Affolter lab) an Eco47III/SmaI EGFP-hZO1 insert was ligated into EcoRV cut pT2cmlc2:EGFP-5xUAS:MCS vector resulting in pT2cmlc2:EGFP-5xUAS:EGFP-hZO1. **A SphI/BglII insert from pUC57_4Xnr (synthetic plasmid with 4XnrUAS (according Akitake et al., 2011) and MCS from ATG:biosynthetics company) was ligated into SphI/BglII cut pT2UASMCS_FRmKate2 (cloned by Y. Blum, Affolter lab)*** resulting in pT24XnrUAS:FR-mKate vector. *** An EcoRI/XhoI PCR amplified FR-mKate insert was ligated into pT25xUAS:MCS resulting in pT2UASMCS_FRmKate2.

4.4.2 Vector maps of cloned constructs

4.4.2.1 pT2fli1ep:Gal4FF

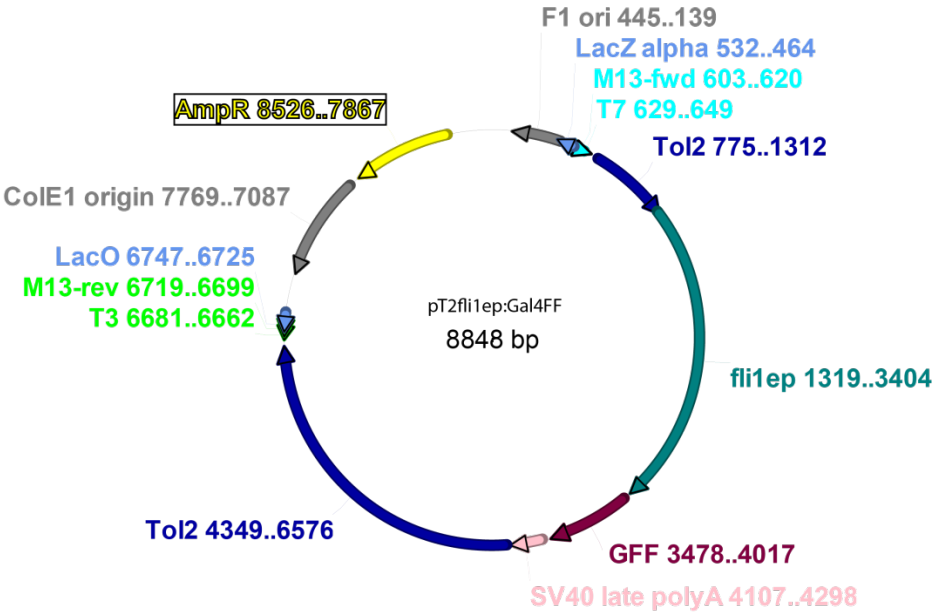

4.4.2.2 pT214xUAS:EGFP-hZO1-*cmlc2*:EGFP

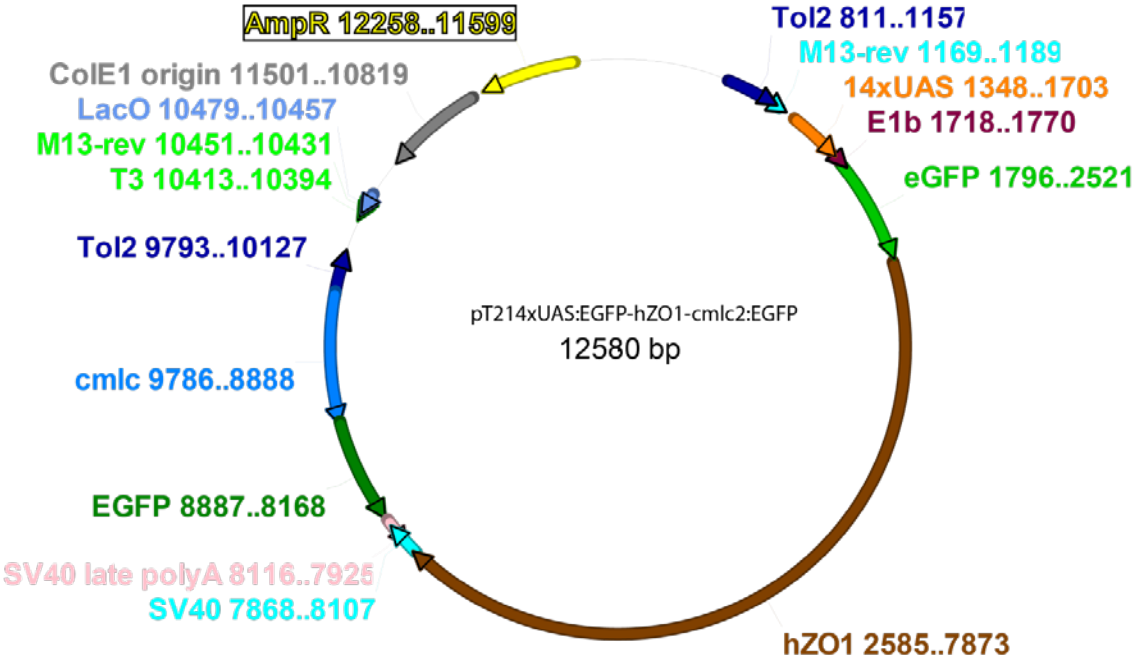

4.4.2.3 pT2fli1ep:Gal4FF-*cmlc2*:EGFP

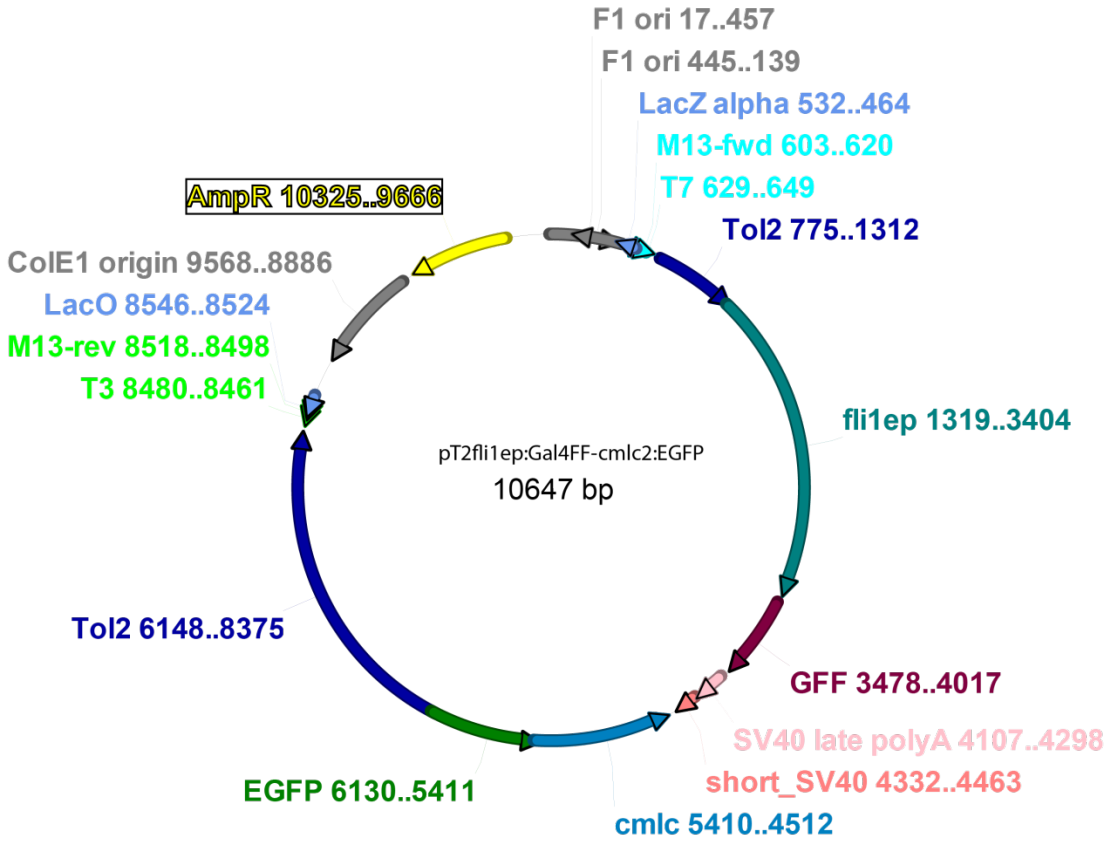

4.4.2.4 pT25xUAS:VEcadΔCD-EGFP

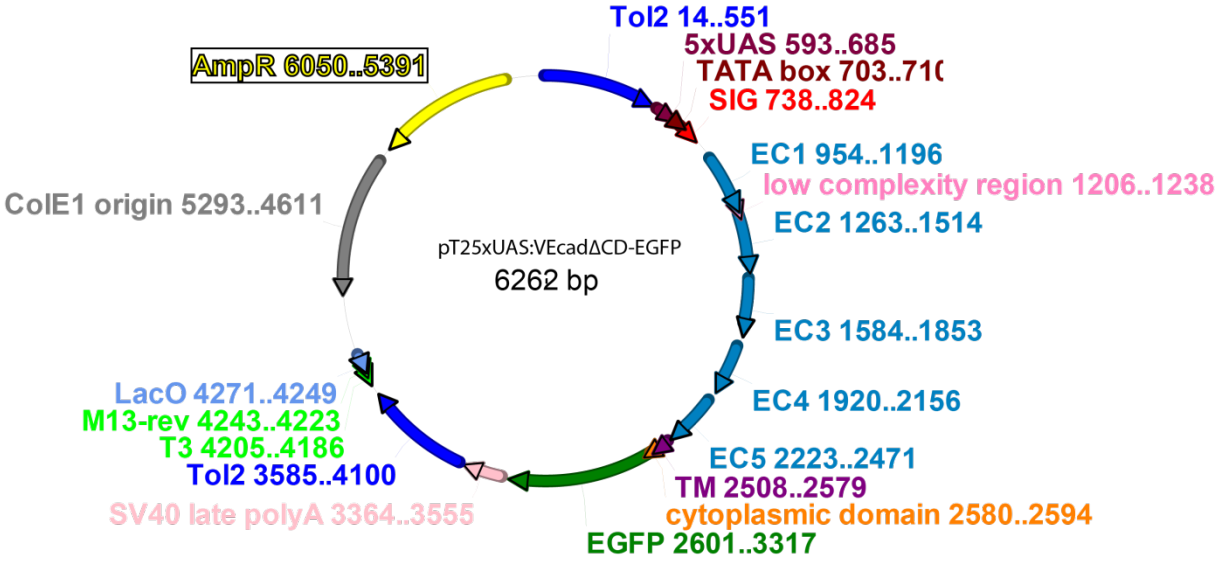

4.4.2.5 pT24XnrUAS:EGFP-hZO1

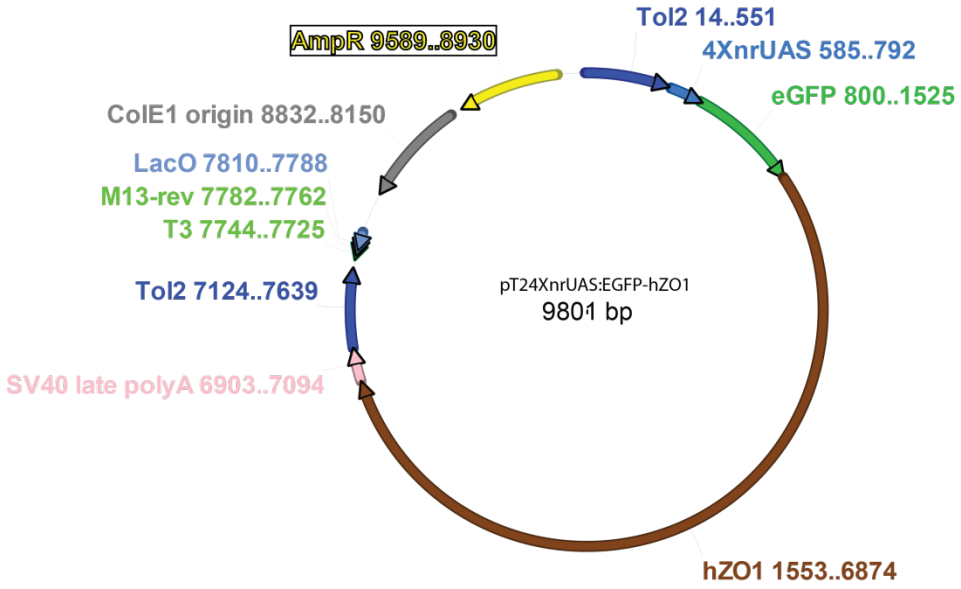

4.4.3 Transgenic zebrafish lines

4.4.3.1 Generation of Tg(UAS:EGFP-hZO1-*cmlc2*:EGFP)$^{ubs5-6}$

Line description:

The Tg(UAS:EGFP-hZO1-*cmlc2*:EGFP)$^{ubs5-6}$ zebrafish lines encode the ORF of the human Zona Occludens gene 1 (ZO1), fused N-terminal to the enhanced version of GFP (Enhanced-GFP = EGFP) downstream of 14xUAS sites. Downstream of the human ZO1 reading frame, a *cmlc2*:EGFP cassette is encoded in reversed orientation.

Generation of line:

Approximately 150 embryos (EK/TL strain) were injected at the one cell stage with pT214xUAS:EGFP-hZO1-cmlc2:EGFP generated construct (see above) and Tol2 transgenesis RNA (concentrations: DNA and RNA both 25ng/µl, 2-4nl/egg). Between 24 hpf and 48 hpf, embryos were screened for transient EGFP expression in the heart. Embryos showing strong transient expression were selected and raised separately. This G0 generation was crossed and screened for germ line transmission. 8 (A-H) transgenic carriers were recovered which displayed EGFP in the heart. Line A, C and F showed mosaic Gal4FF dependent EGFP-hZO1 expression in the vasculature and were used to generate stable F1 generations with the allelic designation ubs5, ubs6 and ubs. Line ubs was not used for this study

Note: In all three alleles, the expression of EGFP-hZO1 was found to be extremely mosaic. This means, even though that the transgene was present (indicated by the *cmlc2*:EGFP cassette) the expression level or fluorescent strength in the ECs ranged from no signal at all to very strong expressing in ECs throughout the endothelium. In ECs with a very high signal, EGFP-hZO1 was often found to be miss-localized and distributed over the whole cell

(background!) which made it difficult to follow the junctional complexes. However, in many cases we detected cells with a strong expression level but low background and thus junctions could be followed more easily.

4.4.3.2 Generation of Tg(fli1ep:Gal4FF;UAS:KAEDErk8)$^{ubs3-4}$

Line description:

The Tg(fli1ep:Gal4FF;UAS:KAEDE^{rk8})$^{ubs3-4}$ zebrafish line encodes Gal4FF, a Gal4 derivative, downstream of the short endothelial specific fli1 enhancer-promoter fragment and the 14xUAS-driven KAEDE transgene. Gal4FF drives KAEDE expression in the vasculature or any other UAS-driven transgene of interest. Both transgenes are separable, i.e. are not on the same chromosome.

Generation of line:

Approximately 150 embryos (UAS:KAEDE^{rk8} line (obtained from ZIRC, originally generated by (Hatta et al., 2006)) were injected at the one cell stage with pT2fli1ep:Gal4FF generated construct (see above) and Tol2 transgenesis RNA (concentrations: DNA and RNA both 25ng/µl, 2-4nl/egg). Embryos were screened for Gal4FF dependent transient KAEDE expression between 24 hpf and 48 hpf. Embryos showing strong transient expression in the developing vasculature were selected and raised separately. These G0 selected fish, were crossed at the adult stage and screened for germ line transmission. 3 transgenic carriers (G0 founders) were recovered which displayed Gal4FF dependent KAEDE expression in the vasculature. These 3 carriers were crossed to UAS:KAEDE fish to generate stable F1 generations with the allelic designation ubs3, ubs4 and ubs2, respectively, which was not further propagated due to a low fecundity of the F1 generation.

Note: The Tg(fli1ep:Gal4FF;UAS:KAEDE^{rk8})$^{ubs3-4}$ zebrafish were crossed to UAS:RFP positive fish (kind gift from K. Kawakami) (Asakawa et al., 2008) to generate Tg(fli1ep:Gal4FF;UAS:RFP)$^{ubs3-4}$ zebrafish lines.

4.4.3.3 Tg(fli1ep:Gal4FF-cmlc2:EGFP;UAS:VEcad∆CD-EGFP)^{ubs12}

Line description:

The Tg(fli1ep:Gal4FF-cmlc2:EGFP;UAS:VEcad∆CD-EGFP)^{ubs12} line encodes a version of VEcadEGFP deficient for the cytoplasmic domain of VEcad downstream of 5xUAS sites. It further encodes a fli1ep:Gal4FF transgene including the *cmlc2*:EGFP transgenesis cassette (Kwan et al., 2007) downstream of Gal4FF.

Generation of line:

Approximately 150 embryos were injected at the one cell stage with generated constructs pT2fli1ep:Gal4FF-*cmlc2*:EGFP and pT25xUAS:VEcad∆CD-EGFP (see above) as well as Tol2 transgenesis RNA (concentrations: DNA and RNA both 25ng/µl, 2-4nl/egg). Embryos displaying transient expression in the heart due to the *cmlc2*:EGFP cassette were selected

and raised to the adult stage. Here, the *cmlc2*:EGFP cassette served as an indirect marker for the UAS transgene integration. From previous experiments we knew that co-injected transgenes often are expressed in the same cells (pers. communication E. Ellertsdottir, Affolter lab and observations L. Herwig). The transgenesis cassette thus served as a positive control for the efficiency of the injections and integration of the pT25xUAS:VEcadΔCD-EGFP construct. From a mass cross of these G0 fish, I isolated 8 fish showing VEcadΔCD-EGFP expression in the vasculature and EGFP expression in the heart. Some ectopic expression was observed in neurons in the region of the neuronal tube. Unfortunately I was not able to identify the founder fish, thus, there might be multiple insertions at different loci. Only 7 fish survived until adult stage and when crossed to fli1ep:Gal4FF;UAS:RFP positive fish, only one of them showed still strong and uniform expression of the UAS-driven transgene in the vasculature. This F1 founder fish was used to generate a stable line Tg(fli1ep:Gal4FF-*cmlc2*:EGFP;UAS:VEcadΔCD-EGFP)^{ubs12} by crossing it either to wild type fish or fli1ep:Gal4FF;UAS:RFP positive fish.

Notes: It should be mentioned that the two transgenes I injected are two individual transgenes, they are not coupled on the same plasmid. The two transgenes might be located on different chromosomes (UAS:reporter can be lost if only selected for the heart marker cassette!). Therefore, the UAS: VEcadΔCD-EGFP transgene needs to be screened visually in every generation. The expression pattern of VEcadΔCD-EGFP is found almost uniformly throughout the whole vasculature. In some cases I observed, a weak expression signal or a total absence of it. The expression in the head vasculature is strong (pers. communication A. Lenard, Affolter lab) and is slightly weaker in the trunk vasculature but again increases in the caudal vein (plexus). However it is not clear whether this is a result of the UAS-transgene itself or the driver Gal4FF which might differentially expressed in this regions.

5 Results[1]

5.1 Distinct Cellular Mechanisms of Blood Vessel Fusion in the Zebrafish Embryo

5.1.1 Analysis of vessel fusion using an endothelial specific transgenic reporter system

In order to drive Gal4 dependent transgenes in the vasculature of the zebrafish and to label single endothelial cells at the (sub)-cellular level, which allows the analysis of relative behaviors of cells during morphogenetic events such as vessel fusion, I have engineered endothelial-specific transgenic reporter systems in the zebrafish, *Danio rerio*. I have generated a DNA construct encoding a Gal4 derivative (Gal4FF) (Asakawa et al., 2008) under the control of the endothelial specific enhancer-promoter element *fli1ep* (Villefranc et al., 2007). Injections of this construct together with Tol2 transgenesis RNA (Kawakami et al., 2004) into fertilized Tg(UAS:KAEDE)^{rk8} zebrafish eggs (Hatta et al., 2006), resulted in transient, mosaic expression of the UAS-driven green to red photoconvertible fluorescent protein KAEDE in endothelial cells (ECs). From these transiently expressing embryos, I successfully isolated three allelic locations of Gal4FF, designated as ubs2-4, from three individual founder fish resulting in the stable Tg(fli1ep:Gal4FF^{ubs2-4};UAS:KAEDE^{rk8}) zebrafish lines. Allele ubs3 and ubs4 were raised as stable stocks, whereas ubs2 was not further propagated due to a low fertility of the F1 generation (pers. communication with J. Torres-Vazquez, Skirball Institute of Biomolecular Medicine, NYC). Although this zebrafish line is endothelial specific, some mosaic, ectopic and weak expression of Gal4-dependent KAEDE can be observed in the notochord and somites as well as cells in the eye region of the ubs3 allele. The ubs4 allele displays weak ectopic expression in the notochord and stronger ectopic expression in neuronal cells in the region of the neural tube (data not shown, pers. observation L. Herwig).

In order to visualize the endothelium in red, I crossed the generated Tg(fli1ep:Gal4FF^{ubs2-4};UAS:KAEDE^{rk8}) with an Tg(UAS: RFP) zebrafish line (Asakawa et al., 2008) and specifically selected RFP positive fish larvae (Figure 15).

[1] The full publications from collaborations can be found in the appendix section 9.2.2, p.107. In 5.5, p.68, each publication is mentioned as an individual chapter, including title, authors, journal information and date of publication. A short explanation of what I have contributed in these papers is found within these chapters too. Each paper, including the full supplementary data, is stored on a DVD in the appendix section.

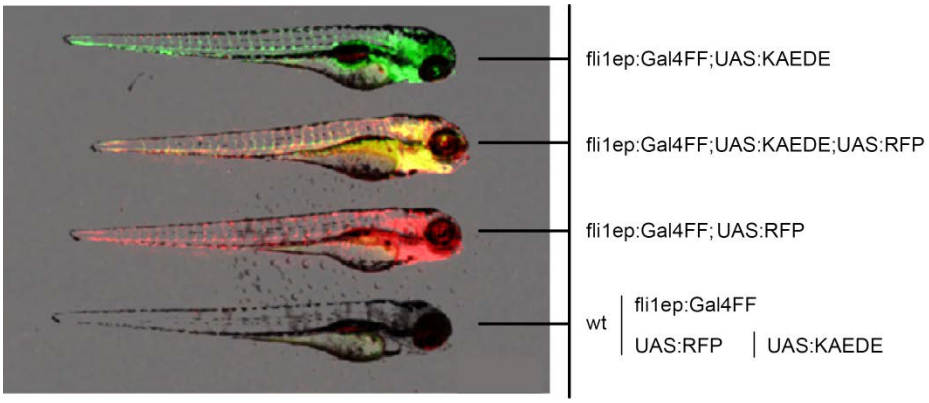

Figure 15 Expression of Gal4FF in different UAS backgrounds. Tg(fli1ep:Gal4FF;**14x**UAS:KAEDE) zebrafish line crossed with a **5x**UAS:RFP transgenic zebrafish line. All different possible genotypes from this cross are listed. Green fish in figure: (Tg(fli1ep:Gal4FF;UAS:KAEDE), this transgenic line allows to convert single cells by UV conversion of the KAEDE protein and trace single endothelial cell behavior during morphogenetic processes by confocal live imaging. Red fish in figure: (Tg(fli1ep:Gal4FF;UAS:RFP), this line can be crossed to any UAS transgenic line available and of interest that does encode a green fluorescent reporter protein. In addition all Gal4FF positive genotypes may be crossed with any non-fluorescent UAS-driven transgene of interest.

These transgenic lines allowed us to undertake two approaches: *First*, the photoconversion of specific regions of interest (ROIs), for example single ECs, from green to red in Tg(fli1ep:Gal4FF;UAS:KAEDE^{rk8}) embryos (Figure 16). *Second,* the visualization of any UAS-driven green fluorescent reporter construct, including constructs labeling finer sub-cellular structures of endothelial cells, such as components of the junctional complexes, within the red labeled endothelium of Tg(fli1ep:Gal4FF;UAS:RFP) embryos.

Thus, since we wanted to investigate the cellular behaviors during vessel fusion by the analysis of the dynamics of endothelial cell-cell junctions, I further engineered a 14xUAS-effector line (Köster and Fraser, 2001) expressing an EGFP tagged version of the human tight junctional protein Zonula Occludens-1 (hZO1), albeit in a highly mosaic fashion, when crossed to Tg(fli1ep:Gal4FF^{ubs3-4}) driver fish (Figure 17). Downstream of the UAS:EGFP-hZO1 transgene, a 900bp enhancer–promoter from the cardiac myosin light chain gene (*cmlc2) fused to EGFP* (*cmlc2*:EGFP) is encoded in reversed orientation. This cassette serves as a transgenesis marker (Kwan et al., 2007) and labels specifically the developing heart (Huang et al., 2003; Auman et al., 2007) and facilitated generation and identification of two UAS:EGFP-hZO1 alleles, ubs5 and ubs6, respectively.

Taken together, these two reporter setups, i.e. Tg(Gal4FF^{ubs3-4};UAS:EGFP-hZO1$^{ubs5-6;}$UAS:RFP) and Tg(fli1ep:Gal4FF^{ubs3-4};UAS:KAEDE^{rk8}) (Figure 16 and Figure 17) allowed the identification and *in vivo* tracking of junctional complexes and individual endothelial cells during the fusion process of ISVs in the zebrafish trunk.

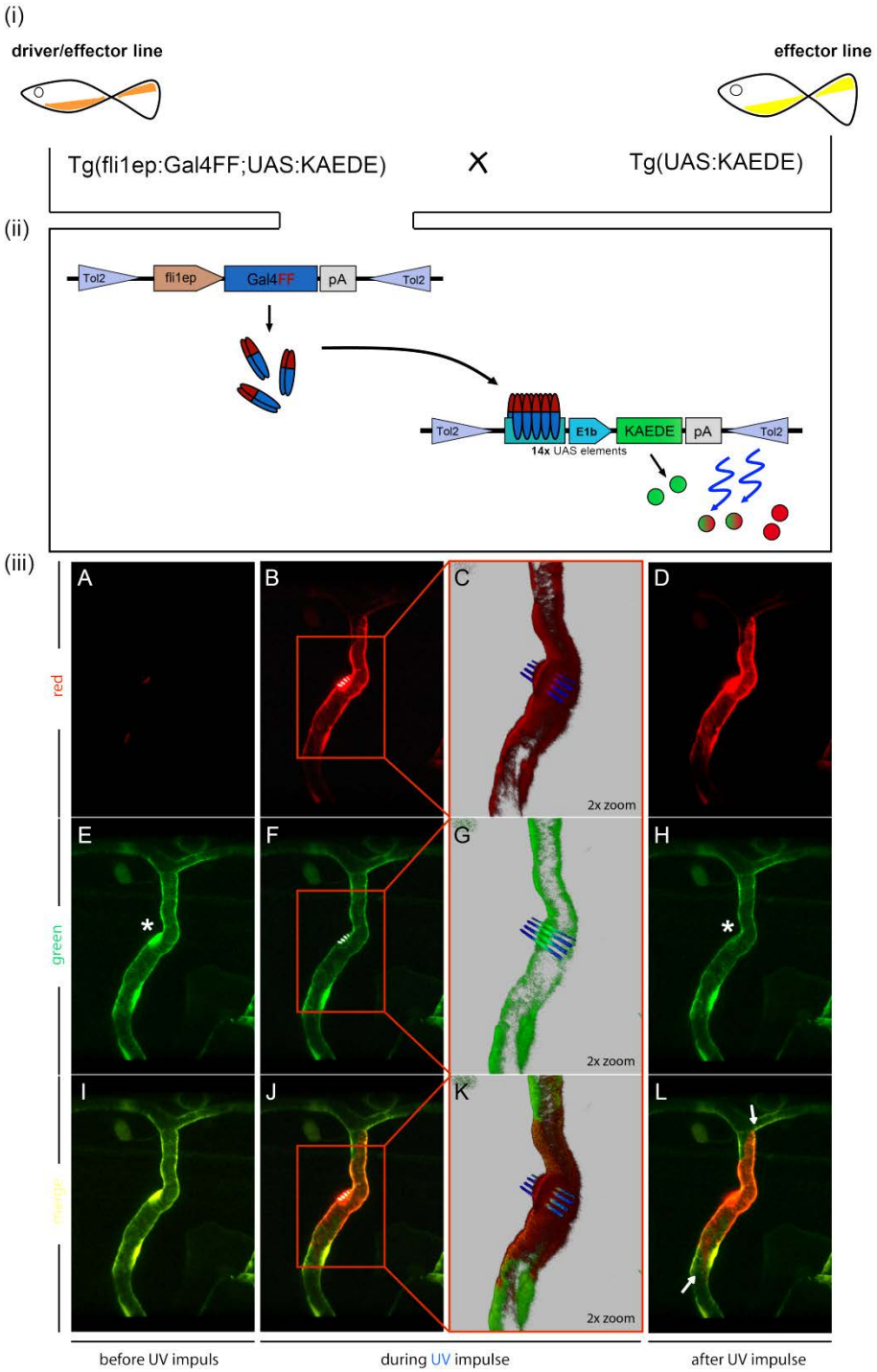

Figure 16 Overview of the UAS:KAEDE reporter system. (i) Crossing between Tg(fli1ep:Gal4FF^{ubs3};UAS:KAEDE^{rk8}) driver-effector line and Tg(UAS:KAEDE)^{rk8} effector line results in double positive transgenic embryos, where (ii) Gal4FF drives endothelial specific expression of the photoconvertible **14x**UAS driven KAEDE protein. (E1b, minimal promoter element; Tol2, left and right transposable tol2-arms for transgenesis; pA, polyadenylation signal (iii) embryos were raised until 2 dpf and a single endothelial cell within the stalk of an ISV was photoconverted by a short UV impulse (ca. 1min) targeting 4 small regions of interest (white points in B, F and J). (C, G) and (K) represent a 2x magnification of the squares in (B, F) and (J) and the laser path of the UV impulse is visible in blue. Different channels for non-converted KAEDE (green: E-H) and converted KAEDE (red: A-D) as well as the merged channel (merge: I-L) are shown. All channels are represented before (left column), during (two middle columns) and after the UV impulse (right column). Green KAEDE fluorescence is strongly reduced and converted into red KAEDE (compare E and H, asterisks) whereas in (L) the boarders of the converted cell are visible (see white arrows).

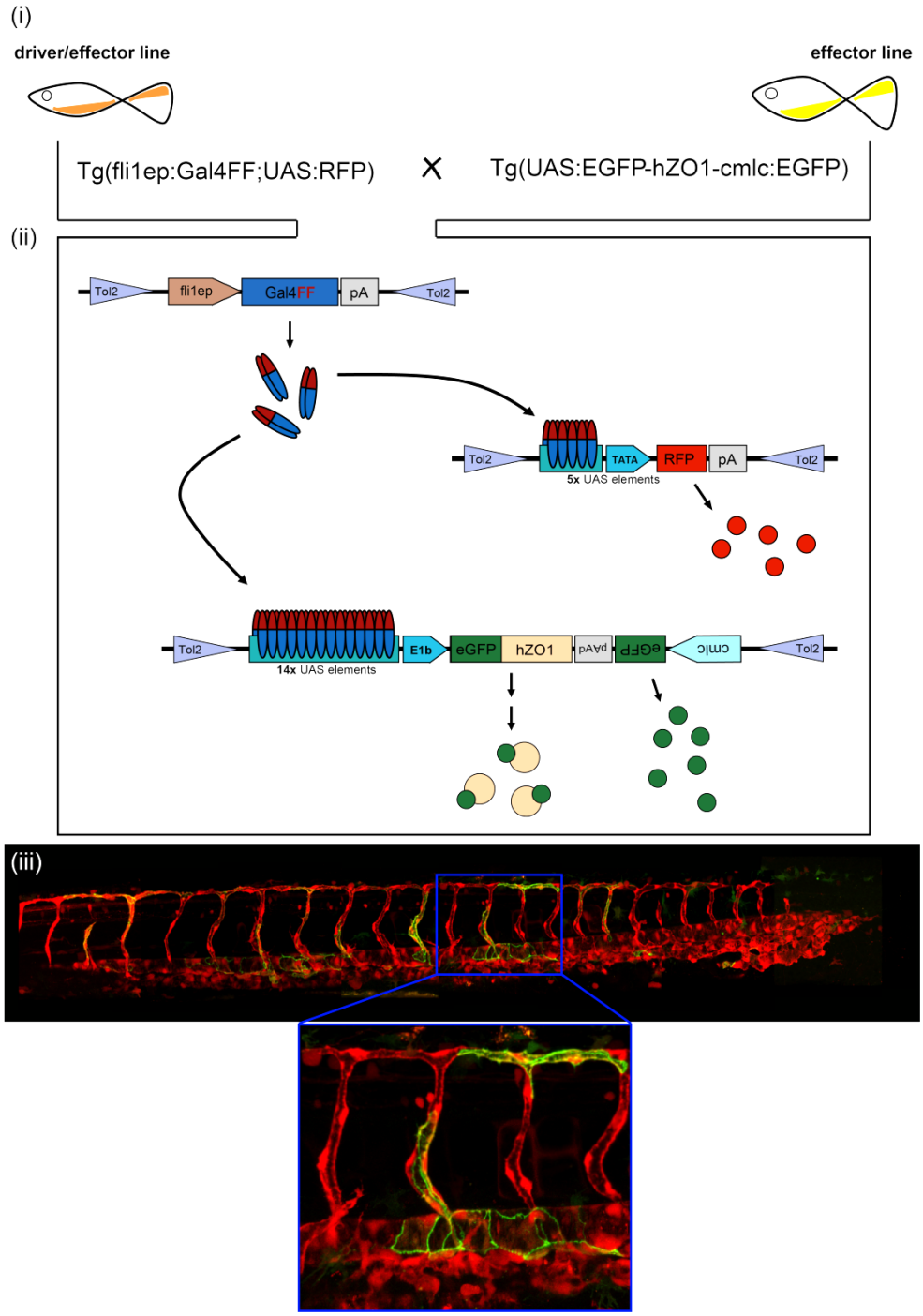

Figure 17 Overview of the UAS:EGFP-hZO1 reporter system. (i) Crossing between Tg(fli1ep:Gal4FF^{ubs3};UAS:RFP) driver-effector line and Tg(UAS:EGFP-hZO1^{ubs5}) effector fish results in triple positive transgenic embryos, where (ii) Gal4FF drives endothelial specific expression of the **5x**UAS-driven RFP and **14x**UAS-driven EGFP-hZO1 protein. The heart marker cassette (*cmlc2*:EGFP) drives EGFP expression in the heart which facilitates selection of EFGP-hZO1 positive fish. (E1b, minimal promoter element; Tol2, left and right transposable tol2-arms for transgenesis; pA, polyadenylation signal) (iii) Single combined confocal pictures (40x, 1.7x zoom) from a triple positive zebrafish trunk that expresses EGFP-hZO1 in a highly mosaic fashion. Magnification of a single picture of the region indicated.

In the following chapter I will summarize the highlights of the publication [2].

Distinct Cellular Mechanisms of Blood Vessel Fusion in the Zebrafish Embryo

Lukas Herwig*, Yannick Blum*, Alice Krudewig, Elin Ellertsdóttir, Anna Lenard, Heinz-Georg Belting and Markus Affolter *these authors contributed equally to this work

Current Biology 21 (2011) 1942–1948

Published online November 22, 2011

This publication was mentioned as an *editor's choice* article in S*cience* 9 December 2011, Network development, Beverly A. Purnell (see 9.3, p.107)

Contribution:

I generated the transgenic zebrafish reporter assay we used in this study to analyze the basic morphogenetic aspects of vessel fusion (see above). I performed the live imaging experiments (using wild type, transgenic and morphant fish embryos) together with Y. Blum. Together we did the data/imaging analysis and discussed and proposed the resulting models. I critically read the manuscript (written by M. Affolter and HG. Belting) during the writing and reviewing process, discussed it and proposed improvements to it. Together with Y. Blum I made, edited or contributed to all the figures.

[2] The full publication and supplementary information can be found in the appendix section of this thesis on page 9.2.1, p. 103; supplementary information (movies and figures) and the full publication are also stored on a DVD enclosed in the appendix section.

5.1.2 Summary of the publication: "Distinct Cellular Mechanisms of Blood Vessel Fusion in the Zebrafish Embryo"

During ISV vessel fusion, neighboring sprouts of ISVs establish contact and subsequently form a lumen between each other. This process of vessel fusion or anastomosis, results in the formation of a new vessel, the dorsal longitudinal anastomotic vessel (DLAV) (Figure 18 and Movie 1 on DVD in appendix), which is found along the anterior-posterior axis, on either side of the neural tube.

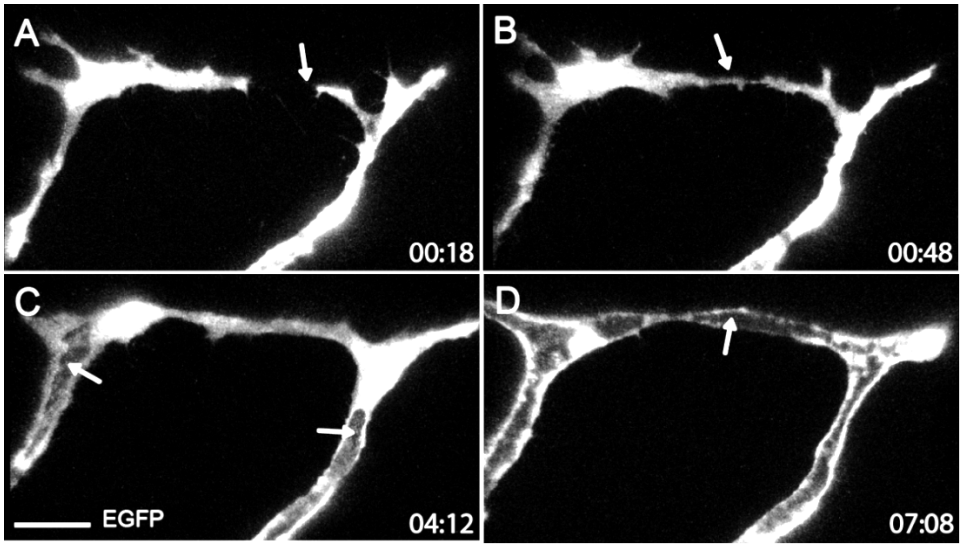

Figure 18 Overview on the process of vessel fusion. (A-D) Different steps during dorsal longitudinal anastomotic vessel (DLAV) formation. Tip cells reach the dorsal side of the embryo and send filopodia in anterior and posterior directions (arrow in 00:18 [hr:min]). The adjacent tip cells contact each other, fuse and form the future DLAV (arrow in 00:48). Later the lumen opens from the stalk and proceeds into the DLAV (arrows in 4:12 and 7:08). Scale bar = 20µm. Figure adapted from Herwig et al., 2011.

As a first step, we compared the expression pattern of our reporter EGFP-hZO1 with the endogenous wild type protein using a VE-cadherin antibody which co-localizes with ZO1 (Blum et al., 2008). We found that EGFP-hZO1 recombinant protein co-localized with endogenous VE-cadherin and thus endogenous ZO1 and is expressed throughout vascular development (Figure 33, p.105). Further, we observed a dynamic behavior of EGFP-hZO1 during the fusion process revealing for the first time, *in vivo*, the dynamics of junctional complexes during blood vessel development.

We next characterized the cellular architecture of the DLVA at 48 hpf, when it is fully lumenized, by the photoconversion of single cells in this vessel in Tg(fli1ep:Gal4FF^{ubs3-4};UAS:KAEDE^{rk8}) embryos. Followed by immunostainings, using a VE-cadherin antibody, we detected different cellular architectures in the DLAV: multicellular tubes as well as seamless tubes (Figure 19). In accordance with these results, live observations at 2 dpf using transgenic fli1ep:Gal4FF^{ubs3};UAS:EGFP-hZO1^{ubs5} embryos revealed the same results (Figure 20).

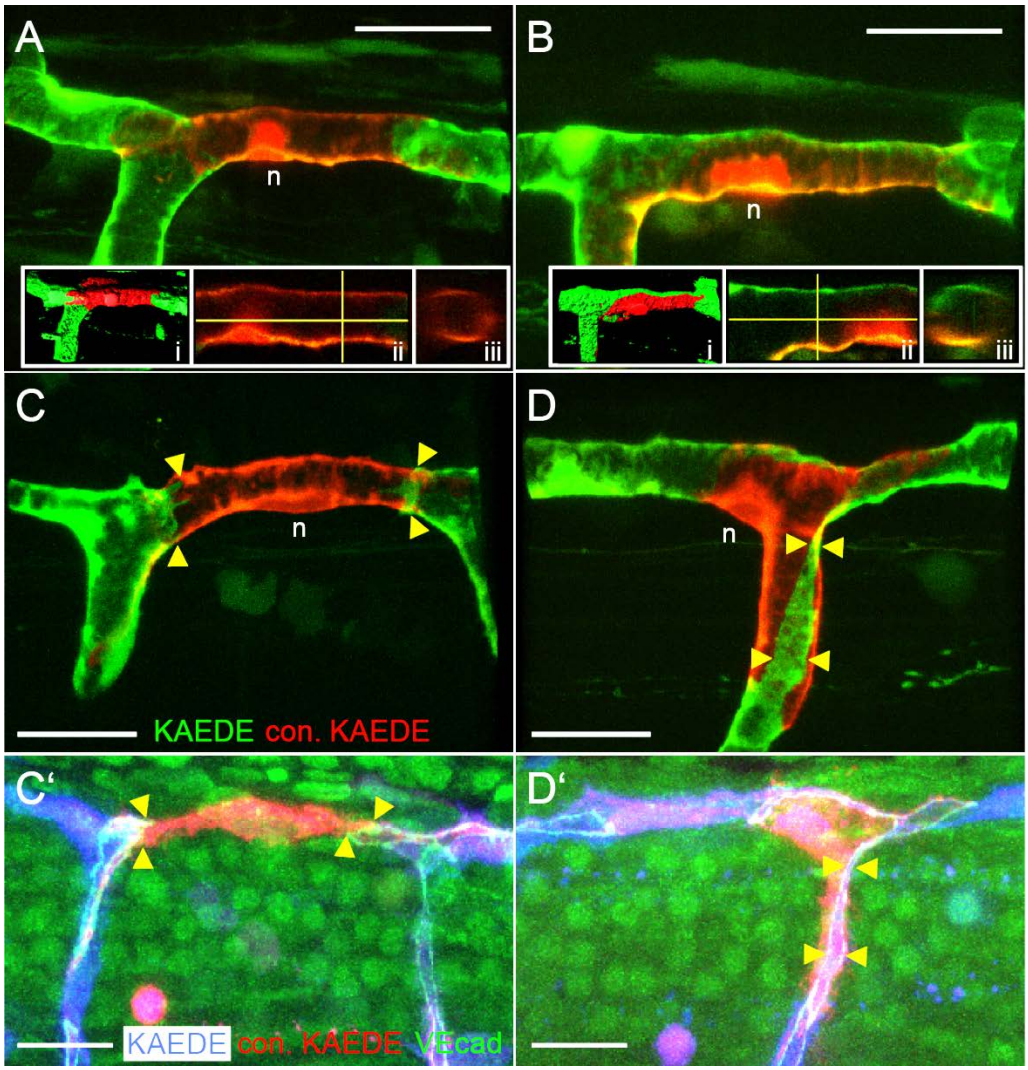

Figure 19 Different vessel architectures in the intersegmental vessel (ISV)/DLAV I. Single, photo-converted cells (red) show a unicellular (A) or a multicellular arrangement (B). Inserts (i–iii) in (A) and (B) show a surface calculation (i), a sagittal section (ii) and a cross-section (iii) at the sites indicated by crosshairs (n = nucleus). (C–D) Single photo-converted cells (red) and corresponding VE-cadherin (VE-cadherin) immunostainings. Arrowheads indicate regions of unicellular (C and C') and multicellular (D and D') tubes. All pictures 48hpf, 63x and 4x zoom, scale bar = 20µm. Figure adapted from Herwig et al., 2011.

We have previously suggested a model for vessel anastomosis (Blum et al., 2008), where at the beginning of each fusion event filopodial extensions of neighboring tip cells contact each other and increase their mutual surface, which is demarcated by a "dot-to-ring-like" transition of junctional proteins (VE-cadherin; ZO1) (see Figure 11, p.27). Following the *in vivo* dynamics of the EGFP-hZO1 protein, localized at these sites of contact, we were able to confirm our previously proposed model. Endothelial cells contact each other and form a dot like spot of junctional protein that, within about 40 min, extends into a ring as the contacting extensions increase their mutual surface (Figure 21 and Movie2). This surface within the elaborating ring-like structure can be classified as an apical membrane compartments as indicated by immunostainings using an antibody against the apical protein Podocalyxin2 (Pdxl2) (Figure 24 and Figure 33, p.105).

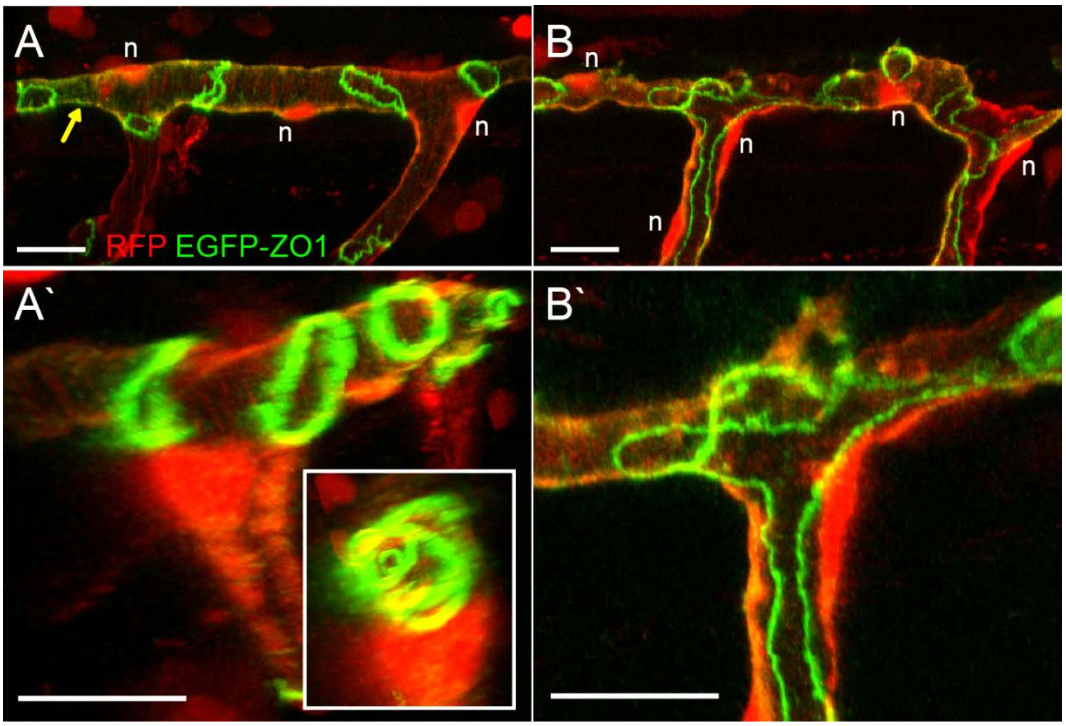

Figure 20 Different vessel architectures in the intersegmental vessel (ISV)/DLAV II. A unicellular tube outlined by EGFP-hZO1 fusion protein is shown in (A), and multicellular/unicellular arrangements represented by EGFP-hZO1 protein are shown in (B). (A) Individual cells (n=nucleus) are separated by each other by junctional rings, no junctions are found along the tubular axis. The yellow arrow in (A), points at delocalized EGFP-hZO1 protein in the cell membrane, most likely due to elevated levels of protein. (B) Multiple junctions run along the axis of the ISV, representing multicellular tubes. These are connected to rings in the DLAV, where again seamless tubes can be found. (A' and B') show different views/angles from (A) and (B). All pictures 48hpf, 63x and 4x zoom, scale bar = 20µm. Figure adapted from Herwig et al., 2011.

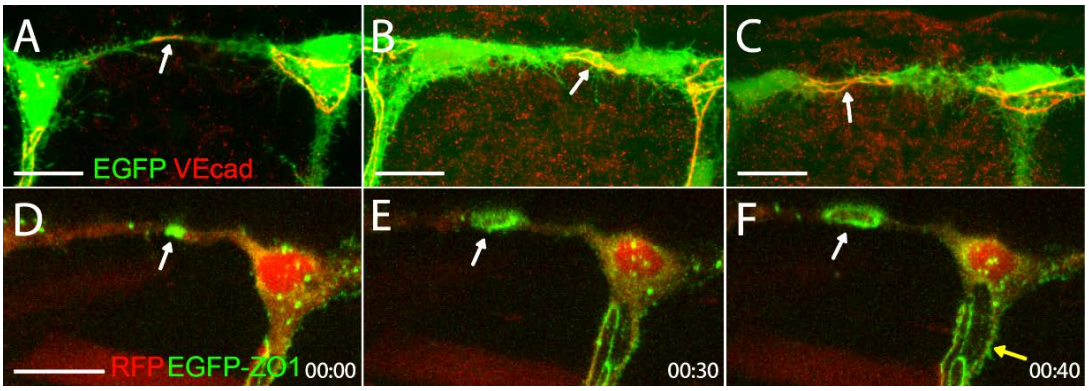

Figure 21 Contact formation during vessel fusion. (A–C) VE-cadherin immunostainings of 30hpf old Tg(fli:EGFP)^{y1} embryos. Dot-like structures, small and larger rings are shown (see white arrows). (D–F) Still pictures of Movie 2 found on DVD in appendix) showing a time-lapse of a Tg(fli1ep:GalFF^{ubs3};UAS:RFP;UAS:EGFP-ZO1^{ubs5}) embryo. An initial contact spot of EGFP-ZO1 (arrow in D) is elaborated into a small (arrow in E) and subsequently into a larger ring (arrow in F). The yellow arrow in (F) points to delocalized EGFP-ZO1 in the cell membrane. 32hpf, 63x, scale bar = 20µm, [hr:min]. Figure adapted from Herwig et al., 2011.

Our *in vivo* analysis of Tg(fli1ep:Gal4FF^{ubs3};UAS:RFP;UAS:EGFP-hZO1^{ubs5}) embryos revealed two distinct cellular morphogenetic mechanisms of how individual neighboring ISVs fuse to each other, which ultimately results in the formation of tubes of different cellular architecture. In a first mechanism, we found neighboring ISVs to fuse by a *cord hollowing* mechanism (see also 3.1.3.2, p.9), that depends on cell rearrangements and results in the formation of a multicellular tube (Figure 22 and Movie3).

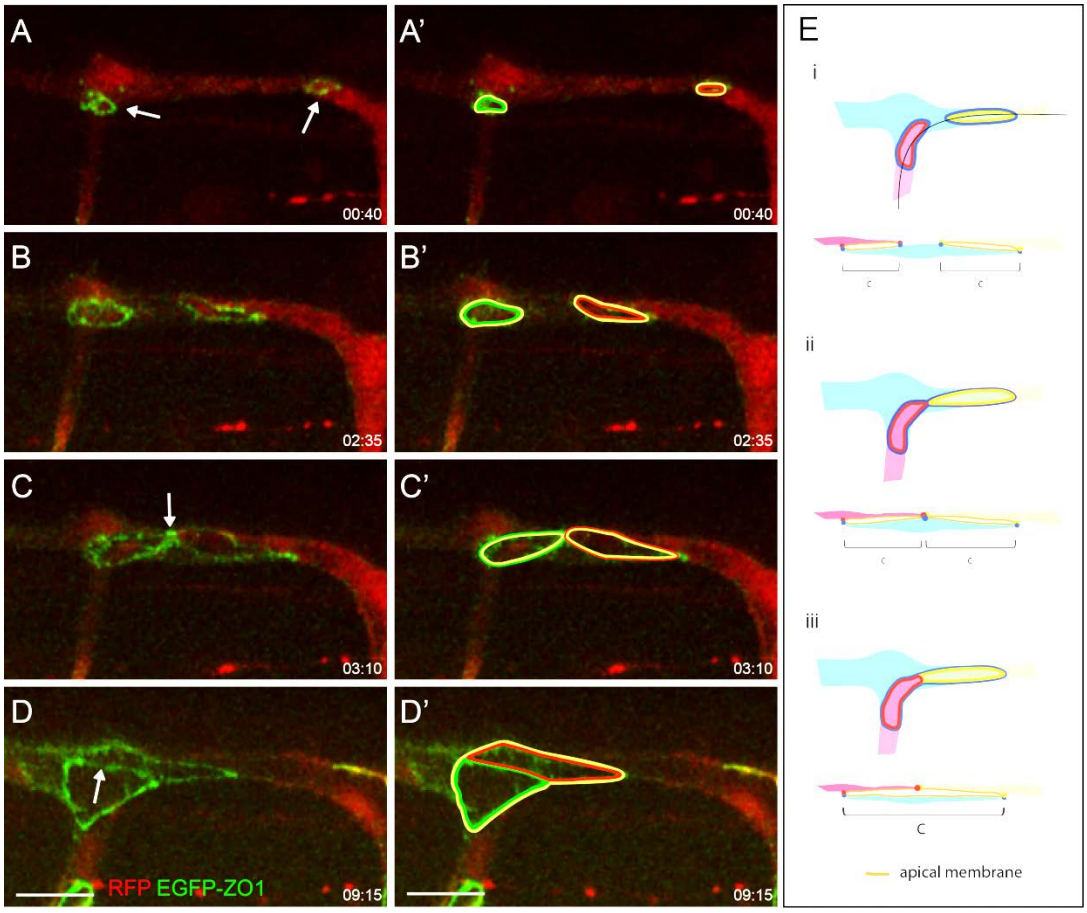

Figure 22 Anastomosis by cord hollowing. Still pictures from Movie 3 on DVD in the appendix, showing a time-lapse figure series of a Tg(fli1ep:GalFF^{ubs3};UAS:RFP;UAS:EGFP-ZO1^{ubs5}) embryo during vessel fusion (total length: 9:20 [hr:min]). (A–C) A tip cell has established contact with an adjacent tip cell (right arrow) and has contact with a stalk cell (left arrow), which results in two rings of EGFP-ZO1 (A). These loops extend and eventually meet (B and C). (A'–D') shows the junctional outline of participating cells (yellow: ''central'' cell, green: stalk cell, red: DLAV cell moving in from posterior). The two initial cell contacts are shown in yellow/green and yellow/red, respectively. When the stalk cell and the adjacent DLAV cell meet, they establish a new contact with ''green and red'' junctions (arrow in D, green and red line in D'). (all pictures, 63x, scale bar = 20µm). (E) Schematic overview of pictures (A-D): (i) several cells (pink, blue and yellow) enlarge their contact surfaces. (ii) Further cell rearrangements generate a novel contact between the pink and yellow cell and lead to a local detachment of the blue cell at the novel contact site (ii-iii). As a result, two local compartments (blue/pink and blue/yellow) merge into a single multicellular lumen. Longitudinal sections along the black line (see (i)) are shown below each step (i-iii). Figure adapted from Herwig et al., 2011.

Here, cell rearrangements of at least three cells increase and bring together two apical membrane compartments, demarcated by junctional rings of EGFP-hZO1 that will coalesce and form a continuous luminal space. In this scenario, a tip cell is connected to a stalk cell and a neighboring tip cell. The two latter ones will rearrange over the central tip cell thereby

bringing together two apical membrane compartments, the one formed between the two tip cells and the one formed between the central tip and stalk cell. This behavior results in the formation of a new junction at the site of contact between the individual membrane compartments. We suggest that dislocation of the tip cell at the site of the newly established contact results in the coalescence of the former individual compartments to one continuous membrane compartment (Figure 22).

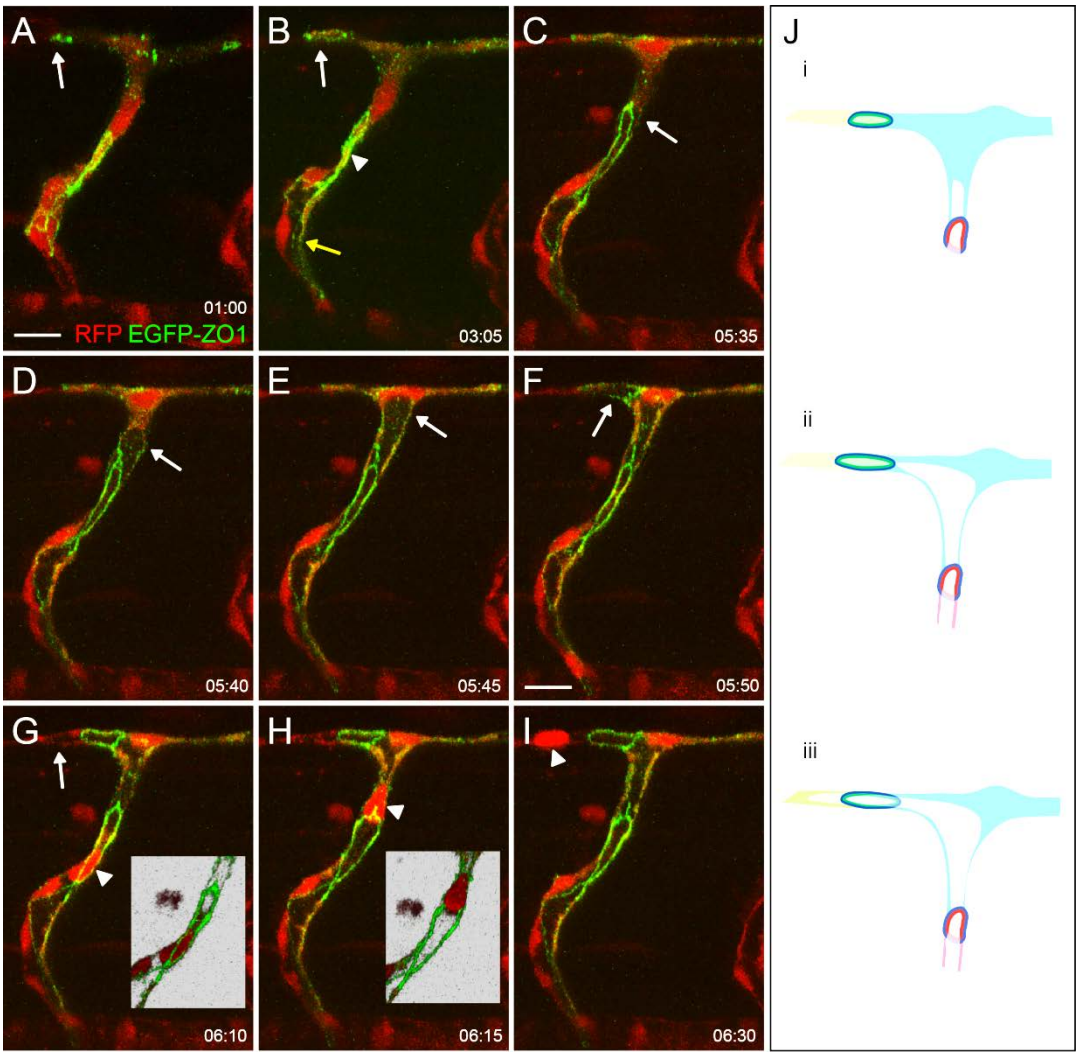

Figure 23 Anastomosis by membrane invagination. Still pictures from Movie 4 on DVD in the appendix, showing a time-lapse of a Tg(fli1ep:GalFF^{ubs3};UAS:RFP;UAS:EGFP-ZO1^{ubs5}) embryo (total length: 10:25 [hr:min]). (A and B) A tip cell has formed initial contacts and subsequently forms loops of EGFP-ZO1 with its adjacent partner (white arrows). The stalk shows a multicellular organization (two lines of EGFP-ZO1, arrowhead in B) and an opening lumen (yellow arrow in B). (C) The lumen projects into the fusion cell (follow arrow from C to E) and finally reaches the left ring of EGFPZO1, which is subsequently inflated (arrow in F). The lumen then continues to extend into the unlabeled fusion cell on the left (arrow in G). A blood cell then passes through the newly formed lumen (follow arrowhead from G–J). Insets show the blood cell passing behind the junction (G) and in front of the junction (H). (all pictures, 63x, scale bar = 20µm). (J) Schematic overview of pictures (A-I): A lumen extends from the dorsal aorta into the stalk and pushes into the "fusion/tip" cell (blue) (i) (The lumen is visualized in a lighter shade of the color of the surrounding cell). As the lumen reaches the distal end of the fusion cell (ii), it merges with a local luminal compartment at the contact and begins to push into the neighboring EC (iii). Figure adapted from Herwig et al., 2011.

In a *second* fusion scenario, we observed a *membrane invagination* mechanism depending on strong cell shape changes in the tip cell, which will generate a seamless or “transcellular” tube. Here, apical membrane invaginates (Figure 24 and Movie 4) and extends through a tip cell until this membrane reaches and coalesces with one of the previously formed apical membrane compartments (at the sites of contact between neighboring ISVs), thereby generating a continuous lumen (Figure 23). A lack of blood pressure does not affect cell rearrangements during ISV fusion, since the observed dynamics of EGFP-ZO1 in zebrafish embryos treated with an ATG-morpholino against *tnnt2a* gene (silent heart) (Sehnert et al., 2002), which blocks the contraction of the heart, are comparable to the wild type condition (Movie 5). However, the apical marker Pdxl2 in this morphant background was only found between junctional complexes, labeled by VE-cadherin antibodies, and a complete absence of the apical protein in seamless regions (regions where no junctions were detected) was observed (Figure 24). This indicates that blood pressure is a driving force for membrane invagination, and thus, is essential for the membrane invagination mechanism; in contrast cell rearrangements during the cord hollowing mechanism seems to be unaffected.

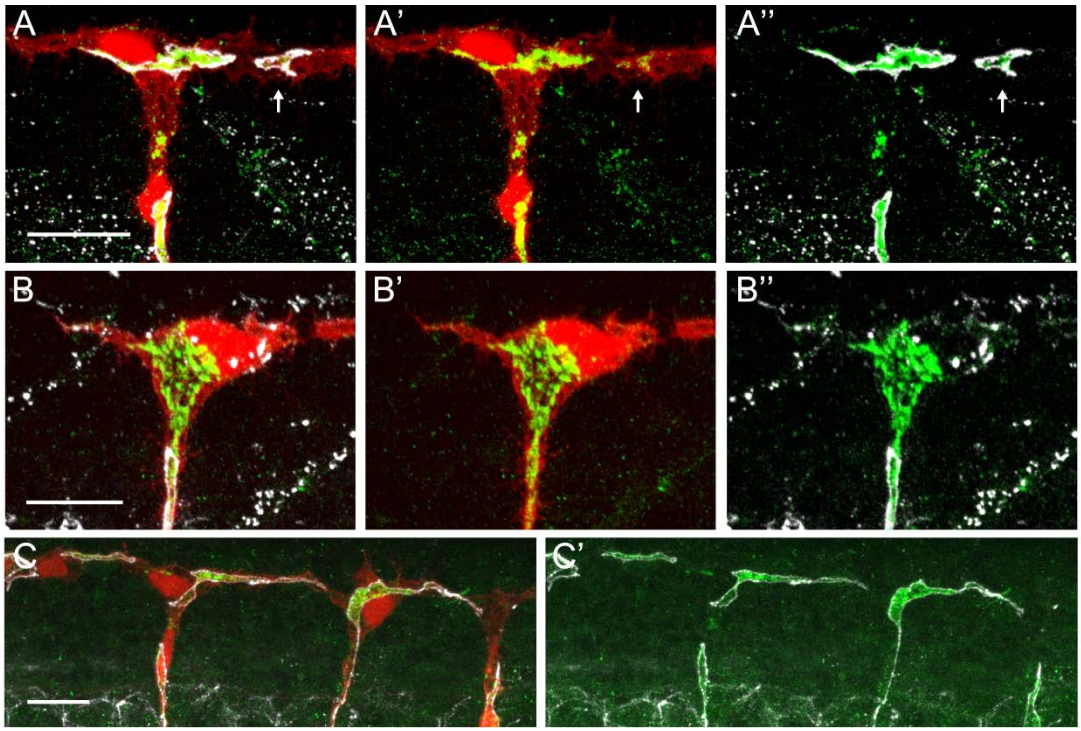

Figure 24 Apical membrane during ISV vessel fusion. Pdxl2 is localized within a junctional ring (arrow) at the contact site of two tip cells at the onset of anastomosis (36 hpf). (B–B’’) Apical membrane invagination of a tip cell at 36 hpf is shown by Pdxl2 immunostaining. (C–C’) In silent heart morphants at the same stage, the Pdxl2 staining is only seen within the junctional rings, indicating that apical membrane invagination does not take place in the absence of blood flow. ZO1 antibody is shown in white, Pdxl2 antibody in green, and kdrl:EGFP in red. Scale bar = 20µm, kdrl = VEGFR2. Figure adapted from Herwig et al., 2011.

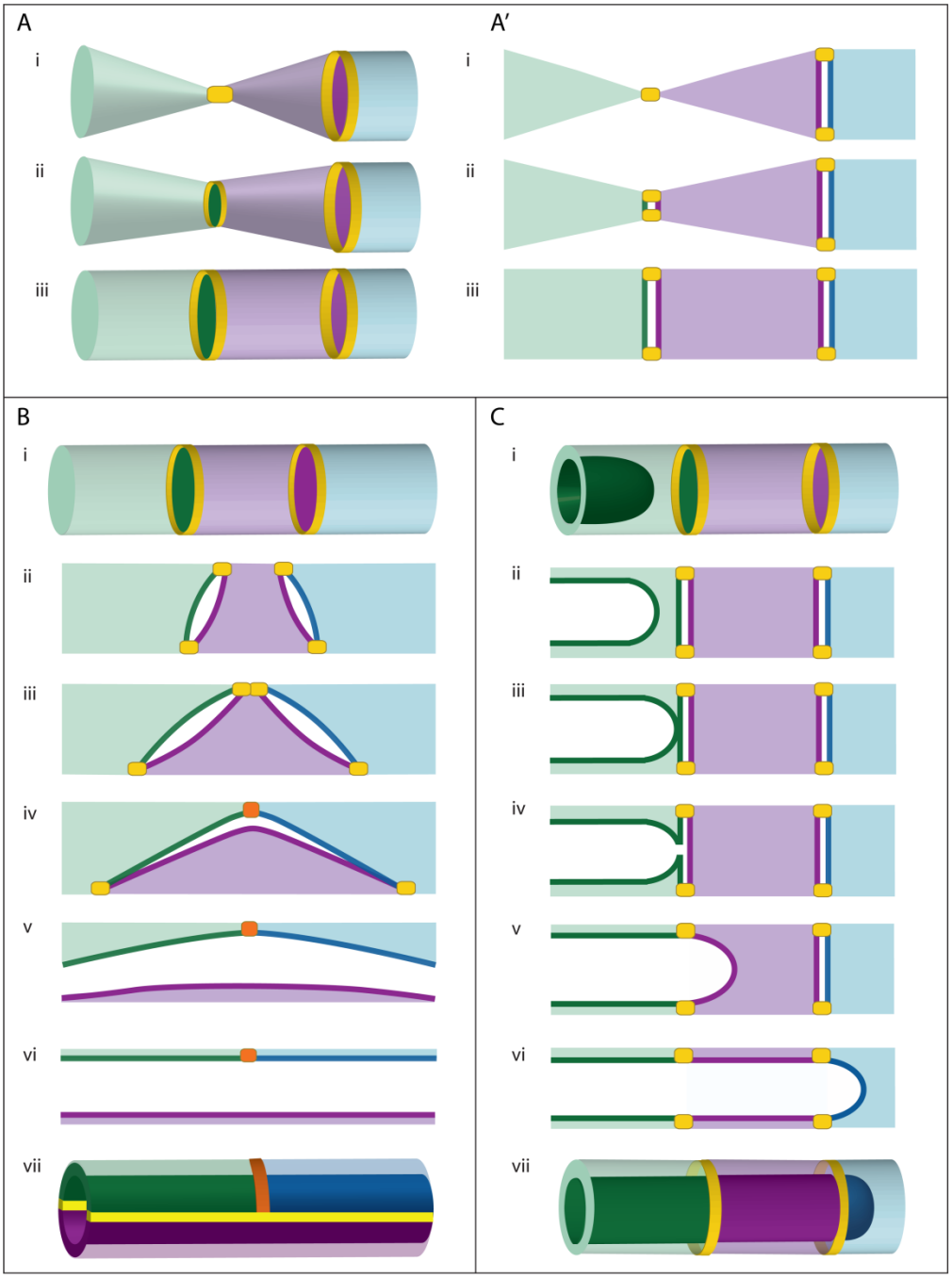

Figure 25 A model of cellular mechanisms during anastomosis. (A and A') Contact formation during vessel fusion is shown in (A) and corresponding sagittal sections in (A'). At the contact site of two neighboring tip cells (green and purple), junctional proteins are deposited (yellow spot in i). As the cells increase their mutual surface, this spot transforms into a ring (ii and iii), and the enclosed membrane compartment becomes apically polarized (dark green and dark purple areas). Subsequently, two different cellular mechanisms are used to complete the fusion process (see B and C). (B) A cord hollowing mechanism results in a multicellular tube. Cell rearrangements bring together two junctional rings, i.e., two apical membrane compartments that then merge into one membrane compartment. This is achieved by the formation of a new junction (orange) between the green and blue cell, which leads to the detachment of the middle cell (purple) at the site of the new contact. (C) Cell membrane invagination leads to the formation of a unicellular, seamless tube. Here, apical membrane of the green cell invaginates into the green cell. It then fuses with its own apical membrane at the previously formed contact side between the green and purple cells (see A). From here the lumen, i.e., the apical membrane of the neighboring cell (dark purple), begins to invaginate. Endothelial cells are shown in green, purple, and blue; apical membranes are shown in dark green, dark purple and dark blue; endothelial cell junctions are shown in yellow; and new endothelial cell junctions are shown in orange. Figure from Herwig et al., 2011.

Taking together, using transgenic zebrafish reporter assays (see also 5.1.1, p48), which allow the labeling of single ECs and endothelial cell-cell junctions in a mosaic fashion, and generation and analysis of a novel apical marker (Pdxl2), we deciphered a *membrane invagination* and *cord hollowing* mechanism during intersegmental vessel fusion in the zebrafish embryo. These two mechanisms lead to the formation of tubes of different cellular architecture, i.e. seamless tubes and multicellular tubes, respectively.

5.2 A VE-cadherin EGFP fusion reporter line

While ZO1 is a general epithelial tight junctional protein, VE-cadherin is an endothelial transmembrane specific adherens protein localized at the adherens junction complex between cells in the endothelium. It is this transmembrane component of the adherens junction complex, that plays a key role in barrier function, angiogenesis and intracellular signaling, which controls cell dynamics and cell cycle progression (reviewed in Harris and Nelson, 2010; Vestweber, 2008, see also 3.1.1, p.4). Therefore, I further engineered a transgenic zebrafish UAS-reporter line carrying an EGFP tagged version of VE-cadherin (Figure 26 and Figure 27). Since a full-length fusion construct was shown to be toxic (personal communication H-G. Belting (Affolter lab) and J. Essner, Iowa State University), my goal was to generate a biological *inert* (non-dominant negative) VE-cadherin recombinant reporter protein, which does not signal and interact with the cytoskeleton of ECs but still exerts its adhesive functions. It is well known that the cytoplasmic domain of cadherins can be bound directly by β-catenin and plakoglobin, which in addition can be both bound by α-catenin (Aberle et al., 1994; Jou et al., 1995; Nieset et al., 1997; Obama and Ozawa, 1997). α-catenin, in turn, binds directly to actin (Rimm et al., 1995). Thus, VE-cadherin is thought to be coupled to the actin cytoskeleton by such cytoplasmic interactions, i.e. by β-catenin, plakoglobin and α-catenin (Harris and Nelson, 2010; Lampugnani and Dejana, 1997). Furthermore, VE-cadherin, in confluent cells, can bind via β-catenin to VEGFR2 and thereby reduces its signaling (Lampugnani et al., 2003; Lampugnani et al., 2006; Rahimi and Kazlauskas, 1999). In addition, a specific conserved amino acid motif (YDEEGGGE) is critical for p120-catenin binding to E-cadherin and VE-cadherin (Thoreson et al., 2000; Ferber et al., 2002). Interestingly, p120-catenin has been suggested to be involved in cell proliferation since cell proliferation is reduced in the presence of a mutant form of VE-cadherin lacking this conserved amino acid motif (Ferber et al., 2002). Furthermore, as mentioned earlier, β-catenin and α-catenin are thought to shuttle from their VE-cadherin binding sites to the nucleus where they can regulate gene expression. Taken together, the cytoplasmic domain of VE-cadherin is likely involved in signaling and actin cytoskeleton interactions.

To this end, I used a full-length VE-cadherin EGFP fusion construct (a kind gift from J. Essner) and deleted the intracellular domain of VE-cadherin by “single-primer mutation technique” (Makarova et al., 2000), which resulted in VEcadΔCD-EGFP. In transient expression experiments I found that this EGFP-tagged deletion construct is expressed in ECs and appeared as dots and lines of stronger signal. This behavior was quiet similar to what I had seen previously in transient expression experiments using a pG1UAS:EGFP-hZO1 construct (Figure 34, p.106) and see also Master Thesis of L. Herwig, 2007, p.63, Figure 28).

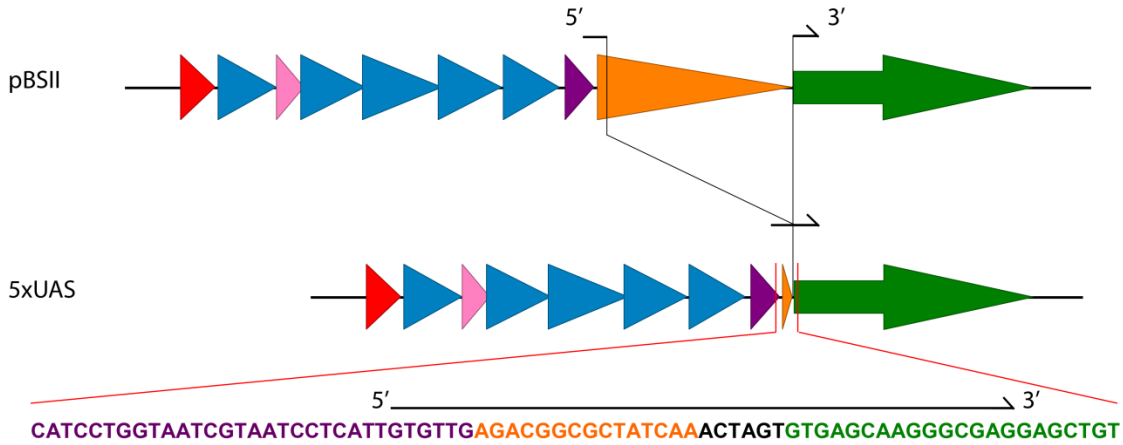

Figure 26 A non-dominant negative VE-cadherin deletion construct. The cytoplasmic domain of VE-cadherin in a full-length EGFP fusion construct was deleted using single-primer technique and cloned downstream of a 5xUAS cassette. Primer sites (3’-header and 5’-tailer = black broken arrow), specific domains (colored triangles) of VE-cadherin, EGFP (green arrow) and sequence after the deletion are given: red, signaling sequence; blue, extracellular domains; pink, ionic region; purple, transmembrane domain; orange, cytoplasmic domain. As visible, the full cytoplasmic domain has been deleted except for the 5 first amino acids of the cytoplasmic domain.

Therefore, in order to generate a stable transgenic zebrafish reporter line, I co-injected the described deletion construct together with a fli1ep:Gal4FF-*cmlc2*:EGFP construct and Tol2 transgenesis RNA into wild type embryos. From transiently expressing embryos I was able to select a positive founder fish that gave rise to a Tg(fli1ep:Gal4FF-*cmlc2*:EGFP;UAS:VEcadΔCD-EGFP) line with the allelic designation ubs12 Figure 27 (for more information see also 4.4.3.3, p.46). In this line, VEcadΔCD-EGFP recombinant protein co-localizes with endogenous ZO1 and is almost uniformly expressed in the whole vasculature (Figure 27 and Figure 35, p.106). Further, I observed a similar dynamic behavior of this protein during the fusion process as seen in the transgenic UAS:EGFP-ZO1 reporter fish and, thus, was able to confirm some of our findings regarding the processes of intersegmental vessel fusion (see below and previous chapter 5.1.2, p.53).

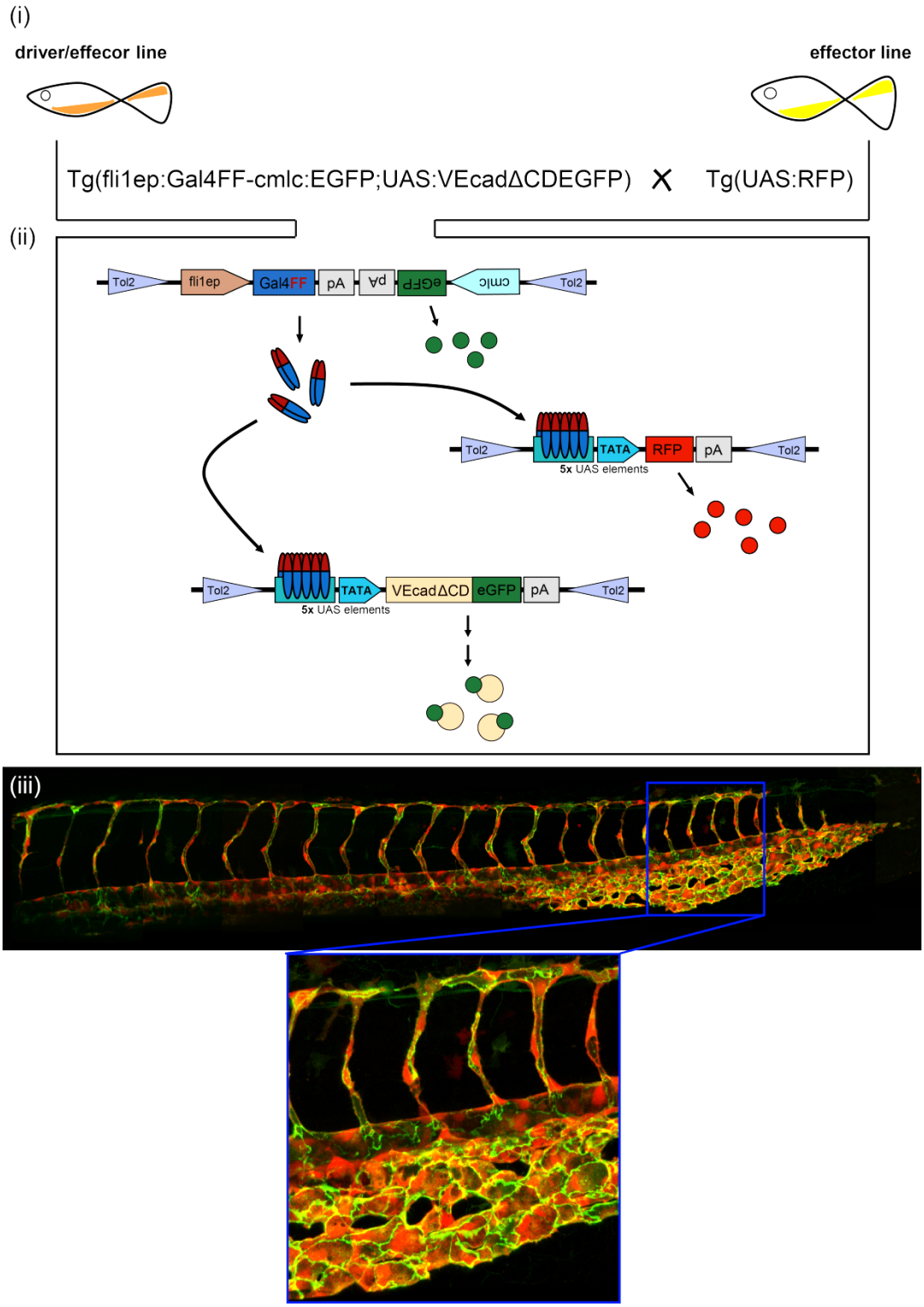

Figure 27 Overview of the VEcadΔCD-EGFP reporter system. (i) Crossing between Tg(fli1ep:Gal4FF-cmlc22:EGFP;UAS:VEcadΔCD-EGFP)^{ubs12} driver-effector line and Tg(UAS:RFP) effector fish results in triple positive transgenic embryos, where (ii) Gal4FF drives endothelial specific expression of the **5x**UAS-driven RFP and **5x**UAS-driven VEcadΔCD-EGFP protein. The heart marker cassette on the fli1ep:Gal4FF allele drives EGFP expression in the heart, and facilitated the generation of the VEcadΔCD-EGFP allele (for more information see 4.4.3.3, p.46). (E1b, minimal promoter element; Tol2, left and right transposable tol2-arms for transgenesis; pA, polyadenylation signal; TATA, TATA-box). (iii) Single combined confocal pictures (40x, 1.7x zoom) from a triple positive zebrafish trunk that expresses VEcadΔCD-EGFP uniformly in the whole vasculature. Magnification of a single picture of the region indicated.

During the fusion process, immediately after filopodial extensions made contact to each other, VEcadΔCD-EGFP became apparent as dot-like structures which elaborated into rings (Figure 28, p.63 and Movie6) as we had seen and described using the UAS:EGFP-hZO1 reporter line (see Figure 21, p.55 and Movie 2). I further was able to observe the membrane invagination mechanisms described above when following VEcadΔCD-EGFP after adjacent tip cells had established their contact (Figure 29 and Movie7, see also Figure 23, p.57 and Movie 4 and Figure 23).

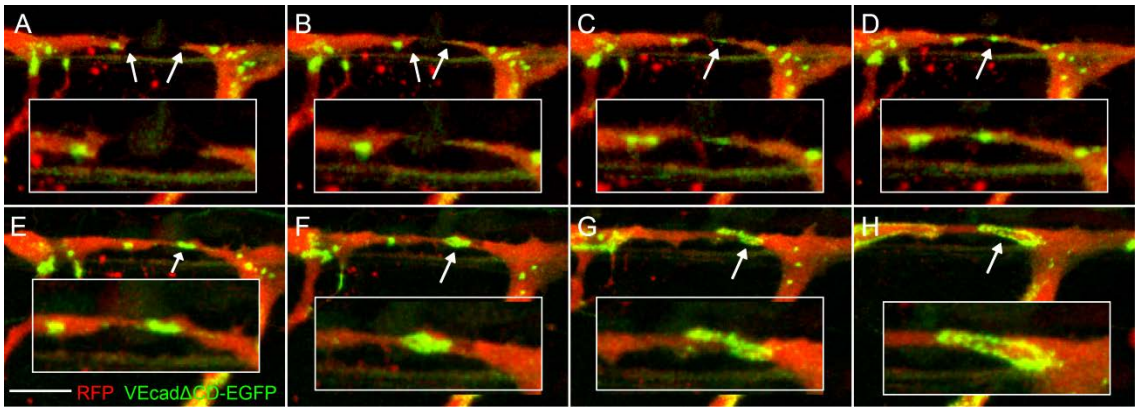

Figure 28 Contact formation visualized by VEcadΔCD-EGFP. (A-H) Still pictures from a time lapse (Movie6 on DVD) of a Tg(fli1ep:Gal4FF;VEcadΔCD-EGFP;UAS:RFP) embryo during intersegmental contact formation. (i) Filopodial extensions of neighboring tip cells contact each other. In (A and B), extensions have not yet established contact. VEcadΔCD-EGFP appears as a small puncta or dots in (C) and then subsequently elaborates into a ring (follow white arrows and insets (C-H)). Picture series from confocal time lapse movie, 32 hpf, with 40x, 1.7x zoom.

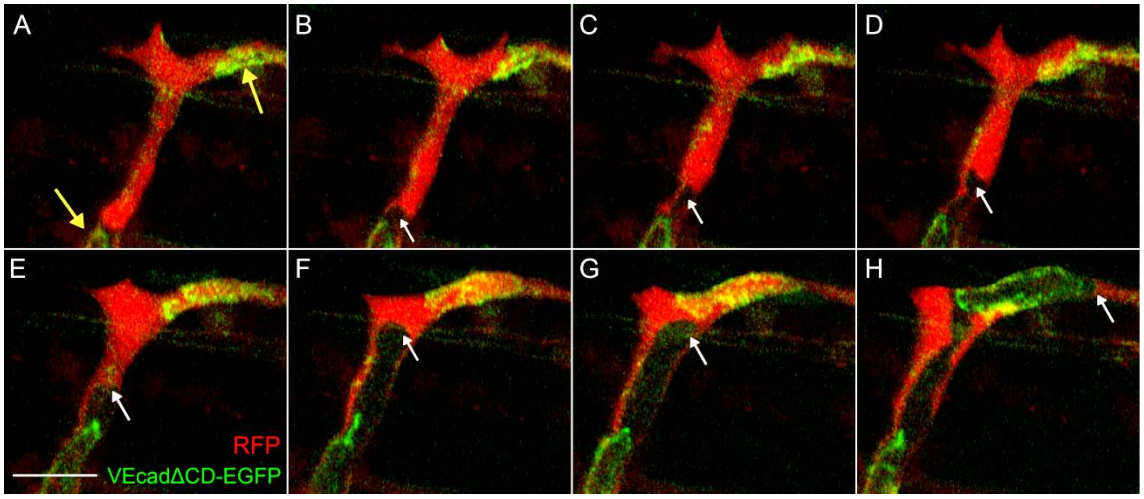

Figure 29 Membrane invagination visualized by VEcadΔCD-EGFP. (A-H) Still pictures from a time lapse (Movie 7 on DVD) of a Tg(fli1ep:Gal4FF;VEcadΔCD-EGFP;UAS:RFP) embryo during intersegmental vessel fusion. (ii) Membrane invagination during ISV vessel fusion is indirectly visualized by VEcadΔCD-EGFP. The tip cell makes contact to one of its neighboring tip cells (yellow arrow in A-H)) while it remains connected to the stalk of the ISV (yellow arrow head in A-H). As visible (follow white arrows in A-H) the membrane invaginates and extends into the fusion cell and eventually reaches and coalesces (H) with the previously formed apical membrane compartment between the neighboring fusion cells resulting in a transcellular lumen (see also Figure 23, p.57). Picture series from confocal time lapse movie, 32 hpf, with 63x, 1.7x zoom.

5.3 Further observations regarding vessel fusion

Using the UAS:EGFP-hZO1 line, that labels the tight junctions of endothelial cells, I was able to observe further fusion events between other endothelial sprouts/vessels than the neighboring ISVs.

During ISV fusion a new vessel, the DLAV, is generated on each side of the neural tube (Isogai et al., 2001 and this thesis). At around 48hpf endothelial cells in each of the bilaterally aligned DLAVs form lumenized sprouts that migrate over the neural tube and eventually fuse with the DLAV on the other side of the tube. These connecting sprouts between the lateral DLAVs seem to be luminized already upon fusion (Figure 36, p.107 and Movie 8). Still, these vessels depict the same mechanism, of dot-to-ring-like junctional elaboration (Figure 30 and Movie 9 and Movie 10).

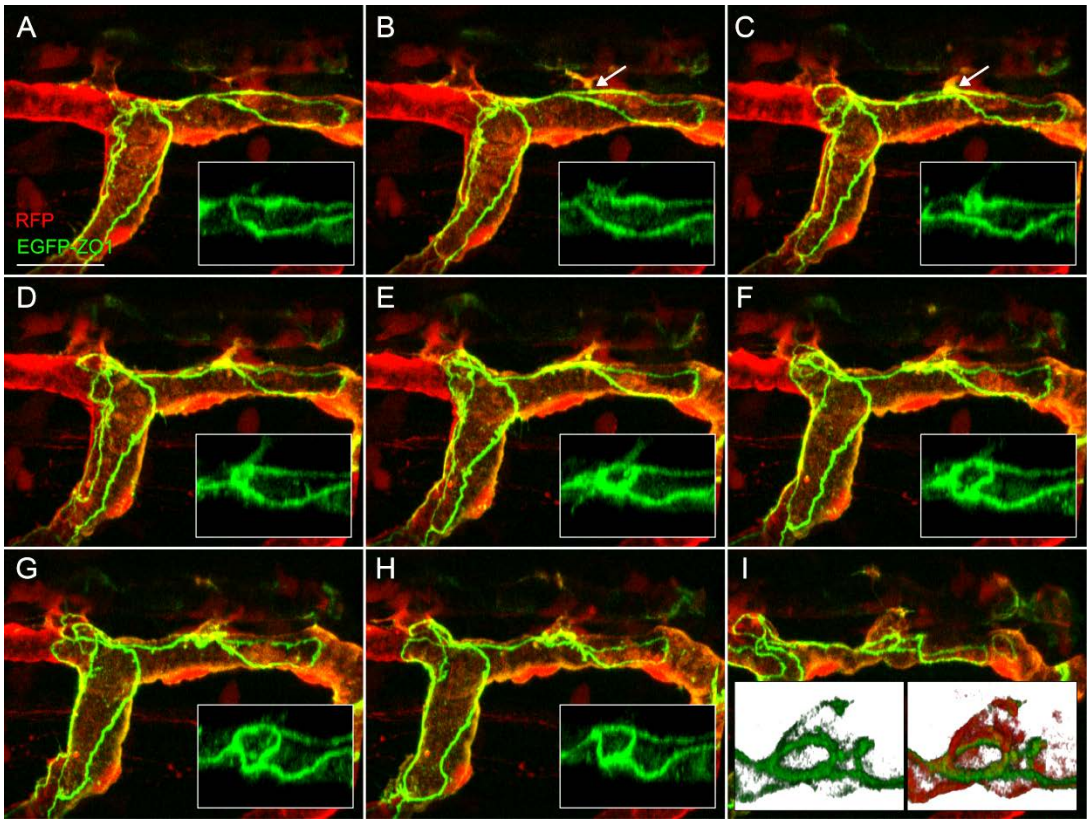

Figure 30 Contact formation between the neighboring DLAVs which run in parallel on each side of the neural tube. (A-H) A sprout from the DLAV located on the other side of the neural tube fuses with the neighboring DLAV. (A) Extensions of a sprout become apparent and (B) make contact to the junction(s) of the neighboring DLAV, as visualized by the dot like deposition of EGFP-hZO1 protein. This dot elaborates into a ring as seen in Figure 21. Small insets represent top view of the site undergoing vessel fusion. (I) The white insets represent a rendering of the site indicated, (green; junctions only, green/red; junctions and cytoplasmic RFP). It is visible, that a unicellular tube is connected to the DLAV by the newly generated ring. Picture series from confocal time lapse movie (see Movie 9 and Movie 10) of a Tg(fli1ep:Gal4FF^{ubs3};UAS:EGFP-hZO1^{ubs5}) embryo, 48hpf, 63x, 2x zoom, scale bar = 20µm.

Further, during secondary sprouting (see also 3.2.4.2.7, p.25), when endothelial sprouts from the posterior cardinal vein connect to the previously formed ISVs, I again observed this behavior. Here, a lumenized sprout contacts the previously formed ISV by filopodial extensions. As soon as a contact is established a junctional ring is formed at the site of contact and finally the two vessels fuse displaying a continuous lumen that allows blood cell circulation, as shown by a number of blood cells passing serendipitously through the newly formed ring and vessel connection (Figure 31 and Movie 11).

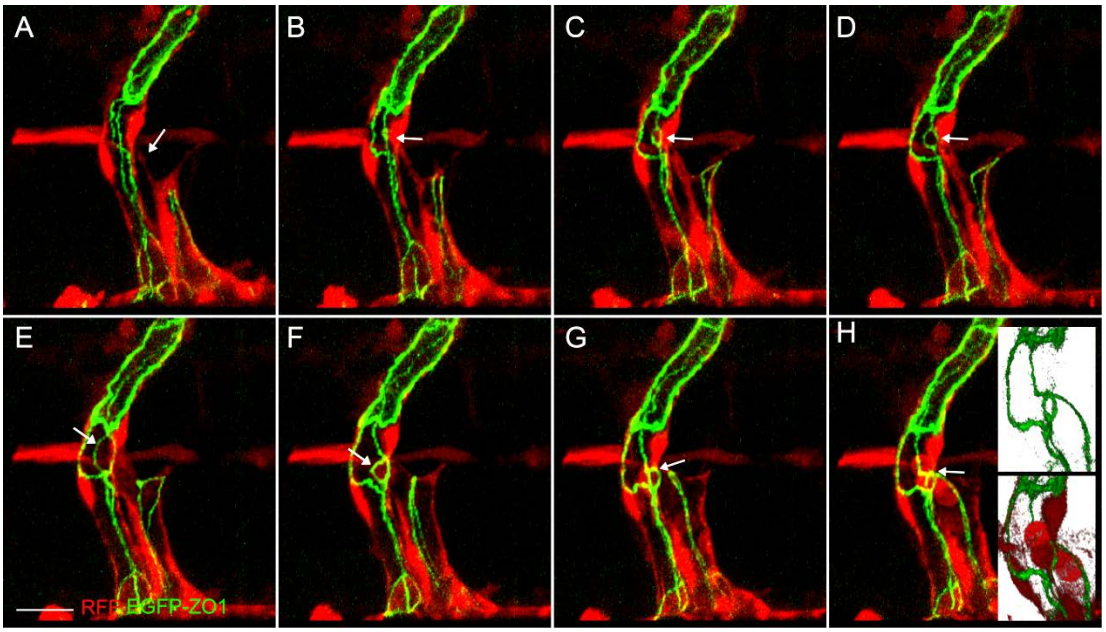

Figure 31 Contact formation between a secondary intersomitic sprout and a primary ISV. (A-H) A secondary sprout fuses with a primary ISV. (A) A filopodial extension is growing towards an ISV (white arrow head) and makes contact to its junctions, as represented by a small dot/circle (white arrow in B). This ring is subsequently transformed into a bigger ring (follow white arrows from (C-G)) and eventually blood cells can pass the two connected vessels (asterisk in H). (H) The white insets represent a rendering of the site indicated. As visible the blood cells pass through the newly generated ring, demonstrating a patent luminal space and a new connection between the former individual vessels. Picture series from confocal time lapse movie (see Movie 11) of a Tg(fli1ep:Gal4FF^{ubs3};UAS:EGFP-hZO1^{ubs5}) embryo, 48hpf, 63x, 2x zoom, scale bar = 20µm.

Interestingly, in both fusion events the filopodial structures connect at sites of endothelial cell-cell contacts since the elaborating rings are formed and integrated at previously established junctional complexes of the target vessels (Figure 30 and Figure 31).

5.4 Transient expression of a non-repetitive UAS-driven EGFP-hZO1 reporter construct

The adaption of the Gal4/UAS system to the zebrafish (Scheer and Campos-Ortega, 1999; Köster and Fraser, 2001) has opened up new possibilities regarding gene expression analysis and the generation and use of novel fluorescent reporter lines. However, we and other laboratories have encountered difficulties maintaining a uniformly expressing UAS reporter line when using the 14xUAS cassette (see also 6.2.2, p.86). Recently, a 4x non-

repetitive UAS-driven GFP reporter construct (4Xnr:GFP) had been shown to be strongly expressed and less silenced than a 14xUAS reporter line over several generations (Akitake et al., 2011). Therefore, I cloned a 4Xnr:EGFP-hZO1 reporter construct and injected it into fertilized Tg(fli1ep:Gal4FF;UAS:RFP) zebrafish eggs at the one cell stage (Figure 32).

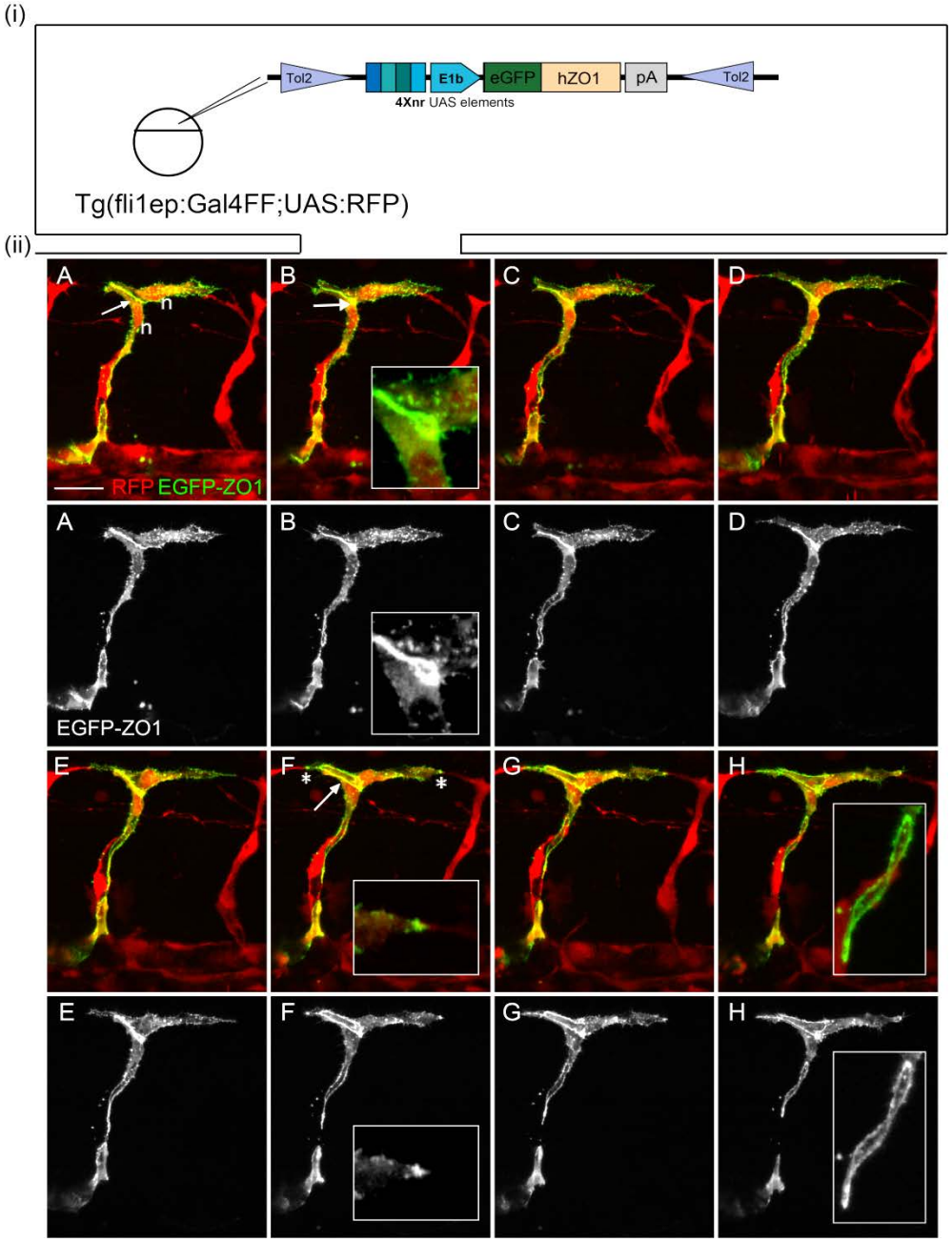

Figure 32 Transient expression of a 4x non-repetitive UAS:EGFP-hZO1 reporter construct. ((A-H) and (A'-H'), green channel only)) 4XnrUAS-driven EGFP-hZO1 localizes to the tight junctional complex in ECs when activated by endothelial specific Gal4FF driver fish. Junction between the tip cell and a stalk cell are visible (white arrow in (A and B) and small inset in (B). This junction subsequently enlarges into a ring between the cells (F). In (F) asterisks and small inset indicate sites of contact formation between the tip cells. (H) A junctional ring connecting two cells is well visible (small inset). Picture series from confocal time lapse movie, 32hpf-38hpf, 40x, 1.7x zoom, scale bar = 20µm, n = nucleus.

These embryos showed strong and transient expression of EGFP-hZO1 in single endothelial cells. The dynamics of EGFP-hZO1 protein in such a cell, followed over time (ca. 32 hpf – 38

hpf), is comparable to behaviors as we have them observed in the stable Tg(UAS:EGFP-hZO1) line I generated (see Figure 17, p.51), which demonstrates the functionality of the construct and makes it a possible candidate for a less mosaic and silenced junctional reporter line. I have injected this construct into fli1ep:Gal4FF positive fish and I am currently screening for putative G0 founder fish.

5.5 Collaborations[3]

5.5.1 Vascular morphogenesis in the zebrafish embryo

Elín Ellertsdóttir, Anna Lenard, Yannick Blum, Alice Krudewig, Lukas Herwig, Markus Affolter, Heinz-Georg Belting

Developmental Biology 341 (2010) 56–65

Published online November 3, 2009

Contribution:

I contributed my critical comments during the writing and reviewing process of this manuscript.

[3] Order of publications: according date of publication.

Developmental Biology 341 (2010) 56–65

Contents lists available at ScienceDirect

Developmental Biology

journal homepage: www.elsevier.com/developmentalbiology

Review

Vascular morphogenesis in the zebrafish embryo

Elín Ellertsdóttir, Anna Lenard, Yannick Blum, Alice Krudewig, Lukas Herwig, Markus Affolter, Heinz-Georg Belting *

Department of Cell Biology, Biozentrum der Universität Basel, Klingelbergstrasse 70, CH-4056 Basel, Switzerland

ARTICLE INFO

Article history:
Received for publication 11 September 2009
Revised 28 October 2009
Accepted 28 October 2009
Available online 3 November 2009

Keywords:
Angiogenesis
Vasculogenesis
Branching morphogenesis
Cell migration
Lumen formation
Development
Zebrafish

ABSTRACT

During embryonic development, the vertebrate vasculature is undergoing vast growth and remodeling. Blood vessels can be formed by a wide spectrum of different morphogenetic mechanisms, such as budding, cord hollowing, cell hollowing, cell wrapping and intussusception. Here, we describe the vascular morphogenesis that occurs in the early zebrafish embryo. We discuss the diversity of morphogenetic mechanisms that contribute to vessel assembly, angiogenic sprouting and tube formation in different blood vessels and how some of these complex cell behaviors are regulated by molecular pathways.

Introduction

Branched tubular organs, such as the insect tracheal system or the vertebrate cardiovascular system, kidney or lung, are found throughout the animal kingdom. Formation of such tubular networks from precursor cells or tissues involves a variety of morphogenetic processes, such as tube formation, elongation, branching and fusion. These processes are brought about by complex cellular behaviors, which include cell polarization, cell migration, cell rearrangements, cell shape changes and cell division. Although tubular organs are extremely diverse in anatomy and function, the cellular activities that govern tube formation and branching morphogenesis appear to be quite similar (Baer et al., 2009; Andrew and Ewald, 2010). In this review, we describe the current understanding of blood vessel formation in the early zebrafish embryo. We are placing special emphasis on the morphogenetic processes that contribute to vascular development and discuss the regulatory components that accompany these events.

In vertebrates, the cardiovascular system constitutes a highly ramified network of tubes that transports gas, nutrients, hormones and metabolites throughout the body. It also has important roles in the regulation of homeostasis and wound healing and is involved in the pathology of numerous diseases including cancer and inflammation (Carmeliet, 2003). The cardiovascular system emerges as one of the first organs during embryonic development and retains morphogenetic plasticity in adult life. Blood vessels are an integral component of all organs and are vital not only for their function but also for their formation during embryonic development (Nikolova and Lammert, 2003; Red-Horse et al., 2007; Sakaguchi et al., 2008). Blood vessels are highly diverse: they differ in size and are specialized depending on their function and the tissue or organ they are embedded in (Aird, 2007; Rocha and Adams, 2009). In general, they consist of an inner epithelium (endothelium) lining the lumen; depending on the type of vessel, this endothelium is surrounded by a basal lamina and by mural cells, such as pericytes and smooth muscle cells, which both support and regulate the function of the endothelium (Armulik et al., 2005).

Over the last decade, the molecular pathways controlling vascular development have attracted much attention, and a large number of key molecules has been identified that regulate different aspects of blood vessel morphogenesis. The basic frameworks of the vascular anatomy are conserved among vertebrates, which makes it possible to assign homologies between distinct blood vessels and to directly compare the formation of these vessels in different vertebrate species (Isogai et al., 2001; see Fig. 1). The zebrafish embryo has proven to be a useful model to study vascular morphogenesis in vivo. The vasculature can be easily visualized using a variety of labeling techniques, such as endothelial specific expression of fluorescent protein or by microangiography (Fig. 1). Its small size, experimental accessibility, optical clarity and rapid development allow to observe cellular activities, such as cell migration, cellular rearrangements and cell divisions, as they occur during blood vessel formation in the embryo. It is also possible to follow cardiovascular mutant phenotypes for several days because oxygenation of the early zebrafish embryo does

* Corresponding author.
E-mail address: heinz-georg.belting@unibas.ch (H.-G. Belting).

0012-1606/$ – see front matter © 2009 Elsevier Inc. All rights reserved.
doi:10.1016/j.ydbio.2009.10.035

5.5.2 Semaphorin-PlexinD1 Signaling Limits Angiogenic Potential via the VEGF Decoy Receptor sFlt1

Tomasz Zygmunt, Carl Michael Gay, Jordan Blondelle, Manvendra K. Singh, Kathleen McCrone Flaherty, Paula Casey Means, Lukas Herwig, Alice Krudewig, Heinz-Georg Belting, Markus Affolter, Jonathan A. Epstein and Jesus Torres-Vazquez

Developmental Cell 21 (2011) 1-14

Published online July 28, 2011

Contribution:

I generated Tg(*fli1ep*:Gal4FF)^{ubs4} zebrafish driver line using the Gateway® system (InvitrogenTM) which was introduced in the lab by A. Krudewig. Together, we generated Figure S4G. I contributed my critical comments during the writing and reviewing process of this manuscript.

Developmental Cell
Article

Semaphorin-PlexinD1 Signaling Limits Angiogenic Potential via the VEGF Decoy Receptor sFlt1

Tomasz Zygmunt,[1,6] Carl Michael Gay,[1,6] Jordan Blondelle,[2] Manvendra K. Singh,[3,5] Kathleen McCrone Flaherty,[1] Paula Casey Means,[1] Lukas Herwig,[4] Alice Krudewig,[4] Heinz-Georg Belting,[4] Markus Affolter,[4] Jonathan A. Epstein,[3,5] and Jesús Torres-Vázquez[1,*]

[1]Department of Cell Biology, Helen L. and Martin S. Kimmel Center for Biology and Medicine at the Skirball Institute, New York University School of Medicine, New York, NY 10016, USA
[2]Université Diderot-Paris 7, Paris, France
[3]Department of Cell and Developmental Biology, Cardiovascular Institute, University of Pennsylvania, Philadelphia, PA 19104, USA
[4]Biozentrum, University of Basel, Ch-4056 Basel, Switzerland
[5]Institute for Regenerative Medicine, University of Pennsylvania, Philadelphia, PA 19104, USA
[6]These authors contributed equally to this work
*Correspondence: jesus.torres-vazquez@med.nyu.edu
DOI 10.1016/j.devcel.2011.06.033

SUMMARY

Sprouting angiogenesis expands the embryonic vasculature enabling survival and homeostasis. Yet how the angiogenic capacity to form sprouts is allocated among endothelial cells (ECs) to guarantee the reproducible anatomy of stereotypical vascular beds remains unclear. Here we show that Sema-PlxnD1 signaling, previously implicated in sprout guidance, represses angiogenic potential to ensure the proper abundance and stereotypical distribution of the trunk's segmental arteries (SeAs). We find that Sema-PlxnD1 signaling exerts this effect by antagonizing the proangiogenic activity of vascular endothelial growth factor (VEGF). Specifically, Sema-PlxnD1 signaling ensures the proper endothelial abundance of *soluble flt1* (*sflt1*), an alternatively spliced form of the VEGF receptor Flt1 encoding a potent secreted decoy. Hence, Sema-PlxnD1 signaling regulates distinct but related aspects of angiogenesis: the spatial allocation of angiogenic capacity within a primary vessel and sprout guidance.

INTRODUCTION

Blood vessels form a pervasive tubular network that distributes oxygen, nutrients, hormones, and immunity factors. The first blood vessels assemble de novo via EC coalescence or vasculogenesis. Later, they expand via angiogenesis, the growth of new blood vessels from preexisting ones. In some locales, this process is stereotypic and vascular sprouts form with evolutionarily conserved and organ-specific distribution, abundance and shapes (Carmeliet, 2005; Isogai et al., 2001; Isogai et al., 2003). For example, zebrafish SeAs sprout bilaterally from the trunk's aorta just anterior to each somite boundary (SB) (Figure 1A). SeA sprouts contain migratory, proliferative and filopodia-rich arterial angiogenic ECs molecularly distinct from the sedentary "phalanx" ECs remaining in the aorta (De Bock et al., 2009; Siekmann and Lawson, 2007; Torres-Vázquez et al., 2004). Normally, only aortic ECs near SBs acquire angiogenic capacity (Ahn et al., 2000; Childs et al., 2002). It is thought that nonendothelial paracrine VEGF signals promote angiogenic capacity, while Notch-mediated lateral inhibition between ECs antagonizes it (Phng and Gerhardt, 2009; Siekmann et al., 2008). However, the mRNA expression of *vegf-a* and Notch pathway genes is inconsistent with the distribution of SeA sprouts. *vegf-a* is not transcribed along SBs, but rather expressed dorsal to the aorta at both the flanking somites' centers and the hypochord, a midline endodermal cell row. Notch pathway genes are expressed continuously along the aorta or broadly through the body (Hogan et al., 2009b; Lawson et al., 2002; Leslie et al., 2007; Phng et al., 2009; Siekmann and Lawson, 2007) (C.M.G., J.B., and J.T.-V., unpublished data). Hence, other cascades likely modulate VEGF and/or Notch signaling at presprouting stages to enable the stereotypical allocation of angiogenic capacity within the aorta. Perturbing these unidentified cascades might change the SeA sprouts' reproducible number or distribution, the ratio of aortic ECs that acquire angiogenic capacity, and/or the responsiveness of these cells to angiogenic cues.

Besides VEGF and Notch activity, proper SeA development requires paracrine Sema-Plxn signaling. Type 3 semas (sema3s) are repulsive guidance cues secreted by somites. Sema3s direct SeA sprout pathfinding by modulating cytoskeletal dynamics via the endothelial Sema3-receptor PlxnD1. Hence, *sema3* or *plxnD1* inactivation yields similar SeA sprout pathfinding defects in zebrafish and mice (Gay et al., 2011). Two observations made in zebrafish make Sema-PlxnD1 signaling a candidate modulator of angiogenic capacity. First, *sema3* and *plxnD1* expression begins hours before SeAs sprout from the aorta at ~21 hr post-fertilization (hpf). Second, loss of Sema-PlxnD1 signaling induces ectopic SeA sprout launching (Childs et al., 2002; Torres-Vázquez et al., 2004).

In wild-type (WT) animals SeA sprouts grow dorsally with a chevron-like shape, bifurcate anteroposteriorly at the neural tube's roof level and interconnect with their ipsilateral neighbors at ~32 hpf forming the paired Dorsal Longitudinal Anastomotic Vessels (DLAVs) (Isogai et al., 2003). In contrast, in *plxnD1* (*out of bounds - obd*) mutants and *plxnD1* morphants, SeA sprouts are misshaped and interconnect ectopically with their ipsilateral

5.5.3 The novel transmembrane protein Tmem2 is essential for coordination of myocardial and endocardial morphogenesis

Roland Totong, Thomas Schell, Fabienne Lescroart, Lucile Ryckebüsch, Yi-Fan Lin, Tomas Zygmunt, Lukas Herwig, Alice Krudewig, Dafna Gershoony, Heinz-Georg Belting, Markus Affolter, Jesus Torres-Vazquez and Deborah Yelon

Development 138 (2011) 4199-4205

Published online October 1, 2011

Contribution:

I generated Tg(*fli1ep*:Gal4FF)^{ubs4} zebrafish driver line using the Gateway® system (InvitrogenTM) which was introduced in the lab by Dr. Alice Krudewig. I contributed my critical comments during the writing and reviewing process of this manuscript.

Development 138, 4199-4205 (2011) doi:10.1242/dev.064261

The novel transmembrane protein Tmem2 is essential for coordination of myocardial and endocardial morphogenesis

Ronald Totong[1], Thomas Schell[1], Fabienne Lescroart[1], Lucile Ryckebüsch[2], Yi-Fan Lin[1,2], Tomasz Zygmunt[1], Lukas Herwig[3], Alice Krudewig[3], Dafna Gershoony[4], Heinz-Georg Belting[3], Markus Affolter[3], Jesús Torres-Vázquez[1] and Deborah Yelon[1,2,*]

SUMMARY

Coordination between adjacent tissues plays a crucial role during the morphogenesis of developing organs. In the embryonic heart, two tissues – the myocardium and the endocardium – are closely juxtaposed throughout their development. Myocardial and endocardial cells originate in neighboring regions of the lateral mesoderm, migrate medially in a synchronized fashion, collaborate to create concentric layers of the heart tube, and communicate during formation of the atrioventricular canal. Here, we identify a novel transmembrane protein, Tmem2, that has important functions during both myocardial and endocardial morphogenesis. We find that the zebrafish mutation *frozen ventricle* (*frv*) causes ectopic atrioventricular canal characteristics in the ventricular myocardium and endocardium, indicating a role of *frv* in the regional restriction of atrioventricular canal differentiation. Furthermore, in maternal-zygotic *frv* mutants, both myocardial and endocardial cells fail to move to the midline normally, indicating that *frv* facilitates cardiac fusion. Positional cloning reveals that the *frv* locus encodes Tmem2, a predicted type II single-pass transmembrane protein. Homologs of Tmem2 are present in all examined vertebrate genomes, but nothing is known about its molecular or cellular function in any context. By employing transgenes to drive tissue-specific expression of *tmem2*, we find that Tmem2 can function in the endocardium to repress atrioventricular differentiation within the ventricle. Additionally, Tmem2 can function in the myocardium to promote the medial movement of both myocardial and endocardial cells. Together, our data reveal that Tmem2 is an essential mediator of myocardium-endocardium coordination during cardiac morphogenesis.

KEY WORDS: Zebrafish, Heart development, Atrioventricular canal, Cardiac fusion

INTRODUCTION

The embryonic heart tube is initially a two-layered structure: the outer layer of muscular myocardium contracts to propel circulation and the inner layer of endothelial endocardium provides continuity with the rest of the vasculature. Myocardial and endocardial cells originate in neighboring regions of the lateral mesoderm (Schoenebeck et al., 2007). During the process of cardiac fusion, both cell types migrate medially in a synchronized fashion and merge at the midline to assemble the heart tube (Bussmann et al., 2007; Holtzman et al., 2007; Moreno-Rodriguez et al., 2006). At later stages, cardiac maturation involves remodeling of both juxtaposed layers during valve formation and trabeculation (Armstrong and Bischoff, 2004; Hinton and Yutzey, 2010; Sedmera et al., 2000). Despite the continual proximity of the myocardium and endocardium, little is known about the mechanisms that coordinate their development.

The coordination of myocardial and endocardial development has been particularly well established in the context of atrioventricular canal (AVC) formation. Both the myocardium and endocardium undergo specialized differentiation in order to create the characteristic morphology of the AVC and to establish the endocardial cushions that will remodel into the atrioventricular valve (Armstrong and Bischoff, 2004; Beis et al., 2005; Chi et al., 2008; Hinton and Yutzey, 2010). Several studies indicate that myocardium-endocardium communication regulates these spatially coincident events (Armstrong and Bischoff, 2004; Hinton and Yutzey, 2010). For example, chick explant experiments suggest that signal transduction between atrioventricular myocardium and atrioventricular endocardium induces endocardial cushion formation (Mjaatvedt et al., 1987). Although several signaling pathways have been implicated in promoting endocardial cushion development (Armstrong and Bischoff, 2004; Beis et al., 2005; Hinton and Yutzey, 2010), it is less clear which genes are responsible for attenuating these signals so as to spatially restrict atrioventricular differentiation.

Myocardium-endocardium coordination is also crucial during cardiac fusion. The synchronization of myocardial and endocardial migration suggests that both tissues respond to the same cues in the extracellular environment. Some cues may emanate from the endoderm: both myocardial and endocardial fusion are inhibited when endodermal specification or morphogenesis is disrupted (e.g. Holtzman et al., 2007; Kikuchi et al., 2001; Kupperman et al., 2000). Additionally, either diminished or excessive deposition of extracellular matrix (ECM) can hinder myocardial and endocardial movement (e.g. Arrington and Yost, 2009; Garavito-Aguilar et al., 2010; Trinh and Stainier, 2004). Furthermore, the myocardium and endocardium may impact the behavior of one another. Cardiomyocytes display aberrant migration patterns in the absence

[1]Developmental Genetics Program and Department of Cell Biology, Kimmel Center for Biology and Medicine, Skirball Institute of Biomolecular Medicine, New York University School of Medicine, New York, NY 10016, USA. [2]Division of Biological Sciences, University of California, San Diego, La Jolla, CA 92093, USA. [3]Biozentrum, University of Basel, CH-4056 Basel, Switzerland. [4]Department of Pharmacology, New York University School of Medicine, New York, NY 10016, USA.

*Author for correspondence (dyelon@ucsd.edu)

Accepted 18 July 2011

The hypothalamic neuropeptide oxytocin is required for formation of the neurovascular interface of the pituitary.

Gutnick A, Blechman J, Kaslin J, Herwig L, Belting HG, Affolter M, Bonkowsky JL, Levkowitz G.

Developmental Cell 21 (2011) 642–654

Published online October 17, 2011

Contribution:

I generated Tg(*fli1ep*:Gal4FF)^{ubs4} zebrafish driver line using the Gateway® system (InvitrogenTM) which was introduced in the lab by Dr. Alice Krudewig. I contributed my critical comments during the writing and reviewing process of this manuscript.

Developmental Cell
Article

The Hypothalamic Neuropeptide Oxytocin Is Required for Formation of the Neurovascular Interface of the Pituitary

Amos Gutnick,[1] Janna Blechman,[1] Jan Kaslin,[2] Lukas Herwig,[3] Heinz-Georg Belting,[3] Markus Affolter,[3] Joshua L. Bonkowsky,[4,5] and Gil Levkowitz[1,*]
[1]Department of Molecular Cell Biology, Weizmann Institute of Science, P.O. Box 26, Rehovot 76100, Israel
[2]Australian Regenerative Medicine Institute, Monash University, Clayton, Victoria 3800, Australia
[3]Biozentrum der Universität Basel, CH-4056 Basel, Switzerland
[4]Department of Pediatrics
[5]Department of Neurobiology and Anatomy
University of Utah, Salt Lake City, UT 84132, USA
*Correspondence: gil.levkowitz@weizmann.ac.il
DOI 10.1016/j.devcel.2011.09.004

SUMMARY

The hypothalamo-neurohypophyseal system (HNS) is the neurovascular structure through which the hypothalamic neuropeptides oxytocin and arginine-vasopressin exit the brain into the bloodstream, where they go on to affect peripheral physiology. Here, we investigate the molecular cues that regulate the neurovascular contact between hypothalamic axons and neurohypophyseal capillaries of the zebrafish. We developed a transgenic system in which both hypothalamic axons and neurohypophyseal vasculature can be analyzed in vivo. We identified the cellular organization of the zebrafish HNS as well as the dynamic processes that contribute to formation of the HNS neurovascular interface. We show that formation of this interface is regulated during development by local release of oxytocin, which affects endothelial morphogenesis. This cell communication process is essential for the establishment of a tight axovasal interface between the neurons and blood vessels of the HNS. We present a unique example of axons affecting endothelial morphogenesis through secretion of a neuropeptide.

INTRODUCTION

The neuroendocrine system is composed of neurosecretory brain cells that transfer hormones into the bloodstream to influence the function of target cells throughout the body. The hypothalamo-neurohypophyseal system (HNS) is a major neuroendocrine conduit through which the brain controls peripheral physiology (Burbach et al., 2001). The anatomy and activities of the HNS are conserved in all vertebrates. Ramon Cajal was the first to provide a description of the nerve fibers that connect the hypothalamus with the posterior pituitary (Cajal, 1911). It has since been established that these hypothalamic neurons themselves secrete neurohormones directly into the blood circulation, a finding that arose from experiments in both fish and mammalian models (Bargmann, 1949; Harris, 1948b; Scharrer, 1928). The hypothalamic neuropeptides arginine-vasopressin (AVP) and oxytocin (OXT) are synthesized in massive magnocellular neurons in the hypothalamus, transported along axons all the way down to the neurohypophysis, where they are secreted (Brownstein et al., 1980). Within the neurohypophysis, AVP and OXT are released from axons of the supraopticohypophyseal tract into fenestrated capillaries, thus leaving the brain and entering the general circulation without disrupting the blood-brain barrier (Burbach et al., 2001).

In the general circulation, secreted AVP regulates water homeostasis by increasing water permeability of the collecting duct of the kidney, and oxytocin regulates labor and milk let down by causing the respective contraction of the smooth muscle of the uterus and of the myoepithelial cells of breast ducts (for review, see Burbach et al., 2001; Gimpl and Fahrenholz, 2001; Verbalis, 2007). These physiological activities are conserved: in teleost fish, the AVP-like neuropeptide (Avpl) (a.k.a. arginine-vasotocin) regulates water balance by affecting filtration in the kidney (Amer and Brown, 1995; Macfarlane and Maetz, 1974; Peter and Fryer, 1983) and oxytocin-like neuropeptide (Oxtl) (a.k.a. isotocin) regulates contraction of smooth muscles in the ovary and oviduct during parturition or oviposition of live bearing and egg laying fish (La Pointe, 1977; Peter and Fryer, 1983). Avpl and Oxtl also regulate blood pressure in the ventral aorta (Chan, 1977; Kulczykowska, 1998; Le Mevel et al., 1993; Peter and Fryer, 1983). The HNS is therefore a central point of interface between the hormonal, neuronal, and vascular systems common to all vertebrate species.

The neurohypophysis is an elaborate three-dimensional structure, which substantially complicates the interpretation of cellular interactions and dynamics based solely on tissue sections. Although the anatomical structures of the neurohypophyseal axons and blood vessels have been the focus of intense study for over a century (Bargmann, 1949; Fink and Smith, 1971; Harris, 1948a; Scharrer, 1928), little progress has been made in uncovering the molecular and cellular processes that underlie formation of the interface between hypothalamic axons and

6 Discussion

6.1 Blood vessel fusion

In this thesis, I have used the zebrafish intersegmental vessels (ISVs) as an *in vivo* model to study single cell morphogenetic mechanisms that underlie the process of blood vessel fusion. During vessel fusion, endothelial cells (EC) face different tasks: ECs need to find their appropriate partners within the tissue, they need to establish a stable contact and finally, they need to form a lumen *de novo*, which will interconnect the two former individual sprouts, resulting in the formation of a new vessel. Using confocal live imaging technique, novel transgenic zebrafish lines (fli1ep:Gal4FF^{ubs3} and UAS:EGFP-hZO1^{ubs4}) and immunostainings, including an apical marker (*zf*-podocalyxin2), we found a specific behavior during contact formation between neighboring extensions of fusing ISVs. Further, we observed two distinct cellular mechanisms - a *membrane invagination* and a *cord hollowing* mechanism - that both can contribute to vessel fusion between the zebrafish ISVs. These two mechanisms are intrinsically connected to lumen formation but use two distinct cellular behaviors, i.e. membrane invagination and cell rearrangements, and lead to the formation of tubes of different cellular architecture - seamless tubes and multicellular tubes, respectively (Figure 25, p.59). The process of vessel fusion, has (up to the publication found in this thesis, Herwig et al. 2011) not been analyzed *in vivo*. However, already more than 20 years ago Kubota and colleagues designed an “endothelial cell tube formation assay” that allows the formation of capillary-like structures by human umbilical vein endothelial cells (HUVECs) when cultured on a basement membrane protein matrix (Kubota et al., 1988). Further, Nakatsu and colleagues have developed an optimized three-dimensional *in vitro* assay using HUVECs, that entails the major steps of angiogenesis, including the sprouting, migration, alignment, proliferation, tube formation, branching, and anastomosis of endothelial sprouts (Nakatsu et al., 2003; Nakatsu and Hughes, 2008). Such *in vitro* assays, including the many steps of angiogenesis, have thus been used for many applications, for instance, the screening for angiogenic or anti-angiogenic factors (Arnaoutova et al., 2009). A major contribution, however, is their use in getting a better molecular understanding of endothelial tube formation during angiogenic sprouting (reviewed in Davis et al., 2011). Although the same genes and morphologic behaviors are required during *in vitro* and *in vivo* tubulogenesis, *in vitro* systems can not model or mimic all the complex interactions that are taking place during angiogenesis *in vivo*. The lack of blood flow or the native environment of blood vessels, for instance, cannot be integrated, or only to a limited extend, when using *in vitro* systems (Nakatsu and Hughes, 2008). Thus, the work using *in vivo* systems of different vertebrate

organisms such as the mouse, zebrafish or chick embryo, has led to important advances in the understanding of angiogenic processes.

6.1.1 Contact formation during blood vessel fusion

As early as neighboring filopodial extensions contact each other during contact formation of fusing ISVs, we observed dot-like cell-cell junctions that are transformed into junctional rings within less than 40 minutes, as the mutual surface of the extensions enlarges (Figure 21, p.55). Using an antibody against zebrafish podocalyxin2 (podocalyxin is a known apical marker in epithelial cells (Meder et al., 2005) belonging to the family of CD34 sialomucins), we observed polarization of the contact area within the elaborated rings (Figure 24, p.58), specifying them as apical membrane compartments. Podocalyxin and CD34 have been recently shown to localize apically during lumen formation of the mouse dorsal aorta (Strilic et al., 2009). In this system, podocalyxin and CD34 are recruited to cell-cell contacts between ECs that initially form a cord-like structure, in which neighboring cells are connected to each other and express junctional molecules (VE-cadherin) all along their entire cell–cell contacts. After the relocalization of junctions between the neighboring ECs (VE-cadherin becomes localized to the cell borders), an apical, future luminal domain is specified by podocalyxin and CDC34 and is outlined by VE-cadherin positive junctions; later, a lumen is formed at this site. This establishment of an apical domain, where a future lumen is going to be formed, is similar to what we have seen at the site of contact formation of anastomosing ISVs. However, we were not able to resolve a luminal space between the two apical membranes at the site of contact. Polarization of these membrane compartments, prior to the morphogenetic movements, that lead to lumen coalescence (see below and Figure 25, p.59), as well as their immediate inflation (see Movie 3 and Movie 4) after coalescence with an extending lumen, however, suggest early formation of an extracellular space between the neighboring membranes in such compartments at the site of contact. The generation of such an extracellular space might be partially explained by electrostatic cell-surface repulsion, generated by sialic acids found on the extracellular domain of podocalyxin. Such electrostatic forces have been shown to be essential for lumen formation in developing blood vessels since removal of the negative charge of sialic acids reduces vascular lumen formation in the DA (Strilic et al., 2010). Further, mice deficient for podocalyxin fail to form a lumenized DA (Strilic et al., 2009). It will be interesting to see whether Pdxl2 has similar functions in the zebrafish during vessel fusion or even at earlier stages when the DA is formed.

The establishment of the observed apical compartments requires the *de novo* formation of apical membrane. It has recently been suggested by Bryant and colleagues that MDCK cells use so called apical membrane initiation sites (AMIS) during the polarization/lumen formation process to specify the site of apical polarization (AMIS: specific sites between contacting

MDCK cells formed at a stage where tight junction markers and podocalyxin cannot be resolved by confocal microscopy). In knockdown experiments Rab11a positive vesicles were found to recruit podocalyxin, initially localized at the periphery of the cells, to AMIS at the future apical/luminal site between neighboring cells. Such AMIS are then transformed into pre-apical patches (PAPs), the sites where the future luminal space will be formed (Bryant et al., 2010) (PAPs: early apical structures where tight junctions are localized differentially from podocalyxin that generates a separation of two opposing plasma membranes, which, however, is not yet resolvable optically (Ferrari et al., 2008)). It was also shown that VE-cadherin knockout mice fail to proper localize podocalyxin and CD34 to the future luminal side (Strilic et al., 2009) and murine endothelial cells, genetically ablated for VE-cadherin, display ectopic podocalyxin at their basal side in 2D culture (Lampugnani et al., 2010). Further, it is suggested that epithelial cell-cell interactions provide important cues regarding the initiation of the polarization of an epithelium. Cell-cell interactions cause the calcium-dependent trafficking of E-cadherin to the sites where cells contact each other. These first contacts appear as E-cadherin positive “spot-like” or “puncta-like” structures in filopodia or lamelipodia (Yonemura et al., 1995; Adams et al., 1996). Such “primordial cell-cell contacts” might serve the cell as positional cues that instruct the cells *where* to localize and activate the polarization machinery (Ebnet et al., 2004). It is then thought that subsequent accumulation of adhesion molecules at these sites recruits the polarity complexes that will initiate formation of adherens junctions (AJs) and tight junctions (TJs) and mediate the polarization process (Willenborg and Prekeris, 2011).We detected VE-cadherin localization as soon as the tip cells make contact to each other (Figure 21, p.55 and Figure 28, p.63), which raises the question, whether these molecules serve the tip cell as a landmark for polarization as the AMIS do in MDCK cells. HG. Belting (Affolter lab) is currently characterizing the role of VE-cadherin during ISV/DLAV formation, analyzing a VE-cadherin null mutant, which displays defects in vessel growth and fusion (pers. communication with H. Belting). The analysis of this mutant alone and in the EGFP-hZO1 background in combination with the Pdxl2 antibody will help to answer the question of whether VE-cadherin is required for proper polarization. Further, following EGFP-hZO1 in VE-cadherin morphant zebrafish embryos, using a splice morpholino (E2I2) against *zf*-VEcad (Nicoli et al., 2007), revealed that tip cells still contact each other but localization of EGFP-hZO1 is less specific and the ring-like structures we observed during contact formation in wild type embryos, are more “diffuse” (data not shown, and see above) indicating that polarization does not occur properly. However, these preliminary results need to be further quantified, as mentioned, by using the Pdxl2 antibody in the VE-cadherin null and EGFP-hZO1 background or by the generation of transgenic fish lines expressing apical fluorescent markers.

6.1.2 Fusion by membrane invagination mechanism

“Seamless endothelial” cells, as described in this thesis (Figure 19, p.54 and Figure 20, p.55) have initially been observed in the diaphragm of the rat by electron microscopy in 1964 by Wolff and colleagues and were reported to be exclusively found in capillaries (Wolff, 1964; Bär et al., 1984). The formation of such seamless tubes *in vivo* has only been elucidated recently by Kamei and colleagues based on a previously suggested model, where ISVs are composed of three ECs arranged in a rod-like fashion, i.e. an inverted T-shaped cell linking to the dorsal aorta, a connecting cell and a T-shaped tip cell, which connects to neighboring ISVs (Childs et al., 2002). Using a cdc42-EGFP live marker, labeling vesicular structures in ECs (Bayless and Davis, 2002) as well as red quantum dot, labeling the forming lumen, it was suggested that in the ISVs these single cells are hollowed out by the stepwise intracellular fusion of vacuoles and vesicles formed *de novo* at distinct sites within the ECs. Here, the intra- and intercellular fusion of these vesicles is thought to extend a growing lumen in a stepwise manner, resulting in seamless vessels (Kamei et al., 2006). However, using our reporter system (Figure 17, p.51), we observed strong morphogenetic movements, i.e. cell shape changes represented by the continuous invagination of membrane into and finally through contacting tip cells of ISVs (Figure 23, p.57 and Movie 4). Specified as an apical membrane, as shown with the Pdxl2 antibody (Figure 24, p.58), this membrane is continuously invaginating through a single, seamless tip cell, with no junctions detected along its whole axis (Figure 24, p.58 and Figure 25, p.59) until the luminal invaginationit reaches and coalesces with the apical compartments at the site of contact. This behavior of membrane invagination generates an extracellular space, the lumen, which continuously extends and passes through the tip cell, and thus can be termed a “transcellular” lumen (Figure 24, p.58 and Figure 25, p.59). This finding is different to the previously proposed model of a stepwise cell hollowing or extension of a lumen through vacuolar fusion events. Furthermore, we did not see any intracellular vesicular/vacuolar fusion events, when doing live imaging experiments using an endothelial specific moesin-EGFP zebrafish reporter line (data not shown and personal communication with Elin Ellertsdottir, Affolter lab).

The membrane invagination mechanism we describe is quite similar to a fusion mechanism in the tracheal system of *Drosophila melanogaster*, where two single tracheal cells of the dorsal trunk, called fusion cells, connect two individual branches to each other (Samakovlis et al., 1996; Tanaka-Matakatsu et al., 1996). During this fusion event, these special fusion cells establish a new contact, demarcated by DE-cadherin which is essential for contact formation (Uemura et al., 1996), and then, systematically, invaginate their membranes towards the common contact site. This results in two seamless “doughnut shaped” cells that interconnect the two former individual sprouts by a continuous lumen. In our model of membrane invagination, we suggest that the growing and invaginating apical membrane in

the tip cell of anastomosing ISVs fuses with the apical membrane which was formed *de novo* at the site of contact between the neighboring tip cells (Figure 25, p.59). Unfortunately, we have not been able to directly follow this membrane fusion event *in vivo*. However, in the tracheal system of *Drosophila melanogaster*, Samakovlis and colleagues proposed that during the fusion mechanism of the tracheal fusion cells, small vesicles assemble in a linear fashion throughout the fusion cells, fuse to each other and finally facilitate the connection with the apical membrane facing the neighboring fusion cell. Thereby, a continuous lumen between the fusion cells is generated (Samakovlis et al., 1996). Two recent studies have resolved these events in more detail. Inside the fusion cells, microtubular tracks, associated with F-actin, are thought to span through the fusion cell along the future luminal axis. These tracks are then used to connect the two apical membranes, the one facing the contact side and the one of the luminal tip invaginating into the fusion cell. Here, guided apical membrane invagination occurs since small membranous vesicles are thought to be transported and localized by these tracks to the growing invaginating membrane and thus, drive its invagination and growth. Finally the two apical membranes become juxtaposed and localized membrane fusion, probably facilitated by vesicle-to-vesicle and vesicle-to-plasma membrane fusion, occurs in this narrow space and causes the opening of the tube (Lee and Kolodziej, 2002; Kakihara et al., 2007). Moreover, it was shown that a mutant of Arf-like 3, a small GTPase that localizes the exocyst complex to the fusing membranes, fails to undergo the intracellular fusion event. Proper localization of the exocyst might thus be a key step in intracellular membrane fusion (Kakihara et al., 2007). Whether these mechanisms are also at work during ISV fusion will be interesting to see. Thus, taken together, our proposed model of membrane invagination into and through the tip cell to at least one of the contact sites resembles the mechanisms that have been described in the tracheal system and thus does not exclude the existence of, probably, very small apical vesicular structures. But it is more likely that such vesicles are transported towards the invaginating membrane where they are integrated by membrane fusion and drive its growth and invagination. Whether this membrane growth is guided in a similar way by microtubular tracks and why the membrane is only growing towards one of the contact sites will be interesting to see. New zebrafish lines such as an UAS:Gtuba2 line (Asakawa and Kawakami, 2010), encoding a GFP tagged version of one of the subunits of the tubulin heterodimer might help to solve these questions.

6.1.3 Fusion by cord hollowing mechanism

In the cord hollowing mechanism, at least three cells migrate, rearrange and thereby bring together two apical membrane compartments at a new contact site, which results in their coalescence and thus the formation of a continuous luminal space. Cord hollowing mechanisms have been described in several systems, for instance, during formation of the

mouse dorsal aorta, the zebrafish intestine and the neural tube (Strilic et al., 2009; Bagnat et al., 2007; Munson et al., 2008). However, in the cord hollowing mechanism in the fusing ISVs that leads to the formation of a multicellular tube, lumen formation is based on cell rearrangements rather than the expansion of small lumens. A very similar mechanism to our proposed model of cord hollowing has been described in the larval stage of the ascidian *Ciona intestinalis* (Dong et al., 2009). Here, a multicellular rod-like cord consisting of about 40 notochordal cells is hollowed out by subsequent cell rearrangements resulting in a multicellular tube. In our model, we suggest that during the cord hollowing mechanism, two individual apical membrane compartments are brought together by cell rearrangements of two outer cells over a central tip cell and that dislocation of the latter results in lumen coalescence (Figure 25, p.59 and Movie 3). Since ECs are extremely thin and elongated in the ISVs, we were not able to resolve this dislocation properly. This dislocation, however, is well seen in the notochordal system of *Ciona intestinalis*, where in the rod-like cord, two cells that initially are not in contact with each other, rearrange over a common neighboring central cell until they contact each other and form a new contact site as indicated by an E-cadherin reporter. As the two outer cells contact each other, the central cell in-between retracts or dislocates, loses its radial symmetry and becomes endothelial-like and part of a multicellular tube. This dislocation results in the coalescence of two neighboring luminal spaces that have been built between the central cell and its two outer neighboring, rearranging cells, prior to their described morphogenetic movements (Dong et al., 2009). Thus, formation of a new junction at the site of contact between the individual compartments and the fast inflating lumen within this region (see Movie 3 and Figure 22, p.56) demonstrate that the two individual membrane compartments must have coalesced, which *per se* is a clear sign of the dislocation of the central cell.

6.1.4 Blood pressure driving apical polarization and membrane invagination

In most cases, epithelial cells have one basolateral and one apical side facing the lumen (Andrew and Ewald, 2010). The tip cell in the ISV is somewhat special since it has to establish an apical surface at three distinct locations that somehow will be transformed into one continuous apical membrane during the vessel fusion process (see also 6.1.5, p.82). These sites are found at the connection to a stalk cell as well as at the newly forming contact sites anterior and posterior to the tip cell (Figure 21, p.55 and Figure 24, p.58). We found blood pressure to be essential to drive apical membrane invagination since in embryos that lack blood pressure (Figure 24, p.58), Pdxl2 is only found between junctions in multicellular regions and is totally absent in unicellular regions. This suggests that pressure drives apical polarization and membrane invagination. Thus, most likely, the tip cell uses first the contact

sites as a landmark or instructive cue regarding polarization (see also 6.1.1, p.77) and then, later, blood pressure as an instructive signal to drive invagination of the membrane. Interestingly, the fusion cells in the dorsal branches of the tracheal system face a similar issue since these cells are connected to a stalk cell, a terminal cell and undergo a fusion event with a neighboring fusion cell. This means, they also have to establish three apical sites at distinct locations that have to be transformed into one continuous apical membrane, which outlines or faces the lumen. However, here, other driving forces than pressure might be responsible for membrane invagination (Gervais et al., 2011 and personal communication A. Ochoa-Espinosa, Affolter lab).

6.1.5 Further considerations and fusion events

To generate a fully lumenized tube, the tip cell will have to bring together its three individual apical membranes by either one of the mechanisms described in this thesis. However, in the movies we analyzed we found that only one of the apical compartments at the contact sites initially coalesced with either an invaginating membrane or with the apical membrane compartment between the tip cell and the stalk by cord hollowing mechanism. How is then the other contact site integrated later into the fusion process? We have not yet fully elucidated how this happens. However, we have seen that at 48hpf fully lumenized unicellular cells exist (Figure 20, p.55), suggesting that a membrane invagination mechanism, as we have described, most likely must have hollowed out the whole cell. It is likely, that this happens in a second membrane invagination process from the side of the DLAV. We have also seen that membrane invagination can follow the cord hollowing mechanism to complete the fusion process (see Movie3, time point 03:45 – 04:55). Most likely, the cells can use these two mechanisms as modules and integrate them into the fusion process where and when they are needed. However, it will be interesting to identify the cues - when and why the two mechanisms are chosen - and molecular key players that trigger and regulate these two mechanisms. Blood pressure seems to be the main driving force for membrane invagination (Figure 24, p.58 and see above). Furthermore, it takes more cells to undergo fusion by cord hollowing. Therefore, does cell number play a role? Does a multicellular environment favor a fusion event by cord hollowing? As seen in the fusion events between the two neighboring DLAVs, these short already lumenized sprouts, budding from a single cell (Figure 36, p.107 and Movie 9), fuse very likely by a membrane invagination mechanism. It will be interesting to see and compare fusion events at distinct anatomical sites and stage of development when different levels of blood pressure and number of ECs are available and to see what other mechanisms cells can use to efficiently generate capillary networks.

As we have shown, contact formation between filopodial extensions of fusing endothelial intersegmental sprouts is demarcated by a dot-to-ring like behavior of junctional complexes (Figure 21, p.55). I have further shown that also secondary sprouts and sprouts from the two neighboring DLAVs behave according to this model (Figure 30, p.64 and Figure 31, p.65). These two latter types of sprouts grow out and make contact to other vessels as lumenized sprouts, which is in contrast to the ISVs which are not lumenized. The ISVs at sites of vessel fusion first make contact and then subsequently form a lumen *de novo*. I further observed that the filopodial extensions in both situations connected to junctional complexes localized between the ECs of the previously formed target vessels. Thus, the new junction was integrated into an established network of junctions. It will be interesting to see whether such later sprouts can only connect to established junctions and whether an increased cell number, i.e. increased number of junctions, would facilitate fusion events. However, fusing endothelial sprouts may also connect and form a ring at the cytoplasm of patent vessels. Interestingly, such an observed junctional connection immediately got integrated into the junctional network by cell rearrangements of the fusing vessels (pers. communication with A. Lenard, Affolter lab). Such efficient integration might be partially explained by the tendency of cells to maximize their interadhesive-bonding energy (see below).

Fusion events in the endothelium are not only restricted to small diameter vessels or capillaries as we have described in our study (Herwig et al., 2011). Larger diameter blood vessels might be formed by fusion events between neighboring smaller blood vessels, as it has been observed in the formation of the descending dorsal aorta (Drake and Fleming, 2000) which is formed by the fusion of smaller bilateral aligned multicellular vessels, the dorsal aortae. Further, at early stages during endocardium formation, multiple endothelial tubes at the midline of the heart are observed which are later transformed into a single blood vessel, the endocardium (Drake et al., 2006). Uniluminal vascular spheroids (multicellular spheres derived from VEGF stimulated embryonic mouse allantois tissue, cultured in hanging drops (Gentile et al., 2008)) have recently been shown to serve as a model for blood vessel assembly, since individual uniluminal vascular spheroids may fuse to each other (Fleming et al., 2011). During these spheroidal fusion events, the cells behave according principles that underlie the differential adhesion hypothesis (DAH). This hypothesis suggests that cells of a mobile, cohesive cell population rearrange in such a way that their inter-adhesive bonding energy is maximized whereas the free energy of the system is minimized (Steinberg, 2007). The morphological behavior of these spheroids during fusion is very similar to the events that have been described during the fusion of the dorsal aortae which suggests that *in vivo* anastomosis of blood vessels may involve a mechanism similar to DAH (Fleming et al., 2011). Furthermore, a novel *in vitro* approach allows the guided formation of perfusable blood vessels and vascular fusion in a microfluidic device consisting of two main

channels and ladder-like microstructures (Yeon et al., 2011). Further, after transplantations, it is critical that the engrafted tissue gets perfused fast and efficiently. A recent study demonstrates that transplanted engineered blood vessels anastomose with the host vasculature in a so called “wrapping and tapping” mechanism. Here, the implanted ECs first wrap around the host vessels at the host-implant interface and cause the reorganization of pericytes and eventually the replacement of the underlying host endothelium and thereby anastomose with the host vessels (Cheng et al., 2011).

6.1.6 Concluding remarks

For the first time, we have described *in vivo* at the single cell level the morphogenetic events that underlie vascular network formation, i.e. vessel fusion or anastomosis, which is essential for normal development and growth of a vertebrate embryo. In general, such single cell resolution analysis as well as the identification of key players will allow a more detailed understanding of the biological processes underlying angiogenesis and probably can be compared to other tubular systems such as the kidney or lung. Detailed morphogenetic and molecular understanding will provide new target sites to design novel drugs interfering with tumor angiogenesis and other vascular processes. Considering this, the combined expertise from (novel) *in vitro* systems (see above) and *in vivo* models, plus the use of novel techniques will not only lead to rapid advances in our understanding of vascular development but will also be of major advantage regarding the design of novel therapeutic treatments.

6.2 The UAS/Gal4 system

The Gal4/UAS system allows indirect expression of any gene of interest in a spatiotemporal manner. Furthermore, transgenes are expressed at high levels when using this system (see also 4.3, p.39). This provides an excellent condition for the expression of an EGFP-hZO1 Gal4-dependent transgene in the endothelium. The expression of an EGFP-hZO1 transgene under the direct control of an endothelial promoter element (flk1) (Jin et al., 2005) was unsuccessful due to several problems, such as toxicity and weak expression levels (personal communication with M. Affolter and H-G. Belting, Affolter lab). Thus, to specifically label endothelial cell-cell junctions, I have adapted the Gal4/UAS system to the vasculature in the zebrafish and generated several transgenic zebrafish lines, including an UAS:EGFP-hZO1 reporter line.

6.2.1 Considerations regarding different Gal4 variants

Initially the Gal4/UAS system was designed for the use in *Drosophila melanogaster* (Brand and Perrimon, 1993; Fischer et al., 1988) but had been soon after adapted to the zebrafish

(Scheer and Campos-Ortega, 1999). The expression of full-length Gal4 and 5 identical copies of UAS sites in the embryo, however, resulted in weak expression of UAS-driven transgenes. Most likely, these weak expression levels resulted from concatemerized transgene integration, which made those transgenes a target for gene silencing (Goll et al., 2009; Akitake et al., 2011) and see below). Thus, to compensate for the weak expression levels Köster and Fraser introduced Gal4-VP16, a more potent Gal4 variant, as well as a 14xUAS multicopy site (Köster and Fraser, 2001; Rorth, 1996; Scheer and Campos-Ortega, 1999 and see below). Later, Tol2 transgenesis technique was introduced, which is thought to allow the integration of transgenes as single copies, preventing the silencing problems caused by concatemerization (Kawakami et al., 2004; Kawakami et al., 2000). Gal4-VP16 is a recombinant protein which encodes the 147 amino acid DNA binding domain of full-length Gal4 and the 58 carboxy-terminal amino acids of the transcriptional activation domain from herpes simplex virus gene *vp16* (Sadowski, 1988)**.** Its modification lead to increased expression levels of transgenes but a high degree of toxicity, i.e. lethal developmental defects were observed and no stable transgenic lines were generated. ‘‘Squelching,’’ the overexpression of a strong transcription activator, for instance Gal4VP16, can cause the inhibition of gene expression by the titration of other transcription factors of the transcription machinery that interact with the activation domain of the overexpressed transcriptional activator (Sadowski, 1988; Gill and Ptashne, 1988). However, a more recent study found only episomal genes to be “squelched”, whereas genes integrated into the chromatin were immune (Rivera et al., 1997), suggesting a reconsideration for the described squelching effect. Whatever the explanation for the observed toxicity, less toxic versions of Gal4-VP16, i.e. Gal4FF and KalTA4 (Distel et al., 2009; Asakawa et al., 2008) have been recently generated. Gal4FF encodes the DNA binding domain of Gal4 plus two 13 amino acid long modificated transcriptional activation domains of VP16 that contain a critical phenylalanine (FF= 2xPADALDD**F**DLDML), whereas KalTA4 encodes a 5’-Kozak sequence (GCCGCCACC) followed by the DNA binding domain and three minimal transactivation domains TA4 (TA4=PADALDD**F**DLDML-PADALDD**G**DLDML-PADALDD**Y**DLDML) (Baron et al., 1997). KalTA4 is codon optimized for the use in zebrafish and a luciferase assay using 5xUAS sites showed 1.5 fold stronger activation than Gal4TA (no Kozak sequence), which itself reaches 74% of the activation level of Gal4VP16 (Distel et al., 2009)**.** Since Gal4VP16 had been shown to be toxic in the zebrafish, I specifically used Gal4FF to generate the endothelial specific Gal4 line (Tg(fli1ep:Gal4FF)$^{ubs2-4}$). In our hands, over several generations, no detectable reduction in the expression level or a toxicity (i.e. embryonic developmental defects or lethality) was observed. Although KalTA4 is codon optimized for the use in zebrafish, both versions are strong activtors and either version, i.e. Gal4FF or KalTA4, is suitable to efficiently drive Gal4-dependent transgenes (pers. communication with

M. Distel, Köster lab). It should be mentioned that all these different versions of the original full-length Gal4 are lacking the transcriptional activation domain ARII of Gal4, which is the essential Gal80 binding site, preventing the transcriptional machinery to be recruited when bound by Gal80 (Ptashne and Gann, 2002). Thus, to generate conditional expression systems using KalTA4 or Gal4FF, other techniques than the use of Gal80 will be needed (see also 6.2.4, p.90). However, despite the availability of the more potent Gal4 derivatives described above, the Chien lab showed that native Gal4 mediated expression but not Gal4VP16 mediated expression of a UAS:GFP-reporter line was inhibited by Gal80. In addition, a temperature sensitive Gal80 was shown to permit or restrict Gal4-mediated expression at high or lower temperatures, respectively (Fujimoto et al., 2011).

6.2.2 Considerations regarding different UAS variants

I was able to generate a Gal4 dependent 14xUAS responder line which visualizes cell-cell junctions by the localization of EGFP-hZO1 at tight junctions. However, the expression pattern of the transgene in this line is extremely mosaic and the expression level of EGFP-hZO1 was further reduced over generations (G0 – F4, personal observation/communication between L. Herwig and Y. Blum and A. Lenard, Affolter Lab). This behaviour is most likely due to epigenetic silencing effects, for instance DNA methylation. In vertebrates DNA (de-)methylation, the covalent addition or removal of a methyl group to a cytosine nucleotide, occurs only at a cytosine followed by a guanine residue, a CpG dinucleotide, and is regulated by DNA methyltransferases (DNMTs). The reversible adding of such methyl groups changes the normal biophysical characteristics of the DNA and is thought to have two major effects, which are inhibition and facilitation of protein binding (Hamilton, 2011; Gibney and Nolan, 2010). DNA methylation is thought to repress genes and has been shown to silence genes in plants, vertebrates and fungi, but is, however, absent in many invertebrate organisms (Miranda and Jones, 2007; Goll and Bestor, 2005). In vertebrates, tandem repeats are thought to be frequently methylated and thus silenced (Garrick, 1998; Miranda and P. A. Jones, 2007). In mice, the homozygous loss of the DNA methyltransferase gene results in strong developmental defects and lethality (Li et al., 1992), which demonstrates that methylation is an essential process during development. The 14x(CGG-N11-CCG)-UAS cassette[1] (Rorth, 1996) I used to generate the EGFP-hZO1 responder line is a tandem repeat and is rich in CpG dinucleotides and thus, very likely, represents a target of methylation and silencing. In a recent study in 2009, Goll and colleagues, have shown that

[1] 14xUAS =
CGGAGTACTGTCCTCCGGGCTGG**CGGAGTACTGTCCTCCG**GCAAGGT**CGGAGTACTGTCCTCCG**ACACTAGAGGT**CGGA**
GTACTGTCCTCCGACGCAAGG**CGGAGTACTGTCCTCCG**GGCTG**CGGAGTACTGTCCTCCG**GCAAGGT**CGGAGTACTGTC**
CTCCGACACTAGAGGT**CGGAGTACTGTCCTCCG**ACGCAAGGT**CGGAGTACTGTCCTCCG**ACACTAGAGGT**CGGAGTACT**
GTCCTCCGACGCAAGGT**CGGAGTACTGTCCTCCG**ACACTAGAGGT**CGGAGTACTGTCCTCCG**ACGCAAGG**CGGAGTACT**
GTCCTCCGGGCTGG**CGGAGTACTGTCCTCCG***GCAAGGGTCGACTCTAGAGGGTATATAATGGATCCCATCGCGTCTCAGC*
CTCACTTTGAGCTCCTCCACAC

this is indeed the case. In this study they used a fluorescent, self-reporting Gal4-VP16 gene/enhancer trap vector and monitored the epigenetically controlled down-regulation (i.e. DNA methylation of the multicopy UAS) of this reporter construct. Initially, stable self-reporting lines showed strong and robust fluorescence, which got mosaic and finally disappeared after several generations. This demonstrates that the silencing effect is heritable, however, it can be reactivated by the increase of Gal4-VP16 expression levels or in mutants lacking DNA methyltransferase-1 (dnmt1) (Goll et al., 2009). The mosaicism we experienced is to some extend advantageous regarding the description of single cellular behaviors during morphogenetic events such as the fusion of neighboring ISVs. If only very few cells express the construct in a visible manner (Figure 22, p.56 and Figure 23, p.57), the labeled junctions can be more easily assigned to individual single cells. A single cell expressing EGFP-hZO1 labels *per se* all its contacts to neighboring cells, and as soon as an unlabeled cell contacts a labeled cell, the new junction becomes visible. Thus, the relative behavior of single cells regarding neighboring cells can be analyzed using such a mosaic reporter line. This facilitated the deciphering and analysis of the two processes described in this thesis (Figure 25, p.59) but made it also extremely time consuming to collect a decent amount of data (time lapse movies) that could be analyzed and quantitated.

In the publication Herwig et al., 2011 we have described the basic behaviors during vessel fusion at the cellular level but we have not yet deciphered the molecular key players controlling this process. The fast analysis of wild type fish, mutants, morphants or chemically treated embryos in a highly mosaic reporter line is tedious, since screening for EGFP-hZO1 positive cells in a mosaic line is time consuming. A junctional reporter line labeling all the endothelial cells, thus, would greatly facilitate the identification of such molecular regulators and their function during the fusion process. Single insertions of a 4x non-repetitive UAS GFP-reporter (4Xnr; four distinct **UAS sites** and a *minimal promoter*)[2] have been shown to be less silenced over three generations in zebrafish larvae than insertions encoding 14 of the same UAS sites (Akitake et al., 2011). Further, to improve expression levels, Distel et al. introduced a GI domain (GI = rabbit β-globin intron) between the stop codon and polyA signal of UAS-driven transgenes which is supposed to increases gene expression as splicing targets the mRNA for nuclear export (Distel et al., 2009; Adam et al., 1995; Perz-Edwards et al., 2001)**.** This might be considered advantageous when working with large open reading frames such as the one of ZO1 which is about 5,3 kb in size. Thus, I cloned a 4XnrUAS:EGFP-hZO1 construct and tested its functionality in transient expression experiments (Figure 32, p.66). It will be interesting and useful to see, whether we can raise a

[2] 4Xnr =
CGGTGGCTTCTAATCCGTGAGTCCTAG**CGGGTGACAGCCCTCCG**TCTTCACAGG**CGGAGGAGAGTCTTCCG**TAGGGTTC CT**CGGAGTACTGTCCTCCG**ACGCGT*GCAAGGGTCGACTCTAGAGGGTATATAATGGATCCCATCGCGTCTCAGCCTCACTT TGAGCTCCTCCACACG*

stable transgenic line expressing this construct. In addition L. Sauteur (Affolter lab) has used the same 4XnrUAS background and does see strong transient and rather uniform expression of different fluorescent reporters in the endothelium (personal communication L. Sauteur). Interestingly, the KAEDE-reporter line encodes the 14xUAS multicopy cassette and has been stable over several generations in our lab. In some of these fish, however, mosaic or weaker expression was detected and in other lines without the 14xUAS cassette a similar phenomenon was observed (pers. communication K. Hatta, Center for Developmental Biology, Riken, Japan). Taken together, depending on the type of experiment, it might be of advantage to generate either a transgenic line encoding 4XnrUAS sites, which should result in a more uniform expression pattern or 14xUAS sites of the same type, where mosaics are more likely to be expected. However, the site of transgene integration (positional effects), is probably still a main issue regarding the generation of good UAS reporter lines (see below).

6.2.3 Technical observations and comments regarding the Gal4/UAS system

The generation of transgenic lines is time consuming, first of all the screening for positive founder fish. Since UAS-driven transgenes in the absence of Gal4 are not visible, founder fish have to be analyzed in a Gal4 background or by PCR technique. In addition, more than one founder fish has to be identified since the genetic environment of site of transgene integration might influence the transgene expression in an enhancing or repressing way (positional effects), which makes it even more time consuming to find good effector lines. It might be possible, that an endogenous enhancer directly interacts with the minimal promoter of the UAS cassette and thus activates the UAS-transgene in a Gal4-independent manner ((Davison et al., 2007) and pers. communication with K. Kawakami, Kawakami lab and M. Müller, Affolter lab)). I have used a *cmlc*2:EGFP transgenesis-cassette, labeling the heart in green (Huang et al., 2003; Kwan et al., 2007; Auman et al., 2007), which facilitated the screening process regarding UAS positive founder fish and later during the screening when doing experiments. This cassette is supposed to be silent in all other tissues except the developing heart. However, if the heart marker cassette is in very close relation to an UAS-driven transgene, the *cmlc2* control region might interact with the UAS sites in one or the other direction (pers. communication with M. Müller, Affolter lab). I have screened G0 and F1 transgenic zebrafish that encode the heart marker cassette upstream of a 5xUAS:life-act-MkOrange cassette in reverted orientation. In this situation, an up-regulation of the otherwise silenced heart marker cassette is likely expected, i.e. the UAS sites upon Gal4FF binding would also activate to some extend the heart marker cassette resulting in a cytoplasmic EGFP background in endothelial cells. Interestingly, in these fish, the heart marker most likely down-regulated the UAS-transgene since I neither observed an EGFP background or

UAS-driven life-act-MkOrange expression, when crossing F1 fish to the endothelial specific Gal4-driver line. The recovered positive founder and F1 fish exclusively expressed EGFP in the heart (data not shown). Interestingly, a 5xUAS-driven rabbit-gp135-RFP (gp135 = podocalyxin), again in the same background (line engineered by Y. Blum), efficiently expressed the transgene but unfortunately displayed a rather cytoplasmic expression pattern of the gp135-RFP and was mosaic to some extend and thus not further analyzed (data not shown). It is of course extremely difficult to explain what is responsible for these variations regarding the UAS transgene expression or repression we experienced when using this *cmlc2*:EGFP-5xUAS background. One explanation might be that in some cases the heart marker cassette simply silences the transgene. Another explanation might be the lack of a real minimal promoter downstream of the 5xUAS element, which in these fish precedes only a minimal TATA sequence. This should result in a weak or even total absence of transcription (pers. communication M. Müller, Affolter lab). However, the transgenic UAS:RFP and UAS:GFP fish, that have been generated encode this minimal TATA element, and show robust and strong expression (Asakawa et al., 2008). The same is true for the Tg(UAS:VEcadΔCD-EGFP) line I generated. It displays strong and uniform expression of the transgene (Figure 27, p.62). It should be mentioned that this three lines mentioned do not encode the heat marker cassette. One might speculate that differences such as the length of DNA between the TATA box and the ATG of the gene of interest might influence transcription or ribosomal binding. If this spacing DNA is too short, transcription might be very inefficient and later also ribosomes fail to bind and thus no or very inefficient translation might occur or transcription itself does not take place at all (pers communication with M. Müller, Affolter lab). However, the VEcad-reporter line does not have a large spacer (4.4.2.4, p.44) and is fully functional regarding transcription and translation (Figure 27, p.62). For the future, I recommend to use an UAS background that encodes a real minimal promoter. The 14xUAS and 4xnr constructs do have such a minimal promoter (E1b) (see figures X and Y). It is a compact promoter of 49 bp and encodes a TATA box (5'-TATATAAT-3') preceding an initiator element from the common carp (Carpio carpio) β-actin gene (5'-CATCGCGTCTCAGC-3') that controls the transcriptional initiation. The last residue corresponds to the +1 nucleotide of polII transcripts (Huang et al., 2006). Further, in the 14xUAS:EGFP-hZO1 line the heart marker cassette is cloned downstream in reverted orientation of the UAS-driven EGFP-hZO1 and thus might not influence the UAS sites (Kwan et al., 2007). This should be considered for future constructs too if a transgenesis cassette is planned to be integrated.

As discussed above, improving techniques can be extremely helpful for the generation of transgenic lines as described in this thesis, but at the same time cause new issues to think

about. Taken together, I suggest, to clone and engineer, UAS-driven constructs/lines in several versions (i.e. with and without a transgenesis cassette, different number of UAS sites) and to carefully analyze what the constructs look like regarding their sequence, locus and relative position between the different coding regions to minimize genetic interference and maximize the expression level of the transgenes.

6.2.4 Outlook

Different groups in the field are constantly improving various components of the Gal4/UAS system (Distel et al., 2009; Köster and Fraser, 2001; Goll et al., 2009; Asakawa et al., 2008). However, none of this group, to date, has established an efficient (fast and accurate, non-leaky) system, that allows "experimentator controlled" conditional expression of a transgene regarding both, space and time, in the endothelium. Such a system, would allow specific overexpression of genes, such as dominant-negative receptors, during the vessel fusion process *in vivo* at the single cellular level. A recent study (Kennedy et al., 2010) has engineered a light inducible *protein-protein interaction system* using two proteins involved into the flowering process of *Arabidopsis thaliana.* Here, illumination by blue light causes dimerization of a basic-loop-helix protein CIB1 and cryptochrome 2 (CRY2), which is a blue light-absorbing photo-sensor that can bind the CIB1 protein when photo-excited (Liu et al., 2008). The group adapted the system to Gal4, and blue light-dependent UAS-driven expression of a reporter was observed in cell culture and thus, might be suitable for the use in zebrafish. However, this system is possibly leaky or it does need a long illumination phase to induce interaction in a certain depth within the tissue of the zebrafish (pers. communication with O. Biehlmaier, Imaging Core Facility (IMCF), Biozentrum Basel). Further, only fluorescent reporters which are illuminated above 500nm can be followed using this system. Another possibility would be to use a photo-activatable CreER^{T2}-system that has recently been designed and reported to be functional and reaching high spatiotemporal resolution. Here a photo-inducible ligand (caged 4-OH cyclofen) is un-caged and activates a CreER^{T2} fusion protein. In a Tg(Eef1α:loxP-GFP-loxP-dsRed2) zebrafish line single cells in the retina have been successfully reported to express dsRed upon two-photon illumination (Resolution et al., 2010). Combination with the Gal4 system (loxP-Gal4-loxP) or a direct Gal4ER^{T2} fusion protein expressed in the vasculature is thinkable. Further, such a system in combination with "cre-recombinase" and "flipase" based insertional mutagenesis as reported by different groups (Madison meeting 2010) might allow to turn mutated genes from ON-OFF-ON or OFF-ON-OFF, respectively, in single cells. It will be useful to adapt/generate such a system described above in combination with Gal4 or alone to analyze at the single cellular level molecular/morphogenetic mechanisms or mutant cells during morphogenetic processes in the endothelium.

6.2.5 Concluding remarks

New molecular technologies or their adaption to the fish field, are growing fast. Examples are: BAC-recombineering (www.ncifcrf.gov/research/brb/protocol.aspx), Tol2 transgenesis (Kawakami et al., 2000), Gal4/UAS system (Scheer and Campos-Ortega, 1999), Cre-Lox system (Langenau et al., 2005; Pan et al., 2005), zinc-finger mutagenesis technique (Meng et al., 2008) or the use of caged morpholinos to down regulate genes at a given time point (Shestopalov et al., 2007) or protein knockout mediated by anti-GFP nanobody (Caussinus et al., 2011). The innovation regarding the engineering and screening for new or improved technologies, and first of all, their combination, will allow to answer biological questions in a more detailed way.

7 Acknowledgements

Sincere thanks goes to Prof. Dr. Markus Affolter who gave me the opportunity to do my PhD thesis in his lab. I specially want to thank him for the great scientific support I experienced during the four years of my PhD. The scientific freedom young students get in his lab enables and encourages discovering the world of biology and science in an enthusiastic way. I very positively think about the Gordon Research Conference on Vascular Cell Biology, held 2011 in Ventura (California), I was able to attend and give a talk, which is certain one of the many highlights during the time I spent in his lab. He always had an open ear and two open office doors for scientific as well as non-scientific issues/ideas to discuss. The great familiar atmosphere in his lab, including numerous parties, apéros, BBQs and skidays made working in his lab very comfortable.

A special thank goes to Yannick Blum who became a very good friend of mine. Together we had much scientific fun and thus, share now a first author ship on a fantastic Current Biology paper. We also spent funny times twice in NYC and on our mountain bikes.

I specially want to thank my parents for their great mental support during these four years.

I further want to thank Dr. Heinz-Georg Belting who always proposed me constructive ideas regarding my project and helped me a lot with preparation of seminars, talks and scientific writings. I also want to mention the other less scientific talking we had. Btw: thanks for letting me and Yannick know about “rose”-bikes.

I want to thank Dr. Elin Ellertsdottir for scientific discussions and her always immediate and enthusiastic help. I thank her for tolerating my, literally spoken, contemporary art project on my bench. I tried at least to change the exhibition twice a year. Further, I want to thank her for reading and improving this thesis.

Further thanks go to Alice Krudewig for much scientific help and the careful reading of this thesis as well as delicious dinners at her place.

I also want to thank Anna Lenard for discussions and “mad-dog”-caused hangovers.

Thank goes to Alex Weiss for many discussions, first of all non-scientifics, parties, “jewish new year” and swimming in summertime.

I thank Fisun Hamaratoglu for many encouraging discussions, with or without good wine.

Thank goes to Dimi Bieli, a young geneticist, who made working in the lab a lot of fun.

I of course want to thank Dr. Martin Müller for genetic discussions and Paul Baumgartner’s cloning tips and tricks.

I want to thank all other people that I have met in the Affolter lab during my PhD, who all helped and supported me.

I also want to thank Helen Preiss for great administrative support and nice talkings.

Last but not least I want to thank the people on the 2nd floor who helped me a lot, especially Kumuthini Kulendra, Karin Mauro, Bernadette Bruno, Gina Evora and Roland Kirchhofer.

8 References

Aberle, H., Butz, S., Stappert, J., Weissig, H., Kemler, R, and Hoschuetzky, H. (1994). Assembly of the cadherin-catenin complex in vitro with recombinant proteins. *Journal of cell science*, **107**, 3655-63.

Abràmoff, M. D., Hospitals, I., Magalhães, P. J., and Abràmoff, M. (2004) Image Processing with ImageJ. *Biophotonics International*, **11**, 36-42.

Achen, M. G., Jeltsch, M, Kukk, E., Mäkinen, T., Vitali, A, Wilks, AF., Alitalo, K, and Stacker, S. a (1998). Vascular endothelial growth factor D (VEGF-D) is a ligand for the tyrosine kinases VEGF receptor 2 (Flk1) and VEGF receptor 3 (Flt4). *Proceedings of the National Academy of Sciences of the United States of America*, **95**, 548-53.

Adam, A., Lin, S., and Hopkins, N. (1995). The Aequorea victoria Green Fluorescent Protein Cyn be Used as a Reporter in Live Zebrafish Embryos. *Developmental biology*, **171**, 123-129.

Adams, R. H. and Eichmann A, (2010),. Axon guidance molecules in vascular patterning. *Cold Spring Harb. Perspect. Biol.* **2**, a001875.

Adams, C. L., Nelson, W J, and Smith, S. J. (1996). Quantitative analysis of cadherin-catenin-actin reorganization during development of cell-cell adhesion. *The Journal of cell biology*, **135**, 1899-911.

Adams, R. H. and Alitalo, K (2007). Molecular regulation of angiogenesis and lymphangiogenesis. *Nature reviews. Molecular cell biology*, **8**, 464-78.

Affolter, M., Itoh, N., Shilo, B., Thiery, J.-Paul, and Werb, Z. (2003). Tube or Not Tube : Remodeling Epithelial Tissues by Branching Morphogenesis Branching morphogenesis involves the restructuring. *Developmental Cell*, **4**, 11-18.

Affolter, M., Zeller, R., and Caussinus, E. (2009). Tissue remodelling through branching morphogenesis. *Nature reviews. Molecular cell biology*, **10**, 831-42.

Akitake, C. M., Macurak, M., Halpern, M. E., and Goll, Mary G (2011). Transgenerational analysis of transcriptional silencing in zebrafish. *Developmental biology*, **352**, 191-201.

Alberts, J., Raff, L., and Walter, R. (2008). Molecular Biology of the Cell 5th edition. Garland Science, Taylor and Francis group. ISBN 978-0-8153-4105-5

Alitalo, Kari, Tammela, T., and Petrova, T. V. (2005). Lymphangiogenesis in development and human disease. *Nature*, **438**, 946-53.

Anderson, D. C., Gill, J. S., Cinalli, R. M., and Nance, J. (2008). Polarization of the C. elegans embryo by RhoGAP-mediated exclusion of PAR-6 from cell contacts. *Science (New York, N.Y.)*, **320**, 1771-4.

Andrew, D. J. and Ewald, A. J. (2010). Morphogenesis of epithelial tubes: Insights into tube formation, elongation, and elaboration. *Developmental biology*, **341**, 34-55.

Armer, H. E. J., Mariggi, G., Png, K. M. Y., Genoud, C., Monteith, A. G., Bushby, A. J., Gerhardt, Holger, and Collinson, L. M. (2009). Imaging transient blood vessel fusion events in zebrafish by correlative volume electron microscopy. *PloS one*, **4**, e7716.

Arnaoutova, I., George, Æ. J., Kleinman, H. K., and Benton, Æ. G. (2009). The endothelial cell tube formation assay on basement membrane turns 20 : state of the science and the art. *Angiogenesis*, 267-274.

Asakawa, K. and Kawakami, K (2010). A transgenic zebrafish for monitoring in vivo microtubule structures. *Developmental dynamics*, **239**, 2695-9.

Asakawa, K., Suster, M. L., Mizusawa, K., Nagayoshi, S., Kotani, T., Urasaki, A., Kishimoto, Y., Hibi, M., and Kawakami, Koichi (2008). Genetic dissection of neural circuits by Tol2 transposon-mediated Gal4 gene and enhancer trapping in zebrafish. *PNAS: Proceedings of the National Academy of Sciences of the United States of America*, **105**, 1255-60.

Assunção Guimarães, C. and Linden, R. (2004). Programmed cell deaths. Apoptosis and alternative deathstyles. *European journal of biochemistry / FEBS*, **271**, 1638-50.

Augustin, H. G., Koh, G. Y., Thurston, Gavin T, and Alitalo, K (2009). Control of vascular morphogenesis and homeostasis through the angiopoietin-Tie system. *Nature reviews. Molecular cell biology*, **10**, 165-77.

Auman, H. J., Coleman, H., Riley, H. E., Olale, F., Tsai, H.-J., and Yelon, D. (2007). Functional modulation of cardiac form through regionally confined cell shape changes. *PLoS biology*, **5**, e53.

Ausprunk, D. and Folkman, J. (1977). Migration and Proliferation of Endothelial Cells in Preformed and Newly Formed Blood Vessels during Tumor Angiogenesis. *Microvascular Research*, **65**, 53-65.

Avraamides, C. J., Garmy-Susini, B., and Varner, J. a (2008). Integrins in angiogenesis and lymphangiogenesis. *Nature reviews. Cancer*, **8**, 604-17.

Baer, M. M., Chanut-Delalande, H., and Affolter, M. (2009). Cellular and molecular mechanisms underlying the formation of biological tubes. *Current topics in Developmental Biology*, 1st ed. Elsevier Inc. ISSN 0070-2153

Bagnat, M., Cheung, I. D., Mostov, Keith E, and Stainier, Didier Y R (2007). Genetic control of single lumen formation in the zebrafish gut. *Nature cell biology*, **9**, 954-60.

Baron, U., Gossen, M., and Bujard, H. (1997). Tetracycline-controlled transcription in eukaryotes: novel transactivators with graded transactivation potential. *Nature*, **25**, 2723-2729.

Bayless, K. J. and Davis, G. E. (2002). The Cdc42 and Rac1 GTPases are required for capillary lumen formation in three-dimensional extracellular matrices. *Journal of cell science*, **115**, 1123-36.

Bernfield, M., Götte, M., Park, P. W., Reizes, O., Fitzgerald, M. L., Lincecum, J., and Zako, M. (1999). Functions of cell surface heparan sulfate proteoglycans. *Annual review of biochemistry*, **68**, 729-77.

Blum, Y., Belting, H.-G., Ellertsdottir, E., Herwig, L., Lüders, F., and Affolter, M. (2008). Complex cell rearrangements during intersegmental vessel sprouting and vessel fusion in the zebrafish embryo. *Developmental biology*, **316**, 312-22.

Bouvrée, K., Larrivée, B., Lv, X., Yuan, L., DeLafarge, B., Freitas, C., Mathivet, T., Bréant, C., Tessier-Lavigne, M., Bikfalvi, A., et al. (2008). Netrin-1 inhibits sprouting angiogenesis in developing avian embryos. *Developmental biology*, **318**, 172-83.

Brand, A H. and Perrimon, N. (1993). Targeted gene expression as a means of altering cell fates and generating dominant phenotypes. *Development*, **118**, 401-15.

Bretscher, A., Edwards, K., and Fehon, R. G. (2002). ERM proteins and merlin: integrators at the cell cortex. *Nature reviews. Molecular cell biology*, **3**, 586-99.

Brown, L. a, Rodaway, A. R. ., Schilling, Thomas F, Jowett, T., Ingham, P. W., Patient, R. K., and Sharrocks, A. D. (2000). Insights into early vasculogenesis revealed by expression of the ETS-domain transcription factor Fli-1 in wild-type and mutant zebrafish embryos. *Mechanisms of Development*, **90**, 237-252.

Brown, P. S., Wang, E., Aroeti, B., Chapin, S. J., Mostov, K E, and Dunn, K. W. (2000). Definition of distinct compartments in polarized Madin-Darby canine kidney (MDCK) cells for membrane-volume sorting, polarized sorting and apical recycling. *Traffic*, **1**, 124-40.

Bryant, D. M., Datta, A., Rodríguez-Fraticelli, A. E., Peränen, J., Martín-Belmonte, F., and Mostov, Keith E (2010). A molecular network for de novo generation of the apical surface and lumen. *Nature cell biology*, **12**, 1035-45.

Buechner, M. (2002). Tubes and the single C. elegans excretory cell. *Trends in cell biology*, **12**, 479-84.

Bär, T., Güldner, F. H., and Wolff, J. R. (1984). “Seamless” endothelial cells of blood capillaries. *Cell and tissue research*, **235**, 99-106.

Carmeliet, P. and Jain, R. K. (2011). Molecular mechanisms and clinical applications of angiogenesis. *Nature*, **473**, 298-307.

Carmeliet, P. and Tessier-Lavigne, M. (2005). Common mechanisms of nerve and blood vessel wiring. *Nature*, **436**, 193-200.

Carmeliet, P., Ferreira, V., Breier, G., Pollefeyt, S., Kieckens, L., Gertenstein, M., Fahrig, M., Risau, Werner, Moons, L., and Eberhardt, K. (1996). Abnormal blood vessel development and lethality in embryos lacking a single VEGF allele. *Nature*, **380**, 435-439.

Castets, M., Coissieux, M.-M., Delloye-Bourgeois, C., Bernard, L., Delcros, J.-G., Bernet, A., Laudet, V., and Mehlen, P. (2009). Inhibition of endothelial cell apoptosis by netrin-1 during angiogenesis. *Developmental cell*, **16**, 614-20.

Caussinus, E., Kanca, O., and Affolter, M. (2011). Fluorescent fusion protein knockout mediated by anti-*GFP nanobody. Nature Structural & Molecular Biology,* **19**, *117-1*21.

Chambers, R. C., Leoni, P., Kaminski, N., Laurent, G. J., and Heller, R. A. (2003). Global Expression Profiling of Fibroblast Responses to Transforming Growth Factor-β1 Reveals the Induction of Inhibitor of Differentiation-1 and Provides Evidence of Smooth Muscle Cell Phenotypic Switching. *The American Journal of Pathology*, **162**, 533-546.

Cheng, G., Liao, S., Kit Wong, H., Lacorre, D. a, di Tomaso, E., Au, P., Fukumura, D., Jain, R. K., and Munn, L. L. (2011). Engineered blood vessel networks connect to host vasculature via wrapping-and-tapping anastomosis. *Blood*, **118**, 4740-9.

Cheng, N., Brantley, D. M., and Chen, J. (2002). The ephrins and Eph receptors in angiogenesis. *Cytokine & growth factor reviews*, **13**, 75-85.

Childs, Sarah, Chen, J.-N., Garrity, D. M., and Fishman, Mark C (2002). Patterning of angiogenesis in the zebrafish embryo. *Development*, **129**, 973-82.

Chung, A. S. and Ferrara, Napoleone (2011). Developmental and Pathological Angiogenesis. *Annual Review of Cell and Developmental Biology*.

Cleaver, O and Krieg, P. (1998). VEGF mediates angioblast migration during development of the dorsal aorta in Xenopus. *Development*, **125**, 3905-14.

Coffin, J. and Poole, T. J. (1988). Embryonic vascular development: immunohistochemical identification of the origin and subsequent morphogenesis of the major vessel primordia in quail embryos. *Development*, **102**, 735-748.

Colas, J.-F. and Schoenwolf, G. C. (2001). Towards a Cellular and Molecular Understanding of. *Developmental Dynamics*, **145**, 117-145.

Costantini, F. and Shakya, R. (2006). GDNF/Ret signaling and the development of the kidney. *BioEssays : news and reviews in molecular, cellular and developmental biology*, **28**, 117-27.

Coultas, L., Chawengsaksophak, K., and Rossant, J. (2005). Endothelial cells and VEGF in vascular development. *Nature*, **438**, 937-45.

Cowin, P. and Wysolmerski, J. (2010). Molecular mechanisms guiding embryonic mammary gland development. *Cold Spring Harbor perspectives in biology*, **2**, a003251.

Datta, A., Bryant, D. M., and Mostov, Keith E (2011). Molecular regulation of lumen morphogenesis. *Current biology,* **21**, R126-36.

Davis, G. E. and Bayless, K. J. (2003). An integrin and Rho GTPase-dependent pinocytic vacuole mechanism controls capillary lumen formation in collagen and fibrin matrices. *Microcirculation*, **10**, 27-44.

Davis, G. E., Stratman, A. N., Sacharidou, A., and Koh, W. (2011). Molecular basis for endothelial lumen formation and tubulogenesis during vasculogenesis and angiogenic sprouting. *International Review of Cell and Molecular Biology*, **288**, 1st ed. Elsevier Inc. ISSN 1937-6448

Davison, J. M., Akitake, C. M., Goll, Mary G, Rhee, J. M., Gosse, N., Baier, H., Halpern, M. E., Leach, S. D., and Parsons, M. J. (2007). Transactivation from Gal4-VP16 transgenic insertions for tissue-specific cell labeling and ablation in zebrafish. *Developmental biology*, **304**, 811-24.

Dejana, Elisabetta (2004). Endothelial cell-cell junctions: happy together. *Nature reviews. Molecular cell biology*, **5**, 261-70.

Dickson, B. J. Netrins. *Current Biology*, **12**, 154-155.

Distel, M., Wullimann, M. F., and Ko, R. W. (2009). Optimized Gal4 genetics for permanent gene expression mapping in zebrafish. *PNAS*, **106**, 13365-13370.

Djonov, V. G., Kurz, H., and Burri, P. H. (2002). Optimality in the developing vascular system: branching remodeling by means of intussusception as an efficient adaptation mechanism. *Developmental dynamics*, **224**, 391-402.

Dong, B., Horie, T., Denker, E., Kusakabe, T., Tsuda, M., Smith, W. C., and Jiang, D. (2009). Tube formation by complex cellular processes in Ciona intestinalis notochord. *Developmental biology*, **330**, 237-49.

Drake, C J and Fleming, P a (2000). Vasculogenesis in the day 6.5 to 9.5 mouse embryo. *Blood*, **95**, 1671-9.

Drake, C J, Davis, L. a, and Little, C D (1992). Antibodies to beta 1-integrins cause alterations of aortic vasculogenesis, in vivo. *Developmental dynamics*, **193**, 83-91.

Drake, Christopher J, Wessels, A., Trusk, T., and Little, C. D. (2006). Elevated vascular endothelial cell growth factor affects mesocardial morphogenesis and inhibits normal heart bending. *Developmental dynamics*, **235**, 10-8.

Ebnet, K., Suzuki, A., Ohno, S., and Vestweber, D. (2004). Junctional adhesion molecules (JAMs): more molecules with dual functions? *Journal of cell science*, **117**, 19-29.

Eichmann, A., Le Noble, F., Autiero, M., and Carmeliet, P. (2005). Guidance of vascular and neural network formation. *Current opinion in neurobiology*, **15**, 108-15.

Elmore, S. (2007). Apoptosis: a review of programmed cell death. *Toxicologic pathology*, **35**, 495-516.

Eriksson, J. and Löfberg, J. (2000). Development of the hypochord and dorsal aorta in the zebrafish embryo (Danio rerio). *Journal of morphology*, **244**, 167-76.

Esko, J. D. and Lindahl, U. (2001). Molecular diversity of heparan sulfate. *Medical Biochemistry*, **108**, 169-173.

Factor, E. G., Dvorak, Harold F, Brown, L. F., Detmar, M., and Dvorak, A. M. (1995). Review. *Angiogenesis*, **146**, 1029-1039.

Feng, W., Wu, H., Chan, L.-N., and Zhang, M. (2008). Par-3-mediated junctional localization of the lipid phosphatase PTEN is required for cell polarity establishment. *The Journal of biological chemistry*, **283**, 23440-9.

Ferber, A., Yaen, C., Sarmiento, E., and Martinez, J. (2002). An octapeptide in the juxtamembrane domain of VE-cadherin is important for p120ctn binding and cell proliferation. *Experimental cell research*, **274**, 35-44.

Ferrara, N. (2009). Vascular endothelial growth factor. *Arteriosclerosis, thrombosis, and vascular biology*, **29**, 789-91.

Ferrara, N., Carver-Moore, K., Chen, H., Dowd, M., Lu, L., and Moore, M. (1996). Heterozygous embryonic lethality induced by targeted inactivation of the VEGF gene. *Nature*, **380**, 439-448.

Ferrara, N. Gerber, H.-P., and LeCouter, J. (2003). The biology of VEGF and its receptors. *Nature medicine*, **9**, 669-76.

Ferrari, A., Veligodskiy, A., Berge, U., Lucas, M. S., and Kroschewski, R. (2008). ROCK-mediated contractility, tight junctions and channels contribute to the conversion of a preapical patch into apical surface during isochoric lumen initiation. *Journal of cell science*, **121**, 3649-63.

Fischer, A., Schumacher, N., Maier, M., Sendtner, M., and Gessler, M. (2004). The Notch target genes Hey1 and Hey2 are required for embryonic vascular development. *Genes & Development*, **18**, 901-911.

Fischer, J. A., Gingiger, E., Maniatis, T., and Ptashne, M. (1988). GAL4 activates transcription in Drosophila. *Nature*, **332**, 853-856.

Fleming, P. A., Argraves, W. S., Gentille, C., Neagu, A., and Drake, Christopher J (2011). Fusion of uniluminal vascular spheroids: a model for assembly of blood vessels. *Developmental Dynamics*, **239**, 398-406.

Forsythe, J. A, Jiang, B. H., Iyer, N. V., Agani, F., Leung, S. W., Koos, R. D., and Semenza, G L (1996). Activation of vascular endothelial growth factor gene transcription by hypoxia-inducible factor 1. *Molecular and cellular biology*, **16**, 4604-13.

Fouquet, B., Weinstein, B M, Serluca, F. C., and Fishman, M C (1997). Vessel patterning in the embryo of the zebrafish: guidance by notochord. *Developmental biology*, **183**, 37-48.

Fraisl, P., Mazzone, M., Schmidt, T., and Carmeliet, P. (2009). Regulation of angiogenesis by oxygen and metabolism. *Developmental cell*, **16**, 167-79.

Fujimoto, E., Gaynes, B., Brimley, C. J., Chien, C-B, and Bonkowsky, J. L. (2011). Gal80 Intersectional Regulation of Cell-Type Specific Expression in Vertebrates. *Developmental dynamics*, **240**, 2324-2334.

Funahashi, Y., Shawber, C. J., Vorontchikhina, M., Sharma, A., Outtz, H. H., and Kitajewski, J. (2010). Notch regulates the angiogenic response via induction of VEGFR-1. *Journal of angiogenesis research*, **2**, 1-10.

Gale, N. W, Dominguez, M. G., Noguera, I., Pan, L., Hughes, V., Valenzuela, D. M., Murphy, A. J., Adams, N. C., Lin, H. C., Holash, J., et al. (2004). Haploinsufficiency of delta-like 4 ligand results in embryonic lethality due to major defects in arterial and vascular development. *PNAS: Proceedings of the National Academy of Sciences of the United States of America*, **101**, 15949-54.

Garrard, S. M., Capaldo, C. T., Gao, L., Rosen, M. K., Macara, I. G., and Tomchick, D. R. (2003). Structure of Cdc42 in a complex with the GTPase-binding domain of the cell polarity protein, Par6. *The EMBO journal*, **22**, 1125-33.

Garrick, D., Fiering, S., Martin, D. I. K., Whitelaw, E. (1998). Repeat-induced gene silencing in mammels. *Nature genetics*, **18**, 56-59.

Gassama-Diagne, A., Yu, W., ter Beest, M., Martin-Belmonte, F., Kierbel, A., Engel, J., and Mostov, K. (2006). Phosphatidylinositol-3,4,5-trisphosphate regulates the formation of the basolateral plasma membrane in epithelial cells. *Nature cell biology*, **8**, 963-70.

Gentile, C., Fleming, Paul A, Mironov, V., Argraves, K. M., Argraves, W. S., and Drake, Christopher J (2008). VEGF-mediated fusion in the generation of uniluminal vascular spheroids. *Developmental dynamics*, **237**, 2918-25.

Gerhardt, Holger, Golding, M., Fruttiger, M., Ruhrberg, C., Lundkvist, A., Abramsson, A., Jeltsch, Michael, Mitchell, C., Alitalo, Kari, Shima, D., et al. (2003). VEGF guides angiogenic sprouting utilizing endothelial tip cell filopodia. *The Journal of cell biology*, **161**, 1163-77.

Gervais, L., Lebreton, G., and Casanova, J. (2011). The making of a fusion branch in the Drosophila trachea. *Developmental biology*, **(e-pub)** 1-7.

Gibney, E. R. and Nolan, C. M. (2010). Epigenetics and gene expression. *Heredity*, **105**, 4-13.

Gill, G. and Ptashne, M. (1988). Negative effect of transcriptional activator GAL4. *Nature*, **334**, 771-775.

Gitler, A. D., Lu, M. M., and Epstein, J. A. (2004). PlexinD1 and Semaphorin Signaling Are Required in Endothelial Cells for Cardiovascular Development. *Development*, **7**, 107-116.

Goll, Mary G, Anderson, R., Stainier, Didier Y R, Spradling, A. C., and Halpern, M. E. (2009). Transcriptional silencing and reactivation in transgenic zebrafish. *Genetics*, **182**, 747-55.

Goll, Mary Grace and Bestor, T. H. (2005). Ukaryotic cytosine ethyltransferases. *Annu. Rev. Biochem.*, **74**, 481-514.

Grazia Lampugnani, M., Zanetti, A., Corada, M., Takahashi, T., Balconi, G., Breviario, F., Orsenigo, F., Cattelino, A., Kemler, Rolf, Daniel, T. O., et al. (2003). Contact inhibition of VEGF-induced proliferation requires vascular endothelial cadherin, beta-catenin, and the phosphatase DEP-1/CD148. *The Journal of cell biology*, **161**, 793-804.

Gridley, T. (2010). Notch Signaling in the Vasculature. *Current topics in Developmental Biology*, **92**, 277-308.

Gu, C., Yoshida, Y., Livet, J., Reimert, D. V., Mann, F., Merte, J., Henderson, C. E., Jessell, T. M., Kolodkin, A. L., and Ginty, D. D. (2005). Semaphorin 3E and plexin-D1 control vascular pattern independently of neuropilins. *Science*, **307**, 265-8.

Gutzman, J. H. and Sive, H. (2010). Epithelial relaxation mediated by the myosin phosphatase regulator Mypt1 is required for brain ventricle lumen expansion and hindbrain morphogenesis. *Development*, **137**, 795-804.

Hamilton, J. P. (2011). Epigenetics : Principles and Practice. *Gastroenterology*, **21205**, 130-135.

Harris, E. S. and Nelson, W James (2010). VE-cadherin: at the front, center, and sides of endothelial cell organization and function. *Current opinion in cell biology*, **22**, 651-8.

Harris, T. J. C. and Tepass, U. (2010). Adherens junctions: from molecules to morphogenesis. *Nature reviews. Molecular cell biology*, **11**, 502-14.

Hatta, K., Tsujii, H., and Omura, T. (2006). Cell tracking using a photoconvertible fluorescent protein. *Nature protocols*, **1**, 960-7.

Hellström, M, Gerhardt, H, Kalén, M, Li, X, Eriksson, U., Wolburg, H, and Betsholtz, C (2001). Lack of pericytes leads to endothelial hyperplasia and abnormal vascular morphogenesis. *The Journal of cell biology*, **153**, 543-53.

Hellström, Mats, Phng, Li-Kun, Hofmann, J. J., Wallgard, E., Coultas, L., Lindblom, P., Alva, J., Nilsson, A.-K., Karlsson, L., Gaiano, N., et al. (2007). Dll4 signalling through Notch1 regulates formation of tip cells during angiogenesis. *Nature*, **445**, 776-80.

Henzel, J. and Press, I. A. (1989). Pituitary growth follicular cells secrete a novel heparin binding factor specific for vascular endothelial cells. *Biochemical and Biophysical Research Communications*, **161**, 851-858.

Herbert, S. P. and Stainier, Didier Y. R. (2011). Molecular control of endothelial cell behaviour during blood vessel morphogenesis. *Nature Reviews Molecular Cell Biology*, **12**, 551-564.

Herbert, S. P., Huisken, J., Kim, T. N., Feldman, M. E., Houseman, B. T., Wang, R. a, Shokat, K. M., and Stainier, Didier Y R (2009). Arterial-venous segregation by selective cell sprouting: an alternative mode of blood vessel formation. *Science*, **326**, 294-8.

Hildebrand, J. D. (2005). Shroom regulates epithelial cell shape via the apical positioning of an actomyosin network. *Journal of cell science*, **118**, 5191-203.

Hogan, B. L. M. and Kolodziej, P. a (2002). Organogenesis: molecular mechanisms of tubulogenesis. *Nature reviews. Genetics*, **3**, 513-23.

Holmes, D. I. R. and Zachary, I. (2005). Protein family review The vascular endothelial growth factor (VEGF) family : angiogenic factors in health and disease. *Genome Biology*, **6**, 209

Houck, K. a, Leung, D. W., Rowland, a M., Winer, J., and Ferrara, N (1992). Dual regulation of vascular endothelial growth factor bioavailability by genetic and proteolytic mechanisms. *The Journal of biological chemistry*, **267**, 26031-7.

Huang, C.-J., Tu, C.-T., Hsiao, C.-D., Hsieh, F.-J., and Tsai, H.-J. (2003). Germ-line transmission of a myocardium-specific GFP transgene reveals critical regulatory elements in the cardiac myosin light chain 2 promoter of zebrafish. *Developmental Dynamics*, **228**, 30-40.

Huang, D. C. and Strasser, A (2000). BH3-Only proteins-essential initiators of apoptotic cell death. *Cell*, **103**, 839-42.

Huang, M., Jia, F.-J., Yan, Y.-C., Guo, L.-H., and Li, Y.-P. (2006). Transactivated minimal E1b promoter is capable of driving the expression of short hairpin RNA. *Journal of virological methods*, **134**, 48-54.

Iden, S., Rehder, D., August, B., Suzuki, A., Wolburg-Buchholz, K., Wolburg, Hartwig, Ohno, S., Behrens, J., Vestweber, D., and Ebnet, K. (2006). A distinct PAR complex associates physically with VE-cadherin in vertebrate endothelial cells. *EMBO reports*, **7**, 1239-46.

Iruela-Arispe, M. L. and Davis, G. E. (2009). Cellular and molecular mechanisms of vascular lumen formation. *Developmental cell*, **16**, 222-31.

Isogai, S, Horiguchi, M, and Weinstein, B. M. (2001). The vascular anatomy of the developing zebrafish: an atlas of embryonic and early larval development. *Developmental biology*, **230**, 278-301.

Isogai, S, Lawson, N. D., Torrealday, S., Horiguchi, M., and Weinstein, B. M. (2003). Angiogenic network formation in the developing vertebrate trunk. *Development*, **130**, 5281-90.

Jahn, R. and Scheller, R. H. (2006). SNAREs-engines for membrane fusion. *Nature reviews. Molecular cell biology*, **7**, 631-43.

Jain, R. K. (2003). Molecular regulation of vessel maturation. *Nature medicine*, **9**, 685-93.

Jakobsson, L., Franco, C. A., Bentley, K., Collins, R. T., Ponsioen, B., Aspalter, I. M., Rosewell, I., Busse, M., Thurston, Gavin, Medvinsky, A., et al. (2010). Endothelial cells dynamically compete for the tip cell position during angiogenic sprouting. *Nature cell biology*, **12**, 943-53.

Jin, S.-W., Beis, D., Mitchell, T., Chen, J.-N., and Stainier, Didier Y R (2005). Cellular and molecular analyses of vascular tube and lumen formation in zebrafish. *Development*, **132**, 5199-209.

Jou, T. S., Stewart, D. B., Stappert, J., Nelson, W J, and Marrs, J. a (1995). Genetic and biochemical dissection of protein linkages in the cadherin-catenin complex. *PNAS: Proceedings of the National Academy of Sciences of the United States of America*, **92**, 5067-71.

Joukov, V., Pajusola, K., Kaipainen, a, Chilov, D., Lahtinen, I., Kukk, E., Saksela, O., Kalkkinen, N., and Alitalo, K (1996). A novel vascular endothelial growth factor, VEGF-C, is a ligand for the Flt4 (VEGFR-3) and KDR (VEGFR-2) receptor tyrosine kinases. *The EMBO journal*, **15**, 1751.

Kaelin, W. G. and Ratcliffe, P. J. (2008). Oxygen sensing by metazoans: the central role of the HIF hydroxylase pathway. Cell review. *Molecular cell*, **30**, 393-402.

Kakihara, K., Shinmyozu, K., Kato, K., Wada, H., and Hayashi, Shigeo (2007). Conversion of plasma membrane topology during epithelial tube connection requires Arf-like 3 small GTPase in Drosophila. *Mechanisms of development*, **125**, 325-36.

Kamei, M., Saunders, W. B., Bayless, K. J., Dye, L., Davis, G. E., and Weinstein, B. M. (2006). Endothelial tubes assemble from intracellular vacuoles in vivo. *Nature*, **442**, 453-6.

Karfunkel, P. (1972). The activity of microtubules and microfilaments in neurulation in the chick. *Journal of Experimental Zoology*, **181**, 289–301.

Kawakami, K, Shima, a, and Kawakami, N (2000). Identification of a functional transposase of the Tol2 element, an Ac-like element from the Japanese medaka fish, and its transposition in the zebrafish germ lineage. *PNAS: Proceedings of the National Academy of Sciences of the United States of America*, **97**, 11403-8.

Kawakami, K., Takeda, H., Kobayashi, M., Matsuda, N., and Mishina, M. (2004). A transposon-mediated gene trap approach identifies developmentally regulated genes in zebrafish. *Developmental cell*, **7**, 133-44.

Kennedy, M. J., Hughes, R. M., Peteya, L. A., Schwartz, J. W., Ehlers, M. D., and Tucker, C. L. (2010). rapid blue-light – mediated induction of protein interactions in living cells. *October*, **7**, 12-16.

Kimmel, C. B., Ballard, W. W., Kimmel, S. R., Ullmann, B., and Schilling, T F (1995). Stages of embryonic development of the zebrafish. *Developmental dynamics*, **203**, 253-310.

Klionsky, D. J. (2007). Autophagy: from phenomenonology to molecular understanding in less than a decade. *Nature reviews. Molecular cell biology*, **8**, 931-937.

Koch, S., Tugues, S., Li, Xiujuan, Gualandi, L., and Claesson-Welsh, L. (2011). Signal transduction by vascular endothelial growth factor receptors. *The Biochemical journal*, **437**, 169-83.

Koh, W., Mahan, R. D., and Davis, G. E. (2008). Cdc42- and Rac1-mediated endothelial lumen formation requires Pak2, Pak4 and Par3, and PKC-dependent signaling. *Journal of cell science*, **121**, 989-1001.

Kubota, Y., Kleinman, H., and Martin, G. (1988). Role of Laminin and Basement Membrane in the Morphological Differentiation of Human Endothelial Cells into Capillary-like Structures. *The Journal of cell biology*, **107**, 1589-1598.

Kundu, M. and Thompson, C. B. (2008). Autophagy: basic principles and relevance to disease. *Annual review of pathology*, **3**, 427-55.

Kwan, K. M., Fujimoto, E., Grabher, C., Mangum, B. D., Hardy, M. E., Campbell, D. S., Parant, J. M., Yost, H. J., Kanki, J. P., and Chien, Chi-Bin (2007). The Tol2kit: a multisite gateway-based construction kit for Tol2 transposon transgenesis constructs. *Developmental dynamics*, **236**, 3088-99.

Köster, R. W. and Fraser, S. E. (2001). Tracing transgene expression in living zebrafish embryos. *Developmental biology*, **233**, 329-46.

Lampugnani, M. G. and Dejana, E (1997). Interendothelial junctions: structure, signalling and functional roles. *Current opinion in cell biology*, **9**, 674-82.

Lampugnani, M. G., Orsenigo, F., Gagliani, M. C., Tacchetti, C., and Dejana, Elisabetta (2006). Vascular endothelial cadherin controls VEGFR-2 internalization and signaling from intracellular compartments. *The journal of cell biology*, **174**, 593-604.

Lampugnani, M. G., Orsenigo, F., Rudini, N., Maddaluno, L., Boulday, G., Chapon, F., and Dejana, Elisabetta (2010). CCM1 regulates vascular-lumen organization by inducing endothelial polarity. *Journal of cell science*, **123**, 1073-80.

Langenau, D. M., Feng, H., Berghmans, S., Kanki, J. P., Kutok, J. L., and Look, A. T. (2005). Cre-lox-regulated transgenic zebrafish model with conditional myc-induced T cell acute lymphoblastic leukemia. *PNAS: Proceedings of the National Academy of Sciences of the United States of America*, **102**, 6068-6073.

Lawson, N D, Scheer, N., Pham, V. N., Kim, C. H., Chitnis, a B., Campos-Ortega, J. a, and Weinstein, B M (2001). Notch signaling is required for arterial-venous differentiation during embryonic vascular development. *Development (Cambridge, England)*, **128**, 3675-83.

Lawson, N. D. and Weinstein, B M (2002). In Vivo Imaging of Embryonic Vascular Development Using Transgenic Zebrafish. *Developmental Biology*, **248**, 307-318.

Lawson, N. D. Vogel, A. M., and Weinstein, B. M. (2002). sonic hedgehog and vascular endothelial growth factor act upstream of the Notch pathway during arterial endothelial differentiation. *Developmental cell*, **3**, 127-36.

Lee, S. and Kolodziej, P. A. (2002). The plakin Short Stop and the RhoA GTPase are required for E-cadherin-dependent apical surface remodeling during tracheal tube fusion. *Development*, **129**, 1509-20.

Le Noble, F., Moyon, D., Pardanaud, L., Yuan, L., Djonov, V., Matthijsen, R., Bréant, C., Fleury, V., and Eichmann, A. (2004). Flow regulates arterial-venous differentiation in the chick embryo yolk sac. *Development (Cambridge, England)*, **131**, 361-75.

Leung, D. W., Cachianes, G., Kuang, W. J., Goeddel, D. V., and Ferrara, N (1989). Vascular endothelial growth factor is a secreted angiogenic mitogen. *Science*, **246**, 1306-9.

Li, E., Bestor, T. H., and Jaenisch, R. (1992). Targeted Mutation of the DNA Methyltransferase Gene Results in Embryonic Lethality. *Cell*, **69**, 915-926.

Lim, a. H., Suli, a., Yaniv, K., Weinstein, B., Li, D. Y., and Chien, C.-B. (2011). Motoneurons are essential for vascular pathfinding. *Development*, **138**, 4813-4813.

Liu, F., Walmsley, M., Rodaway, A., and Patient, R. (2008). Fli1 acts at the top of the transcriptional network driving blood and endothelial development. *Current biology*, **18**, 1234-40.

Liu, H., Yu, X., and Li, K. (2008). Photoexcited CRY2 Interacts with CIB1 to Regulate Transcription and Floral Initiation in Arabidopsis. *Science*, **322**, 1535-1539.

Liu, Z.-Jun, Shirakawa, T., Li, Y., Soma, A., Oka, M., Dotto, G. P., Fairman, R. M., Velazquez, C., Herlyn, M., and Velazquez, O. C. (2003). Regulation of Notch1 and Dll4 by Vascular Endothelial Growth Factor in Arterial Endothelial Cells : Implications for Modulating Arteriogenesis and Angiogenesis Regulation of Notch1 and Dll4 by Vascular Endothelial Growth Factor in Arterial Endothelial Cel. *Society*.

Lobov, I. B., Renard, R. A, Papadopoulos, N., Gale, N W, Thurston, G, Yancopoulos, G D, and Wiegand, S. J. (2007). Delta-like ligand 4 (Dll4) is induced by VEGF as a negative regulator of angiogenic sprouting. *PNAS: Proceedings of the National Academy of Sciences of the United States of America*, **104**, 3219-24.

Lohela, M., Bry, M., Tammela, T., and Alitalo, Kari (2009). VEGFs and receptors involved in angiogenesis versus lymphangiogenesis. *Current opinion in cell biology*, **21**, 154-65.

Low, S. H., Chapin, S. J., Weimbs, T., Kömüves, L. G., Bennett, M. K., and Mostov, K E (1996). Differential localization of syntaxin isoforms in polarized Madin-Darby canine kidney cells. *Molecular biology of the cell*, **7**, 2007-18.

Lu, X., Le Noble, F., Yuan, L., Jiang, Q., De Lafarge, B., Sugiyama, D., Bréant, C., Claes, F., De Smet, F., Thomas, J.-L., et al. (2004). The netrin receptor UNC5B mediates guidance events controlling morphogenesis of the vascular system. *Nature*, **432**, 179-86.

Lubarsky, B. and Krasnow, M. A. (2003). Tube Morphogenesis : Making and Shaping Biological Tubes Many organs are composed of epithelial tubes that. **112**, 19-28.

Mailhos, C., Modlich, U., Lewis, J., Harris, A, Bicknell, R., and Ish-Horowicz, D. (2001). Delta4, an endothelial specific notch ligand expressed at sites of physiological and tumor angiogenesis. *Differentiation;* **69**, 135-44.

Mailleux, A. a, Overholtzer, M., Schmelzle, T., Bouillet, P., Strasser, A., and Brugge, J. S. (2007). BIM regulates apoptosis during mammary ductal morphogenesis, and its absence reveals alternative cell death mechanisms. *Developmental cell*, **12**, 221-34.

Makanya, A. N., Hlushchuk, R., and Djonov, V. G. (2009). Intussusceptive angiogenesis and its role in vascular morphogenesis, patterning, and remodeling. *Angiogenesis*, **12**, 113-23.

Makarova, O., Kamberov, E., and Margolis, B. (2000). Generation of deletion and point mutations with one primer in a single cloning step. *BioTechniques*, **29**, 970-2.

Martin, A. C., Kaschube, M., and Wieschaus, E. F. (2009). Pulsed contractions of an actin-myosin network drive apical constriction. *Nature*, **457**, 495-9.

Martin-Belmonte, F. and Mostov, K. (2008). Regulation of cell polarity during epithelial morphogenesis. *Current opinion in cell biology*, **20**, 227-34.

Martin-Belmonte, F., Gassama, A., Datta, A., Yu, W., Rescher, U., Gerke, V., and Mostov, K. (2007). PTEN-mediated apical segregation of phosphoinositides controls epithelial morphogenesis through Cdc42. *Cell*, **128**, 383-97.

Martin-Belmonte, F. and Mostov, K. (2007). Phosphoinositides Control Membrane Polarity in Epithelial Development. *Cell Cycle* 6:**16** 1957-1961.

Meder, D., Shevchenko, A., Simons, K., and Füllekrug, J. (2005). Gp135/podocalyxin and NHERF-2 participate in the formation of a preapical domain during polarization of MDCK cells. *The Journal of cell biology*, **168**, 303-13.

Meng, X., Noyes, M. B., Zhu, L. J., Lawson, Nathan D, and Wolfe, S. A. (2008). Targeted gene inactivation in zebrafish using engineered zinc-finger nucleases. *Nature biotechnology*, **26**, 695-701.

Metzger, R. J., Klein, O. D., Martin, G. R., and Krasnow, Mark A. (2008). The branching programme of mouse lung development. *Nature*, **453**, 745-50.

Meyer, D., Stiegler, P., Hindelang, C., Mager, A. M., and Remy, P. (1995). Whole-mount in situ hybridization reveals the expression of the Xl-Fli gene in several lineages of migrating cells in Xenopus embryos. *The international journal of developmental biology*, **39**, 909-19.

Miranda, T. B. and Jones, P. A. (2007). DNA Methylation : The Nuts and Bolts of Repression. *Journal of Cellular Physiology*, **213**, 384-390.

Montero-Balaguer, M., Swirsding, K., Orsenigo, F., Cotelli, F., Mione, M., and Dejana, E. (2009). Stable vascular connections and remodeling require full expression of VE-cadherin in zebrafish embryos. *PloS one*, **4**, e5772.

Munson, C., Huisken, J., Bit-Avragim, N., Kuo, T., Dong, P. D., Ober, E. A, Verkade, H., Abdelilah-Seyfried, S., and Stainier, D. Y. R. (2008). Regulation of neurocoel morphogenesis by Pard6 gamma b. *Developmental biology*, **324**, 41-54.

Nakatsu, M. N. and Hughes, C. C. W. (2008). An optimized three-dimensional in vitro model for the analysis of angiogenesis. *Methods in enzymology*, **443**, 65-82.

Nakatsu, M. N., Sainson, R. C. A., Aoto, J. N., Taylor, K. L., Aitkenhead, M., Carpenter, P. M., and Hughes, C. C. W. (2003). Angiogenic sprouting and capillary lumen formation modeled by human umbilical vein endothelial cells (HUVEC) in fibrin gels : the role of fibroblasts and Angiopoietin-1 . *Microvascular Research*, **66**, 102-112.

Neufeld, G, Cohen, T., Gengrinovitch, S., and Poltorak, Z. (1999). Vascular endothelial growth factor (VEGF) and its receptors. *The FASEB journal : official publication of the Federation of American Societies for Experimental Biology*, **13**, 9-22.

Nicoli, S., Ribatti, D., Cotelli, F., and Presta, M. (2007). Mammalian tumor xenografts induce neovascularization in zebrafish embryos. *Cancer research*, **67**, 2927-31.

Nieset, J. E., Redfield, A. R., Jin, F., Knudsen, K. A., Johnson, Keith R, and Wheelock, Margaret J (1997). Characterization of the interactions of α -catenin with α -actinin and β. *Journal of Cell Science*, **1022**, 1013-1022.

Obama, H. and Ozawa, M. (1997). Identification of the domain of alpha-catenin involved in its association with beta-catenin and plakoglobin (gamma-catenin). *The Journal of biological chemistry*, **272**, 11017-20.

Olofsson, B., Korpelainen, E., Pepper, M. S., Mandriota, S. J., Aase, K., Kumar, V., Gunji, Y., Jeltsch, M. M., Shibuya, M, Alitalo, K, et al. (1998). Vascular endothelial growth factor B (VEGF-B) binds to VEGF receptor-1 and regulates plasminogen activator activity in endothelial cells. *PNAS: Proceedings of the National Academy of Sciences of the United States of America*, **95**, 11709-14.

Pan, X., Wan, H., Chia, W., Tong, Y., and Gong, Z. (2005). Demonstration of site-directed recombination in transgenic zebrafish using the Cre / loxP system. *Transgenic Research*, **14**, 217-223.

Pepper, M. S. (1997). Transforming growth factor-beta: vasculogenesis, angiogenesis, and vessel wall integrity. *Cytokine & growth factor reviews*, **8**, 21-43.

Perz-Edwards, a, Hardison, N. L., and Linney, E. (2001). Retinoic acid-mediated gene expression in transgenic reporter zebrafish. *Developmental biology*, **229**, 89-101.

Phng, L-K and Gerhardt, Holger (2009). Angiogenesis: a team effort coordinated by notch. *Developmental cell*, **16**, 196-208.

Phng, Li-Kun, Potente, M., Leslie, J. D., Babbage, J., Nyqvist, D., Lobov, I., Ondr, J. K., Rao, S., Lang, R. a, Thurston, Gavin, et al. (2009). Nrarp coordinates endothelial Notch and Wnt signaling to control vessel density in angiogenesis. *Developmental cell*, **16**, 70-82.

Pola, R., Ling, L. E., Silver, M., Corbley, M. J., Kearney, M., Blake Pepinsky, R., Shapiro, R., Taylor, F. R., Baker, D. P., Asahara, T., et al. (2001). The morphogen Sonic hedgehog is an indirect angiogenic agent upregulating two families of angiogenic growth factors. *Nature medicine*, **7**, 706-11.

Prahst, C., Héroult, M., Lanahan, A. A, Uziel, N., Kessler, O., Shraga-Heled, N., Simons, M., Neufeld, Gera, and Augustin, H. G. (2008). Neuropilin-1-VEGFR-2 complexing requires the PDZ-binding domain of neuropilin-1. *The Journal of biological chemistry*, **283**, 25110-4.

Prekeris, R. (2003). Rabs, Rips, FIPs, and endocytic membrane traffic. *The Scientific World Journal*, **3**, 870-80.

Ptashne, M. and Gann, A. (2002). Genes and Signals 1st ed. Cold Spring Harbor Labaratory Press.

Rahimi, N. and Kazlauskas, A (1999). A role for cadherin-5 in regulation of vascular endothelial growth factor receptor 2 activity in endothelial cells. *Molecular biology of the cell*, **10**, 3401-7.

Resolution, S., Sinha, D. K., Neveu, P., Gagey, N., Aujard, I., Saux, T. L., Rampon, C., Gauron, C., Kawakami, Koichi, Leucht, C., et al. (2010). Photoactivation of the CreER T2 Recombinase for Conditional Site-Specific Recombination. *Zebrafish*, **7,** 199-204.

Rhumbler, L. (1902). Zur Mechanik des Gastrulationsvorganges insbesondere der Invagination. *Archiv für Entwicklungsmechanik der Organismen*, **14**, 401-476.

Ribeiro, C., Neumann, M., Affolter, M., and Universita, B. D. (2004). Genetic Control of Cell Intercalation during Tracheal Morphogenesis in Drosophila. *Current Biology*, **14**, 2197-2207.

Rimm, D. L., Koslov, E. R., Kebriaei, P., Cianci, C. D., and Morrow, J. O. N. S. (1995). Alpha 1(E)-catenin is an actin-binding and -bundling protein mediating the attachment of F-actin to the membrane adhesion complex.. *Physiology*, **92**, 8813-8817.

Risau, W. (1991). Embryonic angiogenesis factors. *Pharmacology & Therapeutics*, **51**, 371-6.

Risau, W. (1997). Mechanisms of angiogenesis. *Nature*, **386**, 671-674.

Risau, W. and Flamme, I. (1995). Vasculogenesis. *Annual review of cell and developmental biology*, **11**, 73-91.

Rivera, V. M., Natesan, S., Gilman, M., and Molinari, E. (1997). Transcriptional squelching re-examined. *Nature*, **390**, 349-350.

Rocha, S. F. and Adams, R. H. (2009). Molecular differentiation and specialization of vascular beds. *Angiogenesis*, **12**, 139-47.

Roman, B. L. and Weinstein, B. M. (2000). Building the vertebrate vasculature: research is going swimmingly. *BioEssays*, **22**, 882-93.

Rorth, P. (1996). A modular misexpression screen in Drosophila detecting tissue-specific phentoypes. *Genetics*, **93**, 12418-12422.

Ruhrberg, C., Gerhardt, Holger, Golding, M., Watson, R., Ioannidou, S., Fujisawa, H., Betsholtz, Christer, and Shima, D. T. (2002). Spatially restricted patterning cues provided by heparin-binding VEGF-A control blood vessel branching morphogenesis. *Genes & Development*, **16**, 2684-98.

Rupp, P. A. and Little, C. D. (2001). Integrins in Vascular Development. *Circulation Research*, **89**, 566-572.

Sadowski, I. (1988). GAL4-VP16 is an unnusually potent transcripton activator. *Nature*, **335,** 563-564.

Saharinen, P., Eklund, L., Miettinen, J., Wirkkala, R., Anisimov, A., Winderlich, M., Nottebaum, A., Vestweber, D., Deutsch, U., Koh, G. Y., et al. (2008). Angiopoietins assemble distinct Tie2 signalling complexes in endothelial cell-cell and cell-matrix contacts. *Nature cell biology*, **10**, 527-37.

Samakovlis, C., Hacohen, N., Manning, G., Sutherland, D. C., Guillemin, K., and Krasnow, M a (1996). Development of the Drosophila tracheal system occurs by a series of morphologically distinct but genetically coupled branching events. *Development*, **122**, 1395-407.

Samakovlis, C., Manning, G., Steneberg, P., Hacohen, N., Cantera, R., and Krasnow, M a (1996). Genetic control of epithelial tube fusion during Drosophila tracheal development. *Development,* **122**, 3531-6.

Santiago-Martínez, E., Soplop, N. H., Patel, R., and Kramer, S. G. (2008). Repulsion by Slit and Roundabout prevents Shotgun/E-cadherin-mediated cell adhesion during Drosophila heart tube lumen formation. *The journal of cell biology*, **182**, 241-8.

Sawyer, J. M., Harrell, J. R., Shemer, G., Sullivan-Brown, J., Roh-Johnson, M., and Goldstein, B. (2010). Apical constriction: a cell shape change that can drive morphogenesis. *Developmental biology*, **341**, 5-19.

Scheer, N. and Campos-Ortega, J. A (1999). Use of the Gal4-UAS technique for targeted gene expression in the zebrafish. *Mechanisms of development*, **80**, 153-8.

Sehnert, A. J., Huq, A., Weinstein, Brant M, Walker, C., Fishman, M., and Stainier, Didier Y. R. (2002). Cardiac troponin T is essential in sarcomere assembly and cardiac contractility. *Nature genetics*, **31**, 106-10.

Semenza, Gregg L (2003). Targeting HIF-1 for cancer therapy. *Nature reviews. Cancer*, **3**, 721-32.

Senger, D. R., Galli, S. J., Dvorak, A. M., Perruzzi, C. A, Harvey, V. S., and Dvorak, H F (1983). Tumor cells secrete a vascular permeability factor that promotes accumulation of ascites fluid. *Science*, **219**, 983-5.

Shalaby, F., Rossant, J., Yamaguchi, T. P., Gertenstein, M., Wu, X.-F., Breitman, M. L., and Schuh, A. C. (1995). Failure of blood-island formation and vasculogenesis in Flk-1-deficient mice. *Nature*, **326**, 62-66.

Shestopalov, I. A., Sinha, S., and Chen, J. K. (2007). Light-controlled gene silencing in zebrafish embryos. *Nature Chemical Biology*, **3**, 650-651.

Shibuya, Masabumi and Claesson-Welsh, L. (2006). Signal transduction by VEGF receptors in regulation of angiogenesis and lymphangiogenesis. *Experimental cell research*, **312**, 549-60.

Siekmann, A. F. and Lawson, Nathan D (2007). Notch signalling limits angiogenic cell behaviour in developing zebrafish arteries. *Nature*, **445**, 781-4.

Siekmann, A. F., Standley, C., Fogarty, K. E., Wolfe, S. A, and Lawson, N. D. (2009). Chemokine signaling guides regional patterning of the first embryonic artery. *Genes & Development*, **23**, 2272-7.

Simon, C. M. (1995). Gotta have GATA. *Nature*, **11**, 9-11.

Soker, S., Takashima, S., Miao, H. Q., Neufeld, G, and Klagsbrun, M. (1998). Neuropilin-1 is expressed by endothelial and tumor cells as an isoform-specific receptor for vascular endothelial growth factor. *Cell*, **92**, 735-45.

Stalmans, I., Ng, Y.-shan, Rohan, R., Fruttiger, M., Bouché, A., Ÿuce, A., Fujisawa, H., Hermans, B., Shani, M., Jansen, S., et al. (2002). Arteriolar and venular patterning in retinas of mice selectively expressing VEGF isoforms. *Journal of Clinical Investigation*, **109**, 327-336.

von Stein, W., Ramrath, A., Grimm, A., Müller-Borg, M., and Wodarz, A. (2005). Direct association of Bazooka/PAR-3 with the lipid phosphatase PTEN reveals a link between the PAR/aPKC complex and phosphoinositide signaling. *Development*, **132**, 1675-86.

Steinberg, M. S. (2007). Differential adhesion in morphogenesis: a modern view. *Current opinion in genetics & development*, **17**, 281-6.

Strilic, B., Kucera, T., Eglinger, J., Ferrara, Napoleone, and Lammert, E. (2009). The Molecular Basis of Vascular Lumen Formation in the Developing Mouse Aorta. *Developmental cell*, **17**, 505-515.

Strilic, B., Lammert, E., Eglinger, J., Zeeb, M., and Krieg, M. (2010). Electrostatic Cell-Surface Repulsion Initiates Lumen Formation in Developing Blood Vessels. *Current Biology*, **20,** 2003-2009.

Suchting, S., Freitas, C., le Noble, F., Benedito, R., Bréant, C., Duarte, A., and Eichmann, A. (2007). The Notch ligand Delta-like 4 negatively regulates endothelial tip cell formation and vessel branching. *PNAS: Proceedings of the National Academy of Sciences of the United States of America*, **104**, 3225-30.

Sumoy, L., Keasey, B., Dittman, T., and Kimelman, D. (1997). A role for notochord in axial vascular development revealed by analysis of phenotype and the exprssion of VEGFR-2 in zebrafish flh and ntl mutant embryos. *Mechanisms of development*, **63**, 15-27.

Suri, C., Jones, P. F., Patan, S., Bartunkova, S., Maisonpierre, P. C., Davis, S., Sato, T. N., and Yancopoulos, G D (1996). Requisite role of angiopoietin-1, a ligand for the TIE2 receptor, during embryonic angiogenesis. *Cell*, **87**, 1171-80.

Suzuki, a, Hamada, K., Sasaki, T., Mak, T. W., and Nakano, T. (2007). Role of PTEN/PI3K pathway in endothelial cells. *Biochemical Society transactions*, **35**, 172-6.

Tammela, T., Zarkada, G., Wallgard, E., Murtomäki, A., Suchting, S., Wirzenius, M., Waltari, M., Hellström, Mats, Schomber, T., Peltonen, R., et al. (2008). Blocking VEGFR-3 suppresses angiogenic sprouting and vascular network formation. *Nature*, **454**, 656-60.

Tanaka-Matakatsu, M., Uemura, T., Oda, H., Takeichi, M., and Hayashi, S (1996). Cadherin-mediated cell adhesion and cell motility in Drosophila trachea regulated by the transcription factor Escargot. *Development*, **122**, 3697-705.

Tarallo, V., Tudisco, L., and De Falco, S. (2011). A placenta growth factor 2 variant acts as dominant negative of vascular endothelial growth factor A by heterodimerization mechanism. *American journal of cancer research*, **1**, 265-274.

Thompson, M. A., Ransom, D. G., Pratt, S. J., Maclennan, H., Kieran, M. W., Iii, H. W. D., Vail, B., Huber, T. L., Paw, B., Brownlie, A. J., et al. (2008). The cloche and spadetail Genes Differentially Affect Hematopoiesis and Vasculogenesis. *New York*, **269**, 248-269.

Thoreson, M. a, Anastasiadis, P. Z., Daniel, J. M., Ireton, R. C., Wheelock, M J, Johnson, K R, Hummingbird, D. K., and Reynolds, a B. (2000). Selective uncoupling of p120(ctn) from E-cadherin disrupts strong adhesion. *The Journal of cell biology*, **148**, 189-202.

Torres-Vázquez, J., Gitler, A. D., Fraser, S. D., Berk, J. D., Van N Pham, Fishman, Mark C, Childs, Sarah, Epstein, J. a, and Weinstein, B. M. (2004). Semaphorin-plexin signaling guides patterning of the developing vasculature. *Developmental cell*, **7**, 117-23.

Tucker, A S. (2007). Salivary gland development. *Seminars in cell & developmental biology*, **18**, 237-44.

Uemura, T., Oda, H., Kraut, R., Hayashi, S, Kotaoka, Y., and Takeichi, M. (1996). Zygotic Drosophila E-cadherin expression is required for processes of dynamic epithelial cell rearrangement in the Drosophila embryo. *Genes & Development*, **10**, 659-671.

Vestweber, D. (2008). VE-cadherin: the major endothelial adhesion molecule controlling cellular junctions and blood vessel formation. *Arteriosclerosis, thrombosis, and vascular biology*, **28**, 223-32.

Villefranc, J. a, Amigo, J., and Lawson, Nathan D (2007). Gateway compatible vectors for analysis of gene function in the zebrafish. *Developmental dynamics*, **236**, 3077-87.

Wang, H. U., Chen, Z. F., and Anderson, D J (1998). Molecular distinction and angiogenic interaction between embryonic arteries and veins revealed by ephrin-B2 and its receptor Eph-B4. *Cell*, **93**, 741-53.

Wang, Y., Kaiser, M. S., Larson, J. D., Nasevicius, A., Clark, K. J., Wadman, S. A, Roberg-Perez, S. E., Ekker, S. C., Hackett, P. B., McGrail, M., et al. (2010). Moesin1 and Ve-cadherin are required in endothelial cells during in vivo tubulogenesis. *Development*, **137**, 3119-28.

Weir, E. K., Hong, Z., Porter, V. a, and Reeve, H. L. (2002). Redox signaling in oxygen sensing by vessels. *Respiratory physiology & neurobiology*, **132**, 121-30.

Weir, E. K., López-Barneo, J., Buckler, K. J., and Archer, S. L. (2005). Acute oxygen-sensing mechanisms. *The New England journal of medicine*, **353**, 2042-55.

Weiss, M. and Orkin, S. H. (1995). GATA transcription factors: key regulators of hematopoiesis. *Experimental hematology*, **23**, 99-107.

Westerfield, M. (2000). The zebrafish book: A guide for the labaratory use of zebrafish (Danio rerio) 4th ed. Eugene: Univ. of Oregon Press. ISBN 978-9994860579

Willenborg, C. and Prekeris, R. (2011). Apical protein transport and lumen morphogenesis in polarized epithelial cells. *Bioscience reports*, **31**, 245-56.

Williams, C. K., Li, J.-L., Murga, M., Harris, A. L., and Tosato, G. (2006). Up-regulation of the Notch ligand Delta-like 4 inhibits VEGF-induced endothelial cell function. *Blood*, **107**, 931-9.

Wolff, J. (1964). Die Ultrastruktur der Blutkapillaren. *Zeitschrift für Zellforschung*, **300**, 290-300.

Wu, H., Rossi, G., and Brennwald, P. (2008). The ghost in the machine: small GTPases as spatial regulators of exocytosis. *Trends in cell biology*, **18**, 397-404.

Xu, K. and Cleaver, O. (2011). Tubulogenesis during blood vessel formation. *Seminars in cell & developmental biology*, **22**, 993-1004.

Yaniv, K. Isogai, S., Castranova, D., Dye, L., Hitomi, J., and Weinstein, Brant M (2006). Live imaging of lymphatic development in the zebrafish. *Nature medicine*, **12**, 711-6.

Yeon, J. H., Hu, Q. P., Ryu, H. R., Chung, M. H., and Jeon, N. L. (2011). Guided formation of perfusable blood vessel and vascular fusion in a microfluidic device. *15th International Conference on miniaturized systems for chemistry and life sciences*, 864-866.

Yonemura, S., Itoh, M., Nagafuchi, A, and Tsukita, S. (1995). Cell-to-cell adherens junction formation and actin filament organization: similarities and differences between non-polarized fibroblasts and polarized epithelial cells. *Journal of cell science*, **108**, 127-42.

You L-R., Lin F-J., Lee T. C., DeMayo J. Francesco., Tsal M-J., Tsal S. (2005). Suppression of Notch signalling by the COUP-TFII transcription factor regulates vein identity. *Nature*, **435**, 98-103.

Yu, W., Datta, A., Leroy, P., O'Brien, L. E., Mak, G., Jou, T.-S., Matlin, K. S., Mostov, Keith E, and Zegers, M. M. P. (2005). Beta1-integrin orients epithelial polarity via Rac1 and laminin. *Molecular biology of the cell*, **16**, 433-45.

Zhong, T. P. (2000). gridlock, an HLH Gene Required for Assembly of the Aorta in Zebrafish. *Science*, **287**, 1820-1824.

Zhong, T P, Childs, S, Leu, J. P., and Fishman, M C (2001). Gridlock signalling pathway fashions the first embryonic artery. *Nature*, **414**, 216-20.

Zovein, A. C., Luque, A., Turlo, K. a, Hofmann, J. J., Yee, K. M., Becker, M. S., Fassler, R., Mellman, I., Lane, T. F., and Iruela-Arispe, M. L. (2010). Beta1 integrin establishes endothelial cell polarity and arteriolar lumen formation via a Par3-dependent mechanism. *Developmental cell*, **18**, 39-51.

van der Zwaag, B., Hellemons, A. J. C. G. M., Leenders, W. P. J., Burbach, J. P. H., Brunner, H. G., Padberg, G. W., and Van Bokhoven, H. (2002). PLEXIN-D1, a novel plexin family member, is expressed in vascular endothelium and the central nervous system during mouse embryogenesis. *Developmental dynamics*, **225**, 336-43.

9 Appendix

9.1 Supplementary figures

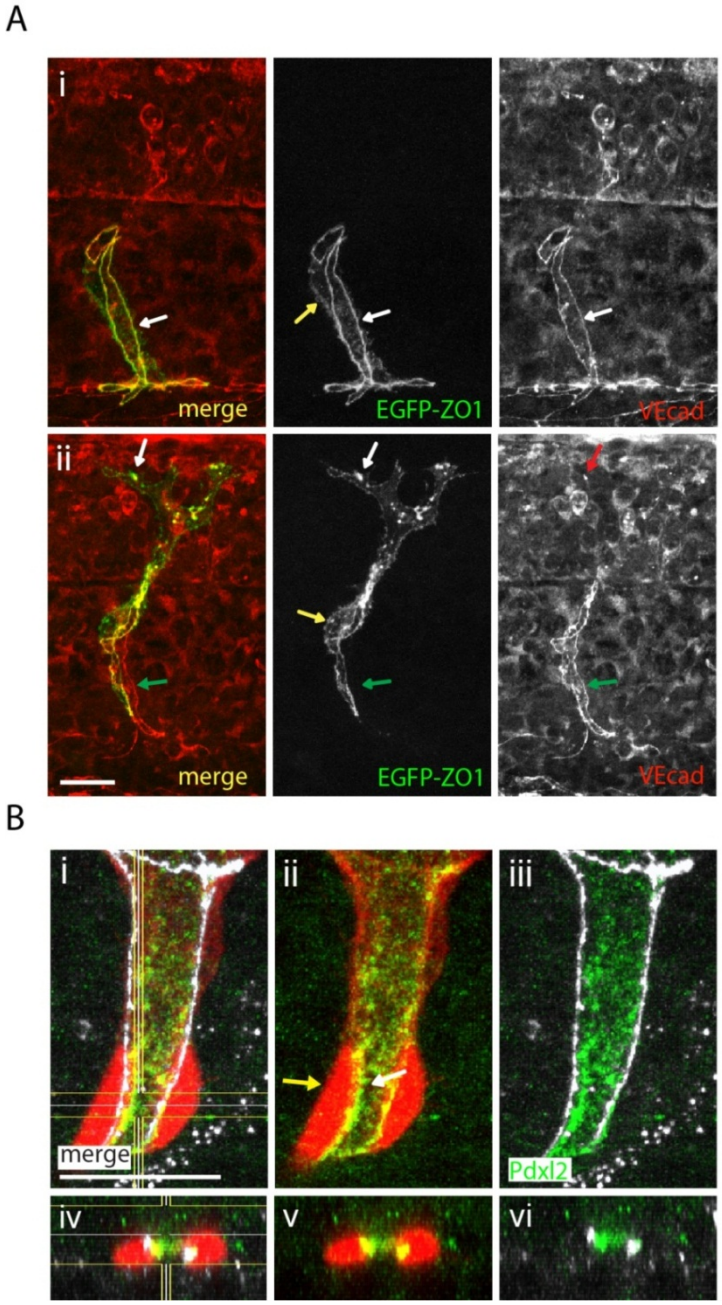

Figure 33 EGFP-ZO1 colocalizes with endogenous VE-cad. (Ai) shows a stalk cell and (Aii) shows a tip cell, where both proteins colocalize along cell junctions and presumptive autocellular contact points (white arrows). Since expression of EGFP-ZO1expression is mosaic, some VE-cad positive junctions are not labeled by EGFP-ZO1 (green arrows). Delocalized ZO1-EGFP protein is found in the cell membrane (yellow arrow**). Luminal localization of Pdxl2 in the zebrafish vasculature.** (B) Optical sections through an ISV at 38hpf showing the distribution of apical and junctional staining in ECs. Sagittal (Bi-iii) and cross (Biv-vi) sections are indicated by crosshairs (i, iv). Pdxl2 is visible only in the luminal site i.e. the apical side (white arrow in ii) of the cells and not the basal side (yellow arrow in ii). (i-vi) ZO1 (white) and Pdxl2 (green) immunolocalization on Tg(*kdrl:EGFP S843*) (red) embryos. The scale bar in all panels represents 20 µm. Figure adapted from Herwig et al, 2011.

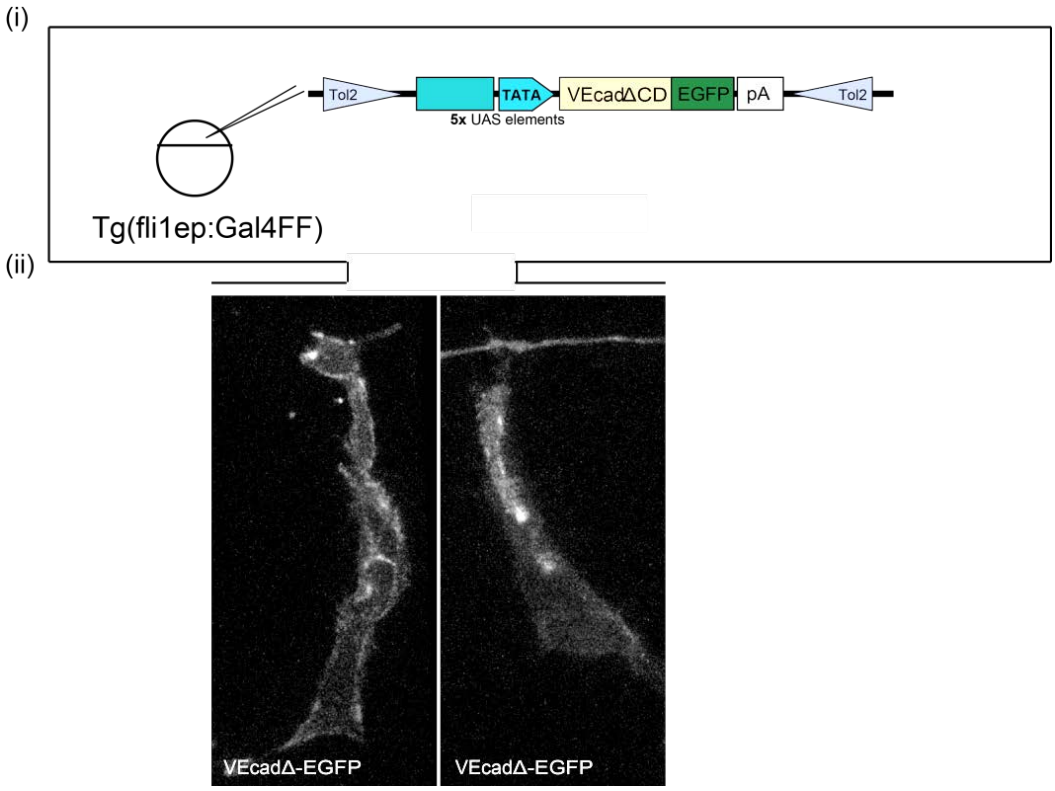

Figure 34 Transient expression of VEcadΔCD-EGFP in endothelial cells. (i) pT25xUAS:VEcadΔCD-EGFP was injected into fertilized eggs from Tg(fli1ep:Gal4FF) zebrafish. Embryos were raised until 32 hpf and checked for transient expression. (ii) Two individual ISVs with ECs expressing VEcadΔCD-EGFP. VEcadΔCD-EGFP localizes as dots and lines in between/in these cells.

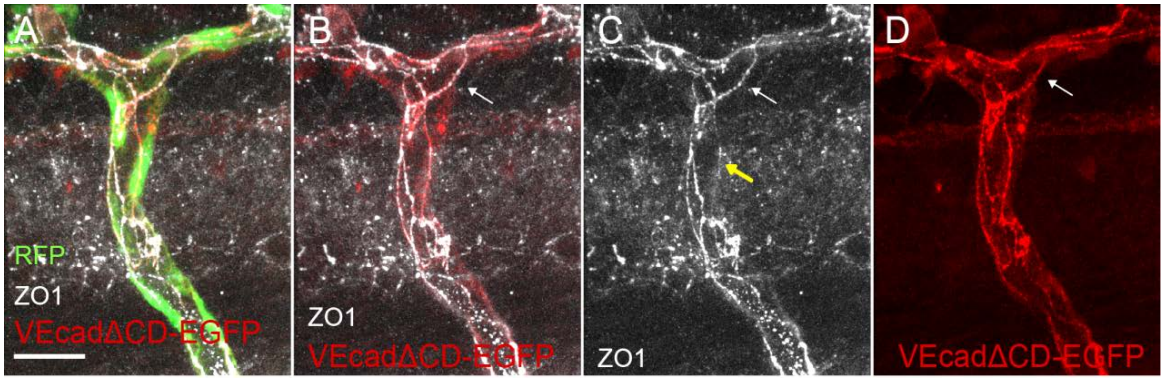

Figure 35 VEcadΔCD-EGFP co-localizes with endogenous ZO1. (A-D) shows upper part and parts of an ISV and the DLAV. Both proteins co-localize along cell junctions (for instance white arrow in (B)). Since expression of EGFP-ZO1expression is mosaic, some VE-cad positive junctions are not labeled by EGFP-ZO1 (green arrows). Delocalized ZO1-EGFP protein is found in the cell membrane (yellow arrow). Figure courtesy of A. Lenard, Affolter lab.

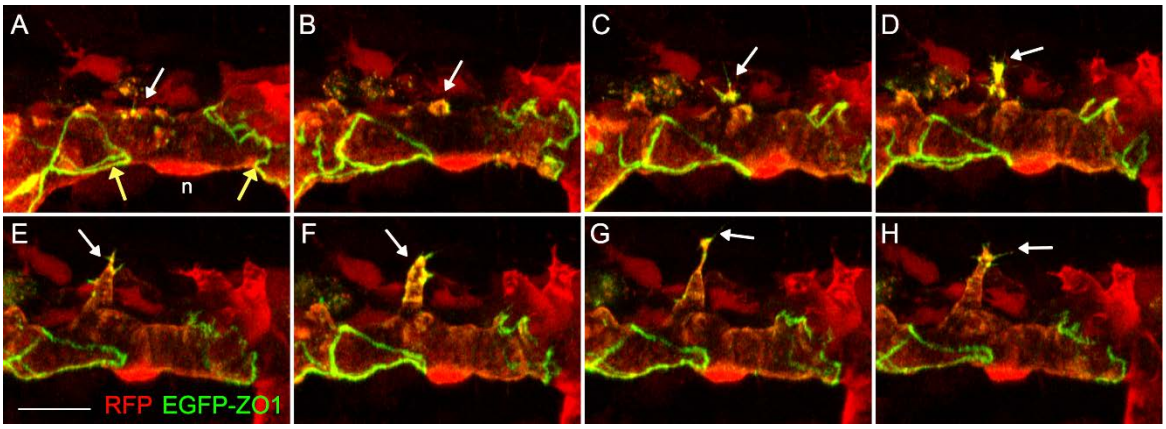

Figure 36 Formation of a sprout in the DLAV at 48 hpf. (A) A seamless EC cell bridging two ISV segments. The two junctional complexes connecting the cell at its anterior and posterior to the nucleus (n) are indicated by yellow arrows. White arrow shows future site of sprout formation. (B-H) The outgrowing lumenized sprout from the DLAV (follow white arrows). EGFP-hZO1 localizes to the tip of the sprout as visible in (C-H).(see Movie8 on DVD)

9.2 Research publications

9.2.1 Publication: Distinct Cellular Mechanisms of Blood Vessel Fusion in the Zebrafish Embryo

followed by

9.2.2 Publications from collaborations[4]

followed by

9.3 *Science*: editor's choice article

9.4 Curriculum vitae

[4] Order of publications: according date of publication.

Current Biology 21, 1942–1948, November 22, 2011 ©2011 Elsevier Ltd All rights reserved DOI 10.1016/j.cub.2011.10.016

Report

Distinct Cellular Mechanisms of Blood Vessel Fusion in the Zebrafish Embryo

Lukas Herwig,[1,2] Yannick Blum,[1,2] Alice Krudewig,[1] Elin Ellertsdottir,[1] Anna Lenard,[1] Heinz-Georg Belting,[1,*] and Markus Affolter[1,*]
[1]Biozentrum der Universität Basel, Klingelbergstrasse 70, CH-4056 Basel, Switzerland

Summary

Although many of the cellular and molecular mechanisms of angiogenesis have been intensely studied [1], little is known about the processes that underlie vascular anastomosis. We have generated transgenic fish lines expressing an EGFP-tagged version of the junctional protein zona occludens 1 (ZO1) to visualize individual cell behaviors that occur during vessel fusion and lumen formation in vivo. These life observations show that endothelial cells (ECs) use two distinct morphogenetic mechanisms, cell membrane invagination and cord hollowing to generate different types of vascular tubes. During initial steps of anastomosis, cell junctions that have formed at the initial site of cell contacts expand into rings, generating a cellular interface of apical membrane compartments, as defined by the localization of the apical marker podocalyxin-2 (Pdxl2). During the cord hollowing process, these apical membrane compartments are brought together via cell rearrangements and extensive junctional remodeling, resulting in lumen coalescence and formation of a multicellular tube. Vessel fusion by membrane invagination occurs adjacent to a preexisting lumen in a proximal to distal direction and is blood-flow dependent. Here, the invaginating inner cell membrane undergoes concomitant apicobasal polarization and the vascular lumen is formed by the extension of a transcellular lumen through the EC, which forms a unicellular or seamless tube.

Results and Discussion

Generation and expansion of vascular beds by vascular remodeling involves a variety of morphogenetic mechanisms such as angiogenic sprout and lumen formation, as well as blood vessel fusion (anastomosis) and vessel pruning. Anastomosis is the essential process that converts dead-end sprouts into a functional vascular network. Angiogenic sprouts are guided by so-called tip cells, which are more motile and send out more filopodia than the trailing stalk cells [2]. During the first step of anastomosis, tip cells from neighboring sprouts establish contact with each other [3, 4]. Subsequently, endothelial cells (ECs) from neighboring sprouts form a continuous endothelium and their lumens are connected. How these events are achieved and coordinated at the cellular level is not known. We have used the zebrafish dorsal longitudinal anastomotic vessels (DLAV) as a model to analyze the cellular mechanisms that underlie vascular anastomosis in vivo. To this end, we generated transgenic reporter lines that label endothelial cell junctions [Tg(*fli1ep:GAL4FF*$^{ubs2-4}$) and Tg(*UAS:EGFP-ZO1*$^{ubs5-6}$), see Figure S1 available online]. These lines allowed us to follow individual cell junctions and, consequently, relative cell movements and cell shape changes, as they occur during vascular remodeling.

The DLAV is formed in a seemingly stereotypic pattern by the anastomosis of neighboring segmental arteries (SA) [5]. Tip cells of individual SAs that have reached the roof of the neural tube extend processes laterally both in rostral and caudal directions. Some of these filopodia emanating from neighboring tip cells eventually contact each other, stabilize, and integrate into the DLAV. During further development, a lumen extends through the SA and the DLAV (see Figure 1A and Figure S1A). We first examined the cellular architecture of the DLAV to determine whether this vessel is made of unicellular or multicellular tubes. By photoconversion of the fluorophore KAEDE in Tg(*fli1ep:GAL4FF*^{ubs3}*; UAS:KAEDE*^{rk8}) embryos, we labeled single cells within the DLAV and determined whether these spanned the circumference of the DLAV either entirely or partially (Figures 1B and 1C). In 16 out of 24 cases, we found cells enclosing the entire lumen representing a unicellular tube, whereas in 8 out of 24 cases, labeled cells covered the vessel only partially, which is indicative for multicellular tubes. To test whether the different cellular arrangements correspond to the patterns of EC junctions, we performed photoconversion experiments and subsequently visualized adherens junctions by immunofluorescence using an antibody against zebrafish-VE-cadherin (zf-VE-cad) [6]. Consistently, we found that unicellular regions did not contain junctions (Figures 1D and 1D′), whereas photoconverted cells, which are nested within a multicellular region, were demarcated by longitudinal lines of VE-cad (Figures 1E and 1E′).

To visualize endothelial cell contacts in vivo, we generated transgenic reporter lines Tg(*UAS:EGFP-ZO1*$^{ubs5-6}$) (Figure S1B). In double transgenic embryos (Tg*fli1ep:GAL4FF*^{ubs3}*; UAS:EGFP-ZO1*^{ubs5}), we compared the localization of the EGFP-zona occludens 1 (ZO1) fusion protein with the distribution of VE-cad and found that it specifically labels cell junctions, albeit in a mosaic fashion (Figure S1C). Furthermore, we confirmed the heterogeneity in vascular architecture described above by the junctional patterns observed in vivo in these embryos. We found regions that had predominantly ring-shaped cell contacts (Figure 1F) as well as regions that contained more complex junctional patterns (Figure 1G). Thus, DLAVs are heterogeneous in their architecture and can consist of different types of tubes: unicellular tubes, multicellular tubes, and tubes of mixed cellular arrangements.

To analyze the cellular dynamics of DLAV formation, we first focused on the initial events of contact formation between neighboring tip cells. From studies using immunofluorescent detection of ZO-1, we previously proposed a model in which interactions between tip cells lead to the generation of junctional spots at the contact sites [6]. These spots elaborate into rings as the cells increase their mutual surface area. Analysis of VE-cad protein revealed identical patterns (Figures 1H–1J). Because this sequence of events was inferred from observations in fixed tissues, we wanted to test this model in

[2]These authors contributed equally to this work
*Correspondence: heinz-georg.belting@unibas.ch (H.-G.B.), markus.affolter@unibas.ch (M.A.)

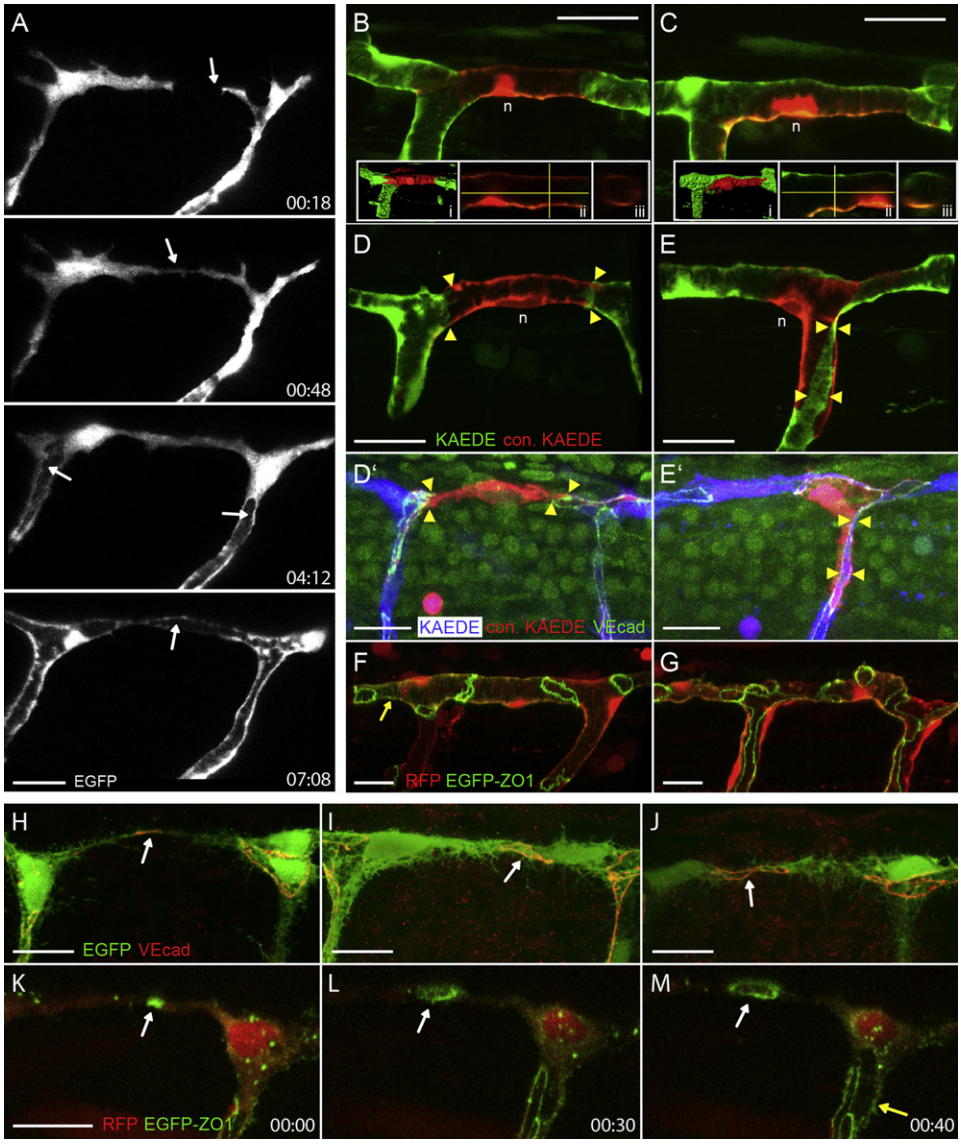

Figure 1. Anastomosis and Heterogeneity of Endothelial Tubes

(A) Still pictures of a time-lapse movie (data not shown) showing steps during dorsal longitudinal anastomotic vessel (DLAV) formation. Tip cells reach the dorsal side of the embryo and send filopodia in anterior and posterior directions (arrow in 00:18 [hr:min]). The tip cells contact each other and form the future DLAV (arrow in 00:48). Later the lumen opens from the stalk and proceeds into the DLAV (arrows in 4:12 and 7:08).

(B–G) Different vessel architectures are found in the intersegmental vessel (ISV)/DLAV. Single, photoconverted cells (red) show a unicellular (B) or a multicellular arrangement (C). Inserts (i–iii) in (B) and (C) show a surface calculation (i), a sagittal section (ii), and a cross-section (iii) at the sites indicated by crosshairs (n = nucleus).

(D–E′) Single photoconverted cells (red) and corresponding VE-cadherin (VE-cad) immunostainings. Arrowheads indicate regions of unicellular (D and D′) and multicellular (E and E′) tubes. A unicellular tube outlined by EGFP-zona occludens 1 (ZO1) fusion protein is shown in (F), and multicellular/unicellular and mixed arrangements represented by EGFP-ZO1 protein are shown in (G). The yellow arrow in (F) points at delocalized EGFP-ZO1 protein in the cell membrane, most likely due to elevated levels of protein.

(H–J) VE-cad immunostainings of 30 hrs postfertilization (hpf) old *fli:EGFP* embryos. Spots and small and larger rings are shown in (H), (I), and (J), respectively (see arrows).

(K–M) Still pictures of Movie S1 showing a time-lapse of a *fli:GAL4FF; UAS:RFP; UAS:EGFP-ZO1* embryo. An initial contact spot of EGFP-ZO1 (arrow in K) is elaborated into a small (arrow in L) and subsequently into a larger loop (arrow in M; Movie S1). The yellow arrow in (M) points to delocalized EGFP-ZO1 in the cell membrane (compare F and Figure S1). Scale bar in all pictures represents 20 μm.

an in vivo situation by performing confocal time-lapse analyses on our EGFP-ZO1 reporter lines. In essence, the pattern of EGFP-ZO1 was congruent with our previous observations, thus confirming the above model (Figures 1K–1M; Movie S1). Moreover, junctional remodeling is extremely dynamic—the transformation from spots to rings occurs within less than 40 min.

Whereas initiation of anastomosis appeared to be consistently associated with formation of ring-shaped junctions, the subsequent establishment of the DLAV showed considerably greater complexity and variety—in respect to (1) junctional remodeling, which corresponds to extensive cell rearrangements, (2) the generation of a continuous endothelium with apical-basal polarity, and (3) lumen formation. After

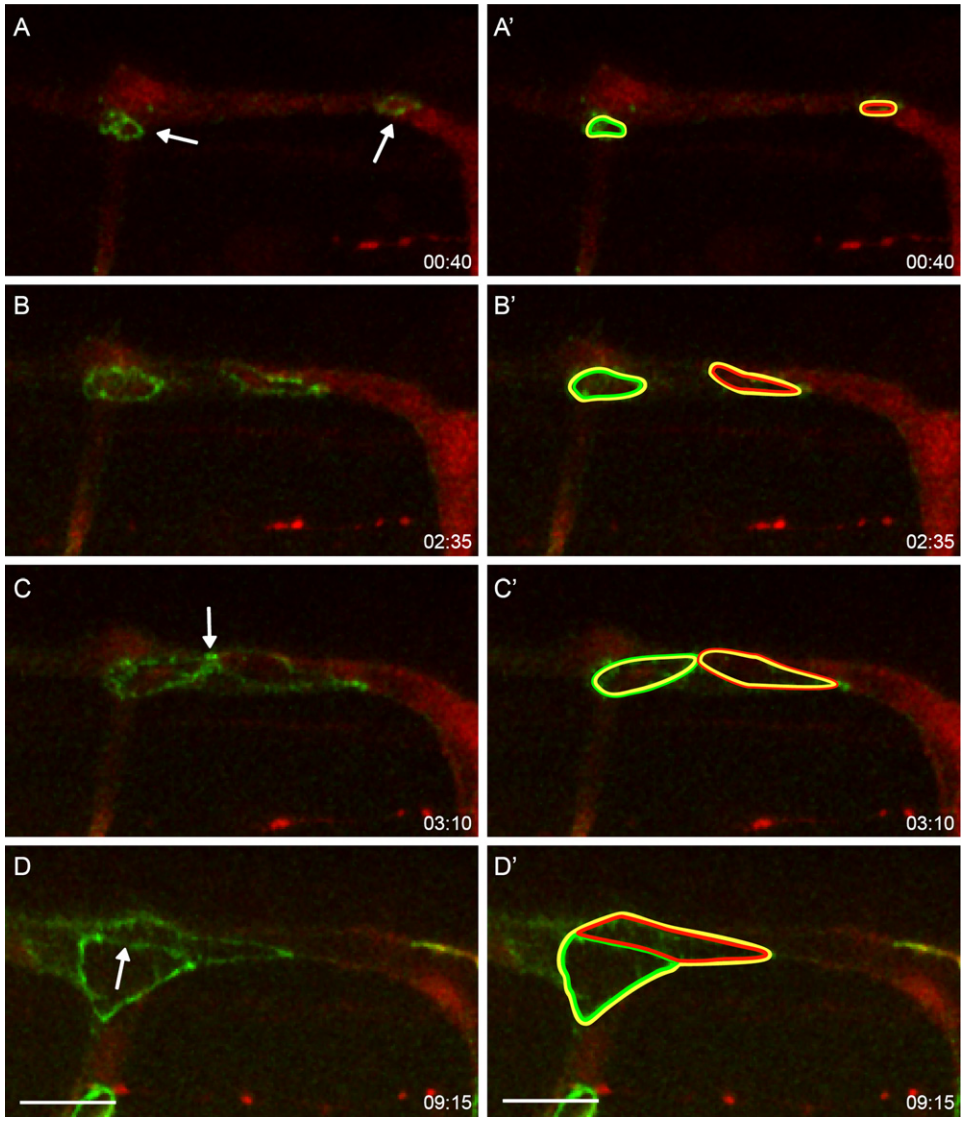

Figure 2. Anastomosis by Cord Hollowing

Still pictures from Movie S2 showing a time-lapse of a *fli:GAL4FF; UAS:RFP; UAS:EGFP-ZO1* embryo (total length: 9:20).

(A–C) A tip cell has established contact with an adjacent tip cell (right arrow) and has contact with a stalk cell (left arrow), which results in two loops of EGFP-ZO1 (A). These loops extend and eventually meet (B and C).

(A′–D′) shows the junctional outline of participating cells (yellow: "central" cell, green: stalk cell, red: DLAV cell moving in from posterior [right]). The two initial cell contacts are shown in yellow/green and yellow/red, respectively. When the stalk cell and the adjacent DLAV cell meet, they establish a new contact with "green and red" junctions (arrow in D, green and red line in D′). Scale bar in all pictures represents 20 μm.

analysis of 15 time-lapse movies representing 19 fusion events, we were able to discern two distinct behaviors with regard to junctional remodeling, which show two alternative cellular mechanisms that underlie DLAV formation (Figure 2; Figure 3).

In many instances (7 out of 19 events), we observed a mechanism that is primarily driven by cell rearrangements (Figure 2; Movie S2). Here, cell contacts between at least three adjacent cells generate two junctional rings, which converge toward each other as the outer cells migrate over a central cell. This convergence ultimately leads to novel contacts between the outer cells, the establishment of a new junction, and the detachment of the medial cell at this site of contact (summarized in Figure S2). Thus, the outcome of this process is the merging of local lumens, which are contained within the junctional rings, to form a continuous luminal space. In principle, this mechanism of luminal coalescence can act locally or, if occurring iteratively, can be used to lumenize longer stretches to generate a patent tube.

In the majority of time-lapse movies (12 out of 19 events), we observed an alternate mechanism of vessel fusion that is intrinsically connected to a different mechanism of lumen formation. In these instances, junctional rings did not move or extend toward each other, the cells exhibited much less migratory behavior, and we did not find continuous adherens junctions along the vascular axis (Figure 3; Movie S3). Instead, the ECs maintained their junctions in a ring shape throughout the process of lumenization. Imaging the dynamics of lumen formation in vivo, either by intravascular quantum dot injection or by lack of cytoplasmic RFP, revealed that the lumen

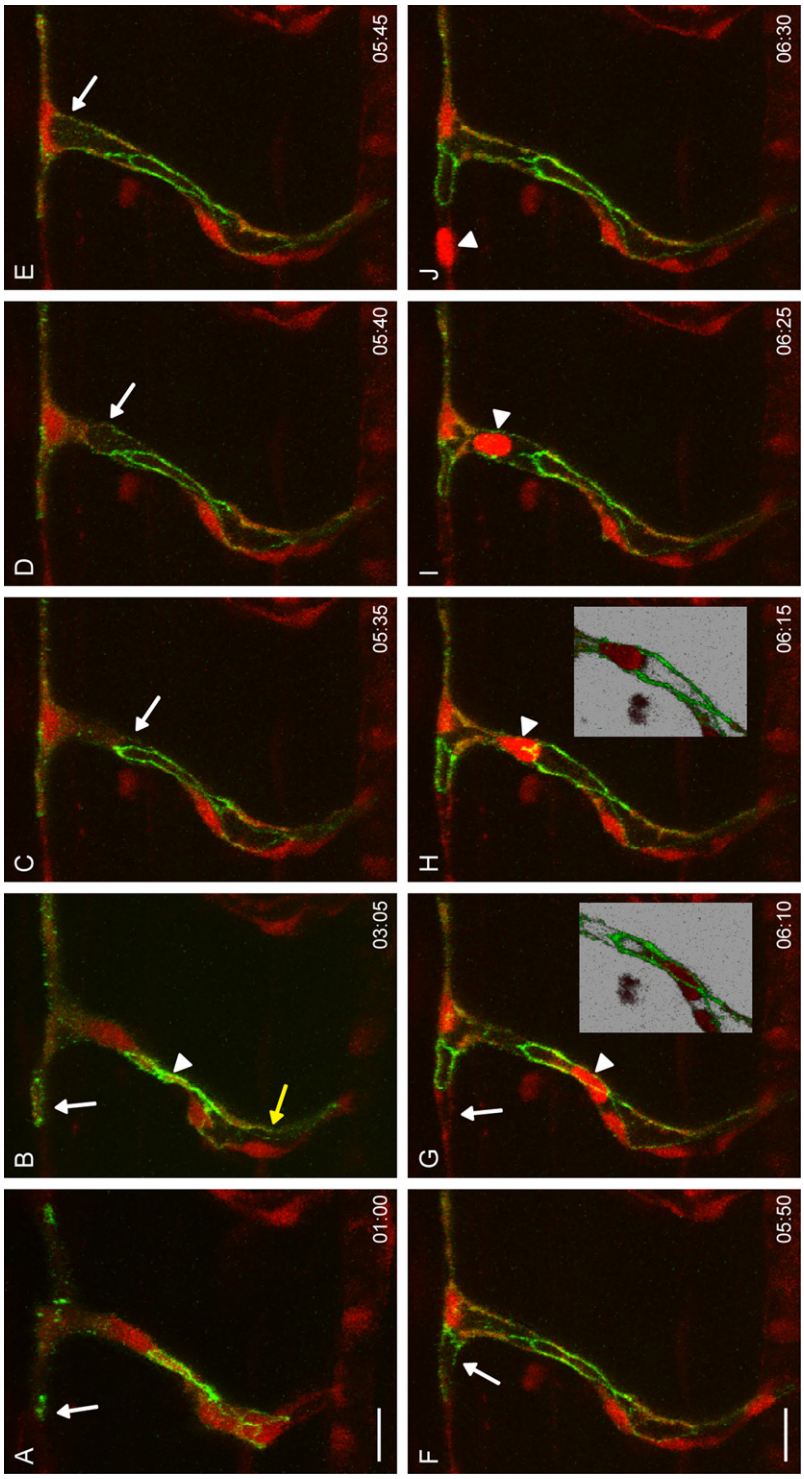

Figure 3. Anastomosis by Membrane Invagination

Still pictures from Movie S3 showing a time-lapse of a Tg(*fli:GAL4FF*^{ubs3}*; UAS:mRFP*^{rk8}*; UAS:EGFP-ZO1*^{ubs5}) embryo (total length: 10:25).

(A and B) A tip cell has formed initial contacts and subsequently forms loops of EGFP-ZO1 with its adjacent partner (white arrows). The stalk shows a multicellular organization (two lines of EGFP-ZO1, arrowhead in B) and an opening lumen (yellow arrow in B).

(C) The lumen projects into the fusion cell (follow arrow from C to E) and finally reaches the left ring of EGFP-ZO1, which is subsequently inflated (arrow in F). The lumen then continues to extend into the unlabeled fusion cell on the left (arrow in G). A blood cell then passes through the newly formed lumen (follow arrowhead from G–J). Insets show the blood cell passing behind the junction (G) and in front of the junction (H). More examples of membrane invagination are shown in Movie S4, Movie S6, and Figures S3B and S3C. Scale bar in all pictures represents 20 μm.

extended through a single cell between two separate sites of contact (Figure S3B; Movie S3; Movie S4, summarized in Figure S2). This mechanism thus leads to a transformation of the tip cell into a "fusion cell," which forms a unicellular tube. This was demonstrated by a blood cell serendipitously passing through the two junctional rings of a hollowed-out EC (insets in Figure 3 and Movie S3).

De novo formation of an epithelial lumen is initiated by the apical-basal polarization of cell membranes [7]. Members of the CD35 family of sialomucins have been shown to localize to the luminal (apical) membrane compartments of ECs in the mammalian vascular system [8]. To examine apical polarization during DLAV formation, we generated antibodies against zebrafish podocalyxin-2 (Pdxl2) and found that it specifically localized to the luminal membranes throughout the zebrafish vasculature (Figure 4A; Figure S1D; data not shown). Importantly, we observed Pdxl2 in membrane compartments within junctional rings shortly after contact formation (Figure 4B), indicating that the future luminal membrane becomes apically polarized during early steps of anastomosis prior to the morphogenetic movements that lead to lumen coalescence during cord hollowing. In agreement with our live observation, we also found Pdxl2 in junction-free segments of DLAVs and intersegmental vessels (ISVs) (Figure S1D). Examination of younger embryos (36 hrs post-fertilization [hpf]) revealed patterns of Pdxl2 protein extending from a multicellular base of SAs into the tip cell (Figure 4C). This continuous Pdxl2 domain is consistent with an expansion of the vascular lumen from a multicellular into a unicellular surrounding and indicates that the tip cell becomes polarized as its cell membrane invaginates.

Because cell membrane invagination occurs directionally and can form a patent lumen within a few hours, we tested whether blood flow is required for lumen formation during anastomosis by the injection of antisense morpholinos against cardiac troponin (silent heart, *sih*, *tnnt2a*) [9] into Tg(*fli:gal4FF;UAS:GFP-ZO1*) embryos. We recorded a total of six time-lapse movies and observed that the initial steps of anastomosis, i.e., the formation and elaboration of the initial junctional rings, were relatively normal and that cell movements appeared unaffected (Figure S3A; Movie S5; data not shown). However, the vascular lumen of *sih* morphants does not inflate, and lumen formation proved difficult to monitor in vivo. Therefore, we used the Pdxl2 antibodies

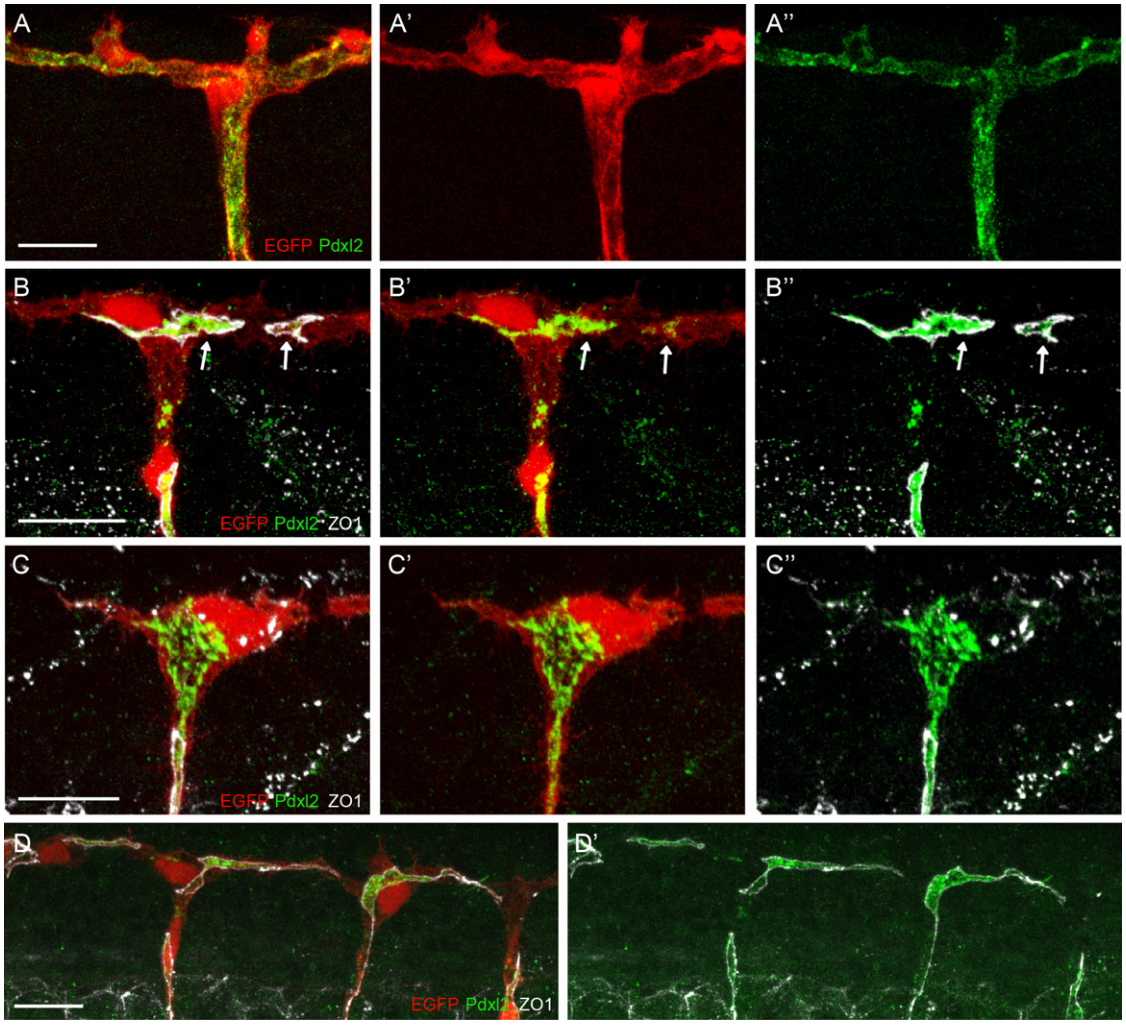

Figure 4. Visualization of Apical Membrane during Anastomosis

(A–A″) Pdxl2 antibodies label apical cell membranes in ISVs and DLAV at 48 hpf.

(B–B″) Pdxl2 is localized within a junctional ring (arrow) at the contact site of two tip cells at the onset of anastomosis (36 hpf).

(C–C″) Apical membrane invaginating into a tip cell at 36 hpf is shown by Pdxl2 immunostaining.

(D–D′) In *sih* morphants at the same stage, the Pdxl2 staining is only seen within the junctional rings, indicating that apical membrane invagination does not take place in the absence of blood flow.

Also compare Movie S3 and Figure S3A. α-ZO1 is shown in white, α-Pdxl2 in green, and *kdrl:EGFP* in red. Scale bar in all pictures represents 20 μm.

to examine the formation of apical cell membranes in *sih* morphant embryos and found that Pdxl2 was largely restricted to multicellular domains except for spurious signals in unicellular regions (Figure 4D). During examination of 60 tip cells at 36 and 48 hpf, respectively, we did not find any occurrence of membrane invagination (see Table S1). These findings indicate that blood flow is dispensable for cell rearrangements during DLAV formation and for EC polarization per se. It is, however, required for membrane invagination, which leads to the formation of unicellular tubes, indicating that blood pressure may be the driving force of this morphogenetic process.

Taken together, we have shown that vascular anastomosis during DLAV formation can occur by very different morphogenetic mechanisms, either by a cord hollowing process generating a multicellular tube or by cell membrane invagination resulting in a unicellular tube, as summarized in Figure 5. In both cases, anastomosis is intrinsically connected with de novo lumen formation at the site of vessel fusion, and the future luminal membrane compartments show apical polarization before the blood vessel becomes patent. At the cellular level, these mechanisms are drastically different because they are driven by cell rearrangements and cell shape changes, respectively. Cord hollowing mechanisms have been described in different vertebrate tissues including the mouse dorsal aorta [8] and the zebrafish neural tube [10, 11] and intestine [12]. However, the cord hollowing mechanism we describe appears unique, because it is driven by cell rearrangements rather than lumen expansion. In contrast, a mechanism of remarkable similarity has been described for hollowing the notochord in the ascidian *Ciona intestinalis* [13]. In both systems, the zebrafish DLAV and *Ciona* notochord, lumenization commences with the de novo establishment of apical domains between neighboring cells and is followed by cell movements and cell shape changes, which result in the fusion of luminal spaces and the formation of a continuous endothelium.

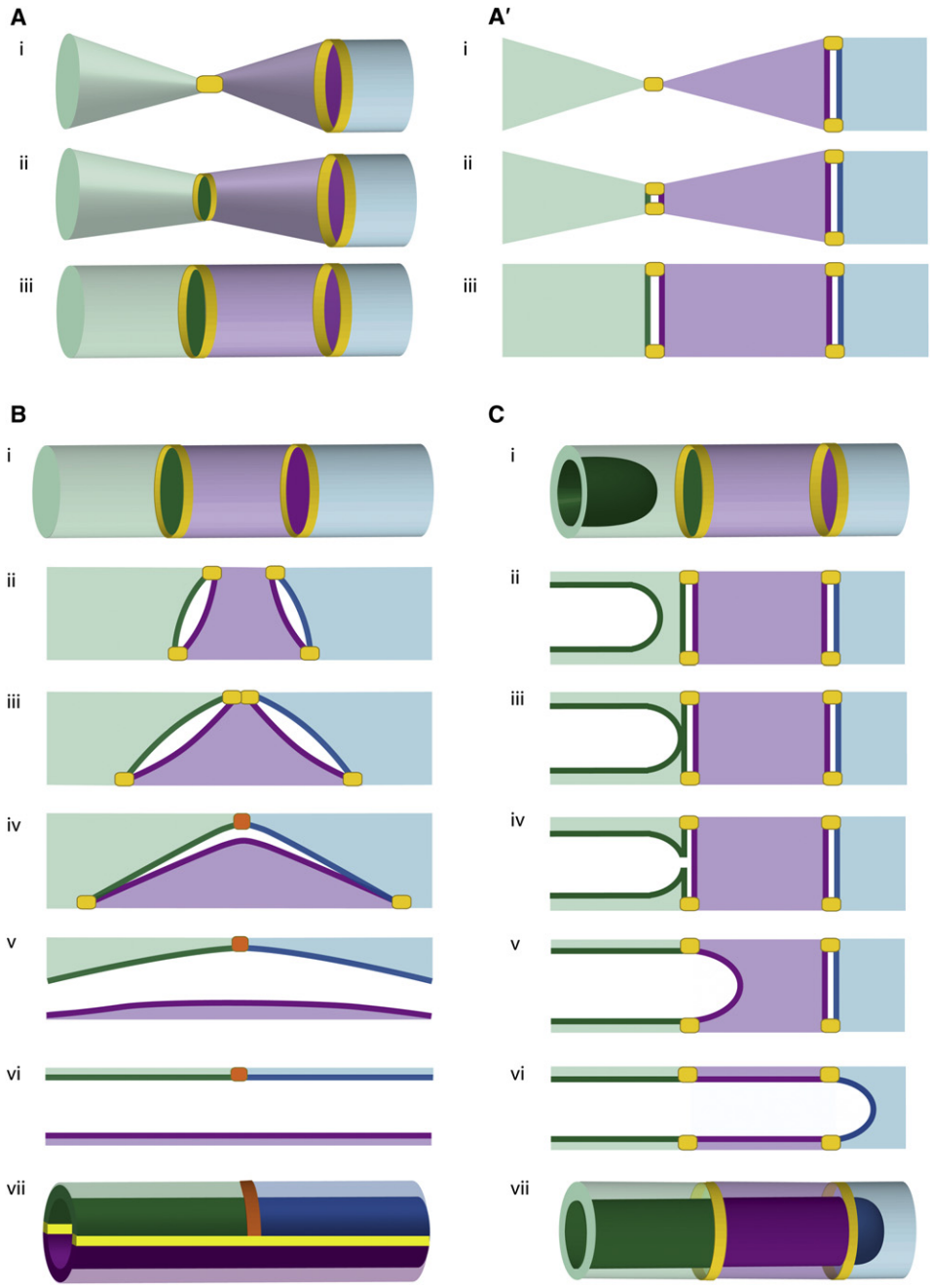

Figure 5. A Model of Cellular Mechanisms during Anastomosis

(A and A′) Contact formation during vessel fusion is shown in (A) and corresponding sagittal sections in (A′). At the contact site of two neighboring tip cells (green and purple), junctional proteins are deposited (yellow spot in i). As the cells increase their mutual surface, this spot transforms into a ring (ii and iii), and the enclosed membrane compartment becomes apically polarized (dark green and dark purple areas). Subsequently, two different cellular mechanisms are used to complete the fusion process (see B and C).

(B) A cord hollowing mechanism results in a multicellular tube. Cell rearrangements bring together two junctional rings, i.e., two apical membrane compartments that then merge into one membrane compartment. This is achieved by the formation of a new junction (orange) between the green and blue cell, which leads to the detachment of the middle cell (purple) at the site of the new contact.

(C) Cell membrane invagination leads to the formation of a unicellular, seamless tube. Here, apical membrane of the green cell invaginates into the green cell. It then fuses with its own apical membrane at the previously formed contact side between the green and purple cells (see A). From here the lumen, i.e., the apical membrane of the neighboring cell (dark purple), begins to invaginate.

Endothelial cells are shown in green, purple, and blue; apical membranes are shown in dark green, dark purple, and dark blue; endothelial cell junctions are shown in yellow; and new endothelial cell junctions are shown in orange.

During the formation of unicellular tubes, the fusion cell undergoes drastic cell shape changes, as the proximal apical cell membrane compartment, which faces the preexisting lumen, invaginates into the cell along the future vascular axis (Figure 5). It thereby generates an extracellular space, which extends through the cell and can be classified as

a "transcellular lumen." According to our model, the invaginating membrane fuses with the distal membrane compartment to convert the fusion cell into a patent tube. Although we are not able to directly visualize membrane fusion in vivo, intracellular cell membrane fusion has been described during the development of the tracheal system of *Drosophila* [14–16]. The fusion cell of the DLAV may be considered analogous to the so-called doughnut cell, which is important for tubular fusion within the *Drosophila* tracheal system and eventually forms a seamless tube. In the case of the tracheal doughnut, it has been shown that this unicellular tube is generated by cell shape changes, which eventually lead to an intracellular membrane fusion [17]. The cell shape changes, which occur during vascular fusion, are far more dramatic than those in the tracheal system. We observed asymmetric cell shape changes, because the tip cell became hollowed in a proximo-distal direction. Furthermore, the direction of invagination was independent of the anatomical orientation and occurred either in a ventral to dorsal or dorsal to ventral direction (Figures S3B and S3C; Movie S4; Movie S6). In all cases, the lumen was formed in a continuous fashion, and we did not detect isolated luminal spaces within the cell.

Here, we have studied the anastomosis of ISVs, which results in the formation of a new vessel, the DLAV. We describe two morphogenetic mechanisms that govern vascular tube formation. These mechanisms, although used by the same type of blood vessel, employ very different cellular activities, cell rearrangements and cell invagination, respectively, to form and connect novel lumens and therefore lead to vessels of distinct cellular architectures. Both mechanisms are used at a comparable rate of instances, suggesting a stochastic selection of the process. Future experiments will explore the parameters, such as blood pressure, vessel size, and cell motility and number, which may influence the choice of mechanism, as well as the molecular mechanisms that underlie blood vessel fusion.

Supplemental Information

Supplemental Information includes three figures, one table, Supplemental Experimental Procedures, and six movies and can be found with this article online at doi:10.1016/j.cub.2011.10.016.

Acknowledgments

We thank Holger Gerhardt for continuous and valuable discussions, Koichi Kawakami for providing tol2-plasmids and Tg(*UAS:RFP*) fish, Chi-Bin Chien for providing pDestTol2CG2, Reinhard Köster for providing UAS-plasmids, Kumuthini Kulendra for fish care, and members of the Affolter group for critically reading the manuscript. A.K. and A.L. are supported by a fellowship from the Werner-Siemens-Foundation (Zug). This work has been supported by the Kantons Basel-Stadt and Basel-Land and by a grant from the Swiss National Science Foundation to M.A.

Received: June 7, 2011
Revised: September 29, 2011
Accepted: October 11, 2011
Published online: November 10, 2011

References

1. Herbert, S.P., and Stainier, D.Y.R. (2011). Molecular control of endothelial cell behaviour during blood vessel morphogenesis. Nat. Rev. Mol. Cell Biol. *12*, 551–564.
2. Gerhardt, H., Golding, M., Fruttiger, M., Ruhrberg, C., Lundkvist, A., Abramsson, A., Jeltsch, M., Mitchell, C., Alitalo, K., Shima, D., and Betsholtz, C. (2003). VEGF guides angiogenic sprouting utilizing endothelial tip cell filopodia. J. Cell Biol. *161*, 1163–1177.
3. Lawson, N.D., and Weinstein, B.M. (2002). In vivo imaging of embryonic vascular development using transgenic zebrafish. Dev. Biol. *248*, 307–318.
4. Ellertsdóttir, E., Lenard, A., Blum, Y., Krudewig, A., Herwig, L., Affolter, M., and Belting, H.-G. (2010). Vascular morphogenesis in the zebrafish embryo. Dev. Biol. *341*, 56–65.
5. Isogai, S., Lawson, N.D., Torrealday, S., Horiguchi, M., and Weinstein, B.M. (2003). Angiogenic network formation in the developing vertebrate trunk. Development *130*, 5281–5290.
6. Blum, Y., Belting, H.-G., Ellertsdottir, E., Herwig, L., Lüders, F., and Affolter, M. (2008). Complex cell rearrangements during intersegmental vessel sprouting and vessel fusion in the zebrafish embryo. Dev. Biol. *316*, 312–322.
7. Martin-Belmonte, F., and Mostov, K. (2008). Regulation of cell polarity during epithelial morphogenesis. Curr. Opin. Cell Biol. *20*, 227–234.
8. Strilić, B., Kucera, T., Eglinger, J., Hughes, M.R., McNagny, K.M., Tsukita, S., Dejana, E., Ferrara, N., and Lammert, E. (2009). The molecular basis of vascular lumen formation in the developing mouse aorta. Dev. Cell *17*, 505–515.
9. Sehnert, A.J., Huq, A., Weinstein, B.M., Walker, C., Fishman, M., and Stainier, D.Y.R. (2002). Cardiac troponin T is essential in sarcomere assembly and cardiac contractility. Nat. Genet. *31*, 106–110.
10. Tawk, M., Araya, C., Lyons, D.A., Reugels, A.M., Girdler, G.C., Bayley, P.R., Hyde, D.R., Tada, M., and Clarke, J.D.W. (2007). A mirror-symmetric cell division that orchestrates neuroepithelial morphogenesis. Nature *446*, 797–800.
11. Munson, C., Huisken, J., Bit-Avragim, N., Kuo, T., Dong, P.D., Ober, E.A., Verkade, H., Abdelilah-Seyfried, S., and Stainier, D.Y.R. (2008). Regulation of neurocoel morphogenesis by Pard6 gamma b. Dev. Biol. *324*, 41–54.
12. Bagnat, M., Cheung, I.D., Mostov, K.E., and Stainier, D.Y.R. (2007). Genetic control of single lumen formation in the zebrafish gut. Nat. Cell Biol. *9*, 954–960.
13. Dong, B., Horie, T., Denker, E., Kusakabe, T., Tsuda, M., Smith, W.C., and Jiang, D. (2009). Tube formation by complex cellular processes in Ciona intestinalis notochord. Dev. Biol. *330*, 237–249.
14. Tanaka-Matakatsu, M., Uemura, T., Oda, H., Takeichi, M., and Hayashi, S. (1996). Cadherin-mediated cell adhesion and cell motility in Drosophila trachea regulated by the transcription factor Escargot. Development *122*, 3697–3705.
15. Steneberg, P., Hemphälä, J., and Samakovlis, C. (1999). Dpp and Notch specify the fusion cell fate in the dorsal branches of the Drosophila trachea. Mech. Dev. *87*, 153–163.
16. Lee, S., and Kolodziej, P.A. (2002). The plakin Short Stop and the RhoA GTPase are required for E-cadherin-dependent apical surface remodeling during tracheal tube fusion. Development *129*, 1509–1520.
17. Kakihara, K., Shinmyozu, K., Kato, K., Wada, H., and Hayashi, S. (2008). Conversion of plasma membrane topology during epithelial tube connection requires Arf-like 3 small GTPase in Drosophila. Mech. Dev. *125*, 325–336.

Current Biology, Volume *21*

Supplemental Information

Distinct Cellular Mechanisms of Blood Vessel Fusion in the Zebrafish Embryo

Lukas Herwig, Yannick Blum, Alice Krudewig, Elin Ellertsdottir, Anna Lenard, Heinz-Georg Belting, and Markus Affolter

Supplemental Inventory

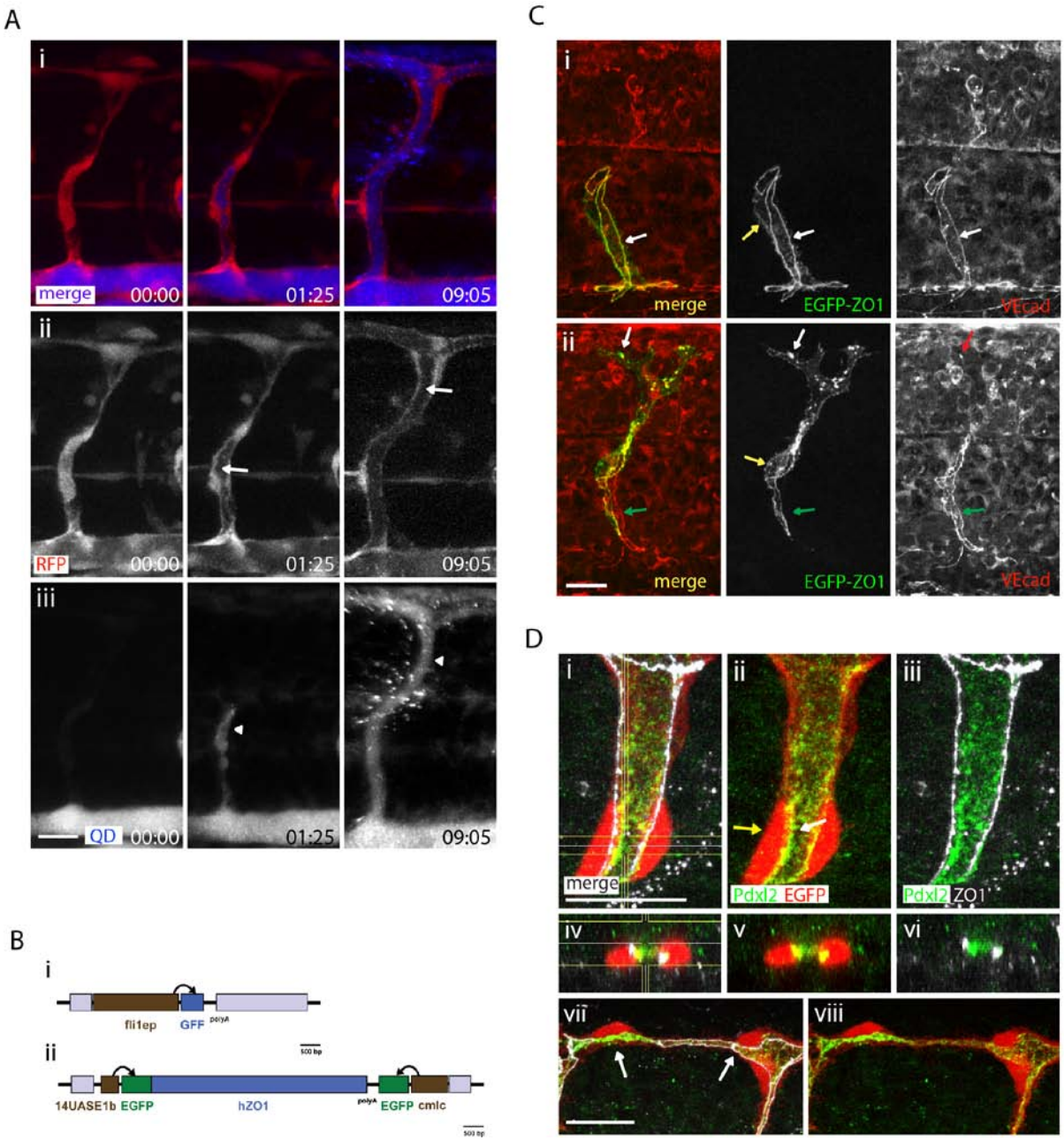
A
i
merge
00:00
01:25
09:05
ii
RFP
00:00
01:25
09:05
iii
QD
00:00
01:25
09:05
B
i
fli1ep
GFF
polyA
ii
500 bp
14UASE1b
EGFP
hZO1
polyA
EGFP
cmlc
500 bp
C
i
merge
EGFP-ZO1
VEcad
ii
merge
EGFP-ZO1
VEcad
D
i
merge
ii
Pdxl2
EGFP
iii
Pdxl2
ZO1
iv
v
vi
vii
viii

Figure S1. QD Labeling of the Lumen and Characterization of *fli1ep:Gal4ff^{ubs3};UAS:ZO1-EGFP^{ubs5}* Transgenic Lines, Related to Figure 1

(A) Lumen formation can be visualized by quantum dot (QD) injection and indirectly by a lack of RFP fluorescence. Picture series from a movie (data not shown). (i) merged images, (ii) RFP, (iii) QD. QD injected into the sinus venosus spread in the circulation visualizing patent lumens. Initially, QD are restricted to the dorsal aorta (DA) (time 00:00 in iii). Later the lumen is successively filled from the DA through the ISV and the DLAV (arrowheads in iii). The distribution of QD in the ISV correlates with a displacement of cytoplasm, which also correlates with a reduction of the cytoplasmic RFP signal (arrows in ii).

(B) DNA Gal4ff-driver and UAS-responder constructs used to generate transgenic reporter lines: Tol2 transposon sequences are shown as grey boxes. (i) schematic of the pT2fli1ep:GAL4FF driver construct, (ii) schematic of pT2UAS:EGFP-hZO1-cmlc2:EGFP responder construct.

(C) EGFP-ZO1 colocalizes with endogenous VE-cad. (i) shows a stalk cell and (ii) shows a tip cell, where both proteins colocalize along cell junctions and presumptive autocellular contact points (white arrows). Since expression of EGFP-ZO1expression is mosaic, some VE-cad positive junctions are not labeled by EGFP-ZO1 (green arrows). Delocalized ZO1-EGFP protein is found in the cell membrane (yellow arrow).

(D) Luminal localization of Pdxl2 in the zebrafish vasculature. Optical sections through an ISV at 38hpf showing the distribution of apical and junctional staining in ECs. Sagittal (i-iii) and cross (iv-vi) sections are indicated by crosshairs (i, iv). Pdxl2 is visible only in the luminal site i.e. the apical side (white arrow in ii) of the cells and not the basal side (yellow arrow in ii). In (vii-viii) the Pdxl2 apical membrane staining in the DLAV at 36 hpf present throughout the cell (left arrow) indicates transcellular lumen formed by a cell invagination process. The Podocalyxin2 apical membrane staining between the junctions (white arrow) indicates extracellular lumen formation by cell rearrangements. (i-viii) ZO1 (white) and Pdxl2 (green) immunolocalization on Tg(*kdrl:EGFP ^{S843}*) (red) embryos. The scale bar in all panels represents 20 μm.

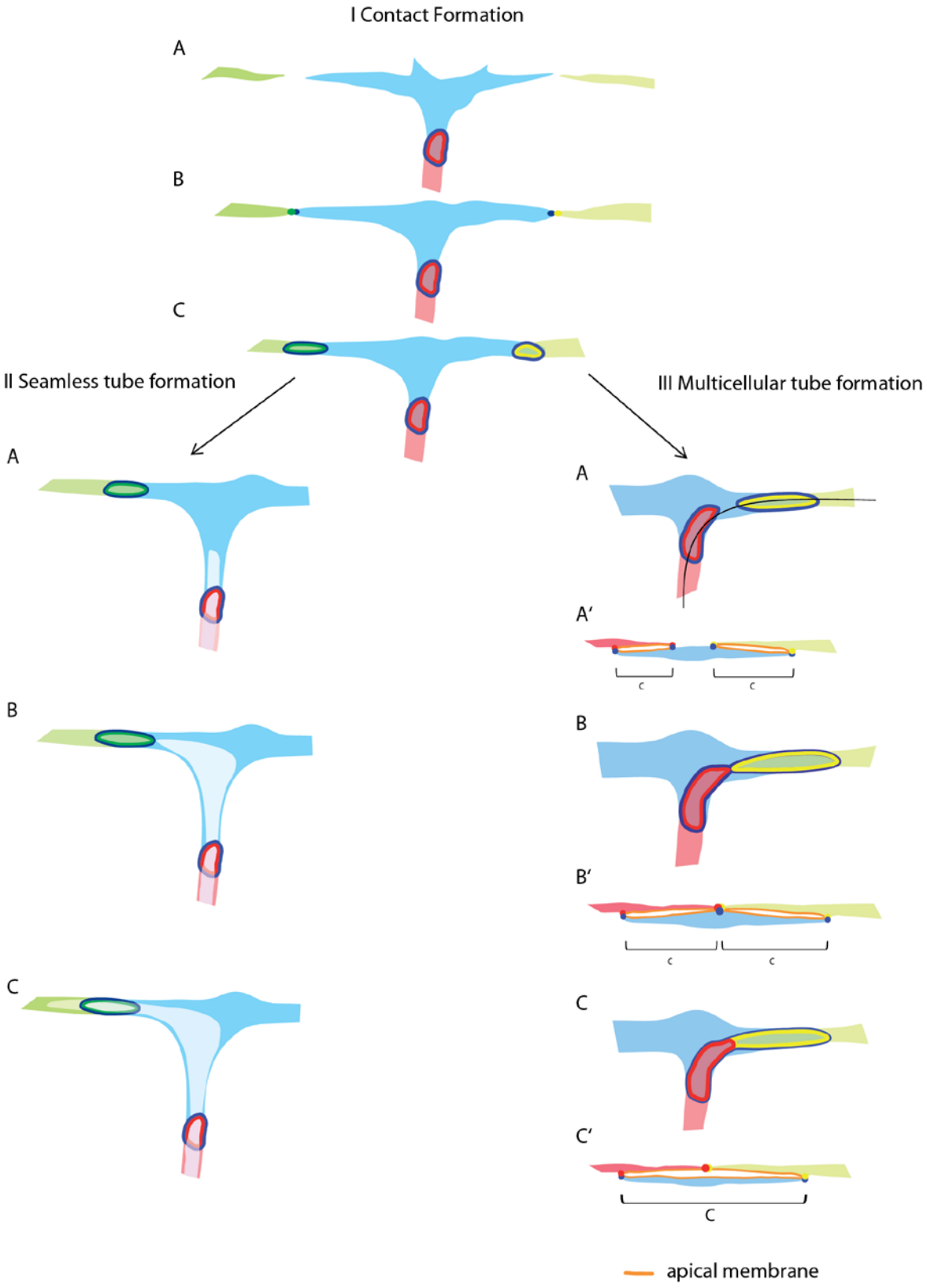
I Contact Formation
A
B
C
II Seamless tube formation
III Multicellular tube formation
A
B
C
A
A'
c
c
B
B'
c
c
C
C'
C
apical membrane

Figure S2. A Schematic Representation of the Sequence of Morphogenetic Events Observed in Movies S2 and S3, Related to Figures 2 and 3

(I) Neighboring tip cells deposit junctional proteins (*EGFP-ZO-1*) at the sites of contact formation (B). These areas expand leading to a transformation of the initial junctional spots into rings. Individual tip cells are shown in green, blue and yellow, respectively). The ISV stalk can be either unicellular or multicellular. For simplicity, a single adjoining stalk cell is shown in pink. Junctions are shown in two colors corresponding to the cell on either site of the cell contact. From here, two different morphogenetic mechanisms lead to two different types of tubes i.e. unicellular/seamless tubes (II) or multicellular tubes (III).

(II) A lumen extends from the dorsal aorta into the stalk and pushes into the "fusion/tip" cell (blue) (A) (The lumen is visualized in a lighter shade of the color of the surrounding cell). As the lumen reaches the distal end of the fusion cell (B), it merges with a local luminal compartment at the contact and begins to push into the neighboring EC (C).

(III) Several cells (pink, blue and yellow) enlarge their contact surfaces (A). Further cell rearrangements generate a novel contact between the pink and yellow cell (B) and lead to a local detachment of the blue cell at the novel contact site (C). As a result, two local compartments (blue/pink and blue/yellow) merge into a single multicellular lumen. (A') to (C') show longitudinal sections along the black line shown in (A). The scale bar in all panels represents 20 μm.

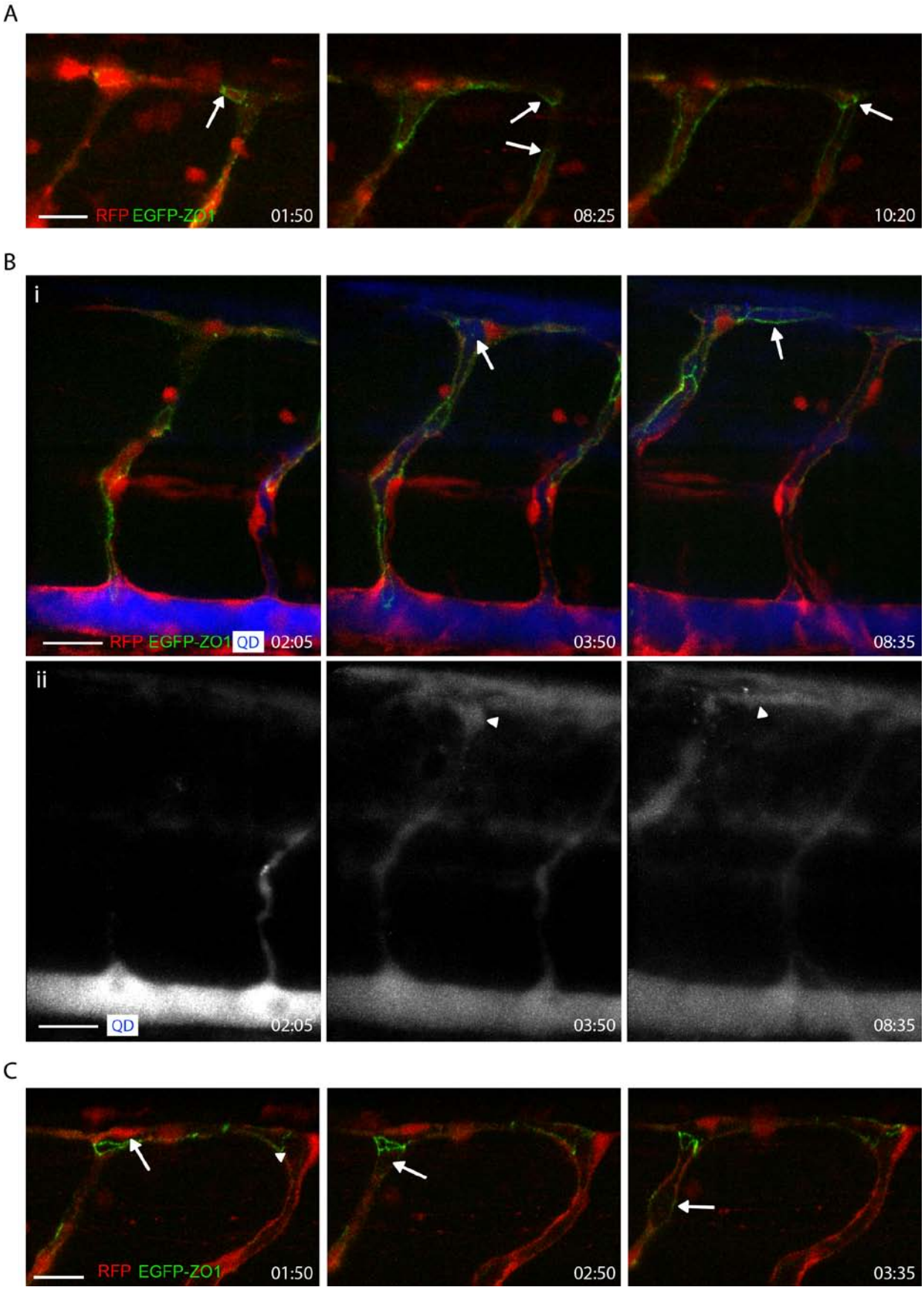
A
RFP EGFP-ZO1
01:50
08:25
10:20
B
i
RFP EGFP-ZO1 QD
02:05
03:50
08:35
ii
QD
02:05
03:50
08:35
C
RFP EGFP-ZO1
01:50
02:50
03:35

Figure S3. Lumen Invagination Visualized by QD Injection, Related to Figure 4

(A) Cell rearrangements do not depend on blood circulation. Series of pictures from movie S3. Fusion spots are transformed into rings (arrow at 01:50) and cell rearrangements (arrows at 08:25 and 10:20) still occur in *sih* morphant embryos.

(B) Microangiography in Tg(*fli1ep:Gal4ff*^{ubs3}*; UAS:RFP; UAS:ZO1-EGFP*^{ubs5}) embryos**.** Still pictures from movie S5. (i) show merge and (ii) show QD channel only. The SA to the left undergoes membrane invagination, similar to the events shown in Fig. 4. By invagination the lumen reaches the proximal site of the dorsal fusion point (arrow and arrowhead at 3:50). Anastomosis is completed when the luminal space within the fusion point becomes filled by QD (arrow and arrowhead at 8:35). (C) Dorsal to ventral lumen invagination. Still pictures from movie S6**.** The lumen extends from the DLAV (arrowhead) into the ISV (follow arrow from 01:50-03:35). The absence of longitudinal junctions indicates a transcellular lumen formation. The scale bar in all panels represents 20 μm.

Table S1. Transcellular Tip Cell Invagination Requires Blood Flow

	Total # of tip cells	# of tip cell invaginations	Percentage of invaginated tip cells
36 hpf uninj.	62	13	20.97%
36 hpf *sih* MO	68	0	0.00%
48 hpf uninj.	19	5	26.32%
48 hpf *sih* MO	61	0	0%

Pdxl2 staining, within a single tip cell. Invagination was inferred from a Pdxl2 domain that stretches continuously from an intercellular junction into the cell (as seen in Fig.4C). uninj. = uninjected embryos

Experimental Procedures

Generation of Transgenic Zebrafish Lines

The plasmids used to generate transgenic fish were constructed using the Gateway® cloning system (Invitrogen) [1] and are schematically shown in figure S1. The Tg(*fli1ep:GAL4FF*$^{ubs2-4}$)activator line has been previously published [2]. pT2UAS:EGFP-ZO1-cmlc:EGFP was generated by ligating a 14xUAS-E1b promoter [3] to a EGFP-hZO1 fragment [4] and cloned into pDestTol2CG2 [5]. Details are provided upon request. Plasmid DNA was coinjected with tol2-mRNA and injected embryos showing transient cardiac EGFP expression were selected and raised separately. Founder fish were screened for germ line transmission. Three carriers showed Gal4FF dependent EGFP-ZO1 expression in the vasculature, two of these, Tg(*UAS:EGFP-ZO1, cmlc:EGFP*$^{UBS5-6}$), were used in this study.

Anti-zf-podocalyxin Antibodies

2 different peptides derived from zf-pdxl2 (XP_692207) were synthesized, coupled to keyhole limpet hemocyanine and used to raise polyclonal anti-sera in rabbits using standard immunization procedures (Peptide Specialty Laboratory, Heidelberg, Germany). Peptide sequences: zf-pdxl2-pep1 (aa470-485): CHSRPSQTRSDYGKLF; zfpdxl2-pep2 (aa573-588): (C)-KPGKDEEDNQEEDTHL.

Immunofluorescence and Imaging

Antibody staining was done as previously described with minor modifications [6]. The following antibodies were used: rabbit anti-zf-pdxl2 1:200 (this study), rabbit anti-zf-CDH5 [6] 1:200; Alexa-568 goat anti-rabbit IgG, 1:1000; Alexa-568 goat anti-mouse IgG, 1:1000; Alexa-633 goat anti-mouse IgG, 1:1000 (All secondary antibodies were purchased from Invitrogen.). Images were taken with a Leica SP5 confocal microscope using a 63x glycerol immersion objective and analyzed using Imaris (Bitplane) and Image J software [7].

In Vivo Time-Lapse Analysis and Embryonic Manipulations

Triple transgenic embryos were selected using a Leica MZ FLIII fluorescent stereomicroscope. Embryos were selected for mRFP ensuring the presence of the fli1ep:GAL4FF and UAS:mRFP transgene and for the presence of the heart marker cmlc2:EGFP. Selected embryos were anaesthetized using tricaine and mounted in a 35 mm glass bottom petri dish (0.17 mm, MatTek), using 0.7% low melting agarose (Sigma) containing 0.01% tricaine and 0,003% PTU. All movies have an initial frame size of 512x512 pixels. Routinely, z-stack consisted of 50-80 slices with a step size of 0.8-1.0 µm. Stacks were taken every 5 minutes, unless noted differently. To label individual ECs KAEDE photoconversion was done on fli1ep:GAL4FF;UAS:Kaede transgenic embryos using a Leica Sp5 confocal microscope by 20-second exposures using a solid-state laser (405nm). At 2 dpf, when nuclei of individual ECs are easily discernible, embryos were anaesthetized with tricaine, mounted in 0.7% low melting agarose and a defined region of interest (ROI) within individual nuclei was exposed to the violet light. 705 nm Quantum Dots (Invitrogen) were injected into the sinus venosus of mounted embryos at a dilution of 1:2 using glass needles (Biomedical Instruments, Jena, Germany) with tip opening of 10 µm and beveled tip.

Fish Maintenance and Stocks

Zebrafish were maintained at standard conditions [8]. Embryos were staged by hours post-fertilization (hpf) at 28.5 °C (Kimmel et al., 1995). Embryos derived from wild-type fish (AB/EK and EK/TL), Tg*(fli1ep:EGFP)*^{y1} [9], Tg*(kdrl:EGFP)*^{S843} [10], Tg*(UAS:Kaede)*^{rk8} [11], Tg*(UAS:RFP)* [12] and Tg*(fli1ep:GAL4FF)*$^{UBS2-4}$ [2] and Tg*(UAS:EGFP-ZO1-cmlc:EGFP)*$^{UBS5-7}$ (this study) were used.

References

1. Villefranc, J.A., Amigo, J., and Lawson, N.D. (2007). Gateway compatible vectors for analysis of gene function in the zebrafish. Dev Dyn *236*, 3077-3087.
2. Zygmunt, T., Gay, C.M., Blondelle, J., Singh, M.K., Flaherty, K.M., Means, P.C., Herwig, L., Krudewig, A., Belting, H.-G., Affolter, M., et al. (2011). Semaphorin-PlexinD1 Signaling Limits Angiogenic Potential via the VEGF Decoy Receptor sFlt1. Developmental cell *21*, 301-314.
3. Köster, R.W., and Fraser, S.E. (2001). Tracing transgene expression in living zebrafish embryos. Developmental biology *233*, 329-346.
4. Riesen, F., Rothen-Rutishauser, B., and Wunderli-Allenspach, H. (2002). A ZO1-GFP fusion protein to study the dynamics of tight junctions in living cells. Histochemistry and Cell Biology *117*, 307-315.
5. Kwan, K.M., Fujimoto, E., Grabher, C., Mangum, B.D., Hardy, M.E., Campbell, D.S., Parant, J.M., Yost, H.J., Kanki, J.P., and Chien, C.-B. (2007). The Tol2kit: a multisite gateway-based construction kit for Tol2 transposon transgenesis constructs. Dev Dyn *236*, 3088-3099.
6. Blum, Y., Belting, H.-G., Ellertsdottir, E., Herwig, L., Lüders, F., and Affolter, M. (2008). Complex cell rearrangements during intersegmental vessel sprouting and vessel fusion in the zebrafish embryo. Developmental Biology *316*, 312-322.
7. Rasband, W.S. (1997-2011). ImageJ, http://imagej.nih.gov/ij/. (Bethesda, Maryland, USA,: U. S. National Institutes of Health).
8. Westerfield, M. (2000). The zebrafish book. A guide for the laboratory use of zebrafish (Danio rerio). 4th Edition, (Eugene: Univ. of Oregon Press).
9. Lawson, N.D., and Weinstein, B.M. (2002). In vivo imaging of embryonic vascular development using transgenic zebrafish. Developmental Biology *248*, 307-318.
10. Jin, S.-W., Beis, D., Mitchell, T., Chen, J.-N., and Stainier, D.Y.R. (2005). Cellular and molecular analyses of vascular tube and lumen formation in zebrafish. Development *132*, 5199-5209.
11. Hatta, K., Tsujii, H., and Omura, T. (2006). Cell tracking using a photoconvertible fluorescent protein. Nat Protoc *1*, 960-967.
12. Asakawa, K., Suster, M.L., Mizusawa, K., Nagayoshi, S., Kotani, T., Urasaki, A., Kishimoto, Y., Hibi, M., and Kawakami, K. (2008). Genetic dissection of neural circuits by Tol2 transposon-mediated Gal4 gene and enhancer trapping in zebrafish. Proc Natl Acad Sci USA *105*, 1255-1260.

Developmental Biology 341 (2010) 56–65

Contents lists available at ScienceDirect

Developmental Biology

journal homepage: www.elsevier.com/developmentalbiology

Review

Vascular morphogenesis in the zebrafish embryo

Elín Ellertsdóttir, Anna Lenard, Yannick Blum, Alice Krudewig, Lukas Herwig, Markus Affolter, Heinz-Georg Belting *

Department of Cell Biology, Biozentrum der Universität Basel, Klingelbergstrasse 70, CH-4056 Basel, Switzerland

ARTICLE INFO

Article history:
Received for publication 11 September 2009
Revised 28 October 2009
Accepted 28 October 2009
Available online 3 November 2009

Keywords:
Angiogenesis
Vasculogenesis
Branching morphogenesis
Cell migration
Lumen formation
Development
Zebrafish

ABSTRACT

During embryonic development, the vertebrate vasculature is undergoing vast growth and remodeling. Blood vessels can be formed by a wide spectrum of different morphogenetic mechanisms, such as budding, cord hollowing, cell hollowing, cell wrapping and intussusception. Here, we describe the vascular morphogenesis that occurs in the early zebrafish embryo. We discuss the diversity of morphogenetic mechanisms that contribute to vessel assembly, angiogenic sprouting and tube formation in different blood vessels and how some of these complex cell behaviors are regulated by molecular pathways.

Introduction

Branched tubular organs, such as the insect tracheal system or the vertebrate cardiovascular system, kidney or lung, are found throughout the animal kingdom. Formation of such tubular networks from precursor cells or tissues involves a variety of morphogenetic processes, such as tube formation, elongation, branching and fusion. These processes are brought about by complex cellular behaviors, which include cell polarization, cell migration, cell rearrangements, cell shape changes and cell division. Although tubular organs are extremely diverse in anatomy and function, the cellular activities that govern tube formation and branching morphogenesis appear to be quite similar (Baer et al., 2009; Andrew and Ewald, 2010). In this review, we describe the current understanding of blood vessel formation in the early zebrafish embryo. We are placing special emphasis on the morphogenetic processes that contribute to vascular development and discuss the regulatory components that accompany these events.

In vertebrates, the cardiovascular system constitutes a highly ramified network of tubes that transports gas, nutrients, hormones and metabolites throughout the body. It also has important roles in the regulation of homeostasis and wound healing and is involved in the pathology of numerous diseases including cancer and inflammation (Carmeliet, 2003). The cardiovascular system emerges as one of the first organs during embryonic development and retains morphogenetic plasticity in adult life. Blood vessels are an integral component of all organs and are vital not only for their function but also for their formation during embryonic development (Nikolova and Lammert, 2003; Red-Horse et al., 2007; Sakaguchi et al., 2008). Blood vessels are highly diverse: they differ in size and are specialized depending on their function and the tissue or organ they are embedded in (Aird, 2007; Rocha and Adams, 2009). In general, they consist of an inner epithelium (endothelium) lining the lumen; depending on the type of vessel, this endothelium is surrounded by a basal lamina and by mural cells, such as pericytes and smooth muscle cells, which both support and regulate the function of the endothelium (Armulik et al., 2005).

Over the last decade, the molecular pathways controlling vascular development have attracted much attention, and a large number of key molecules has been identified that regulate different aspects of blood vessel morphogenesis. The basic frameworks of the vascular anatomy are conserved among vertebrates, which makes it possible to assign homologies between distinct blood vessels and to directly compare the formation of these vessels in different vertebrate species (Isogai et al., 2001; see Fig. 1). The zebrafish embryo has proven to be a useful model to study vascular morphogenesis in vivo. The vasculature can be easily visualized using a variety of labeling techniques, such as endothelial specific expression of fluorescent protein or by microangiography (Fig. 1). Its small size, experimental accessibility, optical clarity and rapid development allow to observe cellular activities, such as cell migration, cellular rearrangements and cell divisions, as they occur during blood vessel formation in the embryo. It is also possible to follow cardiovascular mutant phenotypes for several days because oxygenation of the early zebrafish embryo does

* Corresponding author.
E-mail address: heinz-georg.belting@unibas.ch (H.-G. Belting).

0012-1606/$ – see front matter © 2009 Elsevier Inc. All rights reserved.
doi:10.1016/j.ydbio.2009.10.035

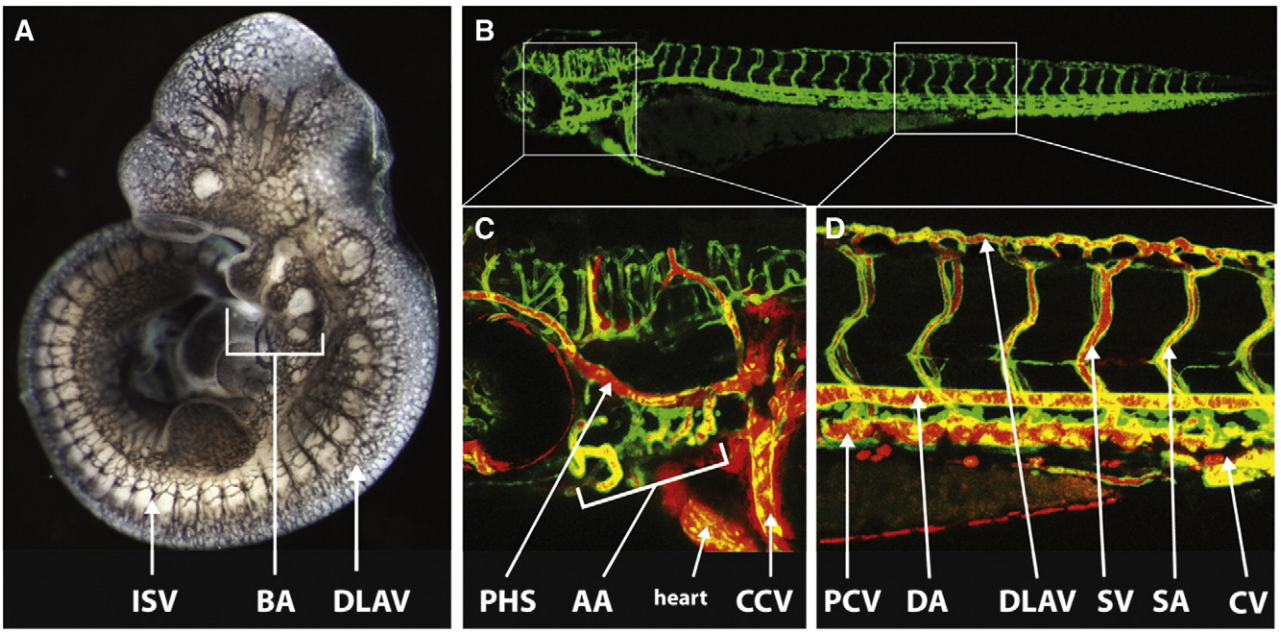

Fig. 1. The vascular system in mouse and fish embryos. (A) Visualization of the vascular system by immunohistochemical localization of PECAM-1 in a day 10 mouse embryo (photo courtesy of Ralf Adams, MPI, Münster, Germany). Owing to the opacity of the mouse embryo, only superficial blood vessels can be seen. BA: branchial arches (1st and 2nd); ISV: intersegmental vessel; DLAV: dorsal longitudinal anastomotic vessel. (B–D) The vascular system in a 3-day-old zebrafish embryo visualized by reporter gene analysis (*TG:flk1:EGFP* in green) and by microangiography using quantum dots (red in panels C and D). Some blood vessels are indicated according to Isogai et al. (2001). AA: aortic arches (1–6); CV: caudal vein; CCV: common cardinal vein; DA: dorsal aorta; PCV: posterior cardinal vein; PHS: primary head sinus; SA: segmental artery; SV segmental vein. At these stages, anatomical similarities between the two species are best observed in the branchial arches and in the ISV of the trunk. ISV and DLAV form quite similarly in both species (Isogai et al., 2003; Walls et al., 2008).

not rely on blood circulation. Furthermore, functional studies by forward and reverse genetics have shown that the molecular components that regulate vascular development are conserved between mammals and fish (Beis and Stainier, 2006; Lawson and Weinstein, 2002b; Thisse, 2002). Thus, the zebrafish embryo presents a unique system in which live imaging can be combined with functional studies to gain a more complete insight into how the molecular and morphogenetic mechanisms are integrated at the (sub)cellular level to shape the vascular tree.

Vasculogenesis

The formation of vertebrate blood vessels is commonly subdivided into two distinct morphogenetic processes, called vasculogenesis and angiogenesis. Vasculogenesis is defined by in situ aggregation of angioblasts into a blood vessel (Coffin and Poole, 1988; Poole and Coffin, 1989; Risau, 1995; Risau et al., 1988), while further sprouting of vessels from existing vessels occurs via a process called angiogenesis (Risau, 1995).

Origin and specification of endothelial cells

Angioblasts are precursors of endothelial cells not yet incorporated into blood vessels. They originate from the ventrolateral mesoderm (Kimmel et al., 1995; Stainier et al., 1995). Analyses of genes expressed in the hematopoietic and endothelial cell lineages have revealed a remarkable conservation between vertebrate species. In particular, transcription factors belonging to the ETS, GATA and LMO families have been shown to control specification of these lineages in mammals as well as fish (De Val et al., 2008; Detrich et al., 1995; Liu and Patient, 2008; Thompson et al., 1998; Zon et al., 1991). At the beginning of somitogenesis, transcription factors, such as *scl*/*tal1* and *lmo2*, which specify angioblasts and hematopoietic cells, are expressed in two domains along the body axis, the anterior and the posterior lateral mesoderm (Dooley et al., 2005; Liao et al., 1998; Patterson et al., 2007). During somitogenesis these cell populations acquire unique gene expression profiles. For example, *flk1*-positive/*scl*-positive precursor cells differentiate into *flk1*-positive/scl-negative and *flk1*-negative/*scl*-positive cells, which will give rise to endothelial and hematopoietic cells, respectively (Gering et al., 1998). There seems to be no transcriptional factor regulating exclusively the endothelial specification but a combination of multiple factors with overlapping expression patterns (reviewed by De Val and Black, 2009).

Formation of the dorsal aorta and the cardinal vein

The basic anatomy of the initial embryonic circulatory system is quite similar among vertebrates. In addition, the first embryonic vessels to appear, the dorsal aorta (DA) and the posterior cardinal vein (PCV), are formed by a distinct morphogenetic mechanism called vasculogenesis in all vertebrates (Isogai et al., 2001). In zebrafish, angioblasts are specified well before the first blood vessels are formed. Expression of molecular markers such as *fli1a* shows that angioblasts are located in two lateral stripes at 12–14 hpf. By 28–30 hpf, the DA and the PVC can be discerned and are fully lumenized (Roman et al., 2002). In vivo imaging, using a *Tg(fli1a:EGFP)* reporter fish line, has shown that angioblasts migrate as individual cells towards the embryonic midline where they coalesce (Lawson and Weinstein, 2002b). During recent years, a considerable amount of research has focused on how this migration process is regulated, how these cells form the axial vessels and how DA and PCV are specified. As indicated in Fig. 2, the PCV forms subsequently to the DA (Eriksson and Löfberg, 2000; Herbert et al., 2009; Jin et al., 2005), and this relationship appears to be conserved among vertebrates (Coffin and Poole, 1988; Hirakow and Hiruma, 1981; Meier, 1980).

Formation of the DA in zebrafish has been studied by transmission electron microscopy (TEM) (Eriksson and Löfberg, 2000; Meier, 1980) and more recently by analysis of transgenic zebrafish embryos (Herbert et al., 2009; Jin et al., 2005; Lawson and Weinstein, 2002b). During vasculogenesis, angioblasts are attracted towards the midline by guidance cues thought to emanate from the endoderm

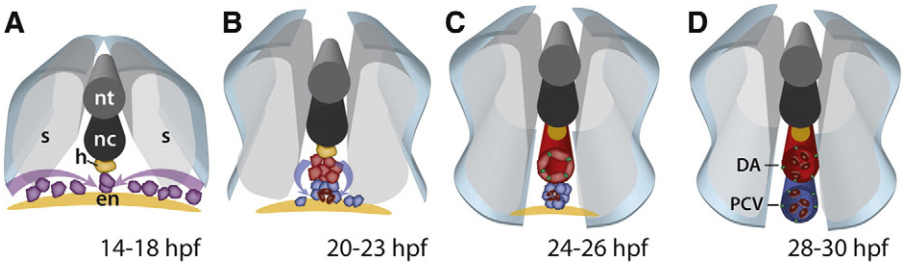

Fig. 2. Phases of vasculogenesis in the zebrafish embryo. Schematic cross sections of the trunk region at representative stages of development (according to Herbert et al., 2009 and Jin et al., 2005). (A) Medial migration. From 14 hpf onward, angioblasts (purple) that originate in the lateral plate mesoderm migrate over the endoderm towards the midline just below the hypochord, where they aggregate to form a vascular cord (B). (B) Arterio-venous segregation and ventral sprouting. At around 17 hpf, angioblasts start to express markers of arterio-venous differentiation, such as *ephrin-b2a* in arterial cells (marked in red). These cells are located in the dorsal portion of the vascular rod and will give rise to the DA, whereas *ephb4a* expressing cells are located more ventrally and will contribute to the PCV and CV. At 21 hpf, angioblasts located in the ventral part of the vascular cord start migrating ventrally and accumulate below the forming DA (B, C). (C) Lumen formation. The DA forms and lumenizes prior to the PCV and CV in the absence of blood cells (brown) by cord hollowing. Venous angioblasts aggregate and coalesce around the blood cells to ultimately form a tube. (D) Functional Vasculature. At 30 hpf, both vessels are fully formed and carry blood flow. Endothelial cell junctions are indicated in green.

(Jin et al., 2005; Fig. 2A). Once the angioblasts have reached the embryonic midline, they form aggregates and tube formation commences (Fig. 2B). TEM studies have shown that angioblasts initially form "aggregates of tightly packed cells" between hypochord and the underlying mesoderm (Eriksson and Löfberg, 2000). These aggregates are discontinuous along the anterior–posterior axis and the cells are spherical at the beginning of the process. At around the 17-somite stage (17.5 hpf), more flattened tube forming cells are found posterior to the 7th–9th somite in the fish embryo. From analysis of transgenic zebrafish, it has been suggested that endothelial cells migrate in two waves to the midline and it has been suggested that the first wave contributes to the DA while the cells of the second wave will form the primary vein (Jin et al., 2005). Alternatively, endothelial cells from both migratory waves may join in a single medial cord and segregate independently from this structure. The latter possibility has recently gained strong support from in vivo time-lapse analyses, which showed that the precursor cells of the caudal vein dissociate from the primordium of the DA by a process termed ventral sprouting (Herbert et al., 2009). Ventral sprouting is initiated around 20 h post-fertilization shortly before the emergence of dorsal sprouts, which will give rise to segmental arteries (SA) (see below) at a time when the DA is not yet lumenized. This finding together with the observation that the expression of the arterial marker *ephrinb2a* (*efnb2a*) is restricted to a subpopulation within the vascular cord suggested that the primary arteries and veins are derived from a common primordium that contains a mixed population of arterial as well as venous angioblasts (Herbert et al., 2009; Jin et al., 2005).

Specification of arterial versus venous fates has been shown to depend on the interaction of the VEGF and Notch signaling pathways (reviewed by Lawson and Weinstein, 2002a; Siekmann et al., 2008). Sonic hedgehog (SHH) signals from the notochord lead to an activation of *vegf-a* expression in ventral somites (Lawson et al., 2002). VEGF-A is sensed by the angioblasts via VEGF-receptor-2/KDR/FLK1 (KDR-Like/KDRL in zebrafish), which leads to the activation of Notch signaling and the transcriptional activation of other factors which results in arterial differentiation in a subset of angioblasts (Cermenati et al., 2008; Lawson et al., 2003; Pendeville et al., 2008; Zhong et al., 2001). In contrast to arterial development, specification of venous fates is independent of VEGF-A signaling (Covassin et al., 2006; Lawson et al., 2003). In agreement with these concepts, modification of VEGF or Notch signaling levels influences the segregation and ventral sprouting behavior. Angioblasts showed excessive ventral migration, when VEGF-A and Notch signals were blocked, whereas downregulation of FLT4 led to a reduction in ventral sprouting (Herbert et al., 2009).

Arterial and venous specification of angioblasts is reflected by particular gene expressions (Lawson and Weinstein, 2002a). Notably, two members of the Eph-ephrin subclass of the receptor tyrosine kinase family are differentially expressed in arteries (EphrinB2/*Efnb2*) and veins (*EphB4*) (Adams et al., 1999; Lawson et al., 2001). Genetic analyses in mouse have demonstrated an important role for bidirectional Ephb4-Efnb2 signaling for vascular morphogenesis (reviewed by Adams and Alitalo, 2007). In mouse and fish, EPHB4-Efnb2 signaling has been shown to be involved in sorting of neuronal cells, which leads to their segregation into adjacent hindbrain segments (Kemp et al., 2009; Mellitzer et al., 1999). To test whether these factors also play a role in the segregation of arterial and venous angioblasts in the primary vascular cord, Herbert and colleagues (2009) modified EPHB4a and EfnB2a levels and interfered with forward and reverse properties of EPHB4a-EfnB2a signaling. Either overexpression or knockdown of EPHB4a/Efnb2a function caused aberrant migration of transplanted angioblasts consistent with defects in arterio-venous segregation. Taken together, these findings show that repulsive EPH4a-EfnB2 signaling regulates arterio-venous segregation, thereby controlling the directionality of angioblast sprouting.

Anterior–posterior differences in artery formation

While the process of vasculogenesis has been best described in the dorsal aorta of the trunk, there is increasing evidence of regional differences in the way the primary vessels form and it has been proposed that distinct cues guide endothelial cells in different domains of the body (Coffin and Poole, 1991; Eriksson and Löfberg, 2000). In agreement with this view, several zebrafish mutants have been isolated that exhibit vascular defects in particular regions of the body (Jin et al., 2007).

Some experiments have shed light on the differences that regulate the formation of the DA of the trunk and the paired lateral dorsal aortae (LDA), which is located in anterior body regions. In an earlier study, the role of the endoderm for formation of the DA was examined in *casanova* (*sox32*) mutants that lack endoderm (Jin et al., 2005). In these embryos, medial migration of angioblasts was slowed but the DA formed normally, suggesting that endoderm is dispensable for DA formation. However, it has more recently been shown that the endoderm plays an essential role for LDA formation in the anterior region of the embryo (Siekmann et al., 2009). Strikingly, mutants for the chemokine receptor *cxcr4a,* which is expressed in the LDA, lack the LDA. CXCR4 is known to bind to CXCL12, which is specifically expressed in the anterior endoderm underlying the developing LDA. Furthermore, loss of CXCL12 function phenocopies the *cxcr4a* deficiency. These findings illustrate the molecular diversity in endothelial cells and the importance of local extrinsic cues for the formation and patterning of the primary aorta.

Transforming a cord into a tube: lumen formation in the primary blood vessels

The morphogenesis of biological tubes has been a longstanding interest in developmental biology and it has been shown that tubes can form in very different ways (Baer et al., 2009; Lubarsky and Krasnow, 2003). After angioblasts have aggregated into a cord-like structure, they ultimately have to assemble a tube. This could in principal occur by different morphogenetic processes, including (i) cell hollowing, where cells form vacuoles that fuse between cells to form a continuous intracellular lumen; (ii) wrapping, where cells migrate in a polarized state and surround the future lumen; (iii) cord hollowing, where cells within the cord attain apical–basal polarity and the lumen is formed by membrane separation and fluid influx; or by (iv) cavitation, where cells in the middle of the rod undergo apoptosis leaving a luminal space behind (Hogan and Kolodziej, 2002; Kucera et al., 2007; Lubarsky and Krasnow, 2003).

Tube formation of the DA has been studied at the cellular level by transgenic and immunofluorescent analyses in zebrafish embryos (Jin et al., 2005). Shortly after angioblasts have formed a cord, the DA begins to lumenize (21 hpf; Figs. 2B, C). Analysis of proteins involved in apical–basal polarization, such as fibronectin or β-catenin, has shown that this process is preceded by endothelial polarization and the formation of junctions between ECs, suggesting that a cord hollowing process forms the lumen of the DA. At the 20-somite stage (19 hpf), cell junctions, as visualized by ZO-1 and Claudin5, are discernable between the cells forming the dorsal aorta (Jin et al., 2005). The mechanisms of lumen formation in the zebrafish dorsal aorta and caudal vein have recently been examined by in vivo time-lapse analyses (Herbert et al., 2009). These studies confirmed a cord hollowing mechanism in the DA, whereas the lumen of the CV is formed by ventrally sprouting venous angioblasts that coalesce around resident blood cells. This mode of lumen formation has not been described before and it is likely to be different from cell wrapping as described above because the sprouting angioblast do not seem to migrate as an epithelial sheet of cells.

In a recent, comprehensive study, lumen formation of the paired dorsal aortae has been examined in the mouse embryo (Strilić et al., 2009). By anatomical and immunofluorescent analyses, Strilić and colleagues show that the lumen of the dorsal aortae forms in discrete steps similar to those observed in the zebrafish and, for the first time, they were able to decipher the molecular mechanisms involved in this process. Consistent with observations in zebrafish, the first steps of lumen formation are initiated upon formation of intercellular adherens junctions between angioblasts. Junctional remodeling then leads to an apical interface between adjacent ECs, followed by an accumulation of anti-adhesive CD34-sialomucins, such as CD34 and Podocalyxin (PODXL). Proper localization of these proteins to the apical surface depends on the presence of VE-cadherin. The subsequent formation of the aortic lumen is driven by a VEGF-A-dependent constriction of the apical surfaces as well as EC elongation induced by the F-actin cytoskeleton. These cell shape changes apparently rely on interactions between Moesin with CD34-sialomucins, which lead to an apical localization of F-actin. This view is supported by the analysis of Moesin and of *Podxl* mutants which both exhibit reduced levels of apical F-actin and a delay in aortic lumen formation. Furthermore, loss of *Podxl* leads to a reduction of Moesin at the sites of endothelial contacts, suggesting that PODXL connects with Moesin in order to recruit F-actin.

In summary, these studies indicate that the morphogenetic mechanisms that drive lumen formation in the dorsal aorta/aortae have been conserved between teleosts and mammals. In either case, coalescence of ECs and subsequent apical–basal polarization of a vascular cord appear to be the primary steps. The lumen is then formed between apical surfaces of apposing ECs by a cord hollowing process. Whether the molecular mechanisms that underlie lumen formation are conserved between fish and mouse remains to be determined. Furthermore, it will be interesting to learn about the morphogenetic processes that may be required to further inflate the lumen.

Angiogenesis

While the primary axial vessels are formed by vasculogenesis, elaboration of the vasculature, i.e. the formation of secondary blood vessels, occurs via angiogenesis, a process by which new blood vessels are generated from a pre-existing one. However, with respect to morphogenetic cell behaviors, angiogenesis can occur in quite different ways. Originally, it has been described as a sprouting process, by which a new vessel is branching off a primary vessel (reviewed by Patan, 2000). In addition to sprouting, a considerably different mode of angiogenesis called intussusception has been described in mammals (reviewed by Makanya et al., 2009). During intussusceptive angiogenesis, a vessel splits along its longitudinal axis into two new branches, thus effectively enlarging the vascular surface area. This process plays an important role in vascular remodeling during plexus formation. In zebrafish, angiogenesis by intussusception has not yet been described and therefore we focus our discussion on sprouting angiogenesis.

Sprouting angiogenesis

Sprouting angiogenesis was described as a general mechanism of microvascular growth during the 1970s, and its relevance for tumor growth and metastasis was soon recognized (Folkman, 1982). Early on angiogenesis was studied in a variety of in vivo and tissue culture systems such as the chorion allantoic membrane of the chick or the corneal pocket (reviewed by Patan, 2000). As an outcome of these studies, sprouting angiogenesis was described as a sequence of events that include (i) migration of ECs toward the angiogenic stimulus, (ii) alignment of ECs in a bipolar mode, (iii) lumen formation and cell divisions distant to the tip of the sprout and (iv) connection of individual sprouts to initiate circulation (Ausprunk and Folkman, 1977; Patan, 2000).

In recent years, much progress has been made in establishing systems in which angiogenic processes can be followed in detail. These include the retinal vasculature of the mouse, which develops postnatally, and the zebrafish embryo, in which all aspects of angiogenesis can be followed in vivo. Embryonic vasculogenesis and angiogenesis in zebrafish occur in ways very similar to those in mammals. In contrast to the latter, zebrafish embryos do not require extra-embryonic vasculogenesis due to their extrauterine development. This greatly facilitates the analysis of embryonic blood vessel formation, as it is not influenced by prior extra-embryonic events. Although all major blood vessels are easily accessible in the zebrafish embryo, the intersegmental blood vessels (ISV) have been most thoroughly studied because of their metameric organization and relatively simple anatomy.

ISV formation in the zebrafish embryo

Formation of ISVs in the zebrafish embryos involves two waves of angiogenic sprouting (Isogai et al., 2003). ECs of the primary wave form the segmental arteries (SA). During the primary wave, ECs sprout from the DA at ~22 hpf. These sprouts grow dorsally and – once they have reached the level of the dorsal neural tube – connect with their neighbors from anterior and posterior segments to form the future dorsal longitudinal anastomotic vessel (DLAV). The second wave, which starts at 32 hpf, involves ECs from the PCV (Yaniv et al., 2006). These sprouts will either connect to an existing SA, thereby transforming it into a vein (SV), or, alternatively, they will grow up to the level of the horizontal myoseptum and form a population of cells

named parachordal lymphangioblasts (PLs) (Hogan et al., 2009; Isogai, 2003). The majority of these cells eventually migrates away from the horizontal myoseptum and contributes to the lymphatic vasculature (Hogan et al., 2009).

Formation of the SA has been described in detail by in vivo time-lapse and immunofluorescent analyses (Blum et al., 2008; Childs et al., 2002; Isogai et al., 2003; Lawson and Weinstein, 2002b). These studies have led to several models of SA morphogenesis. While earlier studies suggested that the SA is made up by 3 cells that are arranged serially in a head to tail fashion (Childs et al., 2002), mosaic analyses and the analysis of endothelial cell junctions showed that SAs are composed of 4–6 cells that extensively overlap along the proximodistal axis of the vessel (Blum et al., 2008). Taken together, these findings suggest a model of SA formation, as shown in Fig. 3. Initially, one or two cells migrate out of the epithelium of the DA forming the sprout (Fig. 3A). During dorsal outgrowth, this sprout consists usually of 3–4 cells, one tip cell and two or three stalk cells (Fig. 3B). When the tip cell has made contacts with its anterior and posterior neighbors, the basic scaffold of the SA is formed (Fig. 3C). Because of cell divisions that occur at varying time points, the stalk can consist of a variable number of cells generating a large degree of morphological heterogeneity, which is illustrated by the variation of junctional patterns (Blum et al., 2008). However, further cell divisions and cellular rearrangements during vessel assembly lead to a paired configuration of cells along the proximodistal extent of the SA, which then forms a lumen. In the following section, we discuss some of the morphogenetic and molecular mechanisms that govern the different aspects of SA formation. Since much progress has also been made in other angiogenesis models, we will discuss them in comparison with SA formation.

Sprouting of SA and SV appears to be triggered by different signals. For example, VEGF-A is critical for SA formation, while it appears dispensable for SV formation, since SV sprout normally in embryos that are mutant for phospholipase C-γ (*plc*-γ , which is a downstream mediator of VEGF-A/VEGFR-2 signaling; Bahary et al., 2007; Habeck et al., 2002; Lawson et al., 2003; Nasevicius et al., 2000; Covassin et al., 2009; Covassin et al., 2006). Here, we will focus on the morphogenesis of the SA. The regulation of angiogenesis by VEGFs and their receptors has been studied in many previous publications in great detail (reviewed by Cébe-Suarez et al., 2006; Matsumoto and Mugishima, 2006; Olsson et al., 2006; Shibuya and Claesson-Welsh, 2006; Yamazaki and Morita, 2006). While early studies focused on general pro-angiogenic functions of VEGF signaling, more specific roles for VEGF signaling in patterning of angiogenic sprouts have recently been revealed (Covassin et al., 2006; Gerhardt et al., 2003; Ruhrberg et al., 2002). Upon VEGF-A/VEGFR-2 signals, ECs initiate the angiogenic program, which entails the loosening of junctional connections with neighboring cells, migratory behavior towards the angiogenic stimulus and cell division (reviewed by Lampugnani and Dejana, 2007). Cells within the nascent sprout respond in different ways to the *VEGF-A*. Whereas cells located at the base (termed stalk cells) show increased rates of proliferation, the leading cell (termed tip cell) sends long and dynamic filopodia into the surrounding environment to guide the growing sprout towards the stimulus (Gerhardt et al., 2003). Endothelial tip and stalk cells do not only have different functions and behaviors (discussed below), they also show differences in gene expression. For example, Platelet derived growth factor B (*Pdgfb*) and *Flt4* are expressed at higher levels in the tip cell than in the stalk cell (Gerhardt et al., 2003; Siekmann and Lawson, 2007).

Patterning and angiogenic behavior of sprouts are regulated by the cooperation of the Notch and VEGFR-2 signaling pathways (Hellström et al., 2007; Siekmann et al., 2008; Siekmann and Lawson, 2007; Suchting et al., 2007; reviewed by Phng and Gerhardt, 2009; Siekmann et al., 2008). The tip cell, receiving the highest level of VEGFR-2 signal, responds with an upregulation of the Notch ligand Delta-like-4 (DLL4), which leads to increased intracellular Notch signaling in the neighboring stalk cells (Hellström et al., 2007). In zebrafish, loss of DLL4 function leads to prolonged angiogenic activity in the ISVs, whereas over-activation of *Notch* signaling leads to a quiescent phenotype (Leslie et al., 2007; Siekmann and Lawson, 2007). DLL4 also regulates angiogenesis by suppressing VEGF-C dependent FLT4 (VEGFR-3) signaling in endothelial cells in mouse and fish (Hogan et al., 2009; Tammela et al., 2008). In zebrafish, VEGF-C/FLT4 signaling is required for venous and lymphatic development (Covassin et al., 2006; Küchler et al., 2006). However, a "kinase-dead" allele of FLT4 is able to rescue the hyperbranching phenotype caused by the loss of *DLL4* function (Hogan et al., 2009). Furthermore, in the absence of DLL4, arterial cells become more sensitive to varying levels of VEGF-C in the embryo (Hogan et al., 2009). These experiments point out a mechanism for how different endothelial lineages can respond specifically to sources of VEGF-C in the trunk. Venous and lymphatic cells, which do not express *dll4*, are able to respond to VEGF-C/FLT4, whereas in arterial cells this pathway is inhibited by DLL4 (Hogan et al., 2009).

Although the molecular mechanisms that control angiogenic behavior in the sprout may not be identical in fish and mouse, there is a common theme in that differences in intracellular Notch signaling confer different cell behaviors along the proximodistal axis of the sprout. Tip cells (low Notch) extend numerous filopodia, are highly migratory and thus display the strongest angiogenic behavior while the proximal stalk cells (high Notch) appear less migratory. It has

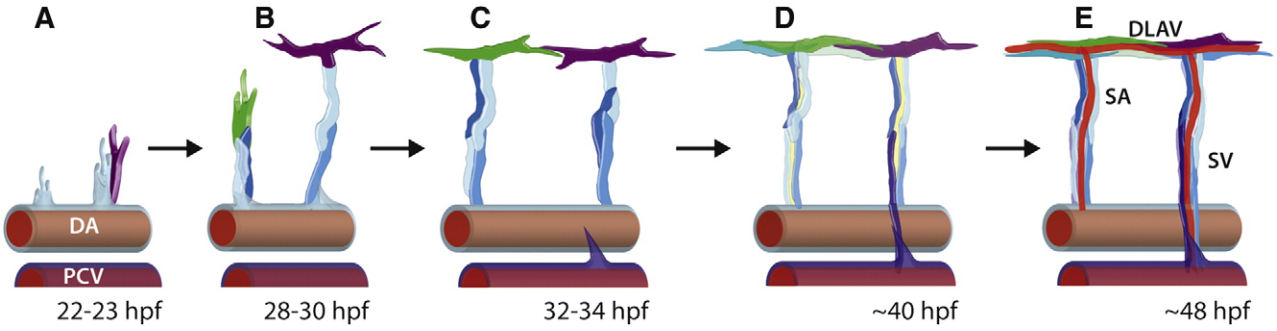

Fig. 3. A model for the morphogenetic events that lead to the formation of ISV and DLAV in the Trunk. Two neighboring sprouts are depicted as representative examples. The leading cells are indicated in green and purple, respectively. At 22 hpf ECs of the DA form sprouts (A) that grow along the somite boundaries up to the dorsal roof of the neural tube (B). During these stages, the sprout consists of 2 to 4 cells that are stabilized by interendothelial junctions (not indicated). At the dorsal side of the embryo, the tip cells send extensions toward their anterior and posterior neighbors to establish connections. During this phase, the ECs establish a scaffold consisting of a vascular cord that is not yet lumenized (B, C). Further cell rearrangements and cell divisions lead to formation of a continuous apical surface that may surround initial luminal spaces (yellow) (D). At around 32 hpf, a secondary wave of angiogenic sprouts emerges from the PCV. These sprouts either generate a group of lymphatic cells, called parachordal lymphangioblasts (not shown), or connect with the adjacent primary vessel (D, on the right), which will become a segmental vein. Blood flow in ISVs commences after SA, SV and DLAV have been established (E).

been proposed that the reduced migratory behavior of stalk cells is important to maintain sprout integrity and connection to the DA (Siekmann et al., 2008).

While the general aspects of angiogenesis in the ISVs of the fish and the postnatal vasculature of the mouse retina are very similar, there appear to be differences in gene expression and pattern of cell proliferation. While in the mouse retina cell proliferation is largely restricted to the stalk (Gerhardt et al., 2003), in fish similar rates can be observed in stalk and tip cells (Blum et al., 2008). Furthermore, based on gene expression—intersegmental sprouts in the fish appear not as polarized as those in the mouse retina. In contrast to the mouse retina, the tip cell markers *dll4* and *flt4* are quite uniformly expressed in tip and stalk cells of the sprouting SA (Hogan et al., 2009; Leslie et al., 2007; Siekmann and Lawson, 2007). Similar to zebrafish, ISV sprouts in the mouse embryo show a relatively even distribution of DLL4 protein (Tammela et al., 2008). These differences between distinct types of blood vessels raise the possibility that, compared to the mouse retina, the state of the tip cell in ISV is less defined. It will be interesting to see whether these differences are due to different interpretations of VEGF/Notch signals or whether they are connected to different morphogenetic processes occurring in the two systems (see below).

How the angiogenic sprout lumenizes is still controversial. Different morphogenetic behaviors and cellular configurations in the sprout can have significant impact on how a vessel is formed. In principle, there are at least 3 different morphogenetic processes of tubulogenesis that may occur in an angiogenic sprout: budding, cord hollowing or cell hollowing (see Fig. 4A). When a novel tube is formed by budding, the ECs that follow the tip cells maintain their epithelial character with a defined apical–basal polarity. During budding, the luminal space of the sprout remains continuous with that of the parent vessel, extending up to the tip cell. Tube branching by budding has been described in many experimental systems including the tracheal system in *Drosophila* and several branched organs in mammals (Baer et al., 2009). Vessel branching by budding appears to occur in larger caliber capillaries that are constantly perfused. In the mouse retina, the lumen is located immediately adjacent to the tip cell (see Fig. 4B). In addition, in vivo time-lapse recording of blood vessels in the zebrafish brain appears consistent with such morphogenetic mode of tubular branching (Huisken and Stainier, 2009).

Formation of ISV does not occur by budding since the initial sprouts do not contain a lumen continuous with the DA (Fig. 4C). Rather, the lumen becomes patent at the time when SA, DLAV and SV have formed proper connections. After labeling circulating blood with fluorescent tracer dyes, it was observed that (from the perspective of the DA) the lumen opens up in a stepwise manner from proximal to

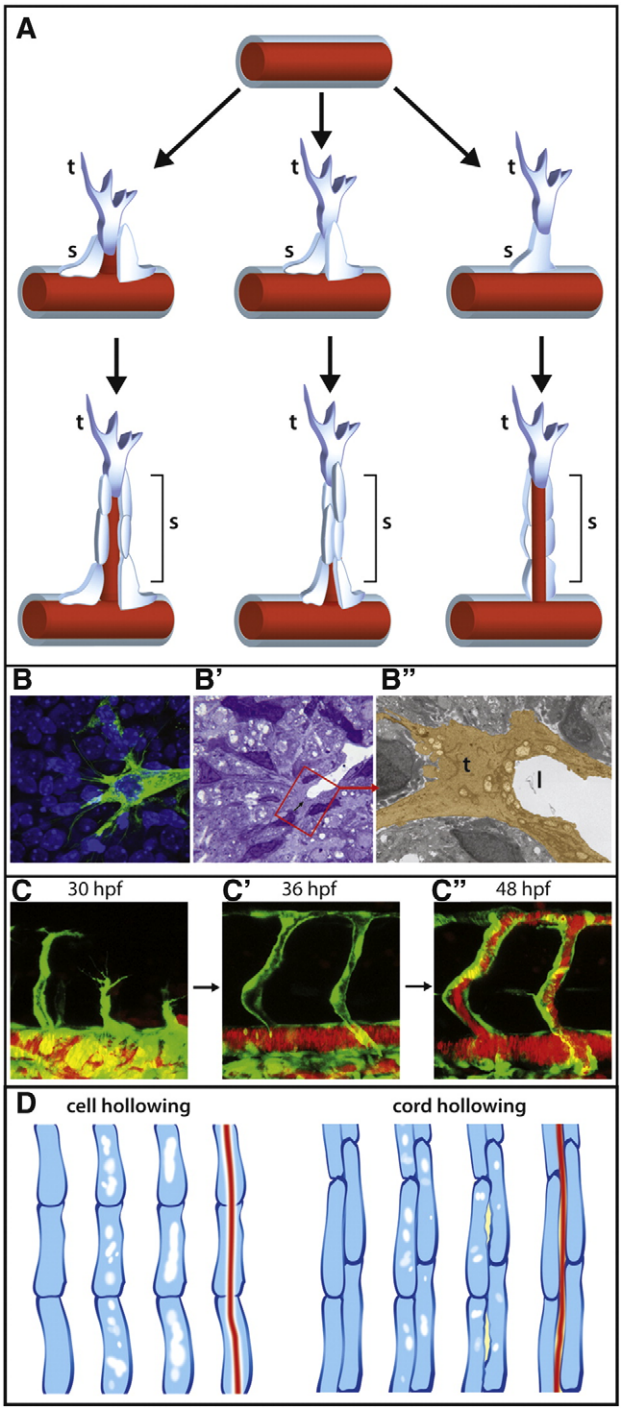

Fig. 4. Different morphogenetic mechanisms that underlie sprouting angiogenesis. (A) Three examples for the cellular organization of an angiogenic sprout. Depending on how the cells are arranged in the sprout, different types of vessels may form. Left: Branching morphogenesis by budding. ECs remain epithelial, while the sprout grows via cell division within the stalk. The lumen remains open and continuous at all times. Middle: Formation of a multicellular tube by cord hollowing. This shows an example, where cells grow in a paired configuration maintaining an apical surface in between. The lumen remains open at the base but is closed in distal region. Close to the tip, cells may be of a more mesenchymal character and undergo cell divisions. Cellular rearrangements will then lead to a continuous apical surface and open up the luminal space. Right: Formation of a unicellular tube with an intracellular lumen. At the tip of a capillary, the lumen may also form within a string of cells. The cells hollow out by vacuole formation followed by exocytosis. This mode of lumen formation will generate a so-called intracellular lumen. (B) Lumen formation behind the leading tip cell in the mouse retina. The lumen of the nascent sprout extends to the tip of the growing sprout. This situation is in agreement with the configuration shown in panel A. Isolectin B4 labeling (green) of an endothelial tip cell projecting long filopodia. Nuclei, Dapi, blue (B). Semithin (B′) and close up of ultrathin (B″) en face section of the sprouting front in the retina illustrating continuous lumen formation (l) just behind the tip cell (t). The endothelial tip cell in panel C is pseudocolored brown. Figure courtesy of Denise Stenzel and Holger Gerhardt, London Research Institute—Cancer Research UK. © Gerhardt et al., 2003. Originally published in J. Cell Biol. doi:10.1083/jcb.200302047. (C) Lumen formation in the ISV and DLAV of a zebrafish embryo. During scaffold formation, neither ISV nor DLAV are perfused, suggesting that the lumen is formed subsequently. Blood flow is initiated after subsequent remodeling and establishment of the intersegmental veins (compare to Fig. 3). Confocal still pictures from an in vivo time-lapse movie of a transgenic zebrafish embryo (*TG:fli1a:EGFP^{y1};gata1:DsRed^{sd2}*). ECs are labeled in green; erythrocytes are labeled in red. (D) Alternate models of lumen formation in the zebrafish ISV. Depending on the cellular arrangement of cells in an angiogenic sprout, de novo lumen formation can occur in at least two different ways. If cells are arranged in a serial fashion, the lumen may be generated by cell hollowing (left, see also A). In this process, ECs pinocytose solutes from extracellular space and form vacuoles that coalesce and fuse to give rise to an intracellular lumen. Eventually intracellular vacuoles of neighboring cells will fuse by exocytosis and form a patent lumen (see Kamei et al., 2006). Alternatively, if cells are arranged in a paired fashion, they may form a lumen by cord hollowing (right, see also A). This process requires establishment of a continuous apical surface that is bounded by at least two ECs. Vacuoles can then be exocytosed into this intercellular space, which will eventually become the vascular lumen.

distal (Kamei et al., 2006). Because vacuole formation and fusion has long been considered an important component of lumen formation, the stepwise expansion of luminal space was interpreted as a succession of vacuolar fusion events that generate a unicellular tube containing an intracellular lumen (Kamei et al., 2006; Fig. 4D). Capillaries that contain intracellular lumens have indeed been described (Bar et al., 1984) and have been called "seamless tubes" because they are characterized by the absence of cell junctions along the longitudinal axis of the vessel. More recently, analyses of cell junctions within nascent sprouts and patent ISVs showed that the cells in the stalk overlap extensively along the proximodistal axis and that ISVs are multicellular tubes containing an extracellular lumen (Blum et al., 2008). This cellular configuration is more consistent with a lumen formation process by cord hollowing (Fig. 4D). In this model, cells in the stalk rearrange to form a continuous apical surface. The lumen is then formed by a process, in which small pre-luminal spaces (rather than vacuoles) are formed by exocytosis and/or paracellular influx of liquids. The stepwise opening of the lumen from the direction of the aorta would then be consistent with the completion of cell rearrangements in the stalk. The events described here would be quite comparable to those described above for the lumen formation in the dorsal aorta.

The three mechanisms discussed here are not necessarily mutually exclusive. For example, it is possible that sprouting angiogenesis contains aspects of both, budding and chord hollowing, depending on the extent to which apical–basal polarity is maintained in the stalk cells. Likewise, it is possible that a single blood vessel contains regions of intracellular as well as regions of extracellular lumen. Taken together, it is clear that different vessels can form by various morphogenetic mechanisms. It remains to be explored what the decisive factors are that determine which mechanism is used. It is likely that parameters such as vessel caliber, blood pressure of the parental vessel as well as cell number within the sprout play important roles.

Guidance cues along the way—endothelial pathfinding

To effectively oxygenate a given organ, blood vessels have to be evenly distributed within this tissue. This can be achieved in different ways, for example by controlling the number of angiogenic sprouts that are generated (e.g. ISV) or by the formation of a plexus (e.g. retinal vasculature in the mouse), which is then remodeled by a pruning process. In recent years, a number of ligands (and their respective receptors) that provide endothelial guidance cues have been described, including the Semaphorin, Netrin, Ephrin and Slit systems (reviewed by Larrivée et al., 2009). Interestingly, these signals were originally described as cues for axonal growth cones (reviewed by Eichmann et al., 2005). It has become clear since that many of the signaling pathways that act during axonal pathfinding are also employed for guidance of angiogenic sprouts.

In the zebrafish, the guidance of angiogenic sprouts is best studied during SA formation. Segmental arteries sprout from the DA at the intersomitic boundary; as they grow out, they follow the intersomitic fissure up to the horizontal myoseptum, from where they change their path to grow more or less straight to the dorsal roof of the neural tube. The exit point of intersegmental sprouts is regulated by molecular guidance cues. In *out of bounds* (*obd*) mutants, angiogenic sprouts form ectopically along the ventral somite border (Childs et al., 2002). Furthermore, these sprouts no longer avoid the ventral somite and the ISVs take on a plexus-like organization. Molecular analyses showed that *obd* encodes the receptor PlexinD1 that is expressed in ECs and interacts with the ligands SEMA3A1/2, which is expressed in ventral somites. Upon ligand binding, a repulsive signal is activated in the ECs prohibiting them from moving into the somite region (Torres-Vazquez, 2004). Recently, it has been shown that the interaction of different Plexins and Semaphorins is also important for the timing of SA sprout formation (Lamont et al., 2009).

Analyses in mouse have uncovered an additional and quite different molecular mechanism that limits the number of sprouts. Bautch and coworkers have shown that a soluble form of FLT-1 (VEGFR-1), sFLT-1, is secreted from ECs adjacent to the forming sprout (Chappell et al., 2009). This isoform is able to bind VEGF, thereby removing it from the environment surrounding the sprout. It is thought that sFLT-1 serves two purposes: it ensures the ordered formation of sprouts from an activated endothelium and it prevents the early sprout to connect back to its original vessel.

The sharing of attracting and repulsive signaling pathways by neurons and ECs appears to be a common theme. In fact, it has been shown that growing neurons and nascent capillaries can walk the same tracks (Mukouyama et al., 2002). It will be interesting to see whether in these instances neurons and ECs simply use the same cues provided by the stromal cells or whether they also navigate by direct cell–cell interactions. It is noteworthy that not only the tip cell but also stalk cells appear to express guidance receptors albeit at lower levels (Larrivée et al., 2009). In zebrafish, for example, the guidance receptor *PlexinD1* is expressed at comparable levels in the tip and the stalk of nascent SA (Torres-Vázquez et al., 2004). This raises the possibility that also stalk cells are involved in angiogenic pathfinding. Indeed, it appears that the tip cell fate is not fixed and that cells at the stalk can become tip cells and vice versa. In murine allantoic explant cultures, migratory ECs are passing each other at the tip (Perryn et al., 2008). In a similar fashion, ECs are changing lead during the outgrowth of vascular cords that sprout from differentiating murine embryonic stem cells (Holger Gerhardt, personal communication). It has been suggested that these tip cell turnovers are regulated by oscillations in Notch signaling along the vascular sprout (Phng and Gerhardt, 2009). It should be noted that these vascular cords are not perfused during early outgrowth and are, in that respect, similar to developing SAs rather than vessels in the postnatal mouse retina.

Cell–cell adhesion during sprouting angiogenesis

The above observations indicate that the angiogenic sprout is highly plastic with regard to signaling events and cell–cell interactions and that cellular rearrangements play an important role in blood vessel morphogenesis. It is generally believed that cellular rearrangements involve remodeling of intercellular junctions (Baer et al., 2009). In *Drosophila*, adherens junctions play an important role for cellular rearrangement during various processes, such as border cell migration or tracheal morphogenesis (Pacquelet and Rørth, 2005; Ribeiro et al., 2004). In the case of border cell migration very different cell behaviors, invasive cell migration and cell adhesion require DE-cadherin. These distinct cellular activities are mediated by homophilic interactions of DE-cadherin between different cell types: interactions among border cells maintain cohesion of the migratory cells while interactions between border cells and nurse cells allow invasive migration into the substratum (Niewiadomska et al., 1999). The role of VE-cadherin during vertebrate angiogenesis is less clear. Mice that are mutant for VE-cadherin die at mid-gestation exhibiting vascular defects that are consistent with a role for VE-cadherin in maintaining vascular integrity (Carmeliet et al., 1999; Crosby, 2005). Further in vitro analyses have also emphasized a role of VE-cadherin in endothelial cell survival and stabilizing the endothelium, in part by antagonizing VEGFR-2 signaling (reviewed by Lampugnani and Dejana, 2007; Vestweber et al., 2009). Recent organotypic cell culture and knockdown experiments in zebrafish point at a role of VE-cadherin in angiogenic sprouting (Abraham et al., 2009). In these studies, quiescent endothelial tubes did not respond to VEGF stimulation unless VE-cadherin function was reduced. They further showed that VE-cadherin suppresses sprouting by inhibiting VEGF-R2/RAC1 signaling. In the zebrafish ISV, knockdown of VE-cadherin led to the formation of ectopic "branch points" along the proximo-

distal axis of the ISV, which were interpreted as prolonged angiogenic behavior of the ECs within the ISV.

While the above results suggest an anti-angiogenic function, other studies indicate a more pro-angiogenic role for VE-cadherin. As discussed above, blood vessel formation is a very dynamic process involving cell rearrangements and cell migration. These dynamics have been studied using murine allantoic explant cultures, which allow to measure the migration of individual and groups of ECs in a process called vasculogenic sprouting, which involves the outgrowth of multicellular sprouts from a primary plexus (Perryn et al., 2008; Rupp et al., 2004). ECs actively migrate over the substrate, frequently passing each other during outgrowth of the vascular rod. These rearrangements are effectively inhibited by addition of a VE-cadherin blocking antibody (Perryn et al., 2008), indicating that VE-cadherin is required for cellular rearrangements as they occur during vasculogenic sprouting. In zebrafish, we have observed that VE-cadherin is also essential for cellular rearrangements during SA formation (H.-G. Belting and M. Affolter, unpublished observation). Therefore, it appears that in addition to functions in vascular integrity and cell survival, VE-cadherin is also involved in sprouting angiogenesis. One can easily imagine that, analogous to the role of DE-cadherin in border cell migration, VE-cadherin may fulfill dual functions at the same time: maintenance of cell–cell contacts and cellular rearrangements.

Conclusions and perspectives

Blood vessel formation includes a spectrum of different morphogenetic processes such as budding, cord hollowing, cell hollowing, cell wrapping and intussusception. The genetic and molecular bases, which initiate and control these different processes is not known. It is clear, however, that ECs of different vascular beds are different in their gene expression profile and that blood vessels are anatomically highly diverse (Rocha and Adams, 2009). Morphogenesis may also be influenced by extraneous factors such as diverse extracellular matrices and signals, shear stress due to blood pressure or differences in cell number (Aird, 2007; Nguyen et al., 2006; Sottile, 2004).

The morphogenetic events that underlie blood vessel formation are likely to determine the way a vessel ultimately lumenizes. During sprouting angiogenesis, larger vessels appear to extend their lumens in conjunction with the outgrowing sprout, while small capillaries may form their lumens de novo by cell hollowing or cord hollowing. The respective contribution to lumen formation in different vessels remains to be determined.

Elaboration of the vascular tree requires additional processes, such as vessel fusion and pruning. How these processes occur at the morphogenetic level has not yet been described in much detail. With regard to vessel fusion, one can envisage that cellular remodeling plays a major role. Furthermore, it is likely that the fusion process occurs differently depending on vessel type. In the zebrafish, the DLAVs form in a non-perfused state and blood circulation commences subsequently. Recently, VE-cadherin localization during DLAV formation revealed that cells from adjacent sprouts undergo extensive rearrangements (Blum et al., 2008). Initial contacts between neighboring sprouts require VE-cadherin, as knockdown of VE-cadherin function leads to slowed-down formation of cell–cell contacts (Montero-Balaguer et al., 2009). It will be interesting to examine the exact cellular mechanisms that drive vessel fusion during DLAV formation and compare them with those occurring in perfused vessels.

Acknowledgments

The authors wish to thank Ralf Adams, Victoria Bautch, Holger Gerhardt, Eckhard Lammert, Stefan Schulte-Merker and Arndt Siekmann for interesting discussions and two anonymous referees for very helpful comments on the original manuscript. This work has been supported by the Kantons Basel-Stadt and Basel-Land, and by the Swiss National Science Foundation. A.L. and A.K. are supported by fellowships from the Werner Siemens-Foundation (Zug).

References

Abraham, S., Yeo, M., Montero-Balaguer, M., Paterson, H., Dejana, E., Marshall, C.J., Mavria, G., 2009. VE-cadherin-mediated cell–cell interaction suppresses sprouting via signaling to MLC2 phosphorylation. Curr. Biol. 19, 1–7.
Adams, R.H., Alitalo, K., 2007. Molecular regulation of angiogenesis and lymphangiogenesis. Nat. Rev., Mol. Cell Biol. 8, 464–478.
Adams, R.H., Wilkinson, G.A., Weiss, C., Diella, F., Gale, N.W., Deutsch, U., Risau, W., Klein, R., 1999. Roles of ephrinB ligands and EphB receptors in cardiovascular development: demarcation of arterial/venous domains, vascular morphogenesis, and sprouting angiogenesis. Genes Dev. 13, 295–306.
Aird, W.C., 2007. Phenotypic heterogeneity of the endothelium: II. Representative vascular beds. Circ. Res. 100, 174–190.
Andrew, D., Ewald, A., 2010. Morphogenesis of epithelial tubes: Insights into tube formation, elongation, and elaboration. Dev. Biol. 341, 66–83.
Armulik, A., Abramsson, A., Betsholtz, C., 2005. Endothelial/pericyte interactions. Circ. Res. 97, 512–523.
Ausprunk, D.H., Folkman, J., 1977. Migration and proliferation of endothelial cells in preformed and newly formed blood vessels during tumor angiogenesis. Microvasc. Res. 14, 53–65.
Baer, M.M., Chanut-Delalande, H., Affolter, M., 2009. Cellular and molecular mechanisms underlying the formation of biological tubes. Curr. Top. Dev. Biol. 89, 137–162.
Bahary, N., Goishi, K., Stuckenholz, C., Weber, G., Leblanc, J., Schafer, C.A., Berman, S.S., Klagsbrun, M., Zon, L.I., 2007. Duplicate VegfA genes and orthologues of the KDR receptor tyrosine kinase family mediate vascular development in the zebrafish. Blood 110, 3627–3636.
Bar, T., Guldner, F.H., Wolff, J.R., 1984. "Seamless" endothelial cells of blood capillaries. Cell Tissue Res. 235, 99–106.
Beis, D., Stainier, D.Y.R., 2006. In vivo cell biology: following the zebrafish trend. Trends Cell Biol. 16, 105–112.
Blum, Y., Belting, H.-G., Ellertsdottir, E., Herwig, L., Lüders, F., Affolter, M., 2008. Complex cell rearrangements during intersegmental vessel sprouting and vessel fusion in the zebrafish embryo. Dev. Biol. 316, 312–322.
Carmeliet, P., 2003. Angiogenesis in health and disease. Nat. Med. 9, 653–660.
Carmeliet, P., Lampugnani, M.G., Moons, L., Breviario, F., Compernolle, V., Bono, F., Balconi, G., Spagnuolo, R., Oosthuyse, B., Dewerchin, M., Zanetti, A., Angellilo, A., Mattot, V., Nuyens, D., Lutgens, E., Clotman, F., de Ruiter, M.C., Gittenberger-de Groot, A., Poelmann, R., Lupu, F., Herbert, J.M., Collen, D., Dejana, E., 1999. Targeted deficiency or cytosolic truncation of the VE-cadherin gene in mice impairs VEGF-mediated endothelial survival and angiogenesis. Cell 98, 147–157.
Cébe-Suarez, S., Zehnder-Fjällman, A., Ballmer-Hofer, K., 2006. The role of VEGF receptors in angiogenesis; complex partnerships. Cell. Mol. Life Sci. 63, 601–615.
Cermenati, S., Moleri, S., Cimbro, S., Corti, P., Del Giacco, L., Amodeo, R., Dejana, E., Koopman, P., Cotelli, F., Beltrame, M., 2008. Sox18 and Sox7 play redundant roles in vascular development. Blood 111, 2657–2666.
Chappell, J.C., Taylor, S.M., Ferrara, N., Bautch, V., 2009. Local guidance of emerging vessel sprouts requires soluble Flt-1 (VEGFR-1). Dev. Cell 1–40.
Childs, S., Chen, J.-N., Garrity, D.M., Fishman, M.C., 2002. Patterning of angiogenesis in the zebrafish embryo. Development 129, 973–982.
Coffin, J.D., Poole, T.J., 1988. Embryonic vascular development: immunohistochemical identification of the origin and subsequent morphogenesis of the major vessel primordia in quail embryos. Development 102, 735–748.
Coffin, J.D., Poole, T.J., 1991. Endothelial cell origin and migration in embryonic heart and cranial blood vessel development. Anat. Rec. 231, 383–395.
Covassin, L.D., Villefranc, J.A., Kacergis, M.C., Weinstein, B.M., Lawson, N.D., 2006. Distinct genetic interactions between multiple Vegf receptors are required for development of different blood vessel types in zebrafish. Proc. Natl. Acad. Sci. U. S. A. 103, 6554–6559.
Covassin, L.D., Siekmann, A.F., Kacergis, M.C., Laver, E., Moore, J.C., Villefranc, J.A., Weinstein, B.M., Lawson, N.D., 2009. A genetic screen for vascular mutants in zebrafish reveals dynamic roles for Vegf/Plcg1 signaling during artery development. Dev. Biol. 329, 212–226.
Crosby, C.V., 2005. VE-cadherin is not required for the formation of nascent blood vessels but acts to prevent their disassembly. Blood 105, 2771–2776.
De Val, S., Black, B.L., 2009. Transcriptional control of endothelial cell development. Dev. Cell 16, 180–195.
De Val, S., Chi, N.C., Meadows, S.M., Minovitsky, S., Anderson, J.P., Harris, I.S., Ehlers, M.L., Agarwal, P., Visel, A., Xu, S.-M., Pennacchio, L.A., Dubchak, I., Krieg, P.A., Stainier, D.Y.R., Black, B.L., 2008. Combinatorial regulation of endothelial gene expression by ETS and forkhead transcription factors. Cell 135, 1053–1064.
Detrich, H.W., Kieran, M.W., Chan, F.Y., Barone, L.M., Yee, K., Rundstadler, J.A., Pratt, S., Ransom, D., Zon, L.I., 1995. Intraembryonic hematopoietic cell migration during vertebrate development. Proc. Natl. Acad. Sci. U.S.A. 92, 10713–10717.
Dooley, K., Davidson, A., Zon, L., 2005. Zebrafish functions independently in hematopoietic and endothelial development. Dev. Biol. 277, 522–536.
Eichmann, A., Yuan, L., Moyon, D., Lenoble, F., Pardanaud, L., Breant, C., 2005. Vascular development: from precursor cells to branched arterial and venous networks. Int. J. Dev. Biol. 49, 259–267.
Eriksson, J., Löfberg, J., 2000. Development of the hypochord and dorsal aorta in the zebrafish embryo (*Danio rerio*). J. Morphol. 244, 167–176.

Folkman, J., 1982. Angiogenesis: initiation and control. Ann. N.Y. Acad. Sci. 401, 212–227.
Gerhardt, H., Golding, M., Fruttiger, M., Ruhrberg, C., Lundkvist, A., Abramsson, A., Jeltsch, M., Mitchell, C., Alitalo, K., Shima, D., Betsholtz, C., 2003. VEGF guides angiogenic sprouting utilizing endothelial tip cell filopodia. J. Cell Biol. 161, 1163–1177.
Gering, M., Rodaway, A.R., Göttgens, B., Patient, R.K., Green, A.R., 1998. The SCL gene specifies haemangioblast development from early mesoderm. EMBO J. 17, 4029–4045.
Habeck, H., Odenthal, J., Walderich, B., Maischein, H., Schulte-Merker, S., consortium, T.s., 2002. Analysis of a zebrafish VEGF receptor mutant reveals specific disruption of angiogenesis. Curr. Biol. 12, 1405–1412.
Hellström, M., Phng, L.-K., Hofmann, J.J., Wallgard, E., Coultas, L., Lindblom, P., Alva, J., Nilsson, A.-K., Karlsson, L., Gaiano, N., Yoon, K., Rossant, J., Iruela-Arispe, M.L., Kalén, M., Gerhardt, H., Betsholtz, C., 2007. Dll4 signalling through Notch1 regulates formation of tip cells during angiogenesis. Nature 445, 776–780.
Herbert, S.P., Huisken, J., Kim, T.N., Feldman, M.E., Houseman, B.T., Wang, R.A., Shokat, K.M., Stainier, D.Y.R., 2009. Arterial-venous segregation by selective cell sprouting: an alternative mode of blood vessel formation. Science 326, 294–298.
Hirakow, R., Hiruma, T., 1981. Scanning electron microscopic study on the development of primitive blood vessels in chick embryos at the early somite-stage. Anat. Embryol. (Berl.) 163, 299–306.
Hogan, B.L., Kolodziej, P.A., 2002. Organogenesis: molecular mechanisms of tubulogenesis. Nat. Rev., Genet. 3, 513–523.
Hogan, B.M., Bos, F.L., Bussmann, J., Witte, M., Chi, N.C., Duckers, H.J., Schulte-Merker, S., 2009. Ccbe1 is required for embryonic lymphangiogenesis and venous sprouting. Nat. Genet. 41, 396–398.
Hogan, B.M., Robert, H., Witte, M., Heloterä, H., Alitalo, K., Duckers, H.J., Schulte-Merker, S., 2009. Vegfc/Flt4 signalling is suppressed by Dll4 in developing zebrafish intersegmental arteries. Development 136, 4001–4009.
Huisken, J., Stainier, D.Y.R., 2009. Selective plane illumination microscopy techniques in developmental biology. Development 136, 1963–1975.
Isogai, S., 2003. Angiogenic network formation in the developing vertebrate trunk. Development 130, 5281–5290.
Isogai, S., Horiguchi, M., Weinstein, B.M., 2001. The vascular anatomy of the developing zebrafish: an atlas of embryonic and early larval development. Dev. Biol. 230, 278–301.
Isogai, S., Lawson, N.D., Torrealday, S., Horiguchi, M., Weinstein, B.M., 2003. Angiogenic network formation in the developing vertebrate trunk. Development 130, 5281–5290.
Jin, S., Herzog, W., Santoro, M., Mitchell, T., Frantsve, J., Jungblut, B., Beis, D., Scott, I., Damico, L., Ober, E., 2007. A transgene-assisted genetic screen identifies essential regulators of vascular development in vertebrate embryos. Dev. Biol. 307, 29–42.
Jin, S.-W., Beis, D., Mitchell, T., Chen, J.-N., Stainier, D.Y.R., 2005. Cellular and molecular analyses of vascular tube and lumen formation in zebrafish. Development 132, 5199–5209.
Kamei, M., Saunders, W.B., Bayless, K.J., Dye, L., Davis, G.E., Weinstein, B.M., 2006. Endothelial tubes assemble from intracellular vacuoles in vivo. Nature 442, 453–456.
Kemp, H.A., Cooke, J.E., Moens, C.B., 2009. EphA4 and EfnB2a maintain rhombomere coherence by independently regulating intercalation of progenitor cells in the zebrafish neural keel. Dev. Biol. 327, 313–326.
Kimmel, C.B., Ballard, W.W., Kimmel, S.R., Ullmann, B., Schilling, T.F., 1995. Stages of embryonic development of the zebrafish. Dev. Dyn. 203, 253–310.
Kucera, T., Eglinger, J., Strilic, B., Lammert, E., 2007. Vascular lumen formation from a cell biological perspective. Novartis Found. Symp. 283, 46–56 discussion 56-60, 238-241.
Küchler, A.M., Gjini, E., Peterson-Maduro, J., Cancilla, B., Wolburg, H., Schulte-Merker, S., 2006. Development of the zebrafish lymphatic system requires VEGFC signaling. Curr. Biol. 16, 1244–1248.
Lamont, R., Lamont, E., Childs, S., 2009. Antagonistic interactions among Plexins regulate the timing of intersegmental vessel formation. Dev. Biol. 331, 199–209.
Lampugnani, M.G., Dejana, E., 2007. Adherens junctions in endothelial cells regulate vessel maintenance and angiogenesis. Thromb. Res. 120 (Suppl 2), S1–S6.
Larrivée, B., Freitas, C., Suchting, S., Brunet, I., Eichmann, A., 2009. Guidance of vascular development: lessons from the nervous system. Circ. Res. 104, 428–441.
Lawson, N.D., Weinstein, B.M., 2002a. Arteries and veins: making a difference with zebrafish. Nat. Rev., Genet. 3, 674–682.
Lawson, N.D., Weinstein, B.M., 2002b. In vivo imaging of embryonic vascular development using transgenic zebrafish. Dev. Biol. 248, 307–318.
Lawson, N.D., Scheer, N., Pham, V.N., Kim, C.H., Chitnis, A.B., Campos-Ortega, J.A., Weinstein, B.M., 2001. Notch signaling is required for arterial-venous differentiation during embryonic vascular development. Development 128, 3675–3683.
Lawson, N.D., Vogel, A.M., Weinstein, B.M., 2002. Sonic hedgehog and vascular endothelial growth factor act upstream of the Notch pathway during arterial endothelial differentiation. Dev. Cell 3, 127–136.
Lawson, N.D., Mugford, J.W., Diamond, B.A., Weinstein, B.M., 2003. Phospholipase C gamma-1 is required downstream of vascular endothelial growth factor during arterial development. Genes Dev. 17, 1346–1351.
Leslie, J.D., Ariza-Mcnaughton, L., Bermange, A.L., Mcadow, R., Johnson, S.L., Lewis, J., 2007. Endothelial signalling by the Notch ligand Delta-like 4 restricts angiogenesis. Development 134, 839–844.
Liao, E.C., Paw, B.H., Oates, A.C., Pratt, S.J., Postlethwait, J.H., Zon, L.I., 1998. SCL/Tal-1 transcription factor acts downstream of cloche to specify hematopoietic and vascular progenitors in zebrafish. Genes Dev. 12, 621–626.
Liu, F., Patient, R., 2008. Genome-wide analysis of the zebrafish ETS family identifies three genes required for hemangioblast differentiation or angiogenesis. Circ. Res. 103, 1147–1154.
Lubarsky, B., Krasnow, M.A., 2003. Tube morphogenesis: making and shaping biological tubes. Cell 112, 19–28.
Makanya, A., Hlushchuk, R., Djonov, V., 2009. Intussusceptive angiogenesis and its role in vascular morphogenesis, patterning, and remodeling. Angiogenesis 12, 113–123.
Matsumoto, T., Mugishima, H., 2006. Signal transduction via vascular endothelial growth factor (VEGF) receptors and their roles in atherogenesis. J. Atheroscler. Thromb. 13, 130–135.
Meier, S., 1980. Development of the chick embryo mesoblast: pronephros, lateral plate, and early vasculature. J. Embryol. Exp. Morphol. 55, 291–306.
Mellitzer, G., Xu, Q., Wilkinson, D.G., 1999. Eph receptors and ephrins restrict cell intermingling and communication. Nature 400, 77–81.
Montero-Balaguer, M., Swirsding, K., Orsenigo, F., Cotelli, F., Mione, M., Dejana, E., 2009. Stable vascular connections and remodeling require full expression of VE-cadherin in zebrafish embryos. PLoS ONE 4, e5772.
Mukouyama, Y.-s., Shin, D., Britsch, S., Taniguchi, M., Anderson, D.J., 2002. Sensory nerves determine the pattern of arterial differentiation and blood vessel branching in the skin. Cell 109, 693–705.
Nasevicius, A., Larson, J., Ekker, S.C., 2000. Distinct requirements for zebrafish angiogenesis revealed by a VEGF-A morphant. Yeast 17, 294–301.
Nguyen, T.-H., Eichmann, A., Le Noble, F., Fleury, V., 2006. Dynamics of vascular branching morphogenesis: the effect of blood and tissue flow. Phys. Rev., E, Stat. Nonlinear Soft Matter Phys. 73, 061907.
Niewiadomska, P., Godt, D., Tepass, U., 1999. DE-cadherin is required for intercellular motility during Drosophila oogenesis. J. Cell Biol. 144, 533–547.
Nikolova, G., Lammert, E., 2003. Interdependent development of blood vessels and organs. Cell Tissue Res. 314, 33–42.
Olsson, A.-K., Dimberg, A., Kreuger, J., Claesson-Welsh, L., 2006. VEGF receptor signalling—in control of vascular function. Nat. Rev., Mol. Cell Biol. 7, 359–371.
Pacquelet, A., Rørth, P., 2005. Regulatory mechanisms required for DE-cadherin function in cell migration and other types of adhesion. J. Cell Biol. 170, 803–812.
Patan, S., 2000. Vasculogenesis and angiogenesis as mechanisms of vascular network formation, growth and remodeling. J. Neuro-oncol. 50, 1–15.
Patterson, L.J., Gering, M., Eckfeldt, C.E., Green, A.R., Verfaillie, C.M., Ekker, S.C., Patient, R., 2007. The transcription factors Scl and Lmo2 act together during development of the hemangioblast in zebrafish. Blood 109, 2389–2398.
Pendeville, H., Winandy, M., Manfroid, I., Nivelles, O., Motte, P., Pasque, V., Peers, B., Struman, I., Martial, J.A., Voz, M.L., 2008. Zebrafish Sox7 and Sox18 function together to control arterial-venous identity. Dev. Biol. 317, 405–416.
Perryn, E.D., Czirók, A., Little, C.D., 2008. Vascular sprout formation entails tissue deformations and VE-cadherin-dependent cell-autonomous motility. Dev. Biol. 313, 545–555.
Phng, L.-K., Gerhardt, H., 2009. Angiogenesis: a team effort coordinated by Notch. Dev. Cell 16, 196–208.
Poole, T.J., Coffin, J.D., 1989. Vasculogenesis and angiogenesis: two distinct morphogenetic mechanisms establish embryonic vascular pattern. J. Exp. Zool. 251, 224–231.
Red-Horse, K., Crawford, Y., Shojaei, F., Ferrara, N., 2007. Endothelium-microenvironment interactions in the developing embryo and in the adult. Dev. Cell 12, 181–194.
Ribeiro, C., Neumann, M., Affolter, M., 2004. Genetic control of cell intercalation during tracheal morphogenesis in Drosophila. Curr. Biol. 14, 2197–2207.
Risau, W., 1995. Differentiation of endothelium. FASEB J. 9, 926–933.
Risau, W., Sariola, H., Zerwes, H.G., Sasse, J., Ekblom, P., Kemler, R., Doetschman, T., 1988. Vasculogenesis and angiogenesis in embryonic-stem-cell-derived embryoid bodies. Development 102, 471–478.
Rocha, S., Adams, R., 2009. Molecular differentiation and specialization of vascular beds. Angiogenesis 12, 139–147.
Roman, B.L., Pham, V.N., Lawson, N.D., Kulik, M., Childs, S., Lekven, A.C., Garrity, D.M., Moon, R.T., Fishman, M.C., Lechleider, R.J., Weinstein, B.M., 2002. Disruption of acvrl1 increases endothelial cell number in zebrafish cranial vessels. Development 129, 3009–3019.
Ruhrberg, C., Gerhardt, H., Golding, M., Watson, R., Ioannidou, S., Fujisawa, H., Betsholtz, C., Shima, D.T., 2002. Spatially restricted patterning cues provided by heparin-binding VEGF-A control blood vessel branching morphogenesis. Genes Dev. 16, 2684–2698.
Rupp, P.A., Czirók, A., Little, C.D., 2004. alphavbeta3 integrin-dependent endothelial cell dynamics in vivo. Development 131, 2887–2897.
Sakaguchi, T.F., Sadler, K.C., Crosnier, C., Stainier, D.Y.R., 2008. Endothelial signals modulate hepatocyte apicobasal polarization in zebrafish. Curr. Biol. 18, 1565–1571.
Shibuya, M., Claesson-Welsh, L., 2006. Signal transduction by VEGF receptors in regulation of angiogenesis and lymphangiogenesis. Exp. Cell Res. 312, 549–560.
Siekmann, A.F., Lawson, N.D., 2007. Notch signalling limits angiogenic cell behaviour in developing zebrafish arteries. Nature 445, 781–784.
Siekmann, A.F., Covassin, L., Lawson, N.D., 2008. Modulation of VEGF signalling output by the Notch pathway. BioEssays 30, 303–313.
Siekmann, A.F., Standley, C., Fogarty, K.E., Wolfe, S.A., Lawson, N.D., 2009. Chemokine signaling guides regional patterning of the first embryonic artery. Genes Dev. 23, 2272–2277.
Sottile, J., 2004. Regulation of angiogenesis by extracellular matrix. Biochim. Biophys. Acta 1654, 13–22.
Stainier, D.Y., Weinstein, B.M., Detrich III, H.W., Zon, L.I., Fishman, M.C., 1995. Cloche, an early acting zebrafish gene, is required by both the endothelial and hematopoietic lineages. Development 121, 3141–3150.

Strilić, B., Kucera, T., Eglinger, J., Hughes, M.R., Mcnagny, K.M., Tsukita, S., Dejana, E., Ferrara, N., Lammert, E., 2009. The molecular basis of vascular lumen formation in the developing mouse aorta. Dev. Cell 17, 505–515.

Suchting, S., Freitas, C., Le Noble, F., Benedito, R., Bréant, C., Duarte, A., Eichmann, A., 2007. The Notch ligand Delta-like 4 negatively regulates endothelial tip cell formation and vessel branching. Proc. Natl. Acad. Sci. U.S.A. 104, 3225–3230.

Tammela, T., Zarkada, G., Wallgard, E., Murtomäki, A., Suchting, S., Wirzenius, M., Waltari, M., Hellström, M., Schomber, T., Peltonen, R., Freitas, C., Duarte, A., Isoniemi, H., Laakkonen, P., Christofori, G., Ylä-Herttuala, S., Shibuya, M., Pytowski, B., Eichmann, A., Betsholtz, C., Alitalo, K., 2008. Blocking VEGFR-3 suppresses angiogenic sprouting and vascular network formation. Nature 454, 656–660.

Thisse, C., 2002. Organogenesis—heart and blood formation from the zebrafish point of view. Science 295, 457–462.

Thompson, M.A., Ransom, D.G., Pratt, S.J., MacLennan, H., Kieran, M.W., Detrich, H.W., Vail, B., Huber, T.L., Paw, B., Brownlie, A.J., Oates, A.C., Fritz, A., Gates, M.A., Amores, A., Bahary, N., Talbot, W.S., Her, H., Beier, D.R., Postlethwait, J.H., Zon, L.I., 1998. The cloche and spadetail genes differentially affect hematopoiesis and vasculogenesis. Dev. Biol. 197, 248–269.

Torres-Vazquez, J., 2004. Semaphorin-plexin signaling guides patterning of the developing vasculature. Dev. Cell 7, 117–123.

Torres-Vázquez, J., Gitler, A.D., Fraser, S.D., Berk, J.D., Pham, V.N., Fishman, M.C., Childs, S., Epstein, J.A., Weinstein, B.M., 2004. Semaphorin-plexin signaling guides patterning of the developing vasculature. Dev. Cell 7, 117–123.

Vestweber, D., Winderlich, M., Cagna, G., Nottebaum, A.F., 2009. Cell adhesion dynamics at endothelial junctions: VE-cadherin as a major player. Trends Cell Biol. 19, 8–15.

Walls, J.R., Coultas, L., Rossant, J., Henkelman, R.M., 2008. Three-dimensional analysis of vascular development in the mouse embryo. PLoS ONE 3, e2853.

Yamazaki, Y., Morita, T., 2006. Molecular and functional diversity of vascular endothelial growth factors. Mol. Divers. 10, 515–527.

Yaniv, K., Isogai, S., Castranova, D., Dye, L., Hitomi, J., Weinstein, B.M., 2006. Live imaging of lymphatic development in the zebrafish. Nat. Med. 12, 711–716.

Zhong, T.P., Childs, S., Leu, J.P., Fishman, M.C., 2001. Gridlock signalling pathway fashions the first embryonic artery. Nature 414, 216–220.

Zon, L.I., Mather, C., Burgess, S., Bolce, M.E., Harland, R.M., Orkin, S.H., 1991. Expression of GATA-binding proteins during embryonic development in *Xenopus laevis*. Proc. Natl. Acad. Sci. U. S. A. 88, 10642–10646.

Developmental Cell
Article

Semaphorin-PlexinD1 Signaling Limits Angiogenic Potential via the VEGF Decoy Receptor sFlt1

Tomasz Zygmunt,[1,6] Carl Michael Gay,[1,6] Jordan Blondelle,[2] Manvendra K. Singh,[3,5] Kathleen McCrone Flaherty,[1] Paula Casey Means,[1] Lukas Herwig,[4] Alice Krudewig,[4] Heinz-Georg Belting,[4] Markus Affolter,[4] Jonathan A. Epstein,[3,5] and Jesús Torres-Vázquez[1,*]

[1]Department of Cell Biology, Helen L. and Martin S. Kimmel Center for Biology and Medicine at the Skirball Institute, New York University School of Medicine, New York, NY 10016, USA
[2]Université Diderot-Paris 7, Paris, France
[3]Department of Cell and Developmental Biology, Cardiovascular Institute, University of Pennsylvania, Philadelphia, PA 19104, USA
[4]Biozentrum, University of Basel, Ch-4056 Basel, Switzerland
[5]Institute for Regenerative Medicine, University of Pennsylvania, Philadelphia, PA 19104, USA
[6]These authors contributed equally to this work
*Correspondence: jesus.torres-vazquez@med.nyu.edu
DOI 10.1016/j.devcel.2011.06.033

SUMMARY

Sprouting angiogenesis expands the embryonic vasculature enabling survival and homeostasis. Yet how the angiogenic capacity to form sprouts is allocated among endothelial cells (ECs) to guarantee the reproducible anatomy of stereotypical vascular beds remains unclear. Here we show that Sema-PlxnD1 signaling, previously implicated in sprout guidance, represses angiogenic potential to ensure the proper abundance and stereotypical distribution of the trunk's segmental arteries (SeAs). We find that Sema-PlxnD1 signaling exerts this effect by antagonizing the proangiogenic activity of vascular endothelial growth factor (VEGF). Specifically, Sema-PlxnD1 signaling ensures the proper endothelial abundance of *soluble flt1* (*sflt1*), an alternatively spliced form of the VEGF receptor Flt1 encoding a potent secreted decoy. Hence, Sema-PlxnD1 signaling regulates distinct but related aspects of angiogenesis: the spatial allocation of angiogenic capacity within a primary vessel and sprout guidance.

INTRODUCTION

Blood vessels form a pervasive tubular network that distributes oxygen, nutrients, hormones, and immunity factors. The first blood vessels assemble de novo via EC coalescence or vasculogenesis. Later, they expand via angiogenesis, the growth of new blood vessels from preexisting ones. In some locales, this process is stereotypic and vascular sprouts form with evolutionarily conserved and organ-specific distribution, abundance and shapes (Carmeliet, 2005; Isogai et al., 2001; Isogai et al., 2003). For example, zebrafish SeAs sprout bilaterally from the trunk's aorta just anterior to each somite boundary (SB) (Figure 1A). SeA sprouts contain migratory, proliferative and filopodia-rich arterial angiogenic ECs molecularly distinct from the sedentary "phalanx" ECs remaining in the aorta (De Bock et al., 2009; Siekmann and Lawson, 2007; Torres-Vázquez et al., 2004). Normally, only aortic ECs near SBs acquire angiogenic capacity (Ahn et al., 2000; Childs et al., 2002). It is thought that nonendothelial paracrine VEGF signals promote angiogenic capacity, while Notch-mediated lateral inhibition between ECs antagonizes it (Phng and Gerhardt, 2009; Siekmann et al., 2008). However, the mRNA expression of *vegf-a* and Notch pathway genes is inconsistent with the distribution of SeA sprouts. *vegf-a* is not transcribed along SBs, but rather expressed dorsal to the aorta at both the flanking somites' centers and the hypochord, a midline endodermal cell row. Notch pathway genes are expressed continuously along the aorta or broadly through the body (Hogan et al., 2009b; Lawson et al., 2002; Leslie et al., 2007; Phng et al., 2009; Siekmann and Lawson, 2007) (C.M.G., J.B., and J.T.-V., unpublished data). Hence, other cascades likely modulate VEGF and/or Notch signaling at presprouting stages to enable the stereotypical allocation of angiogenic capacity within the aorta. Perturbing these unidentified cascades might change the SeA sprouts' reproducible number or distribution, the ratio of aortic ECs that acquire angiogenic capacity, and/or the responsiveness of these cells to angiogenic cues.

Besides VEGF and Notch activity, proper SeA development requires paracrine Sema-Plxn signaling. Type 3 semas (sema3s) are repulsive guidance cues secreted by somites. Sema3s direct SeA sprout pathfinding by modulating cytoskeletal dynamics via the endothelial Sema3-receptor PlxnD1. Hence, *sema3* or *plxnD1* inactivation yields similar SeA sprout pathfinding defects in zebrafish and mice (Gay et al., 2011). Two observations made in zebrafish make Sema-PlxnD1 signaling a candidate modulator of angiogenic capacity. First, *sema3* and *plxnD1* expression begins hours before SeAs sprout from the aorta at ~21 hr post-fertilization (hpf). Second, loss of Sema-PlxnD1 signaling induces ectopic SeA sprout launching (Childs et al., 2002; Torres-Vázquez et al., 2004).

In wild-type (WT) animals SeA sprouts grow dorsally with a chevron-like shape, bifurcate anteroposteriorly at the neural tube's roof level and interconnect with their ipsilateral neighbors at ~32 hpf forming the paired Dorsal Longitudinal Anastomotic Vessels (DLAVs) (Isogai et al., 2003). In contrast, in *plxnD1* (*out of bounds - obd*) mutants and *plxnD1* morphants, SeA sprouts are misshaped and interconnect ectopically with their ipsilateral

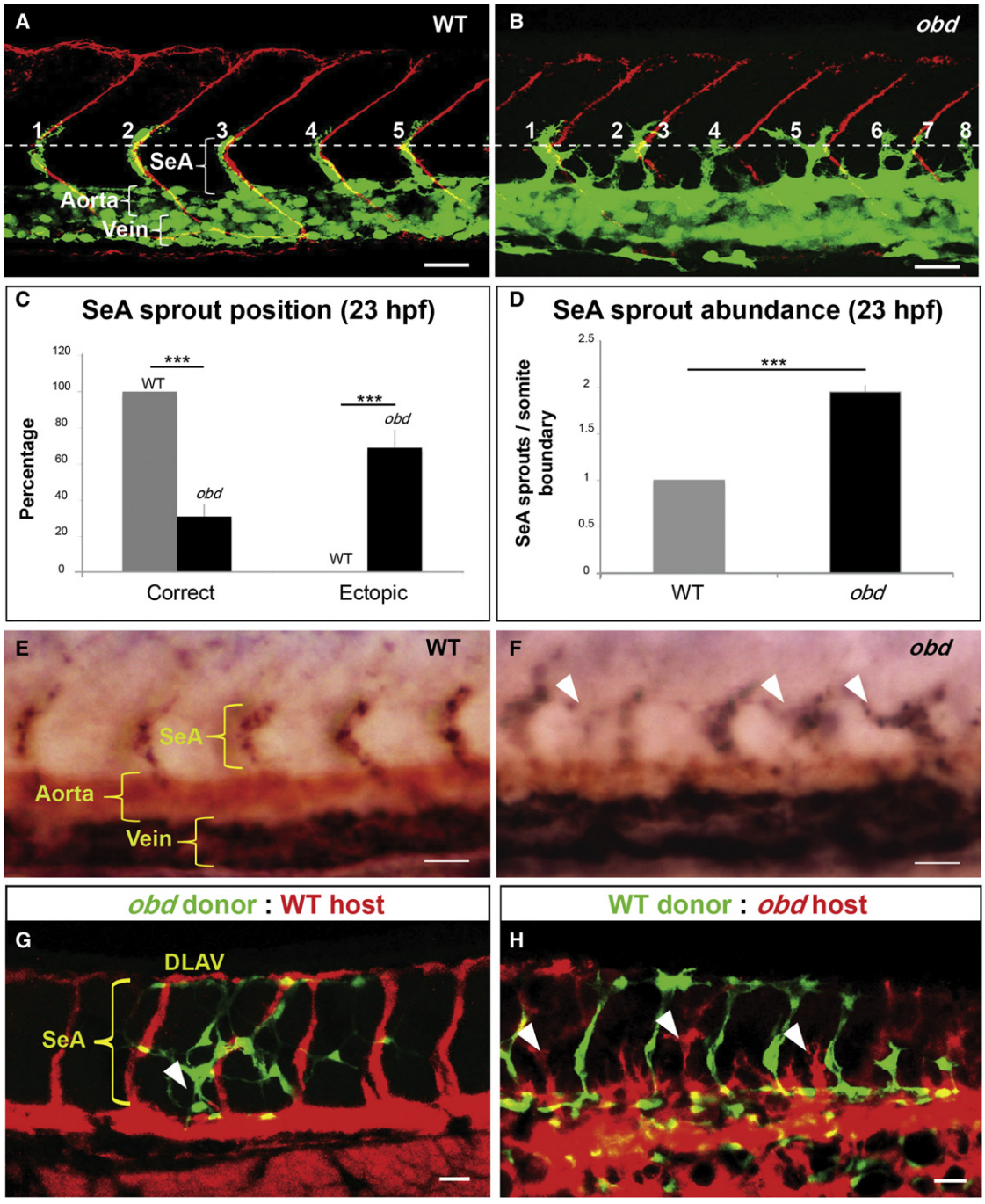

Figure 1. Sema-PlxnD1 Signaling Is Cell Autonomously Required within the Endothelium for Proper SeA Sprout Abundance and Distribution

(A and B) 23 hpf vasculatures, green. SBs, red. Horizontal myoseptum (HM), white dotted line. SeA sprouts, numbered. (A) WT. (B) *obd*.

(C and D) SeA sprout position (C) and abundance (D) in 23 hpf WT and *obd*. n = 8 WT, 12 *obd*. Error bars represent SEM. ***$p < 0.001$.

(E and F) WISH, 28 hpf trunks. Ectopic SeA sprouts, white arrowheads. Riboprobes: *flt4* (blue), *cdh5* (red). WT (E). *obd* (F). n = 10/10 WT, 10/10 *obd*.

(G and H) 32 hpf chimeric vasculatures with ECs of donor (green) and host (red) origin. Examples of ectopic SeA sprouts, white arrowheads.

(A, B, E–H) Anterior, left; dorsal, up. Scale bars represent 30 μm. See Figure S1.

neighbors but form properly placed DLAVs (Childs et al., 2002; Torres-Vázquez et al., 2004). Thus, we further examined Sema-PlxnD1's signaling role during zebrafish SeA development, finding that it plays a presprouting role as a repressor of the aorta's angiogenic potential—the probability that ECs acquire angiogenic capacity. This role stems from its ability to promote *sflt1*'s endothelial abundance and thus antagonize pro-angiogenic VEGF activity (Rahimi, 2006). We propose that

Sema-PlxnD1 signaling allocates angiogenic capacity among aortic ECs in a reproducible spatial pattern, guaranteeing the proper abundance and distribution of SeA sprouts.

RESULTS

Lack of Sema-PlxnD1 Signaling Induces Too Many and Ectopic SeA Sprouts

To investigate if Sema-PlxnD1 signaling modulates angiogenic capacity we measured SeA sprout abundance and positioning in WT and *obd* at 23 hpf, when individual *obd* SeA sprouts are readily identifiable as they are yet to interconnect ectopically. We found *obd* has almost twice the WT's number of SeA sprouts, with most of them launching ectopically (Figures 1A–1D). Hence, Sema-PlxnD1 signaling limits the abundance and defines the position of SeA sprouts.

To molecularly verify the angiogenic character of ECs within *obd* SeA sprouts, we used whole-mount RNA in situ hybridization (WISH) (Moens, 2008) to visualize expression of the pan-endothelial marker *cdh5* (Larson et al., 2004) and *flt4/vegfr-3*, which labels arterial angiogenic ECs within SeA sprouts and the vein (Covassin et al., 2006; Hogan et al., 2009b; Siekmann and Lawson, 2007). *flt4* is expressed in all SeA sprouts and vein of WT and *obd* (Figures 1E and 1F), confirming the angiogenic character of ECs within *obd*'s SeA sprouts and the lack of artery/vein differentiation defects in *obd* (Torres-Vázquez et al., 2004).

Loss of Sema-PlxnD1 Signaling Yields More Angiogenic Cells

To determine if *obd*'s SeA sprout overabundance is associated with too many angiogenic ECs we compared the number of EC nuclei found within developing SeAs and DLAVs of WT and *obd* at 21, 23, and 32 hpf. We found that *obd*'s SeAs/DLAVs collectively harbor more angiogenic ECs than WT (see Figures S1A and S1B available online). We next aimed to compare the WT and *obd* ratios of angiogenic to phalanx arterial ECs. However, SeA sprouts arise while the aorta and vein segregate from each other (Herbert et al., 2009), making the quantification of early aortic EC abundance unfeasible. We thus instead counted EC nuclei in the axial vasculature (aorta and vein taken together) and found that *obd* shows increased axial vasculature EC abundance (Figures S1A and S1B). Hence, loss of Sema-PlxnD1 signaling yields more angiogenic and axial vasculature ECs.

Sema-PlxnD1 Signaling Is Cell-Autonomously Required within the Endothelium

To ask if Sema-PlxnD1 signaling acts cell autonomously to limit the number and define the position of SeA sprouts, we performed cell transplants (Carmany-Rampey and Moens, 2006) to make heterogenotypic WT:*obd* (WT-to-*obd* and *obd*-to-WT) chimeras. We analyzed these at ~32 hpf to determine SeA sprout abundance and distribution and examine the SeA contribution of ECs from donors and hosts (Figures 1G and 1H). We found too many SeA sprouts in WT:*obd* chimeras. As in *obd*, some SeA sprouts launched ectopically and others were positioned correctly. WT ECs were found only within properly positioned SeA sprouts, while *obd* ECs contributed to misshapen SeAs sprouts at both ectopic and correct positions (Figures 1G and 1H and Figure S1C). Control homogenotypic (WT-to-WT and *obd*-to-*obd*) chimeras also showed mosaic SeAs with both host and donor ECs (Figure S1E). Hence, SeAs are not necessarily of clonal origin, in agreement with results from prior transplantation and mosaic transgenic labeling experiments (Childs et al., 2002; Siekmann and Lawson, 2007).

obd ECs found within WT hosts contribute to SeAs/DLAVs much more often than WT ECs contribute to these angiogenic vessels in *obd* hosts (Figures S1C, S1D, and S2C). Since *obd* ECs show exacerbated angiogenic capacity in a WT environment this property is not caused by axial vasculature EC overabundance. Finally, nonendothelial *obd* cells, like ventral somitic muscle fibers (Childs et al., 2002), did not influence the abundance, distribution or anatomical patterning of SeA sprouts (Figure S1C), consistent with *plxnD1*'s endothelial-specific expression (Torres-Vázquez et al., 2004) and the identical vascular phenotypes of mice with global or EC-specific *plxnD1* inactivation (Gay et al., 2011). Thus, Sema-PlxnD1 signaling acts cell autonomously within the endothelium to limit angiogenic potential and ensure the proper abundance and positioning of SeA sprouts.

Aortic ECs with Less Sema-PlxnD1 Signaling (*obd*/+) Become Angiogenic Tip Cells More Often and Are Enriched in the Aorta's Dorsal Side

Each SeA sprout has a spearheading tip cell that becomes "T" shaped during DLAV formation and which is trailed by a few stalk cells (Siekmann and Lawson, 2007). Tip cells embody an enhanced angiogenic state promoted by increased proangiogenic signaling and characterized by exacerbated filopodia dynamics whose acquisition and/or maintenance involves cell competition (Jakobsson et al., 2010; Leslie et al., 2007; Roca and Adams, 2007).

Thus, if Sema-PlxnD1 signaling antagonizes angiogenic potential then ECs with reduced Sema-PlxnD1 signaling levels should acquire an enhanced angiogenic state more often. To test this hypothesis, we used cell transplantation experiments to compare the properties of ECs from WT and *obd*/+ heterozygotes. These embryos have the same number of ECs within both the SeAs/DLAVs and the axial vasculature (Figure S2A) and identical SeA sprout abundance, positioning and patterning (Figures 2A and 2B). We determined the frequency at which donor ECs become tip cells in homogenotypic (WT-to-WT and *obd*/+-to-*obd*/+) and heterogenotypic (WT-to-*obd*/+ and *obd*/+-to-WT) chimeras. To ensure competition between donor and host ECs had occurred, we scored only mosaic SeAs harboring both donor and host ECs. All chimeras showed correctly patterned and positioned SeA sprouts (Figures 2C and 2D and data not shown) and both kinds of homogenotypic chimeras showed identical donor tip cell percentages (Figure 2E). In contrast, the donor tip cell percentage was significantly larger in *obd*/+-to-WT chimeras and smaller in WT-to-*obd*/+ chimeras (Figure 2E).

Hence, the angiogenic capacity and angiogenic positional fate of aortic ECs is not prespecified but is acquired and/or maintained competitively, agreeing with prior related observations (Jakobsson et al., 2010; Siekmann and Lawson, 2007). Indeed, within developing SeA sprouts angiogenic cell nuclei swap

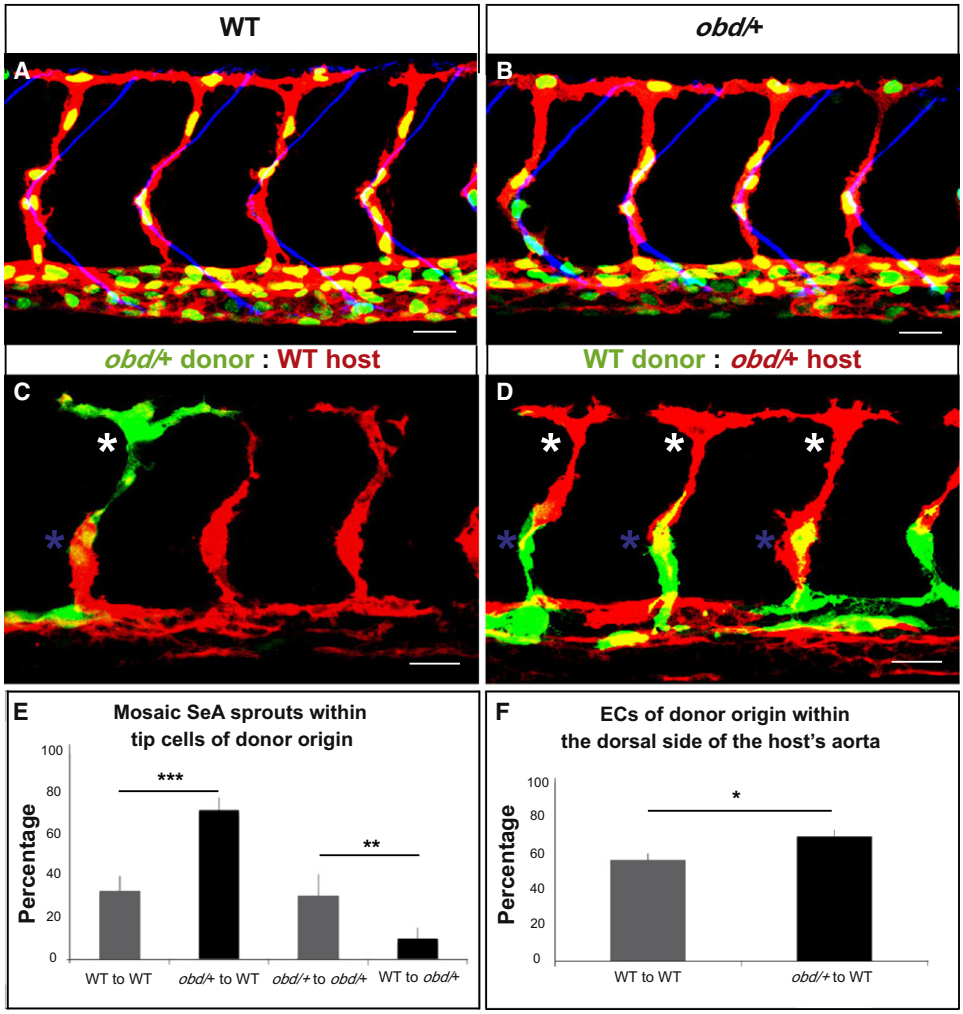

Figure 2. ECs with Less Sema-PlxnD1 Signaling Tend to Become Tip Cells and Occupy the Aorta's Dorsal Side

(A and B) 32 hpf vasculatures. EC nuclei (green), membranes (red). SBs, blue. (A) WT. (B) *obd*/+.

(C and D) 28 hpf vasculatures with ECs of donor (green) and host (red) origin. Asterisks: Tip cells (white), stalk cells (blue).

(E) Percentage of mosaic SeAs with tip cells of donor origin in homogenotypic (gray bars) and heterogenotypic (black bars) chimeras. n = 27 WT to *obd*/+, n = 18 *obd*/+ to *obd*/+, n = 38 *obd*/+ to WT, n = 34 WT to WT. Error bars represent SEM.

(F) Percentage of ECs of donor origin found within the dorsal side of the host's arterial tree in homogenotypic (gray bar) and heterogenotypic (black bar) chimeras.

(E and F) *$p < 0.05$, **$p < 0.01$, ***$p < 0.001$. Error bars represent SEM. n = 24 WT to WT, n = 32 *obd*/+ to WT.

(A–D) Anterior, left; dorsal, up. Scale bars represent 30 μm. See Figure S2 and Movie S1.

positions (Movie S1), suggesting that angiogenic cells within SeA sprouts can exchange places. Thus, the SeA tip cell population scored in Figures 2C–2E likely includes both the angiogenic cells that launched first from the aorta and kept their leading position and those that trailed the original tip cell but later overtook it. Prior studies suggest that migration speed is similar between cells with differential abilities to acquire/maintain a tip cell positional status (Jakobsson et al., 2010). Of note, both WT and *obd*/+ embryos form DLAVs at similar times, suggesting that their SeA sprouts grow with matching speeds. Thus, independently of its roles in guiding SeA sprouts (Gay et al., 2011) and limiting EC abundance (Figures S1A and S1B), Sema-PlxnD1 signaling antagonizes angiogenic responses.

Both the angiogenic potential of *obd* ECs and the angiogenic response of *obd*/+ ECs within WT hosts is enhanced, suggesting that Sema-PlxnD1 signaling acts prior to SeA sprouting. To investigate this possibility and determine its potential cellular basis, we made *obd*/+-to-WT and WT-to-WT chimeras and plotted the distribution of donor ECs within the host's trunk vasculature shortly after SeA sprouts launch (Figure S2B). Consistent with Sema-PlxnD1 signaling's dispensability for artery-vein differentiation (Torres-Vázquez et al., 2004), ECs from both donors contributed to the WT host's aorta equally. However, ECs from *obd*/+ donors were enriched along the aorta's dorsal side (Figure 2F) and *obd* ECs also preferentially occupy this locale in WT hosts (Figures S1C and S2C). In contrast, ECs with a cell autonomous impairment in downstream VEGF signaling that abrogates SeA angiogenesis localize to the aorta's ventral side within WT hosts (Covassin et al., 2009).

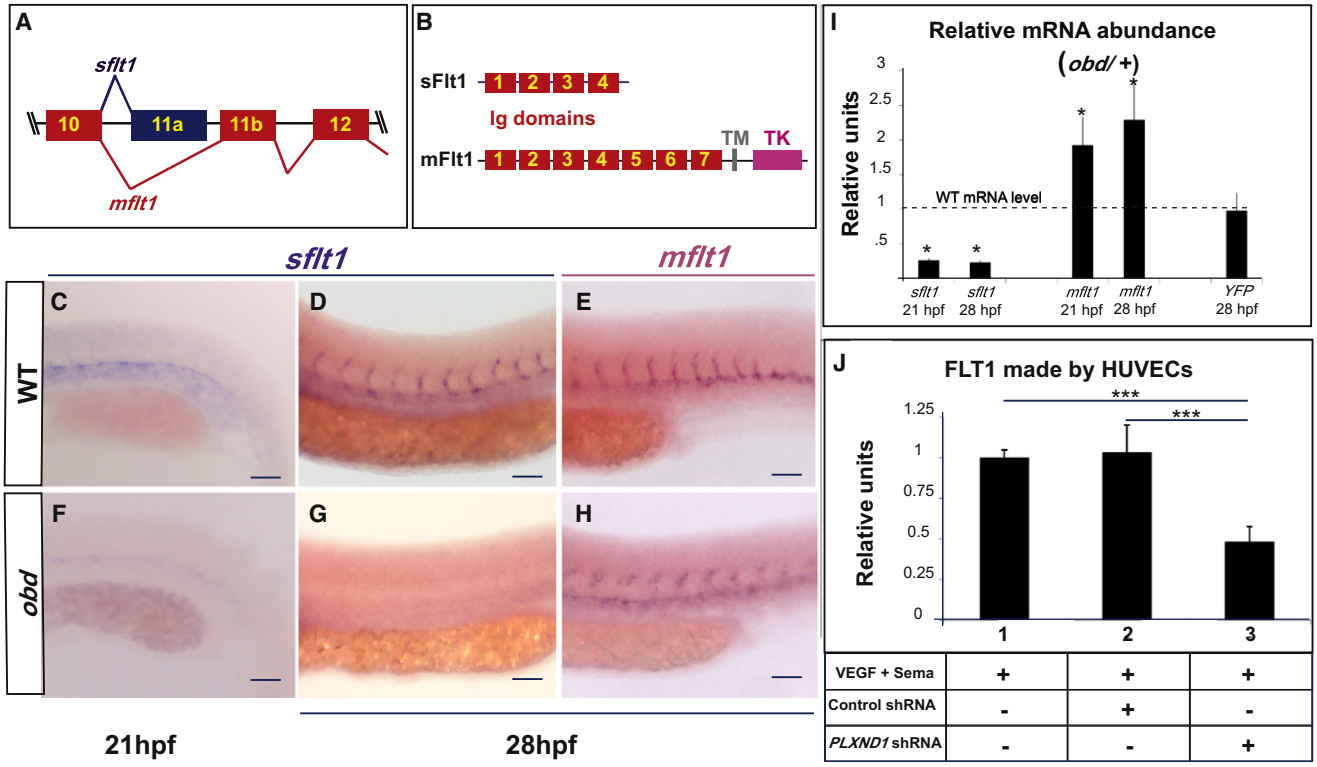

Figure 3. Sema-PlxnD1 Signaling Ensures the Proper Endothelial Abundance of *sflt1*

(A) Alternative *flt1* splicing yields *sflt1* and *mflt1* isoforms with unique eleventh exons. Exons, colored boxes. Introns, black lines.

(B) *sflt1* encodes a soluble 474 aa protein. *mflt1* encodes a 1,273 aa transmembrane protein. Protein domains: Immunoglobulin (Ig, red numbered boxes), transmembrane (TM, gray box), tyrosine kinase (TK, pink box).

(C–H) WISH, embryo trunks (genotypes and ages indicated) hybridized with *sflt1* (C and D, F and G) and *mflt1* (E and H) riboprobes (blue).

(I) qPCR measurements. Relative mRNA abundance of *sflt1*, *mflt1*, and *YFP* (from *Tg(flt1:YFP)*^{hu4624}/+) in 28 hpf *obd*/+ (WT level = 1, dashed line). Error bars represent coefficient of variance *$p < 0.05$.

(J) ELISA-based quantification of FLT1 prepared from cell extracts of HUVECs treated with both VEGF and Sema3E and the control or *PLXND1*-targeting shRNAs. Error bars represent SEM. ***$p < 0.001$.

(C–H) n = 10 embryos per riboprobe, stage and genotype. Pictures of representative examples of stainings observed (10/10 embryos in each category). Anterior, left; dorsal, up. Scale bars represent 50 μm. See Figure S3.

The aorta's dorsal side lies near the trunk's paracrine sources of proangiogenic VEGF (Lawson et al., 2002) and is the aortic angiogenic region (Ahn et al., 2000; Wilkinson et al., 2009). Importantly, *obd*/+ lacks aortic dorsoventral polarization defects: both WT and *obd* display similar expression of the aortic dorsal side marker *tbx20* (data not shown) and make red blood cells, which derive from the aorta's ventral side (data not shown) (Wilkinson et al., 2009).

Hence, Sema-PlxnD1 signaling plays a presprouting role in SeA angiogenesis and the cellular basis for the enhanced angiogenic response of *obd*/+ arterial ECs is, at least, related to their ability to localize early within the WT host's aortic roof, a property likely due to increased VEGF responsiveness. Notably, in heterogenotypic chimeras *plxnD1* genetic dosage affects aortic cell distribution (Figure 2F) and tip cell positional status (Figure 2E) similarly but to different extents. Hence, Sema-PlxnD1 signaling likely exerts other pre-and/or postsprouting effects, like modulating the angiogenic cell's launching schedule and/or positional persistence (Childs et al., 2002; Jakobsson et al., 2010; Kearney et al., 2004).

Sema-PlxnD1 Signaling Regulates the Abundance of the VEGF Antagonist Encoded by *soluble flt1* (*sflt1*)

To determine the molecular mechanism by which Sema-PlxnD1 signaling represses angiogenic potential we used WISH (Moens, 2008) to visualize the expression of twelve components and targets of the VEGF and Notch signaling cascades, including artery-vein differentiation markers (see Supplemental Information). Only *flt1* (*fms-related tyrosine kinase/vegf receptor 1*) (Bussmann et al., 2007; Krueger et al., 2011) expression was visibly affected in *obd*. We found that zebrafish *flt1* pre-mRNA is alternatively spliced into transcripts encoding products similar to the soluble (sFlt1) and membrane (mFlt1) mammalian proteins that function as high-affinity VEGF decoys or receptor/coreceptor tyrosine kinases, respectively (Figures 3A and 3B) (Krueger et al., 2011; Rahimi, 2006). Using isoform-specific riboprobes we detected *sflt1* and *mflt1* transcripts in the WT trunk arterial tree at 21–28 hpf (Figures 3C–3E) (Krueger et al., 2011). In contrast, *sflt1* was barely detectable in *obd* despite robust *mflt1* staining (Figures 3F–3H), suggesting that Sema-PlxnD1 signaling modulates the relative abundance of *flt1* isoforms

and/or *flt1* transcription. We used qPCR to compare the mRNA levels of WT and *obd*/+, which have identical EC abundances. We measured the transcript levels of both *flt1* isoforms and, separately, quantified the *YFP* mRNA output of the *flt1* transcriptional reporter *Tg(flt1:YFP)*^{hu4624} (Hogan et al., 2009a). *obd*/+ shows reduced *sflt1* (4-fold) and increased *mflt1* (3-fold) levels, but unaltered *flt1* transcriptional levels (Figure 3I), and, confocal imaging reveals no clear differences in *Tg(flt1:YFP)*^{hu4624} expression between WT and *obd* (Figure S3C). Finally, ELISA-based measurements of FLT1 from extracts of HUVECs (human umbilical vein ECs) exposed to both VEGF and the canonical PlxnD1 ligand Sema3E reveal that shRNA-mediated *PLXND1* knockdown reduces FLT1 without decreasing *FLT1* transcription (Figure 3J and Figure S3A; see also Figure S3B).

We conclude that Sema-PlxnD1 signaling acts via a posttranscriptional mechanism to ensure *sflt1*'s proper abundance within the trunk's arterial tree and propose this model: *sflt1* acts as a PlxnD1 effector that antagonizes proangiogenic VEGF signaling to limit angiogenic potential.

Partial Reduction of Both *plxnD1* and *sflt1* Enhances SeA Angiogenesis

If the proposed model is true, *plxnD1* and *sflt1* should interact genetically to limit SeA angiogenesis. We tested this prediction with a morpholino (MO) (Morcos, 2007) that inhibits the alternative splicing event that yields *sflt1* (Figures S4A and S4B). The *sflt1*-splice MO induces aberrantly branched SeA sprouts in WT and *obd*-like SeA sprout defects such as ectopic launching and aberrant branching in *obd*/+ heterozygotes (Figures 4B and 4D–4F and Figure S4C). Similarly, a pan-*flt1* splice-blocking MO (Rottbauer et al., 2005) targeting both *sflt1* and *mflt1* also induces *obd*-like SeA sprout defects in *obd*/+ (Figures S4E and S4F). Of note, a different pan-*flt1* MO also induces SeA misbranching in WT (Krueger et al., 2011). Both the expressivity and penetrance of these abnormalities is greater in *sflt1*-splice than in pan-*flt1* morphants, likely due to differences in knockdown efficiencies and the combined effects of inactivating *flt1* isoforms with opposite roles (Figure 4F and Figure S4F) (Rahimi, 2006). In contrast, WT and *obd*/+ treated with mismatched control *sflt1* splice-blocking MO or an *mflt1*-specific splice-blocking MO (Rottbauer et al., 2005) display normal SeA sprouts (Figures 4A and 4C; Figures S4D and S4F).

These observations agree with the vascular organization roles of *plxnD1* (Gay et al., 2011) and *flt1* (Krueger et al., 2011; Rahimi, 2006), the differential activities of *flt1* isoforms (Chappell et al., 2009; Kappas et al., 2008; Rahimi, 2006) and *sflt1*'s low level in *obd*/+ (Figure 3I). In short, *plxnD1* and *sflt1* (but not *mflt1*) interact genetically to modulate SeA sprout positioning, abundance, and patterning.

Endothelial Overexpression of *sflt1*, but not *mflt1*, Inhibits SeA Angiogenesis

Based on our model *sflt1,* like Sema-PlxnD1 signaling, should inhibit SeA angiogenesis. We tested this idea by overexpressing *sflt1* in an endothelial-specific fashion in both WT and *obd* via the GAL4/*UAS* system (Figure S4G). We found that *sflt1* overexpression suppresses SeA sprouting in WT and *obd* (Figures 4G–4H″). To determine if *mflt1* plays similar vascular roles during SeA angiogenesis, we analyzed the effects of *mflt1* overexpression. This treatment does not abrogate SeA sprouting but instead induces ectopic SeA sprouting at low frequency, consistent with the weak *mflt1* proangiogenic activity reported (Rahimi, 2006) (Figure S4H). Hence, within the trunk vasculature *sflt1* and *mflt1* play distinct roles, with *sflt1* acting as an inhibitor of SeA angiogenesis.

sflt1 Inhibits SeA Angiogenesis Cell Autonomously

Based on the model proposed, *sflt1*, like *plxnD1*, should act cell autonomously within the trunk's endothelium to suppress SeA angiogenesis. Given the lack of *flt1* mutants, we tested this prediction by combining *sflt1* overexpression with cell transplantation experiments using donors and hosts carrying different endothelial reporters to distinguish ECs according to their genotype. We made chimeras to determine if overexpressed *sflt1* inhibits SeA sprouting non-cell-autonomously. We transplanted *obd* cells into WT hosts with GAL4/*UAS* system-dependent mosaic endothelial coexpression of *sflt1* and fluorescent DsRed protein. We found that WT aortic ECs overexpressing *sflt1* (DsRed^{+}) fail to form SeA sprouts. However, neighboring *obd* donor and WT host aortic ECs without *sflt1* overexpression (DsRed^{-}) form SeA sprouts (Figures 4I and 4I′). In another experiment, we transplanted cells from *obd* donors with endothelial *sflt1* overexpression (DsRed^{+}) into WT hosts. While the *obd* aortic ECs with *sflt1* overexpression (DsRed^{+}) failed to form SeA sprouts, neighboring WT and donor *obd* ECs not overexpressing *sflt1* (DsRed^{-}) formed SeA sprouts (Figure S4I). Thus, *sflt1* acts cell autonomously despite the potential diffusible nature of its encoded product.

The Exacerbated SeA Angiogenesis of *obd* Requires VEGF Signaling

sflt1 encodes a VEGF signaling antagonist whose levels are greatly reduced in *obd* (Figure 3). To test if VEGF signaling is required for *obd*'s SeA angiogenesis, we chemically inhibited VEGF receptor activation with SU5416 (Herbert et al., 2009). SU5416, but not its vehicle (DMSO), abrogates SeA sprouting in WT and *obd* (Figures 5A, 5B, 5E, and 5F; see also Figure S5B). Similarly, MO-induced *vegfa* activity reduction also abrogates *obd*'s SeA angiogenesis (Childs et al., 2002). These findings indicate *obd*'s excessive SeA angiogenesis is VEGF dependent.

VEGF Signaling Is Enhanced in *obd*

The VEGF cascade splits downstream of the VEGF receptors into PLCG1 (*phospholipase C gamma1; plcg1*) and PI3K^{p110a} (phosphoinositide 3-kinase p110a isoform)-dependent proangiogenic branches (Figure 5M) (Covassin et al., 2009; Graupera et al., 2008). Our model predicts enhanced VEGF signaling in *obd*. Hence, angiogenic deficits due to impaired VEGF signaling, such as those of *plcg1* mutants, should be ameliorated in an *obd* background. *plcg1* lacks SeA sprouts (Figure 5C) (Covassin et al., 2009). However, *obd; plcg1* double mutants show too many and ectopic SeA sprouts (Figure 5D and Figure S5A) that express *flt4* and a trunk arterial tree with reduced *sflt1* abundance (data not shown). *obd; plcg1*'s SeA sprouting recovery requires VEGF signaling, since SU5416 suppresses it (Figure 5H). These observations support the notion that Sema-PlxnD1 cascade inactivation enhances VEGF signaling, suggesting

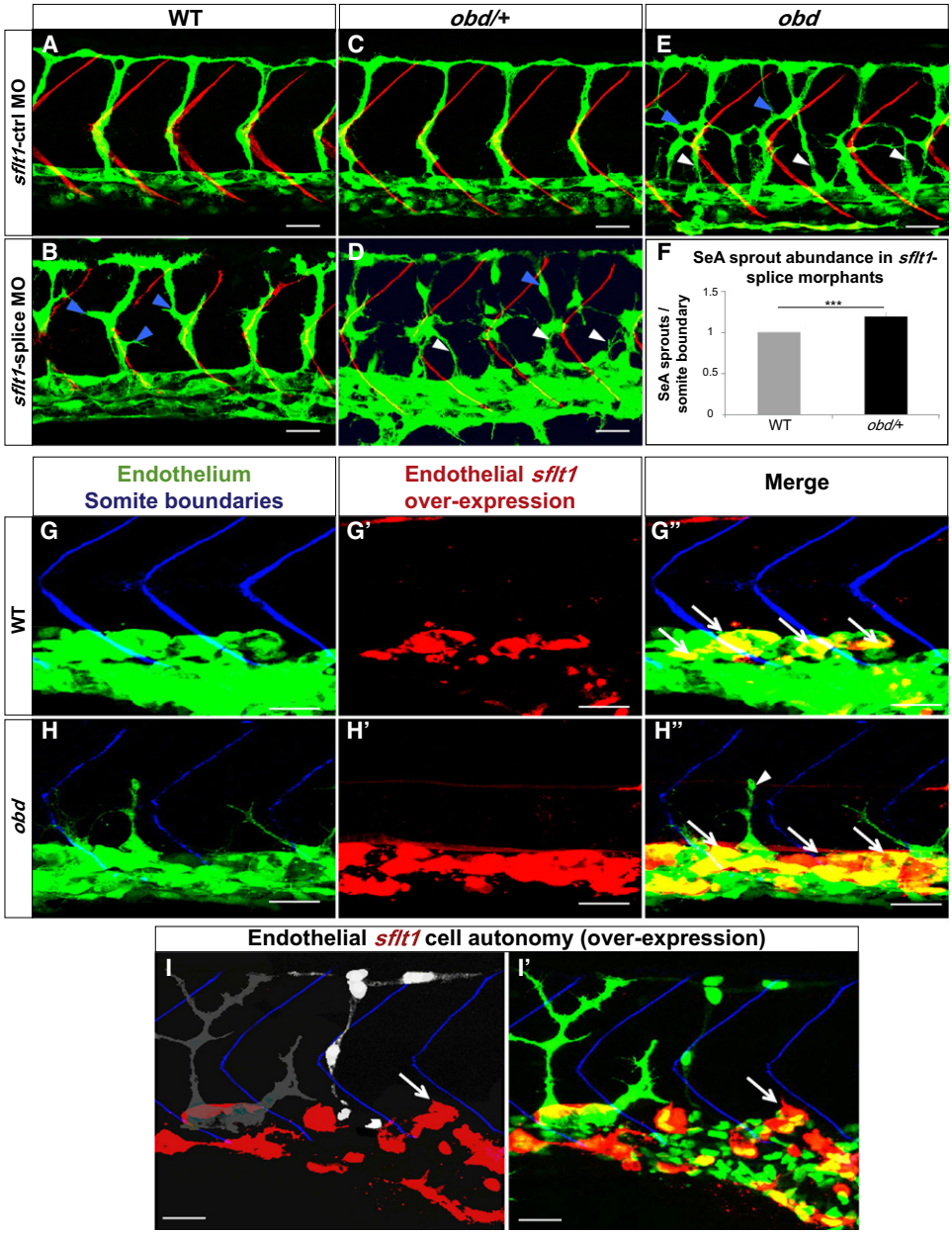

Figure 4. *plxnD1* and *sflt1* Interact Genetically, *sflt1* Limits SeA Angiogenesis Cell Autonomously

(A–I) Thirty-two hpf trunk vasculatures, green.

(A–E) SBs, red. White arrowheads, ectopic SeA sprouts. Blue arrowheads, ectopic SeA branching. (A, C, E) Embryos treated with 20 ng of *sflt1*-ctrl MO: WT (A), *obd*/+ (C), *obd* (E). Embryos treated with 20 ng of *sflt1*-splice MO: WT (B), *obd*/+ (D).

(F) 23 hpf SeA sprout abundance in WT (left, gray bar) and *obd*/+ (right, black bar) *sflt1*-splice morphants. n = 20 WT and n = 19 *obd*/+. Error bars represent SEM. ***$p < 0.001$.

(G–I′) SBs, blue. GAL4FF/*UAS*-mediated endothelial-specific *sflt1* overexpression, red. White arrows, missing SeA sprouts.

(G′–H″) Endothelial *sflt1* overexpression inhibits SeA sprouting. WT (G–G″). *obd* (H and H″), note lack of *sflt1* overexpression (red) in remaining SeA sprout (white arrowhead).

(I and I′) Mosaic vasculature with ECs from both *obd* donor and WT host. Endothelial-specific and mosaic *sflt1* and DsRed coexpression restricted to the WT endothelium (red, I and I′). *obd* ECs express cytosolically targeted EGFP (gray in I; green in I′). WT ECs express nuclear-targeted EGFP (white in I; green in I′). *obd* and WT ECs without *sflt1* overexpression (DsRed-) from SeA sprouts even next to *sflt1* overexpressing WT ECs ($DsRed^+$). WT ECs overexpressing *sflt1* ($DsRed^+$) fail to form SeA sprouts (white arrows, I and I′).

(G–H″) n = 30 embryos with overexpression per genotype, all showing suppression of SeA sprouting. Anterior, left; dorsal, up. Scale bars represent 30 μm. See Figure S4.

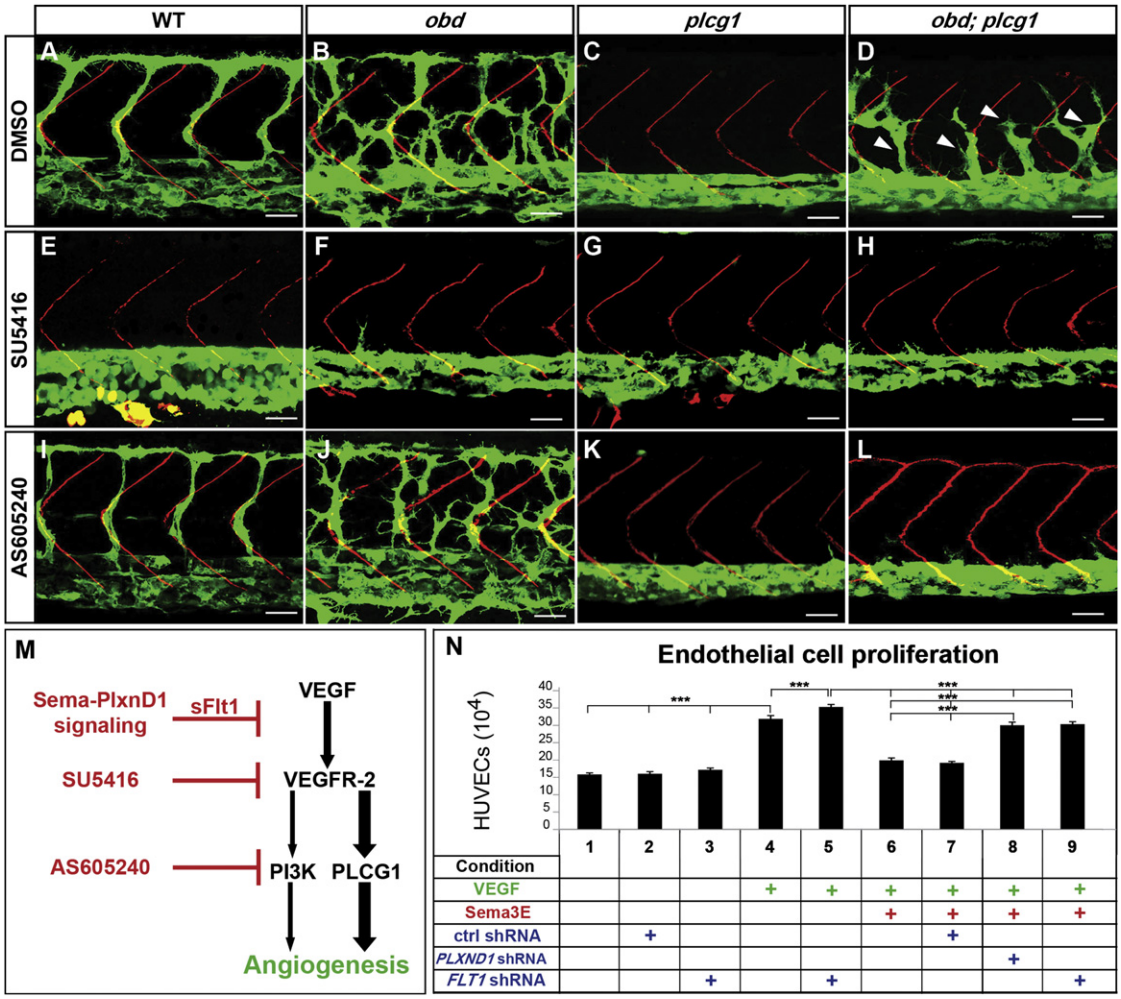

Figure 5. Enhanced VEGF Signaling Causes *obd*'s Exacerbated SeA Angiogenesis

(A–L) Thirty-two hpf trunk vasculatures. WT, *obd, plcg1* and *obd; plcg1* treated with DMSO, SU5416 (VEGFR inhibitor), or AS605240 (PI3K inhibitor). Genotypes, top; treatments, left. Endothelium, green. SBs, red. White arrowheads, recovered SeA sprouts in *obd; plcg1*. Anterior, left; dorsal, up. Scale bars represent 30 μm. n = 18 embryos per genotype and treatment. Pictures show representative phenotypes (18/18 embryos per category).

(M) Diagram of the VEGF cascade and steps inhibited by *sflt1* and drugs used in (E)–(L).

(N) HUVEC proliferation in response to combinations of VEGF, Sema3E, and shRNAs (control, *PLXND1* and *FLT1*). ***$p < 0.001$. Error bars represent SEM. See Figure S5.

that *obd; plcg1*'s angiogenic recovery is VEGF/PI3K^{p110a} dependent.

We tested this possibility via chemical inhibition of PI3K^{p110a} activity with AS605240 (Herbert et al., 2009). PLCG1 function removal has a greater impact on angiogenesis than PI3K^{p110a} inactivation (Covassin et al., 2009; Graupera et al., 2008). Accordingly, AS605240 neither abrogates SeA angiogenesis in WT or *obd* nor ameliorates *plcg1's* angiogenic deficit (Figures 5I–5K). However, AS605240 blocks SeA sprouting in *obd*; *plcg1* (Figure 5L), indicating that proangiogenic VEGF/PI3K^{p110a} activity is limiting under *plcg1*-deficient conditions. Hence, compared with *obd* (Figure 5B), *obd; plcg1* show fewer and stunted SeA sprouts that fail to form DLAVs (Figures 1D, 5D, and 6L).

We further confirmed the link between Sema-PlxnD1 and VEGF signaling by observing that hypomorphic mutants of *kdrl*, which encodes the duplicate canonical VEGF pathway component VEGF receptor 2/VEGFR-2/KDR, show SeA angiogenic deficits (Covassin et al., 2009; Habeck et al., 2002) that are ameliorated in an *obd* background (Figure S5C).

To selectively determine Sema-PlxnD1 signaling's effect on VEGF-induced cellular responses, we used a HUVEC proliferation assay (Figure 5N). We found that VEGF-induced HUVEC proliferation is reduced by Sema3E exposure and that the latter effect is abrogated via *PLXND1* (Bellon et al., 2010; Fukushima et al., 2011; Sakurai et al., 2010; Uesugi et al., 2009) or *FLT1* knockdown (Figure 5N and Figure S5D). Accordingly, VEGF/Sema3E-treated HUVECs make less FLT1 protein upon *PLXND1* knockdown (Figure 3J). Of note, *PLXND1* knockdown in HUVECs does not affect *FLT1* transcription (Figure S5D), paralleling our in vivo data indicating that Sema-PlxnD1 signaling modulates *sflt1* abundance posttranscriptionally (Figures 3C–3I and Figure S3C).

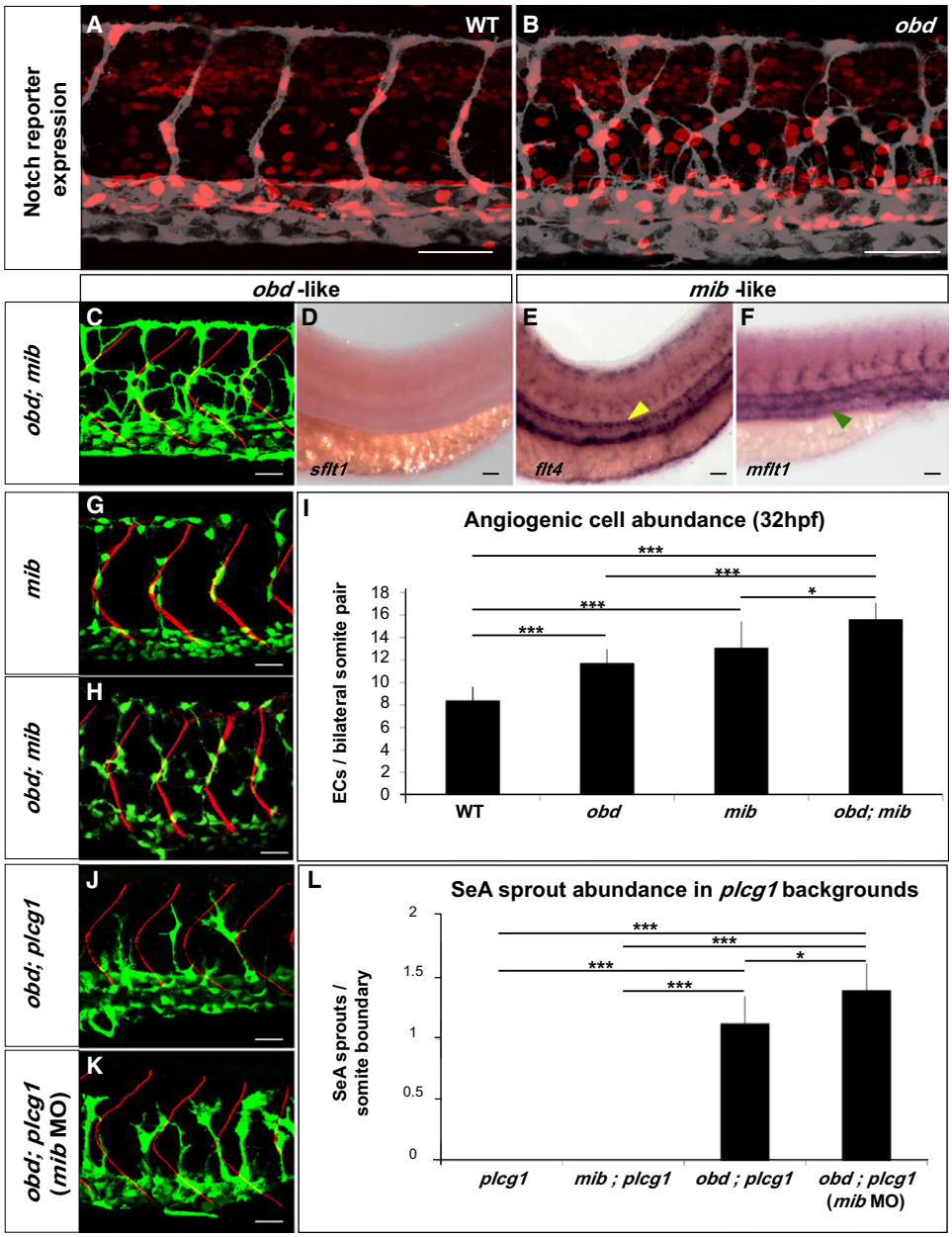

Figure 6. Notch Signaling Loss Does Not Phenocopy *obd*

(A and B) Expression of Notch's activity nuclear reporter *Tg(Tp1bglob:hmgb1-mCherry)*^{ih11} (red) in the endothelium (gray) of WT (A) and *obd* (B).

(C–F) *obd; mib*. (C) Endothelium, green. SBs, red. (D–F) WISH with *sflt1*, *flt4* and *mflt1* riboprobes, as indicated. Double mutant phenotypes classed as *obd*-like (C and D) or *mib*-like (E and F) based on the mutant they resemble most. Note lack of *sflt* (as in Figure 3G) and ectopic aortic *flt4* (yellow arrowhead; as in Figure S6A) and venous *mflt1* stainings (green arrowhead, as in Figure S6B).

(G–I) Angiogenic cell abundance within the trunk's arterial tree of WT, *obd*, *mib* (G) and *obd; mib* (H) in *Tg(fli1:nEGFP)*^{y7} embryos.

(G–H) EC nuclei, green. SBs, red.

(I) Quantification; n = 10 per genotype.

(J–L) SeA sprout abundance in *plcg*, *mib; plcg*, *obd*; *plcg* (J) and *obd; plcg* embryos injected with 10 ng of *mib* MO (*mib* MO) (K).

(J and K) Endothelium, green. SBs, red.

(L) n = 8, 7, 11 and 9 for *plcg*, *mib; plcg*, *obd; plcg* and *obd; plcg* (*mib* MO), respectively.

Scale bars represent 50 μm (A, B, and D–F), 30 μm (C, G, H, J, and K).

(I and L) *p < 0.05, ***p < 0.001. Error bars represent SEM.

(A–F, G, H, J, and K) Anterior, left; dorsal, up. Trunk images and quantifications: 32 hpf (A–C, G–L), 28 hpf (D–F). See Figure S6.

WISHs suggest that *sflt1*'s level in the trunk's arterial tree is independent of VEGF signaling: SU5416 treatment does not reduce *sflt1* abundance in WT nor increases it in *obd* (Figure S5B). Hence, *obd*'s decreased *sflt1* abundance is not secondary to enhanced VEGF signaling but rather at least one of its causes.

Sema-PlxnD1 and Notch Signaling Play Distinct and Additive Roles in SeA Angiogenesis

Notch signaling also negatively regulates SeA sprouting (Leslie et al., 2007; Siekmann and Lawson, 2007). We thus compared the arterial tree phenotypes induced by loss of Sema-PlxnD1 and Notch signaling. We found that unlike *obd*, SeA sprout abundance and distribution are normal in *mind bomb* (*mib*) mutants, in which a ubiquitin ligase required for Notch signaling is inactive (Figure S6A) (Itoh et al., 2003; Lawson et al., 2002; Lawson and Weinstein, 2002). Likewise, Notch pathway inactivation via mutations in either *mib* or *delta-like ligand 4* (*dll4*), which encodes a Notch ligand expressed in the trunk's arterial tree (Leslie et al., 2007), fails to ameliorate the angiogenic deficit of *plcg1* (Figure S6C).

Studies in other systems and/or vascular beds suggest Notch signaling promotes *flt1* expression (Bussmann et al., 2011; del Toro et al., 2010; Funahashi et al., 2010; Harrington et al., 2008; Jakobsson et al., 2010; Suchting et al., 2007), prompting us to ask if Notch signaling is reduced in *obd* or modulates the trunk's arterial tree expression of *flt1* and its isoforms.

WISH expression analysis of Notch pathway components (*deltac*, *dll4 notch5*, and *gridlock*) and targets (*gridlock, ephrin-B2a*, *flt4*, and *ephB4a*) fails to uncover evidence for reduced Notch signaling in *obd* (data not shown) and, endothelial expression of the transgenic Notch signaling reporters *Tg(Tp1bglob:hmgb1-mCherry)*^{jh11} and *Tg(Tp1bglob:eGFP)*^{um14} (Nicoli et al., 2010; Parsons et al., 2009) is similar in WT and *obd* (Figures 6A and 6B and data not shown), consistent with the notion that in *obd* Notch activity is preserved.

Visual comparison of the expression of the *flt1* transcriptional reporter (Hogan et al., 2009a, 2009b) in WT, *obd* mutants and *mib* morphants (Figure S3C) reveals no significant differences. *Tg(flt1:YFP)*^{hu4624} expression is also unaffected in *dll4* morphants (Geudens et al., 2010). Moreover, WISH of *mib* mutants reveals no visible reduction in *sflt1* or *mflt1* abundance but rather a mild enhancement in *sflt1* and *mflt1* venous expression (Figure S6B). Consistent with the role of Notch signaling in artery/vein differentiation and angiogenesis, *mib* displays ectopic aortic *flt4* expression (Figure S6A) (Lawson et al., 2001; Siekmann and Lawson, 2007).

To elucidate the relationship between Sema-PlxnD1 and Notch signaling, we analyzed the anatomical, cellular and molecular vascular phenotypes of *obd; mib* and the combined impact of inactivating both pathways on *plcg1's* SeA angiogenesis deficit. We found that within the arterial tree *obd; mib* show *obd*-like SeA anatomical organization and *sflt1* abundance (Figures 6C and 6D) but *mib*-like *flt4* and *mflt1* expression patterns (Figures 6E and 6F). This mix of *obd*- and *mib*-like phenotypes reveals that Sema-PlxnD1 and Notch signaling play distinct vascular roles.

Yet we also find additive genetic interactions between both pathways: *obd; mib* have greater angiogenic cell abundance than *obd* or *mib* (Figures 6G–6I) (Leslie et al., 2007; Siekmann and Lawson, 2007). Likewise, silencing *mib* (Itoh et al., 2003) in *obd; plcg* further increases their SeA sprout abundance (Figures 6J–6L). Hence, in this sensitized background Notch signaling seems to play a minor role as a negative regulator of SeA sprout abundance, consistent with the loss of SeA sprouting induced by overexpression of constitutive-active Notch forms, the complex interplay between VEGF and Notch signaling and the lateral inhibition role of the latter (Jakobsson et al., 2010; Roca and Adams, 2007; Siekmann and Lawson, 2007). While these additive interactions suggest that Sema-PlxnD1 and Notch signaling modulate common aspects of angiogenic development, these pathways clearly make qualitatively and quantitatively different contributions via molecularly distinct mechanisms. For example, while both pathways antagonize VEGF signaling, they modulate different pathway components, namely *sflt1* and *flt4*. Together, these observations indicate that Notch signaling remains active in *obd* and that Sema-PlxnD1 signaling functions without Notch activity (Figure 7A), underscoring the distinct roles of Sema-PlxnD1 and Notch signaling in SeA angiogenesis.

DISCUSSION

Our findings reveal that Sema-PlxnD1 signaling acts as a pre-sprouting repressor of angiogenic potential in the trunk's arterial tree. We posit that Sema-PlxnD1 signaling fulfills this role, at least in part, by maintaining *sflt1*'s proper endothelial abundance to antagonize proangiogenic VEGF signaling (Figure 7A). We propose that the somitic *sema3a* and endothelial *plxnD1* expression preceding SeA sprouting (Torres-Vázquez et al., 2004) (Figure 7B) reproducibly yield differences in Sema-PlxnD1 signaling level, and thus in *sflt1* abundance, along the aorta (Figure 7C). Although the proposed variation in WT *sflt1* aortic levels appears beyond the resolution of WISH, we find that ECs from *obd*/+ donors (which have less *sflt1*) are more likely to become SeA tip cells in WT hosts. Indeed, ECs with the lowest *Flt1* abundance make the angiogenic sprouts of WT and *Flt1*^{lacZ}/+ mouse retinas and ES cell-derived vessels (Chappell et al., 2009).

Our WISH and qPCR data indicate that loss or reduction of Sema-PlxnD1 signaling leads to low *sflt1* abundance within both the aorta and SeA sprouts. Accordingly, our cell transplants show that Sema-PlxnD1 signaling acts cell autonomously to spatially restrict the aorta's angiogenic capacity (Figure 7D) and limit the angiogenic responses of ECs within SeA sprouts (Figure 7E).

While sFlt1 can act non-cell autonomously (Ambati et al., 2006); (Chappell et al., 2009; Kearney et al., 2004), its effective range is context dependent (Goldman et al., 1998; James et al., 2009; Kendall and Thomas, 1993). In the trunk's arterial tree the antiangiogenic effects of endothelial-specific *sflt1* overexpression appear cell autonomous. sFlt1 forms VEGF-bridged inhibitory complexes with the proangiogenic receptors Flk1/Kdr (Bussmann et al., 2008; Kendall et al., 1996) and mFlt1 (Kendall and Thomas, 1993) and binds to the endothelial extracellular matrix, which abundantly surrounds the aorta (Jin et al., 2005; Orecchia et al., 2003). Both observations suggest how sFlt1's effective range might be limited within the aorta.

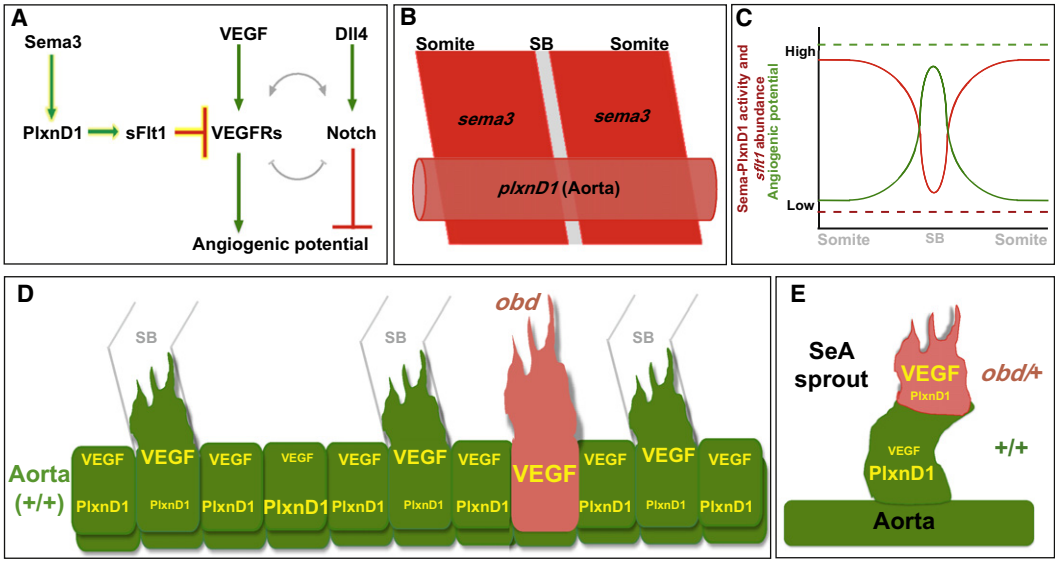

Figure 7. Model for How Sema3-PlxnD1 Signaling Restricts Angiogenic Potential along the Aorta and Limits Angiogenic Responses within SeA Sprouts

(A) Sema3-PlxnD1 signaling inhibits VEGF's proangiogenic effects via sFlt1, limiting angiogenic potential. The complex cross-regulation (gray lines) between the VEGF and Notch cascades implies Sema-PlxnD1 signaling impacts Notch activity indirectly.

(B) Somitic *sema3*s (dark red) and endothelial *plxnD1* (light red) expression precedes SeA sprouting (SB, gray) (Roos et al., 1999; Torres-Vázquez et al., 2004; Yee et al., 1999).

(C) WT aortic Sema-PlxnD1 signaling levels (red solid line) are highest in ECs next to the somites and lowest in ECs next to SBs, where angiogenic potential (green solid line) is highest. *obd* lacks Sema-PlxnD1 activity and thus *sflt1* abundance is greatly reduced (red dotted line), leading to uniformly enhanced angiogenic potential levels (green dotted line) that yield too many and ectopic SeA sprouts.

(D and E) VEGF signaling and angiogenic responses are cell autonomously enhanced by loss (*obd*) or decreased (*obd*/+) endothelial *plxnD1* activity, as exemplified by *obd* to WT (D) and *obd*/+ to WT (E) chimeras. VEGF signaling and PlxnD1 activity levels are indicated by font size.

Alternatively, sFlt1 might act in an intracrine manner, as proposed for mFlt1 (Lee et al., 2007b).

Our model implies that PlxnD1 signaling in response to paracrine Sema3 cues is key for the proper spatial modulation of angiogenic capacity within the aorta (Gay et al., 2011). Yet our findings do not rule out the potential involvement of autocrine Sema3 cues in PlxnD1 signaling prior to and/or during SeA sprouting (Banu et al., 2006; Kutschera et al., 2011; Lamont et al., 2009; Serini et al., 2003; Toyofuku et al., 2007). Similarly, endothelial Sema-PlxnD1 signaling could impact the proangiogenic activity of both paracrine and autocrine VEGFs (Childs et al., 2002; Covassin et al., 2006; da Silva et al., 2010; Hogan et al., 2009b; Lee et al., 2007a; Siekmann and Lawson, 2007; Tammela et al., 2008).

Our study reveals a key mechanistic link between Sema-PlxnD1 and VEGF signaling (Bellon et al., 2010; Fukushima et al., 2011; Sakurai et al., 2010; Uesugi et al., 2009). Consistent with defects in exon selection during *flt1*'s alternative splicing and/or alterations in the mRNA stability of *flt1* isoforms, impaired Sema-PlxnD1 signaling leads to contrasting posttranscriptional changes in *sflt1* and *mflt1* abundance. Sema-PlxnD1 signaling inactivates Ras-related proteins, antagonizes integrin and PI3K signaling and modulates cytoskeletal dynamics (Gay et al., 2011). How these PlxnD1-mediated events are connected to *flt1*'s posttranscriptional regulation and angiogenesis will be addressed by future studies.

Here we show that Sema-PlxnD1 and Notch signaling can function independently of each other and play largely distinct cellular and molecular roles. However, Sema-PlxnD1 activity antagonizes VEGF responsiveness and Notch and VEGF signaling are linked by complex feedback loops (Jakobsson et al., 2009; Lobov et al., 2007; Williams et al., 2006). Hence, we anticipate functional interactions between both pathways via the VEGF cascade. For example, it is likely that the enhanced VEGF signaling of ECs with less Sema-PlxnD1 activity allows them to exert a stronger Dll4/Notch-mediated lateral inhibition upon their neighbors, enabling the former to more often become angiogenic and/or, acquire and/or keep a tip cell positional status (Jakobsson et al., 2010; Leslie et al., 2007; Siekmann and Lawson, 2007). Remarkably, the combined loss of both Sema-PlxnD1 (*plxnD1*) and Notch signaling (*mib*) signaling does not enable every aortic EC to sprout, suggesting that other pathways and/or mechanisms limit the trunk's arterial tree angiogenic capacity.

Together with prior studies (Gay et al., 2011), our findings indicate that Sema-PlxnD1 signaling regulates distinct yet interconnected aspects of angiogenic development: the spatial allocation of angiogenic capabilities and the guidance of growing sprouts. It is likely that these roles, and their bases, are evolutionarily conserved (see Gay et al., 2011). Changes in *sflt1* abundance induce congenital vascular malformations (Acevedo and Cheresh, 2008), gestational hypertension (Rahimi, 2006) and are associated with cancer (Aref et al., 2005). Hence, mutations and polymorphisms that affect Sema-PlxnD1 signaling are likely modifiers of these diseases. Conversely, alterations in *sflt1* abundance and/or activity might impact Sema-PlxnD1 signaling dependent processes like cardiovascular and nervous system

development and both tumor angiogenesis and metastasis (Gay et al., 2011; Raab and Plate, 2007; Takahashi and Shibuya, 2005). Overall, the regulation of *sflt1* abundance via Sema-PlxnD1 signaling has broad biomedical implications beyond angiogenesis and provides a new way of understanding how Sema and VEGF signals might be integrated in many contexts.

EXPERIMENTAL PROCEDURES

Zebrafish

Embryos and adults kept and handled using standard laboratory conditions under New York University IACUC guidelines. Zebrafish stocks and genotyping methods/reagents described in the Supplemental Information.

Imaging

Live and fluorescently immunostained embryos imaged via confocal microscopy, whole mount RNA in situ hybridized embryos and drug treated animals imaged via transmitted light microscopy. All embryos mounted sideways. Details are in the Supplemental Information.

SeA Sprout Abundance and Position Quantification

Quantifications done using confocal images of immunofluorescently stained 23 hpf *Tg(fli:EGFP)^{y1}* embryos. SeA sprouts: individual EGFP-positive aortic dorsal projections that reach or surpass the horizontal myoseptum (HM; see Figure 1). SeA sprout positions: Correct (SeA base abuts directly the anterior side of neighboring somite boundary), ectopic (all other base locations). SeA sprouts were counted in four adjacent anterior trunk segments and averaged to yield a SeA sprouts/somite boundary ratio. Student's t test (homocedastic, two-tail distribution) was used to analyze the differences between the means of cell number data sets.

Endothelial Cell Abundance Quantification

We used 21, 23, and 32 hpf *Tg(fli1:nEGFP)^{y7}*; *Tg(flk1:ras-mCherry)^{s896}* and *Tg(flk1:EGFP-NLS)*; *Tg(flk1:ras-mCherry)^{s896}* immunofluorescently stained embryos to visualize EC nuclei and vascular anatomy. Confocal sections across the width of the anterior trunk were collected and 3D-projected with Imaris 6.2.1 software (Bitplane AG). EGFP-positive nuclei were marked (measurement point application) and counted. Since WT SeAs launch next to somite boundaries (SBs) but *obd* SeAs arise from these and other sites we divided the trunk vasculature into segments delimited by the posterior and anterior halves of consecutive bilateral somite pairs and counted EC nuclei within each segment. Based on their location, EC nuclei were assigned to the axial vessels (AxV; aorta and vein), the SeAs and/or DLAVs. AxV (rather than aortic- and venous-specific) EC abundance was scored since the aorta and vein are not fully distinct at 21 and 23 hpf (Herbert et al., 2009). We counted ECs in three consecutive trunk segments (located dorsal to the yolk extension) and averaged them to obtain ECs/bilateral somite pair ratios for each location. Student's t test (homocedastic, two-tail distribution) was used to analyze the differences between the means of EC number data sets. Note: not every EC whose nucleus is labeled by *Tg(fli1:nEGFP)^{y7}* (green) is marked by *Tg(flk1:ras-mCherry)^{s896}* (red) due to the latter's expression mosaicism (Figure S1A).

Cell Transplants

Cell transplants done with 3–4 hpf donor and host blastula-stage embryos as in (Carmany-Rampey and Moens, 2006). Thirty to 50 cells were aspirated from the donor's animal pole and placed into the host's lateral margin zone. Donors and hosts carried distinct endothelial-specific reporters to easily identify the source of ECs within chimeras.

plxnD1's *Cell Autonomy*

We used both WT and *obd* as *Tg(fli:EGFP)^{y1}* donors and as *Tg(flk1:ras-mcherry)^{s896}* hosts. 1 nl of a 5% solution of lineage tracer (dextran Alexa Fluor 647; Invitrogen) was injected into 1-cell-stage donors. Chimeras fixed at 32 hpf.

Quantification of Mosaic SeA Sprouts with Tip Cells of Donor Origin

We used both WT and *obd*/+ as *Tg(fli:EGFP)^{y1}* donors and as *Tg(flk1:ras-mcherry)^{s896}* hosts. Chimeras fixed at 28 hpf.

Quantification of the Distribution of ECs of Donor Origin within the Trunk Vasculature of Chimeras

We used both WT and *obd*/+ as *Tg(flk1:EGFP-NLS)* donors. *Tg(flk1:ras-mcherry)^{s896}* used as hosts. Chimeras fixed at 21–23 hpf. Embryos with ECs of donor origin within the trunk's vascular tree were selected. Confocal images of their whole trunk vasculature were taken and analyzed as described in Figure S2B.

sflt1's *Cell Autonomy*

We used *Tg(fli:EGFP)^{y1}* donors and *Tg(flk1:EGFP-NLS)* hosts. Endothelial-specific, *sflt1* mosaic overexpression in donors or hosts done using the *Tg(fliep:gal4ff)^{ubs4}* GAL4 driver line and the bidirectional *UAS* vector *pTol [DsRed::UAS::sFlt1]*.

Whole-Mount RNA In Situ Hybridization (WISH)

WISH performed as in (Moens, 2008). The list of analyzed genes and riboprobe synthesis protocols are in the Supplemental Experimental Procedures.

Morpholino Oligo (MO) Injection

MOs (Gene Tools, LLC) were injected into 1-cell-stage *Tg(fli1:EGFP)^{y1}* embryos as in (Morcos, 2007). MO sequences and validation methods are in the Supplemental Experimental Procedures.

Drug Treatments

Embryos were dechorionated before treatment. Treatments began at 16 (Figures 5A–5L) or 20 hpf (Figure S5B; to prevent the dramatic aortic size reduction induced by earlier treatments). Control embryos were treated with 0.025% dimethyl sulfoxide (DMSO; Sigma) in water. Inhibitor-treated embryos were incubated in 0.25 μM AS605240 or 0.5 μM SU5416 (Sigma) aqueous solutions of 0.025% DMSO.

Quantitative Real-Time Polymerase Chain Reaction (qPCR)

Total mRNA (zebrafish embryos) and RNA (HUVECs) extraction and cDNA synthesis done as per Supplemental Experimental Procedures. qPCR DNA products amplified with Power SYBR Green 2X Master Mix (Applied Biosystems) as per manufacturer's instructions. Whole embryo qPCR products were quantified with a 7900HT Real-Time PCR System (Applied Biosystems). Relative *sflt1*, *mflt1*, and *YFP* mRNA levels normalized to *bactin2* transcript abundance. For shRNA control experiments, products were quantified with a PRISM 7900 (Applied Biosystems). Relative *PLXND1* and *FLT1* levels normalized to *glyceraldehyde-3-phosphate* (*GAPDH*) abundance. Primer sequences are in the Supplemental Experimental Procedures.

ACCESSION NUMBERS

The sequence of the sflt1 mRNA can be accessed at GenBank (accession number: HQ322130, released upon publication).

SUPPLEMENTAL INFORMATION

Supplemental Information includes six figures, Supplemental Experimental Procedures, and one movie and can be found with this article online at doi:10.1016/j.devcel.2011.06.033.

ACKNOWLEDGMENTS

We thank N.C. Chi, C-B. Chien, S. Childs, A. Chitnis, S.L. Johnson, K. Kawakami, N.D. Lawson, M. Parsons, S. Schulte-Merker, D. Stainier, B.M. Weinstein, and the Zebrafish International Resource Center for reagents; G. Fishell, E.J.A. Hubbard, H. Knaut, J.F. Nance, D.B. Rifkin, K.L. Targoff, J.E. Treisman, S.R. Schwab, F. Ulrich, K.A. Yaniv, and D. Yelon for discussions; J. Zavadil (NYU Cancer Institute Genomics Facility), D. Dalfo, and J.-Y. Roignant for qPCR advice; and D. Chan for administrative help. We were supported by Werner Siemens-Foundation, Switzerland (A.K.), NICHD Training Program grant 5T32HD007520-05 (C.M.G.), and The David Himelberg Foundation and NHLBI (J.T.-V.). Author breakdown is as follows: T.Z., C.M.G., J.T.-V. (ideas, experiments, data analysis, fish lines, plasmids, writing); J.B., P.C.M. (experiments, data analysis); K.M.F. (experiments, fish lines, husbandry

support, writing); M.K.S. (ideas, cell culture experiments, data analysis, writing); L.H., A.K., H.-G.B., M.A. (*Tg(fliep:gal4ff)*^{ubs4} line); J.A.E. (ideas, data analysis). All authors commented on the manuscript.

Received: January 21, 2011
Revised: May 20, 2011
Accepted: June 27, 2011
Published online: July 28, 2011

REFERENCES

Acevedo, L.M., and Cheresh, D.A. (2008). Suppressing NFAT increases VEGF signaling in hemangiomas. Cancer Cell *14*, 429–430.

Ahn, D.G., Ruvinsky, I., Oates, A.C., Silver, L.M., and Ho, R.K. (2000). tbx20, a new vertebrate T-box gene expressed in the cranial motor neurons and developing cardiovascular structures in zebrafish. Mech. Dev. *95*, 253–258.

Ambati, B.K., Nozaki, M., Singh, N., Takeda, A., Jani, P.D., Suthar, T., Albuquerque, R.J., Richter, E., Sakurai, E., Newcomb, M.T., et al. (2006). Corneal avascularity is due to soluble VEGF receptor-1. Nature *443*, 993–997.

Aref, S., El Sherbiny, M., Goda, T., Fouda, M., Al Askalany, H., and Abdalla, D. (2005). Soluble VEGF/sFLt1 ratio is an independent predictor of AML patient out come. Hematology *10*, 131–134.

Banu, N., Teichman, J., Dunlap-Brown, M., Villegas, G., and Tufro, A. (2006). Semaphorin 3C regulates endothelial cell function by increasing integrin activity. FASEB J. *20*, 2150–2152.

Bellon, A., Luchino, J., Haigh, K., Rougon, G., Haigh, J., Chauvet, S., and Mann, F. (2010). VEGFR2 (KDR/Flk1) signaling mediates axon growth in response to semaphorin 3E in the developing brain. Neuron *66*, 205–219.

Bussmann, J., Bakkers, J., and Schulte-Merker, S. (2007). Early endocardial morphogenesis requires Scl/Tal1. PLoS Genet. *3*, e140.

Bussmann, J., Lawson, N., Zon, L., and Schulte-Merker, S.; Zebrafish Nomenclature Committee. (2008). Zebrafish VEGF receptors: a guideline to nomenclature. PLoS Genet. *4*, e1000064.

Bussmann, J., Wolfe, S.A., and Siekmann, A.F. (2011). Arterial-venous network formation during brain vascularization involves hemodynamic regulation of chemokine signaling. Development *138*, 1717–1726.

Carmany-Rampey, A., and Moens, C.B. (2006). Modern mosaic analysis in the zebrafish. Methods *39*, 228–238.

Carmeliet, P. (2005). Angiogenesis in life, disease and medicine. Nature *438*, 932–936.

Chappell, J.C., Taylor, S.M., Ferrara, N., and Bautch, V.L. (2009). Local guidance of emerging vessel sprouts requires soluble Flt-1. Dev. Cell *17*, 377–386.

Childs, S., Chen, J.N., Garrity, D.M., and Fishman, M.C. (2002). Patterning of angiogenesis in the zebrafish embryo. Development *129*, 973–982.

Covassin, L.D., Villefranc, J.A., Kacergis, M.C., Weinstein, B.M., and Lawson, N.D. (2006). Distinct genetic interactions between multiple Vegf receptors are required for development of different blood vessel types in zebrafish. Proc. Natl. Acad. Sci. USA *103*, 6554–6559.

Covassin, L.D., Siekmann, A.F., Kacergis, M.C., Laver, E., Moore, J.C., Villefranc, J.A., Weinstein, B.M., and Lawson, N.D. (2009). A genetic screen for vascular mutants in zebrafish reveals dynamic roles for Vegf/Plcg1 signaling during artery development. Dev. Biol. *329*, 212–226.

da Silva, R.G., Tavora, B., Robinson, S.D., Reynolds, L.E., Szekeres, C., Lamar, J., Batista, S., Kostourou, V., Germain, M.A., Reynolds, A.R., et al. (2010). Endothelial alpha3beta1-integrin represses pathological angiogenesis and sustains endothelial-VEGF. Am. J. Pathol. *177*, 1534–1548.

De Bock, K., De Smet, F., Leite De Oliveira, R., Anthonis, K., and Carmeliet, P. (2009). Endothelial oxygen sensors regulate tumor vessel abnormalization by instructing phalanx endothelial cells. J. Mol. Med. *87*, 561–569.

del Toro, R., Prahst, C., Mathivet, T., Siegfried, G., Kaminker, J.S., Larrivee, B., Breant, C., Duarte, A., Takakura, N., Fukamizu, A., et al. (2010). Identification and functional analysis of endothelial tip cell-enriched genes. Blood *116*, 4025–4033.

Fukushima, Y., Okada, M., Kataoka, H., Hirashima, M., Yoshida, Y., Mann, F., Gomi, F., Nishida, K., Nishikawa, S., and Uemura, A. (2011). Sema3E-PlexinD1 signaling selectively suppresses disoriented angiogenesis in ischemic retinopathy in mice. J. Clin. Invest. *121*, 1974–1985.

Funahashi, Y., Shawber, C.J., Vorontchikhina, M., Sharma, A., Outtz, H.H., and Kitajewski, J. (2010). Notch regulates the angiogenic response via induction of VEGFR-1. J Angiogenes Res *2*, 3.

Gay, C.M., Zygmunt, T., and Torres-Vázquez, J. (2011). Diverse functions for the semaphorin receptor PlexinD1 in development and disease. Dev. Biol. *349*, 1–19.

Geudens, I., Herpers, R., Hermans, K., Segura, I., Ruiz de Almodovar, C., Bussmann, J., De Smet, F., Vandevelde, W., Hogan, B.M., Siekmann, A., et al. (2010). Role of delta-like-4/Notch in the formation and wiring of the lymphatic network in zebrafish. Arterioscler. Thromb. Vasc. Biol. *30*, 1695–1702.

Goldman, C.K., Kendall, R.L., Cabrera, G., Soroceanu, L., Heike, Y., Gillespie, G.Y., Siegal, G.P., Mao, X., Bett, A.J., Huckle, W.R., et al. (1998). Paracrine expression of a native soluble vascular endothelial growth factor receptor inhibits tumor growth, metastasis, and mortality rate. Proc. Natl. Acad. Sci. USA *95*, 8795–8800.

Graupera, M., Guillermet-Guibert, J., Foukas, L.C., Phng, L.K., Cain, R.J., Salpekar, A., Pearce, W., Meek, S., Millan, J., Cutillas, P.R., et al. (2008). Angiogenesis selectively requires the p110alpha isoform of PI3K to control endothelial cell migration. Nature *453*, 662–666.

Habeck, H., Odenthal, J., Walderich, B., Maischein, H., and Schulte-Merker, S.; Tübingen 2000 screen consortium. (2002). Analysis of a zebrafish VEGF receptor mutant reveals specific disruption of angiogenesis. Curr. Biol. *12*, 1405–1412.

Harrington, L.S., Sainson, R.C., Williams, C.K., Taylor, J.M., Shi, W., Li, J.L., and Harris, A.L. (2008). Regulation of multiple angiogenic pathways by Dll4 and Notch in human umbilical vein endothelial cells. Microvasc. Res. *75*, 144–154.

Herbert, S.P., Huisken, J., Kim, T.N., Feldman, M.E., Houseman, B.T., Wang, R.A., Shokat, K.M., and Stainier, D.Y. (2009). Arterial-venous segregation by selective cell sprouting: an alternative mode of blood vessel formation. Science *326*, 294–298.

Hogan, B.M., Bos, F.L., Bussmann, J., Witte, M., Chi, N.C., Duckers, H.J., and Schulte-Merker, S. (2009a). Ccbe1 is required for embryonic lymphangiogenesis and venous sprouting. Nat. Genet. *41*, 396–398.

Hogan, B.M., Herpers, R., Witte, M., Heloterä, H., Alitalo, K., Duckers, H.J., and Schulte-Merker, S. (2009b). Vegfc/Flt4 signalling is suppressed by Dll4 in developing zebrafish intersegmental arteries. Development *136*, 4001–4009.

Isogai, S., Horiguchi, M., and Weinstein, B.M. (2001). The vascular anatomy of the developing zebrafish: an atlas of embryonic and early larval development. Dev. Biol. *230*, 278–301.

Isogai, S., Lawson, N.D., Torrealday, S., Horiguchi, M., and Weinstein, B.M. (2003). Angiogenic network formation in the developing vertebrate trunk. Development *130*, 5281–5290.

Itoh, M., Kim, C.H., Palardy, G., Oda, T., Jiang, Y.J., Maust, D., Yeo, S.Y., Lorick, K., Wright, G.J., Ariza-McNaughton, L., et al. (2003). Mind bomb is a ubiquitin ligase that is essential for efficient activation of Notch signaling by Delta. Dev. Cell *4*, 67–82.

Jakobsson, L., Bentley, K., and Gerhardt, H. (2009). VEGFRs and Notch: a dynamic collaboration in vascular patterning. Biochem. Soc. Trans. *37*, 1233–1236.

Jakobsson, L., Franco, C.A., Bentley, K., Collins, R.T., Ponsioen, B., Aspalter, I.M., Rosewell, I., Busse, M., Thurston, G., Medvinsky, A., et al. (2010). Endothelial cells dynamically compete for the tip cell position during angiogenic sprouting. Nat. Cell Biol. *12*, 943–953.

James, J.M., Gewolb, C., and Bautch, V.L. (2009). Neurovascular development uses VEGF-A signaling to regulate blood vessel ingression into the neural tube. Development *136*, 833–841.

Jin, S.W., Beis, D., Mitchell, T., Chen, J.N., and Stainier, D.Y. (2005). Cellular and molecular analyses of vascular tube and lumen formation in zebrafish. Development *132*, 5199–5209.

Kappas, N.C., Zeng, G., Chappell, J.C., Kearney, J.B., Hazarika, S., Kallianos, K.G., Patterson, C., Annex, B.H., and Bautch, V.L. (2008). The VEGF receptor Flt-1 spatially modulates Flk-1 signaling and blood vessel branching. J. Cell Biol. *181*, 847–858.

Kearney, J.B., Kappas, N.C., Ellerstrom, C., DiPaola, F.W., and Bautch, V.L. (2004). The VEGF receptor flt-1 (VEGFR-1) is a positive modulator of vascular sprout formation and branching morphogenesis. Blood *103*, 4527–4535.

Kendall, R.L., and Thomas, K.A. (1993). Inhibition of vascular endothelial cell growth factor activity by an endogenously encoded soluble receptor. Proc. Natl. Acad. Sci. USA *90*, 10705–10709.

Kendall, R.L., Wang, G., and Thomas, K.A. (1996). Identification of a natural soluble form of the vascular endothelial growth factor receptor, FLT-1, and its heterodimerization with KDR. Biochem. Biophys. Res. Commun. *226*, 324–328.

Krueger, J., Liu, D., Scholz, K., Zimmer, A., Shi, Y., Klein, C., Siekmann, A., Schulte-Merker, S., Cudmore, M., Ahmed, A., and le Noble, F. (2011). Flt1 acts as a negative regulator of tip cell formation and branching morphogenesis in the zebrafish embryo. Development *138*, 2111–2120.

Kutschera, S., Weber, H., Weick, A., De Smet, F., Genove, G., Takemoto, M., Prahst, C., Riedel, M., Mikelis, C., Baulande, S., et al. (2011). Differential endothelial transcriptomics identifies semaphorin 3G as a vascular class 3 semaphorin. Arterioscler. Thromb. Vasc. Biol. *31*, 151–159.

Lamont, R.E., Lamont, E.J., and Childs, S.J. (2009). Antagonistic interactions among Plexins regulate the timing of intersegmental vessel formation. Dev. Biol. *331*, 199–209.

Larson, J.D., Wadman, S.A., Chen, E., Kerley, L., Clark, K.J., Eide, M., Lippert, S., Nasevicius, A., Ekker, S.C., Hackett, P.B., and Essner, J.J. (2004). Expression of VE-cadherin in zebrafish embryos: a new tool to evaluate vascular development. Dev. Dyn. *231*, 204–213.

Lawson, N.D., and Weinstein, B.M. (2002). In vivo imaging of embryonic vascular development using transgenic zebrafish. Dev. Biol. *248*, 307–318.

Lawson, N.D., Scheer, N., Pham, V.N., Kim, C.H., Chitnis, A.B., Campos-Ortega, J.A., and Weinstein, B.M. (2001). Notch signaling is required for arterial-venous differentiation during embryonic vascular development. Development *128*, 3675–3683.

Lawson, N.D., Vogel, A.M., and Weinstein, B.M. (2002). sonic hedgehog and vascular endothelial growth factor act upstream of the Notch pathway during arterial endothelial differentiation. Dev. Cell *3*, 127–136.

Lee, S., Chen, T.T., Barber, C.L., Jordan, M.C., Murdock, J., Desai, S., Ferrara, N., Nagy, A., Roos, K.P., and Iruela-Arispe, M.L. (2007a). Autocrine VEGF signaling is required for vascular homeostasis. Cell *130*, 691–703.

Lee, T.H., Seng, S., Sekine, M., Hinton, C., Fu, Y., Avraham, H.K., and Avraham, S. (2007b). Vascular endothelial growth factor mediates intracrine survival in human breast carcinoma cells through internally expressed VEGFR1/FLT1. PLoS Med. *4*, e186.

Leslie, J.D., Ariza-McNaughton, L., Bermange, A.L., McAdow, R., Johnson, S.L., and Lewis, J. (2007). Endothelial signalling by the Notch ligand Delta-like 4 restricts angiogenesis. Development *134*, 839–844.

Lobov, I.B., Renard, R.A., Papadopoulos, N., Gale, N.W., Thurston, G., Yancopoulos, G.D., and Wiegand, S.J. (2007). Delta-like ligand 4 (Dll4) is induced by VEGF as a negative regulator of angiogenic sprouting. Proc. Natl. Acad. Sci. USA *104*, 3219–3224.

Moens, C. (2008). Whole mount RNA. In situ hybridization on zebrafish embryos: mounting. Cold Spring Harb Protoc. 10.1101/pdb.prot5038.

Morcos, P.A. (2007). Achieving targeted and quantifiable alteration of mRNA splicing with Morpholino oligos. Biochem. Biophys. Res. Commun. *358*, 521–527.

Nicoli, S., Standley, C., Walker, P., Hurlstone, A., Fogarty, K.E., and Lawson, N.D. (2010). MicroRNA-mediated integration of haemodynamics and Vegf signalling during angiogenesis. Nature *464*, 1196–1200.

Orecchia, A., Lacal, P.M., Schietroma, C., Morea, V., Zambruno, G., and Failla, C.M. (2003). Vascular endothelial growth factor receptor-1 is deposited in the extracellular matrix by endothelial cells and is a ligand for the alpha 5 beta 1 integrin. J. Cell Sci. *116*, 3479–3489.

Parsons, M.J., Pisharath, H., Yusuff, S., Moore, J.C., Siekmann, A.F., Lawson, N., and Leach, S.D. (2009). Notch-responsive cells initiate the secondary transition in larval zebrafish pancreas. Mech. Dev. *126*, 898–912.

Phng, L.K., and Gerhardt, H. (2009). Angiogenesis: a team effort coordinated by notch. Dev. Cell *16*, 196–208.

Phng, L.K., Potente, M., Leslie, J.D., Babbage, J., Nyqvist, D., Lobov, I., Ondr, J.K., Rao, S., Lang, R.A., Thurston, G., and Gerhardt, H. (2009). Nrarp coordinates endothelial Notch and Wnt signaling to control vessel density in angiogenesis. Dev. Cell *16*, 70–82.

Raab, S., and Plate, K.H. (2007). Different networks, common growth factors: shared growth factors and receptors of the vascular and the nervous system. Acta Neuropathol. *113*, 607–626.

Rahimi, N. (2006). VEGFR-1 and VEGFR-2: two non-identical twins with a unique physiognomy. Front. Biosci. *11*, 818–829.

Roca, C., and Adams, R.H. (2007). Regulation of vascular morphogenesis by Notch signaling. Genes Dev. *21*, 2511–2524.

Roos, M., Schachner, M., and Bernhardt, R.R. (1999). Zebrafish semaphorin Z1b inhibits growing motor axons in vivo. Mech. Dev. *87*, 103–117.

Rottbauer, W., Just, S., Wessels, G., Trano, N., Most, P., Katus, H.A., and Fishman, M.C. (2005). VEGF-PLCgamma1 pathway controls cardiac contractility in the embryonic heart. Genes Dev. *19*, 1624–1634.

Sakurai, A., Gavard, J., Annas-Linhares, Y., Basile, J.R., Amornphimoltham, P., Palmby, T.R., Yagi, H., Zhang, F., Randazzo, P.A., Li, X., et al. (2010). Semaphorin 3E initiates antiangiogenic signaling through plexin D1 by regulating Arf6 and R-Ras. Mol. Cell. Biol. *30*, 3086–3098.

Serini, G., Valdembri, D., Zanivan, S., Morterra, G., Burkhardt, C., Caccavari, F., Zammataro, L., Primo, L., Tamagnone, L., Logan, M., et al. (2003). Class 3 semaphorins control vascular morphogenesis by inhibiting integrin function. Nature *424*, 391–397.

Siekmann, A.F., and Lawson, N.D. (2007). Notch signalling limits angiogenic cell behaviour in developing zebrafish arteries. Nature *445*, 781–784.

Siekmann, A.F., Covassin, L., and Lawson, N.D. (2008). Modulation of VEGF signalling output by the Notch pathway. Bioessays *30*, 303–313.

Suchting, S., Freitas, C., le Noble, F., Benedito, R., Bréant, C., Duarte, A., and Eichmann, A. (2007). The Notch ligand Delta-like 4 negatively regulates endothelial tip cell formation and vessel branching. Proc. Natl. Acad. Sci. USA *104*, 3225–3230.

Takahashi, H., and Shibuya, M. (2005). The vascular endothelial growth factor (VEGF)/VEGF receptor system and its role under physiological and pathological conditions. Clin. Sci. *109*, 227–241.

Tammela, T., Zarkada, G., Wallgard, E., Murtomäki, A., Suchting, S., Wirzenius, M., Waltari, M., Hellström, M., Schomber, T., Peltonen, R., et al. (2008). Blocking VEGFR-3 suppresses angiogenic sprouting and vascular network formation. Nature *454*, 656–660.

Torres-Vázquez, J., Gitler, A.D., Fraser, S.D., Berk, J.D., Van, N. Pham, Fishman, M.C., Childs, S., Epstein, J.A., Weinstein, B.M., and Weinstein, B.M. (2004). Semaphorin-plexin signaling guides patterning of the developing vasculature. Dev. Cell *7*, 117–123.

Toyofuku, T., Yabuki, M., Kamei, J., Kamei, M., Makino, N., Kumanogoh, A., and Hori, M. (2007). Semaphorin-4A, an activator for T-cell-mediated immunity, suppresses angiogenesis via Plexin-D1. EMBO J. *26*, 1373–1384.

Uesugi, K., Oinuma, I., Katoh, H., and Negishi, M. (2009). Different requirement for Rnd GTPases of R-Ras GAP activity of Plexin-C1 and Plexin-D1. J. Biol. Chem. *284*, 6743–6751.

Wilkinson, R.N., Pouget, C., Gering, M., Russell, A.J., Davies, S.G., Kimelman, D., and Patient, R. (2009). Hedgehog and Bmp polarize hematopoietic stem cell emergence in the zebrafish dorsal aorta. Dev. Cell *16*, 909–916.

Williams, C.K., Li, J.L., Murga, M., Harris, A.L., and Tosato, G. (2006). Up-regulation of the Notch ligand Delta-like 4 inhibits VEGF-induced endothelial cell function. Blood *107*, 931–939.

Yee, C.S., Chandrasekhar, A., Halloran, M.C., Shoji, W., Warren, J.T., and Kuwada, J.Y. (1999). Molecular cloning, expression, and activity of zebrafish semaphorin Z1a. Brain Res. Bull. *48*, 581–593.

Development 138, 4199-4205 (2011) doi:10.1242/dev.064261

The novel transmembrane protein Tmem2 is essential for coordination of myocardial and endocardial morphogenesis

Ronald Totong[1], Thomas Schell[1], Fabienne Lescroart[1], Lucile Ryckebüsch[2], Yi-Fan Lin[1,2], Tomasz Zygmunt[1], Lukas Herwig[3], Alice Krudewig[3], Dafna Gershoony[4], Heinz-Georg Belting[3], Markus Affolter[3], Jesús Torres-Vázquez[1] and Deborah Yelon[1,2,*]

SUMMARY

Coordination between adjacent tissues plays a crucial role during the morphogenesis of developing organs. In the embryonic heart, two tissues – the myocardium and the endocardium – are closely juxtaposed throughout their development. Myocardial and endocardial cells originate in neighboring regions of the lateral mesoderm, migrate medially in a synchronized fashion, collaborate to create concentric layers of the heart tube, and communicate during formation of the atrioventricular canal. Here, we identify a novel transmembrane protein, Tmem2, that has important functions during both myocardial and endocardial morphogenesis. We find that the zebrafish mutation *frozen ventricle* (*frv*) causes ectopic atrioventricular canal characteristics in the ventricular myocardium and endocardium, indicating a role of *frv* in the regional restriction of atrioventricular canal differentiation. Furthermore, in maternal-zygotic *frv* mutants, both myocardial and endocardial cells fail to move to the midline normally, indicating that *frv* facilitates cardiac fusion. Positional cloning reveals that the *frv* locus encodes Tmem2, a predicted type II single-pass transmembrane protein. Homologs of Tmem2 are present in all examined vertebrate genomes, but nothing is known about its molecular or cellular function in any context. By employing transgenes to drive tissue-specific expression of *tmem2*, we find that Tmem2 can function in the endocardium to repress atrioventricular differentiation within the ventricle. Additionally, Tmem2 can function in the myocardium to promote the medial movement of both myocardial and endocardial cells. Together, our data reveal that Tmem2 is an essential mediator of myocardium-endocardium coordination during cardiac morphogenesis.

KEY WORDS: Zebrafish, Heart development, Atrioventricular canal, Cardiac fusion

INTRODUCTION

The embryonic heart tube is initially a two-layered structure: the outer layer of muscular myocardium contracts to propel circulation and the inner layer of endothelial endocardium provides continuity with the rest of the vasculature. Myocardial and endocardial cells originate in neighboring regions of the lateral mesoderm (Schoenebeck et al., 2007). During the process of cardiac fusion, both cell types migrate medially in a synchronized fashion and merge at the midline to assemble the heart tube (Bussmann et al., 2007; Holtzman et al., 2007; Moreno-Rodriguez et al., 2006). At later stages, cardiac maturation involves remodeling of both juxtaposed layers during valve formation and trabeculation (Armstrong and Bischoff, 2004; Hinton and Yutzey, 2010; Sedmera et al., 2000). Despite the continual proximity of the myocardium and endocardium, little is known about the mechanisms that coordinate their development.

The coordination of myocardial and endocardial development has been particularly well established in the context of atrioventricular canal (AVC) formation. Both the myocardium and endocardium undergo specialized differentiation in order to create the characteristic morphology of the AVC and to establish the endocardial cushions that will remodel into the atrioventricular valve (Armstrong and Bischoff, 2004; Beis et al., 2005; Chi et al., 2008; Hinton and Yutzey, 2010). Several studies indicate that myocardium-endocardium communication regulates these spatially coincident events (Armstrong and Bischoff, 2004; Hinton and Yutzey, 2010). For example, chick explant experiments suggest that signal transduction between atrioventricular myocardium and atrioventricular endocardium induces endocardial cushion formation (Mjaatvedt et al., 1987). Although several signaling pathways have been implicated in promoting endocardial cushion development (Armstrong and Bischoff, 2004; Beis et al., 2005; Hinton and Yutzey, 2010), it is less clear which genes are responsible for attenuating these signals so as to spatially restrict atrioventricular differentiation.

Myocardium-endocardium coordination is also crucial during cardiac fusion. The synchronization of myocardial and endocardial migration suggests that both tissues respond to the same cues in the extracellular environment. Some cues may emanate from the endoderm: both myocardial and endocardial fusion are inhibited when endodermal specification or morphogenesis is disrupted (e.g. Holtzman et al., 2007; Kikuchi et al., 2001; Kupperman et al., 2000). Additionally, either diminished or excessive deposition of extracellular matrix (ECM) can hinder myocardial and endocardial movement (e.g. Arrington and Yost, 2009; Garavito-Aguilar et al., 2010; Trinh and Stainier, 2004). Furthermore, the myocardium and endocardium may impact the behavior of one another. Cardiomyocytes display aberrant migration patterns in the absence

[1]Developmental Genetics Program and Department of Cell Biology, Kimmel Center for Biology and Medicine, Skirball Institute of Biomolecular Medicine, New York University School of Medicine, New York, NY 10016, USA. [2]Division of Biological Sciences, University of California, San Diego, La Jolla, CA 92093, USA. [3]Biozentrum, University of Basel, CH-4056 Basel, Switzerland. [4]Department of Pharmacology, New York University School of Medicine, New York, NY 10016, USA.

*Author for correspondence (dyelon@ucsd.edu)

Accepted 18 July 2011

of endocardial cells, implying that myocardium-endocardium communication influences the direction of cell movement (Holtzman et al., 2007). However, the molecular basis for myocardium-endocardium interactions during cardiac fusion is not yet clear.

To elucidate the molecular mechanisms underlying myocardium-endocardium communication, we have investigated the zebrafish mutation *frozen ventricle* (*frv*). Zygotic *frv* mutants display ectopic AVC characteristics, and maternal-zygotic *frv* mutants exhibit defects in cardiac fusion. Positional cloning indicates that the *frv* locus encodes Tmem2, a previously uncharacterized transmembrane protein. Tissue-specific rescue experiments suggest that Tmem2 acts in the endocardium to spatially restrict atrioventricular differentiation, whereas during cardiac fusion Tmem2 acts in the myocardium to promote the medial movement of both myocardial and endocardial cells. Together, our studies illuminate crucial roles of a novel molecule, Tmem2, in regulating the coordination of myocardial and endocardial morphogenesis.

MATERIALS AND METHODS

Zebrafish

We discovered the recessive lethal mutation *frozen ventricle* (*frv*^{sk38}) through routine intercrosses in the Skirball zebrafish facility. To obtain maternal-zygotic *frv* embryos, we generated germline replacement chimeras through transplantation, as previously described (Ciruna et al., 2002). Donor embryos were generated by intercrossing *frv* heterozygotes, and wild-type host embryos were screened for germ cells derived from *frv*$^{-/-}$ donors. We raised 273 chimeric embryos and recovered eight fertile adult females. These females were bred to male *frv* heterozygotes to generate maternal-zygotic *frv* mutants.

In situ hybridization

We conducted in situ hybridization using previously reported probes for *myl7* (ZDB-GENE-991019-3), *notch1b* (ZDB-GENE-990415-183), *bmp4* (ZDB-GENE-980528-2059), *versican* (ZDB-GENE-011023-1), *tbx2b* (ZDB-GENE-990726-27) and *cdh5* (ZDB-GENE-040816-1). Mutant embryos were identified by PCR genotyping.

Immunofluorescence

We performed MF20/S46 whole-mount immunofluorescence as previously described (Alexander et al., 1998). To detect Dm-grasp, we used the monoclonal antibody zn-5 (ZIRC; 1:10), rabbit polyclonal anti-GFP (Invitrogen; 1:100), goat anti-mouse IgG Alexa 594 (Invitrogen; 1:100) and goat anti-rabbit IgG Alexa 488 (Invitrogen; 1:100). Embryos were fixed in 4% PFA at 4°C overnight and were cut coronally posterior to the common cardinal vein to facilitate antibody penetration. Staining was performed in PBS with 0.5% Triton X-100 and 1% DMSO. Confocal images were obtained using a Zeiss LSM510 microscope, and *z*-stacks were rendered in three dimensions and analyzed with Volocity software (Perkin Elmer).

Positional cloning of *frv*

Meiotic mapping demonstrated that the *frv* mutation is located on chromosome 5, between SSLP markers z61852 and z22523. Analysis of SNPs narrowed the interval to a region containing five candidate genes. Sequencing of the coding region of *tmem2* (GenBank HQ997922) revealed a nonsense mutation in *frv*.

mRNA and morpholino injection

Embryos were injected at the one-cell stage with 200-500 pg mRNA or 8-13.5 ng anti-*tmem2* morpholino (MO) (5′-AGCAGTCCAAGCATACC-ATTACTCC-3′; Gene Tools). Capped mRNA was synthesized from a pCS2 vector containing the *tmem2* or *tmem2-gfp* coding sequence. The MO blocks splicing between exon 4 and intron 4-5, which is predicted to result in a truncated protein that contains the first 404 amino acids of Tmem2 and 44 amino acids encoded by intronic sequence.

Transgenes

We used the Gateway system (Kwan et al., 2007; Villefranc et al., 2007) to create the transgenes *Tg(myl7:tmem2-gfp)*, *Tg(kdrl:gal4vp16)* and *Tg(uas:tmem2-gfp)*. We employed Tol2 transposase-mediated transgenesis for both transient transgene expression and generation of transgenic founders (Fisher et al., 2006). Additional transgenic lines used were *Tg(kdrl:GRCFP)* (Cross et al., 2003) and *Tg(fliep:gal4ff)*^{ubs4}, which drives endothelium-specific expression of the GAL4-VP16 derivative Gal4FF and is described elsewhere (Zygmunt et al., 2011).

RESULTS AND DISCUSSION

frv restricts atrioventricular differentiation to the atrioventricular canal

The zebrafish mutation *frozen ventricle* (*frv*) has a distinctive impact on cardiac morphology and function. At 48 hours post-fertilization (hpf), embryos homozygous for *frv* exhibited contractility and dysmorphic cardiac chambers, with poor demarcation of the AVC and an abnormal separation between the ventricular myocardium and endocardium (Fig. 1A-H). By 72 hpf, the *frv* mutant ventricle ceased to contract, although atrial function seemed unaffected, inspiring the use of *frozen ventricle* as the locus name.

Expression patterns of cardiac genes appeared normal during the initial steps of heart tube assembly in *frv* mutants (see Fig. S1 in the supplementary material). By contrast, defects in expression of the AVC markers *notch1b*, *bmp4*, *versican*, and *tbx2b* were evident in *frv* mutants by 48 hpf. In wild-type embryos, expression of each of these markers becomes restricted to the AVC (Hurlstone et al., 2003; Walsh and Stainier, 2001) (Fig. 1I-K, see Fig. S2A in the supplementary material). In *frv* mutants, none of these markers became properly restricted (Fig. 1L-N, see Fig. S2B in the supplementary material): *notch1b* expression was evident in the ventricular endocardium, *bmp4* expression was expanded into the ventricular myocardium, and *versican* and *tbx2b* expression expanded into both the ventricular and atrial myocardium. Additionally, *frv* mutants exhibited expanded localization of the adhesion molecule Dm-grasp. Dm-grasp is normally detectable in differentiated endocardial cells within the AVC, but not in the remainder of the endocardium (Beis et al., 2005) (Fig. 1O-Q). In *frv* mutants, Dm-grasp was found throughout the entire ventricular endocardium, as well as in the AVC endocardium (Fig. 1R-T). Thus, the presence of ectopic atrioventricular characteristics in the *frv* mutant ventricle indicates an important role for *frv* in the regional restriction of atrioventricular differentiation.

Positional cloning of *frv* reveals a novel transmembrane protein

To gain insight into the molecular mechanisms of *frv* function, we positionally cloned the gene encoded by the *frv* locus. Meiotic mapping of *frv* identified a 0.28 cM genetic interval, and the annotated zebrafish genome assembly indicated five candidate genes in this region (Fig. 2A). Examination of the coding sequence of one of these genes, *transmembrane protein 2* (*tmem2*), revealed a nonsense mutation in *frv* mutant genomic DNA that is predicted to truncate the Tmem2 protein (Fig. 2B). To test the hypothesis that loss of *tmem2* function is responsible for the *frv* mutant phenotype, we injected *tmem2* mRNA into *frv* mutant embryos and found that this can rescue the *frv* mutant defects in chamber morphology, ventricular contractility and Dm-grasp distribution (see Table S1 and Fig. S3G-I in the supplementary material). Injection of *tmem2* mRNA did not cause any detectable phenotype in wild-type embryos. Additionally, we found that injection of anti-*tmem2* morpholinos (MOs) into wild-type embryos could cause

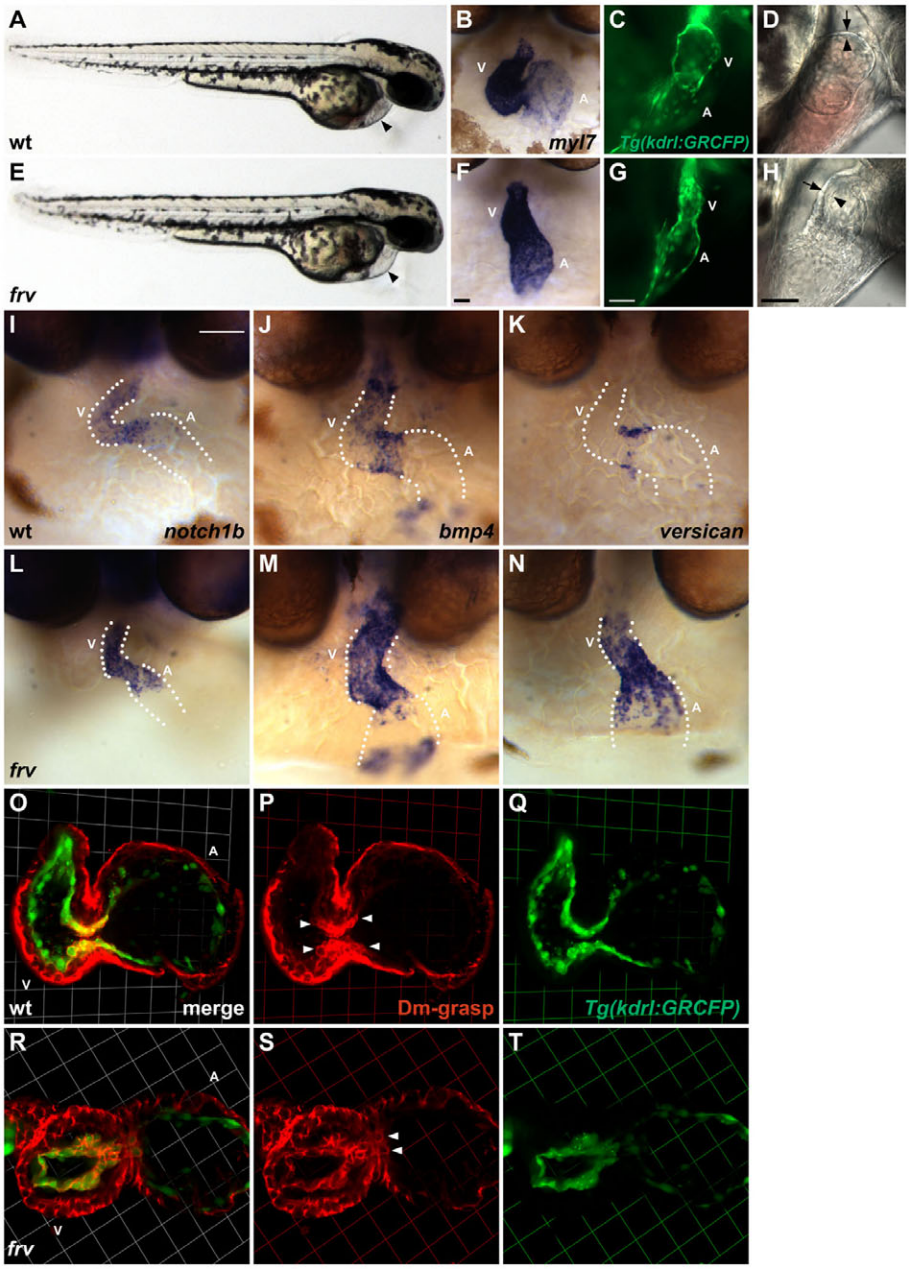

Fig. 1. The *frv* mutation disrupts myocardial and endocardial morphogenesis. (**A**,**E**) Lateral views of wild-type (wt) and *frv* mutant zebrafish embryos at 48 hpf reveal mild pericardial edema in *frv* mutants (arrowheads). Other than their cardiac defects, *frv* mutants appear morphologically normal. (**B**,**F**) Frontal views depict *myl7* expression in wild type (B) and in *frv* mutants (F) at 48 hpf. (**C**,**G**) Lateral views showing endocardial expression of *Tg(kdrl:GRCFP)* in wild type (C) and in *frv* mutants (G) at 52 hpf. (**D**,**H**) Lateral views at 52 hpf depict the close juxtaposition of the ventricular endocardium (arrowhead) and myocardium (arrow) in wild type (D) and their greater separation in *frv* mutants (H). (**I-N**) Frontal views depict expression of atrioventricular canal (AVC) markers in wild type (I-K) and in *frv* mutants (L-N) at 48 hpf. Dotted lines outline the chambers flanking the AVC. (**O-T**) Three-dimensional projections of selected confocal sections of wild-type (O-Q) and *frv* mutant (R-T) hearts expressing *Tg(kdrl:GRCFP)* (green) in the endocardium at 57 hpf. Immunofluorescence reveals Dm-grasp (red) throughout the myocardium and in the AVC endocardium (arrowheads). In *frv* mutants, Dm-grasp is also seen ectopically in the ventricular endocardium. Grids are 23 μm per segment. A, atrium; V, ventricle. Scale bars: 50 μm.

dysmorphic chambers, reduced ventricular contractility and ectopic Dm-grasp (see Fig. S3J-L in the supplementary material). Together, the linkage, nonsense mutation, rescue and MO phenocopy data indicate that disruption of the *tmem2* gene is the cause of the *frv* phenotype.

Tmem2 is predicted to be a type II transmembrane protein with a single transmembrane helix, a short cytoplasmic tail and a long extracellular portion (Fig. 2B). A BLAST local alignment search detected two identifiable domains – a G8 domain and a GG domain – within the extracellular sequence (Fig. 2B), consistent with previous bioinformatic analysis of the human TMEM2 homolog (see Fig. S4 in the supplementary material) (Guo et al., 2006; He et al., 2006). The structure of Tmem2 is highly conserved: Tmem2 homologs are detectable in a wide variety of vertebrate genomes, including *Homo sapiens*, *Mus musculus*, *Gallus gallus*, *Xenopus tropicalis* and *Takifugu rubripes*, all of which share at least 63% amino acid similarity with zebrafish Tmem2 (see Fig. S4 in the supplementary material). However, we were unable to identify Tmem2 homologs in *Caenorhabditis elegans* or *Drosophila melanogaster*. Despite its conservation among vertebrates, no prior studies have investigated Tmem2 function. Thus, our data provide novel evidence of an essential role for Tmem2.

Endocardial expression of *tmem2* represses inappropriate atrioventricular differentiation

The *frv* phenotype indicates that Tmem2 prevents atrioventricular differentiation in the ventricular endocardium, but it is not clear in which tissue Tmem2 acts to execute this role. Human and mouse Tmem2 homologs are expressed in a wide array of tissues (Scott et al., 2000). Consistent with this, we found broad expression of *tmem2* throughout the early zebrafish embryo, and we also detected a maternal supply of *tmem2* (see Fig. S5 in the supplementary material).

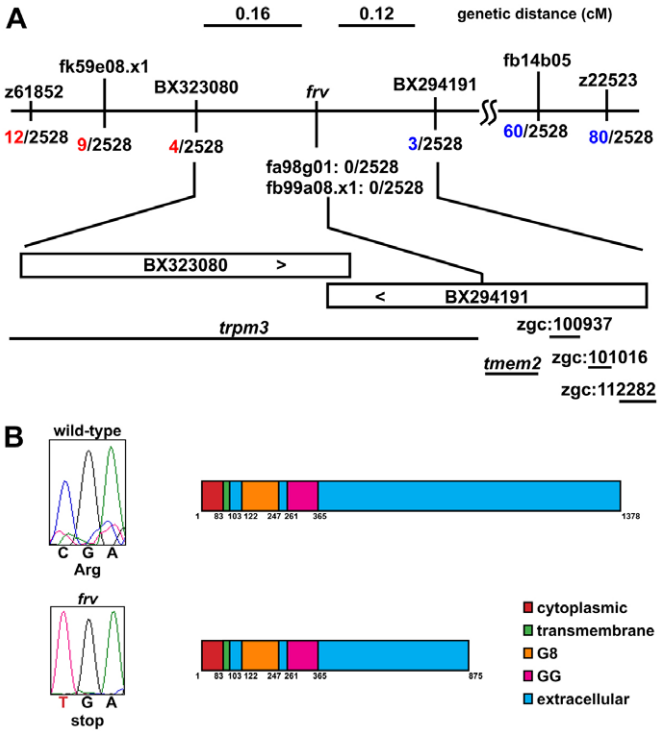

Fig. 2. The *frv* locus encodes the transmembrane protein Tmem2. (**A**) Meiotic and physical maps of the zebrafish genomic region containing *frv*. Meiotic mapping revealed a 0.28 cM interval for *frv* defined by SNPs on the ends of overlapping contigs (BX323080, BX294191). Fractions indicate the number of proximal (red) and distal (blue) recombination events out of 2528 meioses. Five candidate genes are shown as represented in Ensembl. (**B**) The predicted structures of Tmem2 protein in wild-type and *frv* mutant embryos. Amino acid positions defining the domains are indicated. Histograms demonstrate that *frv* mutants contain a C-to-T transition at position 2623 of the *tmem2* coding region. This mutation changes an Arg codon to a premature stop codon at amino acid position 875 and is predicted to result in a truncated Tmem2 protein.

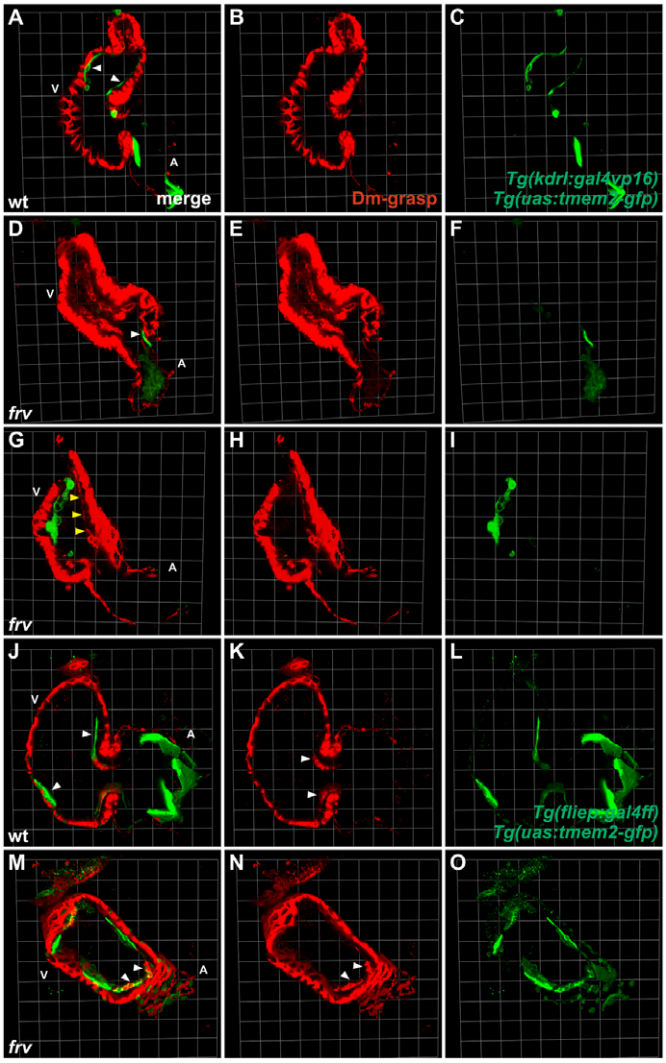

Fig. 3. Endocardial expression of *tmem2* rescues the *frv* mutant endocardium. Three-dimensional projections of selected confocal sections of wild-type (A-C,J-L) and *frv* mutant (D-I,M-O) zebrafish hearts expressing *tmem2-gfp* (green) in the endocardium at 57 hpf. Immunofluorescence indicates Dm-grasp localization (red). (A-I) Transient mosaic expression of *tmem2-gfp* is driven by injection of the transgenes *Tg(kdrl:gal4vp16)* and *Tg(uas:tmem2-gfp)*. (J-O) Mosaic expression of *tmem2-gfp* is driven by stably integrated *Tg(fliep:gal4ff)* and *Tg(uas:tmem2-gfp)* transgenes. (**A-C**,**J-L**) Expression of *tmem2-gfp* in ventricular endocardium (A,J, arrowheads) does not affect wild-type development. (**D-F**) Ectopic Dm-grasp remains in the *frv* mutant ventricle when *tmem2-gfp* is expressed only in atrial endocardium (D, arrowhead). (**G-I**) Mosaic expression of *tmem2-gfp* in the ventricular endocardium of *frv* mutants suppresses ectopic Dm-grasp localization. Ventricular endocardium that does not express *tmem2-gfp* retains ectopic Dm-grasp (G, arrowheads). (**M-O**) Broad *tmem2-gfp* expression in the ventricular endocardium rescues ectopic Dm-grasp expression in an *frv* mutant. AVC endocardium still expresses Dm-grasp as in wild type (compare M,N with K, arrowheads). Endocardial expression of *tmem2-gfp* does not improve ventricular contractility, but does reduce the abnormal gap between the myocardium and endocardium. Grids are 23 μm per segment.

Since the expression pattern of *tmem2* does not clarify its site of action, we designed tissue-specific transgenes to test whether expression of *tmem2* in the myocardium or endocardium could rescue the *frv* mutant phenotype. These transgenes drive expression of a fusion protein in which the C-terminus of Tmem2 is tagged with GFP. Tmem2-GFP appears functionally equivalent to Tmem2: injection of *tmem2-gfp* mRNA yielded results similar to injection of *tmem2* mRNA (see Table S1 in the supplementary material).

Expression of *tmem2* throughout the myocardium, driven by the stably integrated transgene *Tg(myl7:tmem2-gfp)* (see Fig. S6A-C in the supplementary material), was not sufficient to rescue the ectopic atrioventricular characteristics in *frv* mutants (see Fig. S7 in the supplementary material). Expression of *tmem2* in the endocardium was more challenging to attain. Since no endocardium-specific driver is available, we employed endothelial drivers (Jin et al., 2005; Villefranc et al., 2007). First, we used the transgenes *Tg(kdrl:gal4vp16)* and *Tg(uas:tmem2-gfp)* to generate transient mosaic expression within the endocardium (Fig. 3A-C). Expression of *tmem2* in atrial endocardium did not alter the *frv* mutant phenotype (Fig. 3D-F; n=4). By contrast, we observed loss of ectopic Dm-grasp in ventricular endocardial cells exhibiting mosaic *tmem2* expression (Fig. 3G-I; n=5). In an effort to generate a more thorough rescue of the *frv* endocardium, we next employed the stably integrated driver *Tg(fliep:gal4ff)* (Zygmunt et al., 2011). Unfortunately, stable integration of both *Tg(fliep:gal4ff)* and *Tg(uas:tmem2-gfp)* did not result in uniform expression of *tmem2* throughout the endocardium (Fig. 3J-L, see Fig. S6D in the

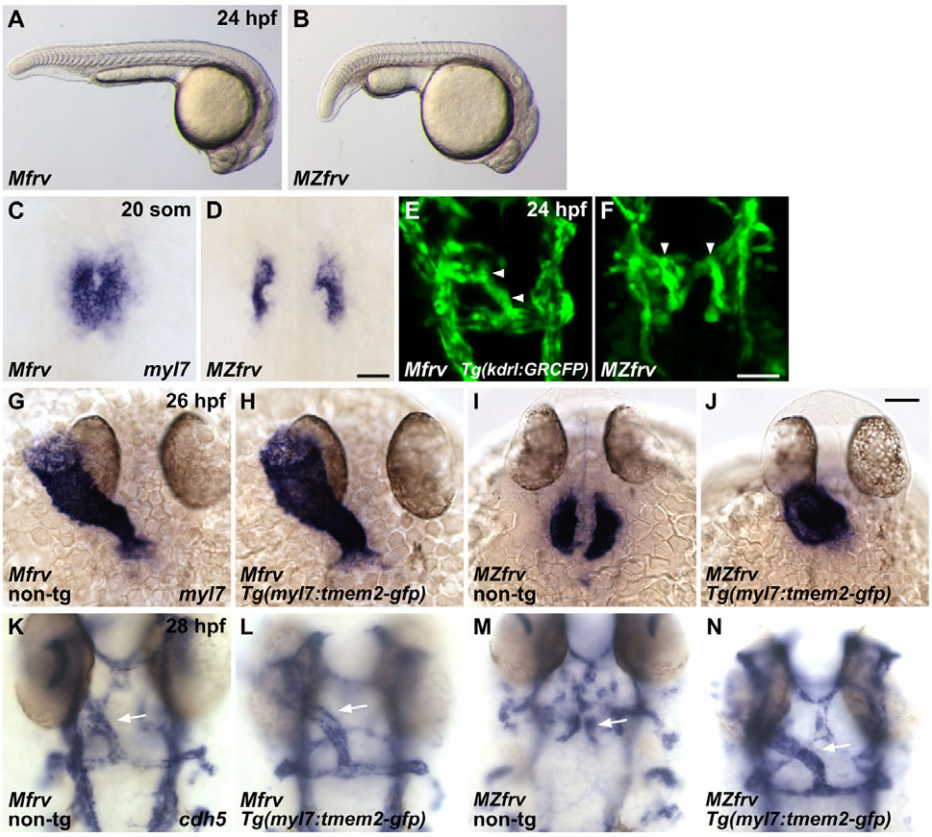

Fig. 4. Maternal-zygotic *frv* mutants exhibit myocardial and endocardial fusion defects that are rescued by myocardial *tmem2* expression. (**A**,**B**) Lateral views of zebrafish maternal (*Mfrv*) and maternal-zygotic (*MZfrv*) *frv* mutant siblings reveal body length and yolk extension defects in *MZfrv* embryos at 24 hpf. (**C**,**D**,**G-J**) Dorsal views depict *myl7* expression at 20 somites (som) and 26 hpf. (**E**,**F**) Dorsal views depict endocardial expression of *Tg(kdrl:GRCFP)* (arrowheads) at 24 hpf. (**K-N**) Dorsal views depict endocardial expression of *cdh5* (arrows) at 28 hpf In *Mfrv* embryos, expression of *Tg(myl7:tmem2-gfp)* has no effect on myocardial or endocardial morphogenesis (G,H,K,L), whereas in *MZfrv* embryos expression of *Tg(myl7:tmem2-gfp)* rescues both myocardial and endocardial fusion (I,J,M,N). Non-transgenic (non-tg) and transgenic siblings were distinguished by examination of fluorescence before fixation. Comparable results were obtained with two independent transgenic founders. Scale bars: 50 μm.

supplementary material), potentially owing to epigenetic silencing of *Tg(uas:tmem2-gfp)* (Goll et al., 2009). Accordingly, the effects of this transgene combination in *frv* mutants were comparable to the effects of mosaic expression of *Tg(kdrl:gal4vp16)* and *Tg(uas:tmem2-gfp)* (*n*=3); however, in one *frv* mutant, broad expression of *tmem2* in the ventricular endocardium eliminated the ectopic Dm-grasp (Fig. 3M-O). These data indicate that the activity of Tmem2 in the ventricular endocardium is sufficient to prevent the ectopic assumption of atrioventricular characteristics. Moreover, our data imply the existence of repressive mechanisms that restrain atrioventricular differentiation in the ventricle.

Tmem2 facilitates medial migration of both myocardium and endocardium

Given the contrast between the broad expression pattern of *tmem2* and the specific defects in *frv* mutants, we suspected that the maternal supply of *tmem2* partially compensates for the loss of zygotic *tmem2* function. To uncover additional roles of *tmem2*, we generated maternal-zygotic *frv* (*MZfrv*) mutant embryos via germline replacement (Ciruna et al., 2002). *MZfrv* mutants underwent gastrulation normally and began to display morphological defects during somitogenesis; by contrast, maternal *frv* (*Mfrv*) mutants appeared normal (Fig. 4A,B, see Fig. S8 in the supplementary material). Cardiac defects emerged in *MZfrv* mutants at an earlier stage than in zygotic *frv* mutants. Whereas cardiac fusion proceeded normally in *Mfrv* mutants, the medial migration of *MZfrv* cardiomyocytes was significantly hindered (Fig. 4C,D). However, the bilateral populations of cardiomyocytes were not permanently separated, and they eventually formed two linked sets of dysmorphic chambers (see Fig. S9 in the supplementary material). Additionally, *MZfrv* mutants displayed abnormal endocardial migration. Instead of meeting at the midline to form an endocardial tube, *MZfrv* endocardial cells were substantially delayed in their medial migration and remained bilaterally separate (Fig. 4E,F). Therefore, Tmem2 is crucial for facilitating cell movement during cardiac fusion.

Myocardial expression of *tmem2* promotes both myocardial and endocardial fusion

The failure of both myocardial and endocardial fusion in *MZfrv* mutants suggested the possibility that both phenotypes result from a primary defect in endoderm formation. However, endodermal specification and morphogenesis appeared normal in *MZfrv* mutants (data not shown). We therefore hypothesized that Tmem2 functions in migrating cardiac cells. Using the stably integrated transgene *Tg(myl7:tmem2-gfp)*, we found that myocardial expression of *tmem2* could rescue myocardial migration in *MZfrv* mutants; although morphogenesis was still slightly delayed in rescued embryos, cardiac fusion was complete and heart tube extension was under way by 26 hpf (Fig. 4G-J, see Fig. S10A-D in the supplementary material; *n*=15). Remarkably, the positive effects of *Tg(myl7:tmem2-gfp)* expression extended to the endocardium. Myocardial expression of *tmem2* rescued endocardial migration in *MZfrv* mutants, such that the endocardial cells reached the midline and extended into a tube (Fig. 4K-N, see Fig. S10E-H in the supplementary material; *n*=12). These data demonstrate that Tmem2 activity in the myocardium is sufficient to facilitate both myocardial and endocardial fusion. Moreover, our data provide the first evidence for a myocardial factor that influences the migration of endocardial cells.

Tmem2 is essential for the coordination of myocardial and endocardial morphogenesis

Our studies provide the first demonstration that the previously unappreciated transmembrane protein Tmem2 has multiple important functions during development. Notably, Tmem2 is

essential for two crucial aspects of cardiac morphogenesis: the spatial restriction of atrioventricular differentiation during AVC formation and the medial migration of cardiac cells during cardiac fusion. In each context, we have identified one location where Tmem2 can function – in the endocardium during AVC formation and in the myocardium during cardiac fusion – although our results do not rule out additional sites for Tmem2 activity during these processes. Our data suggest intriguing mechanisms for the coordination of myocardial and endocardial morphogenesis by Tmem2, and it is attractive to speculate that Tmem2 might play similar roles during AVC differentiation and cardiac fusion.

The transmembrane localization of Tmem2 evokes the hypothesis that it could facilitate myocardium-endocardium signaling. Perhaps certain signals repress atrioventricular differentiation in the ventricle, and Tmem2 plays a permissive role in facilitating signal reception by the endocardium. Similarly, Tmem2 could act to limit the activity of inductive signals that specify AVC endocardium; for example, the similarities between *frv* mutants and *apc* mutants suggest a possible role of Tmem2 in restricting Wnt signaling (Hurlstone et al., 2003; Verhoeven et al., 2011). During cardiac fusion, Tmem2 might facilitate the transduction of an unknown myocardial-to-endocardial motility cue; however, this scenario seems unlikely because the endocardium can move to the midline in *hand2* mutants, which possess very few cardiomyocytes (Garavito-Aguilar et al., 2010). Alternatively, rather than influencing specific signaling pathways, Tmem2 might impact myocardial and endocardial morphogenesis by modulating the extracellular environment. Perhaps Tmem2 influences ECM organization between the endocardium and myocardium in a manner that normally insulates the ventricular endocardium from myocardial signals that induce atrioventricular differentiation. Likewise, since specific parameters of ECM composition are known to be fundamental for cardiac fusion (Arrington and Yost, 2009; Garavito-Aguilar et al., 2010; Trinh and Stainier, 2004), Tmem2 could play a permissive role in ensuring the appropriate ECM organization to facilitate both myocardial and endocardial movement. Whatever the molecular role of Tmem2, its activity, as described here, broadens our comprehension of the mechanisms that underlie the coordination of myocardial and endocardial development. Elucidating the biochemical basis for Tmem2 function will further advance our understanding of the roles of this novel developmental regulator.

Note added in proof

An accompanying paper (Smith et al., 2011) characterizes the phenotype caused by zebrafish mutations referred to as *wickham* (*wkm*) and reports that the *wkm* locus encodes *tmem2*. Complementation tests performed by breeding *frv* heterozygotes to *wkm* heterozygotes have demonstrated that the two mutant alleles fail to complement each other: summarizing the results of five independent clutches, 27.7% (49/177) of the progeny display a phenotype indistinguishable from that of zygotic *frv* mutants. These data further reinforce the conclusion that the *frv* and *wkm* mutations disrupt the same gene: *tmem2*.

Acknowledgements

We thank L. Pandolfo, K. McCrone, E. Reynolds and C. McDaniel for expert zebrafish care, and T. J. Cardozo, T. Evans, D. Fitch, A. Joyner, H. Knaut and members of the Yelon laboratory for constructive discussions.

Funding

Work in the Yelon laboratory is supported by grants from the National Institutes of Health, American Heart Association and March of Dimes. Deposited in PMC for release after 12 months.

Competing interests statement

The authors declare no competing financial interests.

Supplementary material

Supplementary material for this article is available at http://dev.biologists.org/lookup/suppl/doi:10.1242/dev.064261/-/DC1

References

Alexander, J., Stainier, D. Y. and Yelon, D. (1998). Screening mosaic F1 females for mutations affecting zebrafish heart induction and patterning. *Dev. Genet.* **22**, 288-299.

Armstrong, E. J. and Bischoff, J. (2004). Heart valve development: endothelial cell signaling and differentiation. *Circ. Res.* **95**, 459-470.

Arrington, C. B. and Yost, H. J. (2009). Extra-embryonic syndecan 2 regulates organ primordia migration and fibrillogenesis throughout the zebrafish embryo. *Development* **136**, 3143-3152.

Beis, D., Bartman, T., Jin, S. W., Scott, I. C., D'Amico, L. A., Ober, E. A., Verkade, H., Frantsve, J., Field, H. A., Wehman, A. et al. (2005). Genetic and cellular analyses of zebrafish atrioventricular cushion and valve development. *Development* **132**, 4193-4204.

Bussmann, J., Bakkers, J. and Schulte-Merker, S. (2007). Early endocardial morphogenesis requires Scl/Tal1. *PLoS Genet.* **3**, e140.

Chi, N. C., Shaw, R. M., De Val, S., Kang, G., Jan, L. Y., Black, B. L. and Stainier, D. Y. (2008). Foxn4 directly regulates tbx2b expression and atrioventricular canal formation. *Genes Dev.* **22**, 734-739.

Ciruna, B., Weidinger, G., Knaut, H., Thisse, B., Thisse, C., Raz, E. and Schier, A. (2002). Production of maternal-zygotic mutant zebrafish by germ-line replacement. *Proc. Natl. Acad. Sci. USA* **99**, 14919-14924.

Cross, L. M., Cook, M. A., Lin, S., Chen, J. N. and Rubinstein, A. L. (2003). Rapid analysis of angiogenesis drugs in a live fluorescent zebrafish assay. *Arterioscler. Thromb. Vasc. Biol.* **23**, 911-912.

Fisher, S., Grice, E. A., Vinton, R. M., Bessling, S. L., Urasaki, A., Kawakami, K. and McCallion, A. S. (2006). Evaluating the biological relevance of putative enhancers using Tol2 transposon-mediated transgenesis in zebrafish. *Nat. Protoc.* **1**, 1297-1305.

Garavito-Aguilar, Z. V., Riley, H. E. and Yelon, D. (2010). Hand2 ensures an appropriate environment for cardiac fusion by limiting fibronectin function. *Development* **137**, 3215-3220.

Goll, M. G., Anderson, R., Stainier, D. Y., Spradling, A. C. and Halpern, M. E. (2009). Transcriptional silencing and reactivation in transgenic zebrafish. *Genetics* **182**, 747-755.

Guo, J., Cheng, H., Zhao, S. and Yu, L. (2006). GG: a domain involved in phage LTF apparatus and implicated in human MEB and non-syndromic hearing loss diseases. *FEBS Lett.* **580**, 581-584.

He, Q. Y., Liu, X. H., Li, Q., Studholme, D. J., Li, X. W. and Liang, S. P. (2006). G8: a novel domain associated with polycystic kidney disease and non-syndromic hearing loss. *Bioinformatics* **22**, 2189-2191.

Hinton, R. B. and Yutzey, K. E. (2010). Heart valve structure and function in development and disease. *Annu. Rev. Physiol.* **73**, 29-46.

Holtzman, N. G., Schoenebeck, J. J., Tsai, H. J. and Yelon, D. (2007). Endocardium is necessary for cardiomyocyte movement during heart tube assembly. *Development* **134**, 2379-2386.

Hurlstone, A. F., Haramis, A. P., Wienholds, E., Begthel, H., Korving, J., Van Eeden, F., Cuppen, E., Zivkovic, D., Plasterk, R. H. and Clevers, H. (2003). The Wnt/beta-catenin pathway regulates cardiac valve formation. *Nature* **425**, 633-637.

Jin, S. W., Beis, D., Mitchell, T., Chen, J. N. and Stainier, D. Y. (2005). Cellular and molecular analyses of vascular tube and lumen formation in zebrafish. *Development* **132**, 5199-5209.

Kikuchi, Y., Agathon, A., Alexander, J., Thisse, C., Waldron, S., Yelon, D., Thisse, B. and Stainier, D. Y. (2001). casanova encodes a novel Sox-related protein necessary and sufficient for early endoderm formation in zebrafish. *Genes Dev.* **15**, 1493-1505.

Kupperman, E., An, S., Osborne, N., Waldron, S. and Stainier, D. Y. (2000). A sphingosine-1-phosphate receptor regulates cell migration during vertebrate heart development. *Nature* **406**, 192-195.

Kwan, K., Fujimoto, E., Grabher, C., Mangum, B., Hardy, M., Campbell, D., Parant, J., Yost, H., Kanki, J. and Chien, C. (2007). The Tol2kit: a multisite gateway-based construction kit for Tol2 transposon transgenesis constructs. *Dev. Dyn.* **236**, 3088-3099.

Mjaatvedt, C. H., Lepera, R. C. and Markwald, R. R. (1987). Myocardial specificity for initiating endothelial-mesenchymal cell transition in embryonic chick heart correlates with a particulate distribution of fibronectin. *Dev. Biol.* **119**, 59-67.

Moreno-Rodriguez, R. A., Krug, E. L., Reyes, L., Villavicencio, L., Mjaatvedt, C. H. and Markwald, R. R. (2006). Bidirectional fusion of the heart-forming fields in the developing chick embryo. *Dev. Dyn.* **235**, 191-202.

Schoenebeck, J. J., Keegan, B. R. and Yelon, D. (2007). Vessel and blood specification override cardiac potential in anterior mesoderm. *Dev. Cell* **13**, 254-267.

Scott, D. A., Drury, S., Sundstrom, R. A., Bishop, J., Swiderski, R. E., Carmi, R., Ramesh, A., Elbedour, K., Srikumari Srisailapathy, C. R., Keats, B. J. et al. (2000). Refining the DFNB7-DFNB11 deafness locus using intragenic polymorphisms in a novel gene, TMEM2. *Gene* **246**, 265-274.

Sedmera, D., Pexieder, T., Vuillemin, M., Thompson, R. P. and Anderson, R. H. (2000). Developmental patterning of the myocardium. *Anat. Rec.* **258**, 319-337.

Smith, K. A., Lagendijk, A. K., Courtney, A. D., Chen, H., Paterson, S., Hogan, B. M., Wicking, C. and Bakkers, J. (2011). Transmembrane protein 2 (Tmem2) is required to regionally restrict atrioventricular canal boundary and endocardial cushion development. *Development* **138**, 4193-4198.

Trinh, L. A. and Stainier, D. Y. (2004). Fibronectin regulates epithelial organization during myocardial migration in zebrafish. *Dev. Cell* **6**, 371-382.

Verhoeven, M. C., Haase, C., Christoffels, V. M., Weidinger, G. and Bakkers, J. (2011). Wnt signaling regulates atrioventricular canal formation upstream of BMP and Tbx2. *Birth Defects Res. A Clin. Mol. Teratol.* **91**, 435-440.

Villefranc, J. A., Amigo, J. and Lawson, N. D. (2007). Gateway compatible vectors for analysis of gene function in the zebrafish. *Dev. Dyn.* **236**, 3077-3087.

Walsh, E. C. and Stainier, D. Y. (2001). UDP-glucose dehydrogenase required for cardiac valve formation in zebrafish. *Science* **293**, 1670-1673.

Zygmunt, T., Gay, C. M., Blondelle, J., Singh, M. K., Flaherty, K. M., Means, P. C., Herwig, L., Krudewig, A., Belting, H.-G., Affolter, M. et al. (2011). Semaphorin-PlexinD1 signaling limits angiogenic potential via the VEGF decoy receptor sFlt1. *Dev. Cell* (in press).

Developmental Cell
Article

The Hypothalamic Neuropeptide Oxytocin Is Required for Formation of the Neurovascular Interface of the Pituitary

Amos Gutnick,[1] Janna Blechman,[1] Jan Kaslin,[2] Lukas Herwig,[3] Heinz-Georg Belting,[3] Markus Affolter,[3] Joshua L. Bonkowsky,[4,5] and Gil Levkowitz[1,*]
[1]Department of Molecular Cell Biology, Weizmann Institute of Science, P.O. Box 26, Rehovot 76100, Israel
[2]Australian Regenerative Medicine Institute, Monash University, Clayton, Victoria 3800, Australia
[3]Biozentrum der Universität Basel, CH-4056 Basel, Switzerland
[4]Department of Pediatrics
[5]Department of Neurobiology and Anatomy
University of Utah, Salt Lake City, UT 84132, USA
*Correspondence: gil.levkowitz@weizmann.ac.il
DOI 10.1016/j.devcel.2011.09.004

SUMMARY

The hypothalamo-neurohypophyseal system (HNS) is the neurovascular structure through which the hypothalamic neuropeptides oxytocin and arginine-vasopressin exit the brain into the bloodstream, where they go on to affect peripheral physiology. Here, we investigate the molecular cues that regulate the neurovascular contact between hypothalamic axons and neurohypophyseal capillaries of the zebrafish. We developed a transgenic system in which both hypothalamic axons and neurohypophyseal vasculature can be analyzed in vivo. We identified the cellular organization of the zebrafish HNS as well as the dynamic processes that contribute to formation of the HNS neurovascular interface. We show that formation of this interface is regulated during development by local release of oxytocin, which affects endothelial morphogenesis. This cell communication process is essential for the establishment of a tight axovasal interface between the neurons and blood vessels of the HNS. We present a unique example of axons affecting endothelial morphogenesis through secretion of a neuropeptide.

INTRODUCTION

The neuroendocrine system is composed of neurosecretory brain cells that transfer hormones into the bloodstream to influence the function of target cells throughout the body. The hypothalamo-neurohypophyseal system (HNS) is a major neuroendocrine conduit through which the brain controls peripheral physiology (Burbach et al., 2001). The anatomy and activities of the HNS are conserved in all vertebrates. Ramon Cajal was the first to provide a description of the nerve fibers that connect the hypothalamus with the posterior pituitary (Cajal, 1911). It has since been established that these hypothalamic neurons themselves secrete neurohormones directly into the blood circulation, a finding that arose from experiments in both fish and mammalian models (Bargmann, 1949; Harris, 1948b; Scharrer, 1928). The hypothalamic neuropeptides arginine-vasopressin (AVP) and oxytocin (OXT) are synthesized in massive magnocellular neurons in the hypothalamus, transported along axons all the way down to the neurohypophysis, where they are secreted (Brownstein et al., 1980). Within the neurohypophysis, AVP and OXT are released from axons of the supraopticohypophyseal tract into fenestrated capillaries, thus leaving the brain and entering the general circulation without disrupting the blood-brain barrier (Burbach et al., 2001).

In the general circulation, secreted AVP regulates water homeostasis by increasing water permeability of the collecting duct of the kidney, and oxytocin regulates labor and milk let down by causing the respective contraction of the smooth muscle of the uterus and of the myoepithelial cells of breast ducts (for review, see Burbach et al., 2001; Gimpl and Fahrenholz, 2001; Verbalis, 2007). These physiological activities are conserved: in teleost fish, the AVP-like neuropeptide (Avpl) (a.k.a. arginine-vasotocin) regulates water balance by affecting filtration in the kidney (Amer and Brown, 1995; Macfarlane and Maetz, 1974; Peter and Fryer, 1983) and oxytocin-like neuropeptide (Oxtl) (a.k.a. isotocin) regulates contraction of smooth muscles in the ovary and oviduct during parturition or oviposition of live bearing and egg laying fish (La Pointe, 1977; Peter and Fryer, 1983). Avpl and Oxtl also regulate blood pressure in the ventral aorta (Chan, 1977; Kulczykowska, 1998; Le Mevel et al., 1993; Peter and Fryer, 1983). The HNS is therefore a central point of interface between the hormonal, neuronal, and vascular systems common to all vertebrate species.

The neurohypophysis is an elaborate three-dimensional structure, which substantially complicates the interpretation of cellular interactions and dynamics based solely on tissue sections. Although the anatomical structures of the neurohypophyseal axons and blood vessels have been the focus of intense study for over a century (Bargmann, 1949; Fink and Smith, 1971; Harris, 1948a; Scharrer, 1928), little progress has been made in uncovering the molecular and cellular processes that underlie formation of the interface between hypothalamic axons and

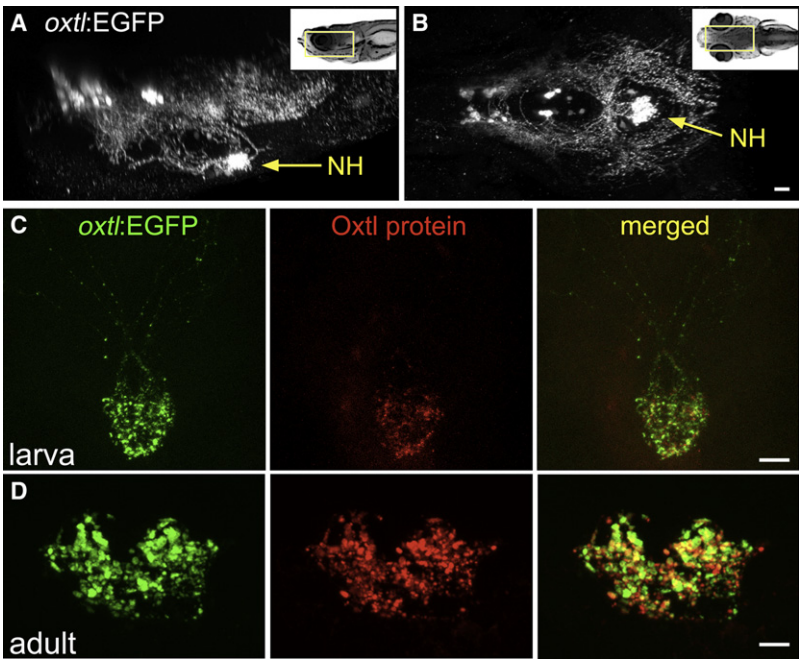

Figure 1. Oxytocinergic Reporter Transgene Tags HN Projections

(A and B) 3D reconstruction of the hypothalamic-neurohypophseal system of an optically sectioned 9-day-old zebrafish embryo carrying the *oxtl:*EGFP transgene (anterior to the left; A, lateral view; B, ventral view). Axonal projections to the neurohypophysis (NH) are highly visible in *oxtl:*EGFP transgenic animals due to extensive arborization of NH nerve termini.

(C and D) Immunohistochemical analysis of Oxytocin protein in *oxtl:*EGFP transgenic zebrafish showing colocalization of EGFP+ and Oxytocin+ nerve termini in the neurohypophysis of either 6-day-old larva (C, anterior up) or coronally sectioned adult (D); 14-day-old).

Scale bars, 20 μm. See also Figure S1 and Movie S1.

hypophyseal vasculature. Here, we present a unique transgenic approach in which both zebrafish oxytocinergic axonal termini and vascular endothelia cells within the neurohypophysis are labeled. We use this system to analyze the morphogenesis of the neurohypophyseal axonal trajectories and neuroendocrine vasculature in live zebrafish embryos and demonstrate that neurohypophyseal angiogenesis is regulated by the developing hypothalamo-neurohypophyseal nerve termini. Our results suggest that local secretion of oxytocin into the neurohypophysis is an intrinsic developmental event essential for the formation of the hypophyseal neurovascular connection.

RESULTS

Cellular Organization of the Zebrafish HNS

The optically transparent zebrafish embryo offers a unique tool to study the ontogenesis of the HNS in vivo without the need for surgical intervention, although the formation and structure of the zebrafish neurohypophysis is, to date, still poorly characterized. We recently identified the genomic regulatory region of the zebrafish *oxtl* gene and have generated a transgenic reporter line, *oxtl*:EGFP, in which zebrafish oxytocinergic cell bodies in the hypothalamus are labeled (Blechman et al., 2011). We first examined whether this line can be used to track axonal projections from the hypothalamus to the neurohypophysis. Three-dimensional reconstitution of optically-sectioned 9-day-old *oxtl*:EGFP larvae revealed extensive EGFP-positive axonal trajectories of oxytocinergic neurons throughout the nervous system (Figures 1A and 1B; see Movie S1 available online). In particular, we observed a prominent *oxtl*:EGFP+ tract originating from the two hemispheres of the neurosecretory preoptic areas (NPO) converging into the midline and terminating at the ventral part of the hypothalamus at the presumed location of the pituitary (Figure 1B). Immunostaining of the *oxtl*:EGFP with an anti-oxytocin antibody confirmed that these ventral hypothalamic axonal termini colocalize with oxytocinergic-positive vesicles of the presumed neurohypophysis of embryonic and adult brains (Figures 1C and 1D and Figure S1). To further validate this observation we crossed the *oxtl*:EGFP line with another transgenic line in which the adenohypophyseal pituitary cell-type, prolactin (Prl) is labeled (Liu et al., 2003, 2006). Two-color imaging of this double-transgenic line revealed that the ventral hypothalamic oxytocinergic trajectories terminate near the Prl-positive adenohypophyseal cells (Figure 2A). This transgenic system provided us with a new tool to study the morphogenesis of the zebrafish preopticohypophyseal axonal tract analogous to the supraopticohypophyseal tract in mammals.

We next visualized the neurovascular interface within the neurohypophysis by crossing our HNS specific line with a vascular endothelial reporter expressing mCherry in *vegfr2*-positive cells (Chi et al., 2008; Jin et al., 2005). Previous work, based on microangiography, has provided an extensive map of the vascular network in the zebrafish head (Isogai et al., 2001). Using our axovasal double transgenic line, we were able to identify GFP+ oxytocinergic projections converging posteriorly and medially into the neurohypophysis, arborizing extensively and interfacing with a formation of blood vessels previously annotated as palatocerebral veins (Figures 2B and 2E and Movies S2 and S3). The hypothalamo-neurohypophyseal (HN) axonal termini project onto the posterior part of this loop-shaped vascular structure. To ascertain the position of this structure in relation to the adenohypophysis, we generated double transgenic lines with labeled blood vessels (*vegfr2:*EGFP or *vegfr2:*mCherry) and adenohypophyseal cell types (*pomc*:GFP or *prl*:RFP). Three-dimensional image reconstruction of the ventral diencephalon in these embryos revealed that these blood vessels engulf part of the pituitary area abutting the adenohypophysis (Figures 2C and 2D and Movie S4). The NH is positioned in a pocket-like indentation formed by the ventrally located adenohypophysis (Figures 2B′ and 2D′).

The vessels forming the hypophyseal vascular structure has been previously annotated as median palatocerebral vein (MPLV) and palatocerebral vein (PLV) (Isogai et al., 2001). As we now identify these vessels as the zebrafish hypophyseal vessels, we set out to reassess their arterial and venous identity. We performed live imaging of hypophyseal blood flow using

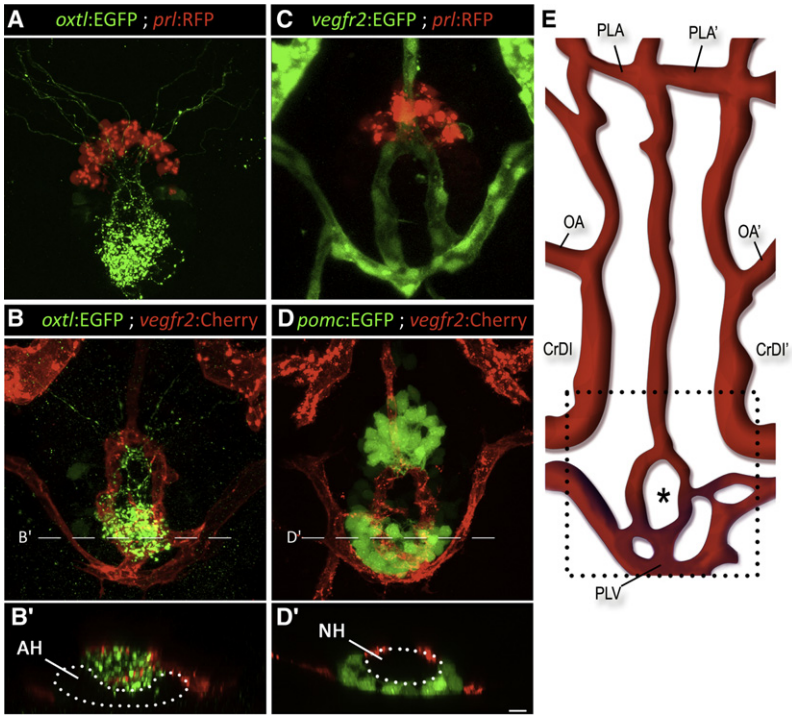

Figure 2. Axovasal Interactions in the Zebrafish Pituitary

(A–D) Three-dimensional reconstructions of the hypophysis of 9-day-old zebrafish embryos carrying pairs of transgenic fluorescent markers of different hypophyseal components. (A) The *oxtl:EGFP* transgene (green) marks oxytocinergic axons terminating at the neurohypophysis, just dorsal and posterior to the adenohypophyseal prolactin-producing cells marked with *prl:RFP* (red).

(B) Double transgenic animals expressing *oxtl:EGFP* (green) together with the vascular endothelial marker *vegfr2:Cherry* (red) reveal a distinct, previously unidentified structure of the zebrafish hypophyseal vasculature.

(C and D) Hypophyseal vasculature, visualized by either *vegfr2:EGFP* or *vegfr2:Cherry*, together with the adenohypophyseal markers *prl:RFP* and *pomc:EGFP*. The ring-like vascular structure resided dorsal to the adenohypophysis. (B′) and (D′) show optical Z-slices that demonstrate the position of the NH in an indentation of the adenohypophysis.

(E) Schematic map of ventral head vasculature of the zebrafish larvae, including the location of the hypophyseal vasculature. The asterisk marks the location of the neurohypophysis.

AH, adenohypophysis; CrDI, cranial division of the internal carotid artery; NH, neurohypophysis; OA, optic artery; PLA, palatocerebral artery; PLV, palatocerebral vein; *pomc*, proopiomelanocortin; *prl*, prolactin; *vegfr*, vascular endothelial growth factor receptor. Scale bar, 20 μm. See also Movies S2–S4.

time-lapse microscopy of a triple transgenic line with labeled erythrocytes (*gata1*:dsRed), blood vessels (*vegfr2*:EGFP) and adenohypophyseal cells for positional reference (*prl*:RFP). By following individual dsRed+ erythrocytes, we determined the direction of blood flow into and out of the hypophysis to the lateral venous sinuses (Figure 3A and Movie S5). This allowed us to deduce the identity of the hypophyseal artery and veins (Figure 3B and Figure S2).

Taken together, our analyses identify the organization of the zebrafish neurovascular HNS structure in relation to the other pituitary cell populations (Figure 3C).

Morphogenesis of the Hypothalamo-Neurohypophyseal System

We set out to delineate the morphogenic events leading to the formation of axovasal contact between hypothalamic axons and neurohypophyseal blood capillaries. Although the expression of oxytocin is apparent from the Prim-15 stage (30–36 hr; Unger and Glasgow, 2003), we found that our *oxtl*:EGFP did not express sufficient levels of the EGFP protein to detect axonal expression at this embryonic stage (data not shown). To resolve this, we sought an earlier transgenic reporter that would allow detection of the initial stages of hypophyseal innervation. We previously reported that the homeodomain-containing protein Orthopedia (Otp) is expressed in hypothalamic neuronal progenitors, including the magnocellular oxytocinergic neurons of the NPO area (Blechman et al., 2007; Machluf et al., 2011). Moreover, we recently identified a genomic *cis*-regulatory region driving expression of the zebrafish *otpb* gene in the NPO (Fujimoto et al., 2011). We made use of this *cis*-regulatory element to generate a transgenic *otpb*:EGFP-caax line driving expression of a membrane-tagged EGFP in Otp+ cell bodies and axons, including hypothalamo-neurohypophyseal (HN) projections (Figures 4A–4C). We analyzed neurovascular formation at 36, 54, and 72 hr using an *otpb:caax-EGFP;fli:dsRed* double transgenic line. This analysis shows that HN axonal projections innervate the neurohypophysis before the vessels are formed and a tight neurovascular interface is established between 2 and 3 days of development (Figures 4D–4F).

A dynamic analysis of hypophyseal vascularization/angiogenesis has never been reported. We used time-lapse microscopy to track vascular endothelial cells in the ventral diencephalon of zebrafish embryos carrying the *vegfr2*:Cherry vascular reporter transgene in which a membrane-localized monomeric Cherry is expressed in endothelial precursors and mature vessels (Chi et al., 2008). The embryos were imaged from 2 days postfertilization (dpf), when the hypophyseal vascular structure is yet absent, through 3 dpf, at which time the vascular loop around the neurohypophysis is fully established. Three-dimensional reconstitution followed by cell tracking of such time-lapse movies (n = 4) showed that formation of the hypophyseal artery begins prior to that of the veins; the artery is initiated at the hypophysis itself and extends anteriorly until it connects with the palatocerebral arteries at day 2.5 (Figure 4G). As the primary lateral vein sinuses extend forward through the diencephalon, they sprout medially and wrap around the posterior edge of the neurohypophysis to form the hypophyseal veins. These fuse bilaterally with one another and with the hypophyseal arteries to form a ring around the neurohypophysis and connect it to the general circulation at approximately 3 days. (Figure 4G and Movie S6). High-resolution 3D rendering of an embryo fixed at this time point clearly shows that the hypophyseal veins connect bilaterally to the primary vein sinuses (Figure S2).

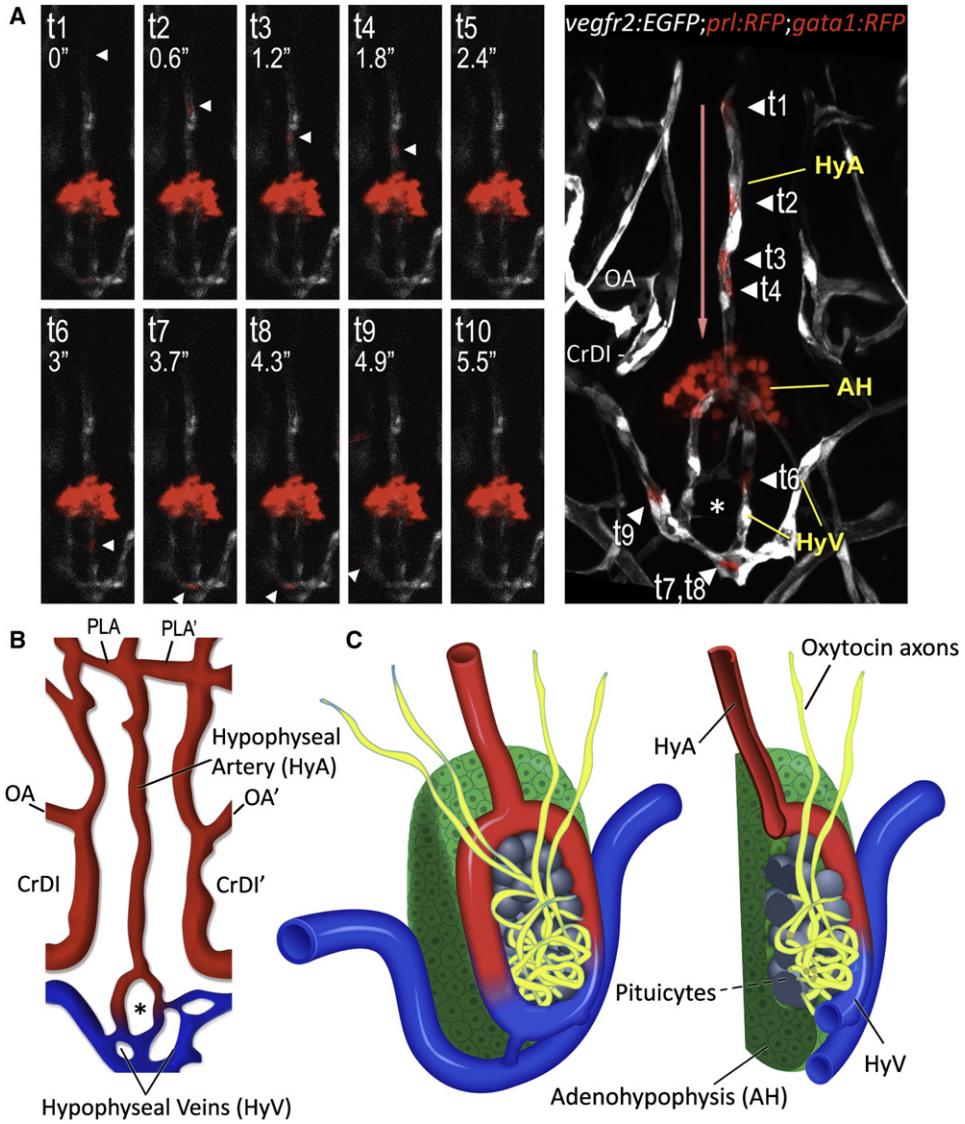

Figure 3. 3D Structure of the Hypophyseal Neurovascular Interface

(A and B) Identification of hypophyseal arteries and veins by real-time analysis of hypophyseal blood flow.

(A) Confocal time-lapsed images (t1–t10) of a single gata1+ blood cell (arrowhead) traveling from the hypophyseal artery into the neurohypophysis and its outflow through the hypophyseal veins. Superposition of all time points and the direction of blood flow (red arrow) are shown in the right panel. Adjacent Prl-RFP+ adenohypophyseal cells (arrow) served as a positional landmark.

(B) Schematic map of ventral head vasculature of the zebrafish larvae, including the newly annotated hypophyseal artery (red) and veins (blue). AH, adenohypophysis, CrDI, cranial division of the internal carotid artery; HyA, hypophyseal artery; HyV, hypophyseal veins; OA, optic artery; PLA, palatocerebral artery.

(C) Schematic representation of the 3D structure of the zebrafish pituitary depicting the various cellular components of the adeno- and neurohypophysis. A longitudinal section of this structure is shown on the right.

See also Figure S2 and Movie S5.

The above analyses of neurohypophyseal axons and blood vessels highlight key cellular events of HNS morphogenesis: (1) HN axons appears at the site of the prospective neurohypophysis as early as 24–36 hr after fertilization. (2) Endothelial cells forming the hypophyseal artery and veins appear at 2 days, approximately 24 hr after the axons start to innervate the neurohypophysis. (3) It takes another 24 hr for the endothelial cells of the artery and veins of the hypophysis to sprout and fuse to form the aforementioned loop-like structure, creating a tight interface with the neurohypophyseal axons.

Hypothalamic Neurons Are Necessary for Pituitary Vascular Organization

During its morphogenesis, the neurohypophysis becomes a point of intersection between axons and vessels. We next examined the interdependence of blood vessels for axon patterning in the neurohypophysis. The zebrafish mutant *cloche* (*clo*) has an overall deficiency of endothelial and hematopoietic lineages, including a complete lack of head vasculature (Stainier et al., 1995). We examined whether the neurohypophyseal axonal projections are affected in *cloche* mutants by comparing

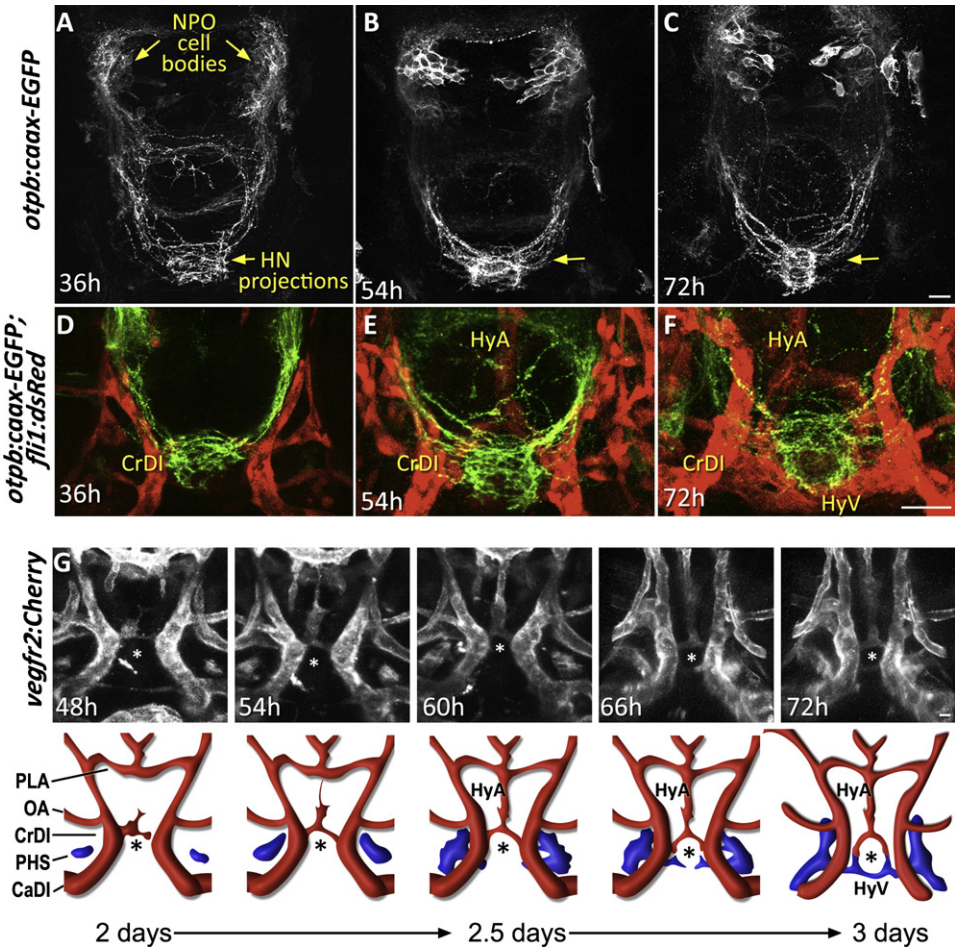

Figure 4. Morphogenesis of the Neurohypophysis

(A–C) Dynamics of hypophyseal innervation. Images of transgenic *otpb:caax-EGFP* embryos reveal that innervation of the hypophysis by neurons of the neurosecretory preoptic nucleus (NPO) occurs as early as 36 hr postfertilization and becomes well established by 54 hr. Scale bar, 20 μm.

(D–F) Dynamics of neurovascular interface. Images of double transgenic *otpb:caax-EGFP;fli1:dsRed* embryos at different developmental stages showing innervation of the neurohypophysis prior to hypophyseal vessel formation.

(G) Dynamics of hypophyseal vascularization. Time-lapsed (48–72 hr) confocal microscopy was used to track vascular endothelial cells in the ventral diencephalon of *vegfr2:Cherry* embryos. The upper panels display snapshots of critical stages in the formation of the hypophyseal loop-like structure. A schematic representation of the corresponding images with arterial (red) and venous (blue) color-coding is shown at the bottom.

CrDI, cranial division of the internal carotid artery; HyA, hypophyseal artery; HyV, hypophyseal veins; OA, optic artery; PHS, primary head sinus; PLA, palatocerebral artery. The asterisk (*) demarcates the location of the neurohypophysis. See also Movie S6.

oxytocinergic-positive neurohypophyseal axonal termini in mutant and wild-type siblings. This analysis revealed no significant differences in oxytocinergic immune-reactive projections indicating that the presence of endothelial cells/vessels is not required for HN innervation (Figures 5A and 5B; n = 13/15). This result is consistent with the observation that axons begin to innervate the NH before the blood vessel network is established (Figures 4D–4F).

We next examined whether the presence of HN neuronal tracts is important for morphogenesis of the neuroendocrine vasculature. We undertook a conditional HN cell ablation strategy using tissue-specific expression of the nitroreductase (NTR), an enzyme that converts the prodrug metronidazole into a cytotoxic agent (Curado et al., 2008; Davison et al., 2007). We chose to target Otp+ neurons as this cell population includes all NPO neurons that innervate the neurohypophysis (Figure 4 and Machluf et al., 2011). To this end, we generated a transgenic line, *otpb*:*Gal4;UAS:*NTR-Cherry, in which the NTR-Cherry fusion protein is expressed in Otp+ neurons using a tissue-specific Gal4 transgene to drive an NTR-Cherry that was placed under multiple Gal4 upstream activation sequences (Davison et al., 2007). We crossed the *otpb*:*Gal4;UAS:*NTR-Cherry fish with the vascular-specific *vegfr2:EGFP* line to generate triple transgenic embryos in which vascular development can be monitored in the presence or absence of Otp+ HN cells. The metronidazole drug was applied to embryos at 24–72 hr, from the stage at which the first HN neuronal tracts are detected and until the intact hypophyseal vascular structure is formed and contacts the axons. The efficiency of HN cell ablation was assessed by monitoring NTR-Cherry+ (Figures 5D and 5J) and *oxtl*+ neurons (Figures S3A and S3B) in control and metronidazole-treated triple transgenic (*otpb*:*Gal4;UAS:*NTR-Cherry;*vegfr2:EGFP*) embryos.

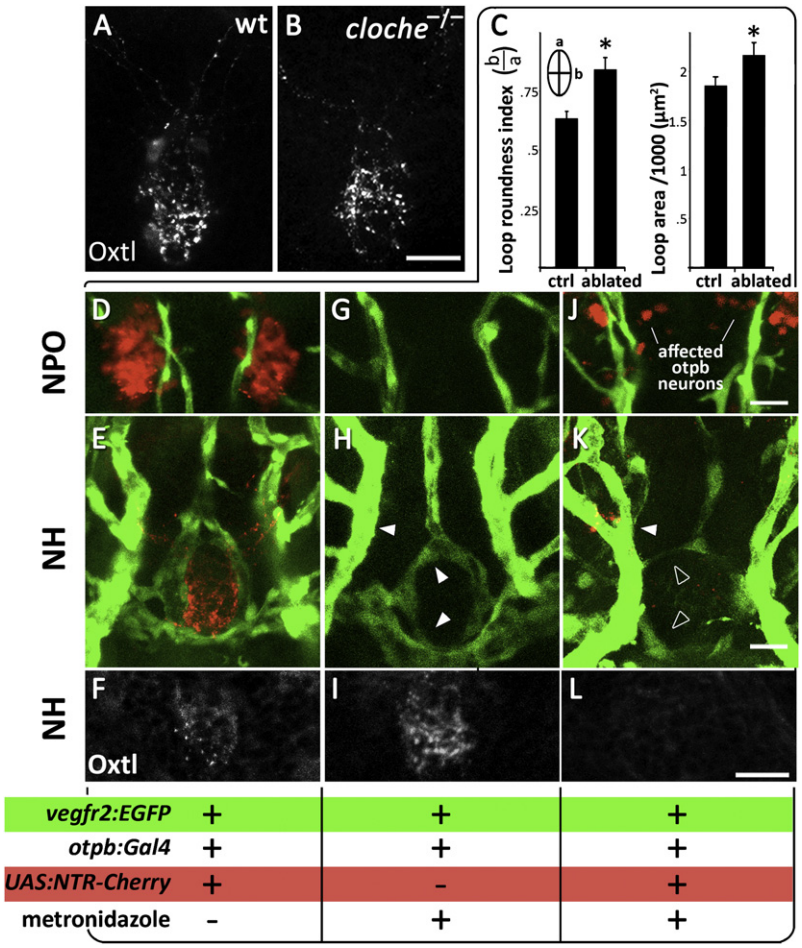

Figure 5. Abnormal Development of Pituitary Vasculature in the Absence of HN Innervation

(A and B) Immunostaining of oxytocin (Oxtl) in wild-type (A) and the endothelial-deficient mutant *cloche* (−/−) (B) mutants, which lack all blood vessels.

(C–L) Genetic cell ablation of Otp+ neurons of the neurosecretory preoptic nucleus (NPO). (C) Quantitative analysis of the vascular phenotype caused by HN neuronal ablation (see text). Using the Gal4/UAS system (*otpb*:Gal4;*UAS*:NTR-Cherry) to drive expression of a Nitroreductase-Cherry (NTR-Cherry) fusion protein only in Otp+ neurons make these cells and their projections visible (red) and susceptible to the prodrug metronidazole. This transgenic fish was crossed to the vascular reporter line, *vegfr2:*EGFP, to generate a triple transgenic line (D–F and J–L). Double transgenic line (*otpb*:Gal4;*vegfr2*:EGFP, G–I) expressing vascular EGFP but not the NTR-Cherry protein served as a control for nonspecific drug toxicity. The presence of Cherry+ neurons (D, G, J), EGFP+ blood vessels (E, H, and K) and oxytocin immunoreactivity (F, I, and L) were monitored in three experimental conditions; the respective genotypes as well as the application of the metronidazole killing agent are indicated below. Filled and empty arrowheads indicate normal and abnormal blood vessels, respectively.

See also Figure S3.

To verify the deleterious effects of Otp+ cell ablation on HN neurosecretion, we measured the levels of the Oxytocin protein in the neurohypophysis by anti-oxytocin immunostaining and determined that Otp+ cell ablation causes a marked decrease in neurohypophyseal oxytocin levels (Figures 5F, 5I, and 5L and Figure S3C).

We then went on to analyze the head vasculature in metronidazole-treated *vegfr2:EGFP* embryos carrying the *otpb*:*Gal4* and *UAS:*NTR-Cherry transgenes, as compared to siblings not carrying them. As expected, application of the metronidazole prodrug to embryos not carrying the *UAS:*NTR-Cherry transgene had no significant effect on hypophyseal or other blood vessels, indicating that in the absence of NTR-Cherry, metronidazole treatment is not toxic and does not affect vasculature (Figures 5G–5I, n = 15/15). In contrast, Otp+ cell ablation in metronidazole-treated triple transgenic (*vegfr2:EGFP*;*otpb*:*Gal4*;*UAS:*NTR-Cherry) embryos was accompanied by a marked impairment of hypophyseal vasculature, indicating that impaired HN neurosecretion is associated with hypophyseal vascular abnormality (Figures 5J–5L, n = 12/15). While the hypophyseal vasculature of normal embryos tightly surrounds the neurohypophysis forming an elliptical loop (Figures 5E and 5H), ablation of Otp+ neurons caused abnormalities characterized by: failure to close the neurohypophyseal vascular loop, incomplete connection of the hypophyseal artery to the PLA and overall thin hypophyseal vascular structures (Figure 5K). We used two measurable parameters to quantify changes to this morphology (Figure 5C): (1) "loop roundness index"– samples with ablated axons display a more round loop as opposed to the ellipsoid shaped loop in the control samples, and (2) "loop area"– axonal ablated embryos exhibit a significant increase in the loop area. In short, ablation of Otp+ neurons led a significantly rounder loop surrounding a larger area (n = 15, *$p < 0.05$). In all cases, all neighboring head vessels remained unaffected.

These results suggest that a tissue interaction between HN neurons projecting to the neurohypophysis and endothelial cells contributes to the formation of an intact neurohypophyseal vascular structure. We hypothesize that HN axons provide a proangiogenic cue necessary for morphogenesis of the hypophyseal vasculature and establishment of a functional neurovascular connection.

Oxytocin and Its Receptor Are Required for Pituitary Vascular Morphogenesis

We set out to identify a secreted axonal-derived cue that might be involved in pituitary vascular morphogenesis. Previous studies have effectively shown that vascular endothelial cells of many tissues express oxytocin receptor (Jankowski et al., 2004; Thibonnier et al., 1999; Wakasa et al., 2009). Furthermore, recent reports have demonstrated that oxytocin stimulates migration and sprouting of human endothelial cells in vitro (Cassoni et al., 2006; Cattaneo et al., 2008). These findings, together with our finding that the neurohypophysis is innervated before its vascularization (Figure 3) and the coincidence of vascular abnormality with HN oxytocin levels (Figure 5), have led us to hypothesize that hypophyseal secretion of oxytocin acts as

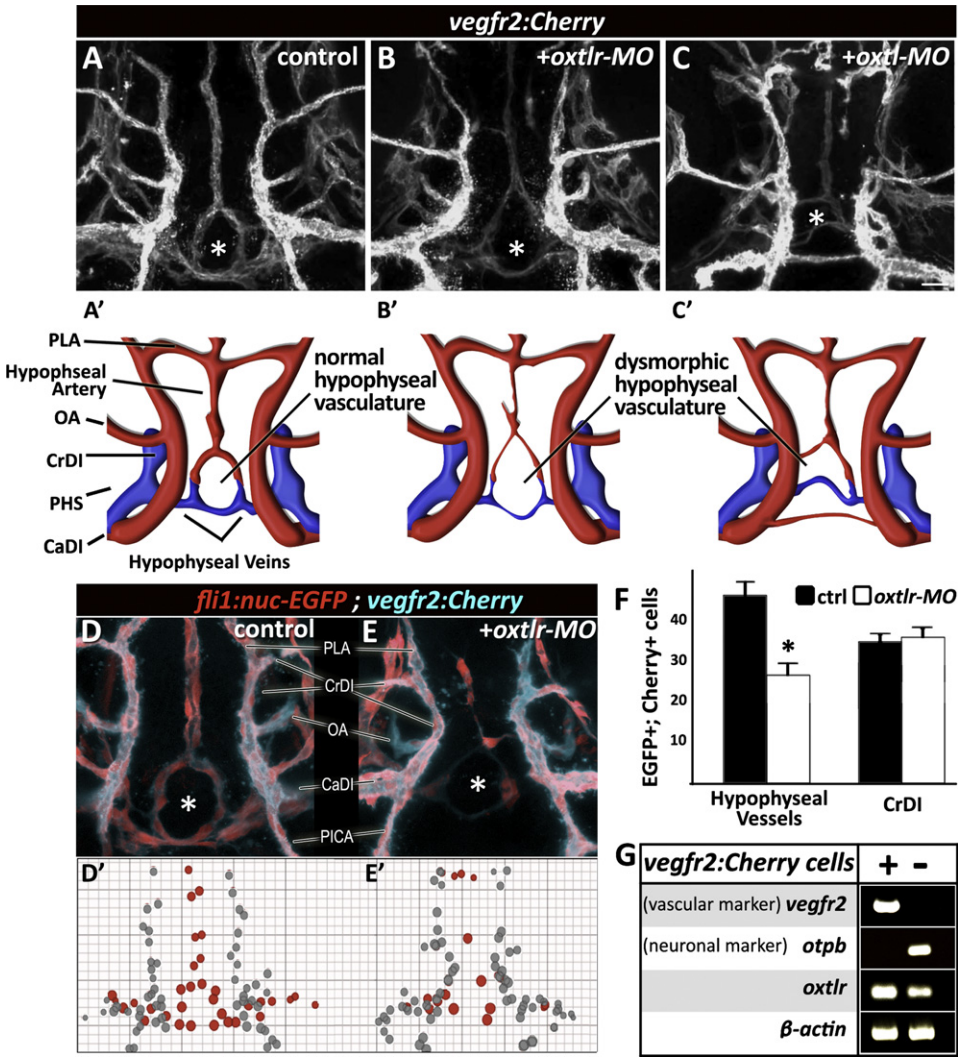

Figure 6. Oxytocin and Its Receptor Are Necessary for Pituitary Vascularization

(A–D) High-resolution confocal images of the head vasculature of 3-day-old embryos following targeted knockdown of the gene encoding for oxytocin (*oxtl*-MO) or oxytocin receptor (*oxtlr*-MO) using antisense morpholino oligonucliotides, leads to severe impairment of neurohypophyseal vasculature, but does not impede development of neighboring vessels. A schematic representation of the corresponding phenotype with arterial (red) and venous (blue) color-coding is shown in (A′)–(C′).

(D and E) By crossing nuclear- and membrane-tagged fluorescent vascular reporter lines, we are able to count the number of vascular endothelial cells in each vessel. A dot-plot histogram showing the x,y positions of EGFP+;Cherry+ endothelial cells nuclei of the hypophyseal vessels as well as the adjacent internal carotid arteries (CrDI, between the PICA and the PLA) is shown in (D′) and (E′). Individual cells belonging to the hypophyseal vessels (red) and CrDI (gray) are color coded. The *oxtlr*-MO-injected embryos (E) display a markedly reduced number of endothelial cells in the hypophyseal vessel but no change in the nearby internal carotid artery.

(F) Bar histogram showing EGFP+;Cherry+ cell counts in the internal carotid arteries and hypophyseal vessels in control and following *oxtlr* knockdown. *$p < 0.01$, $n = 14$.

(G) RT-PCR analysis of *vegfr2:*Cherry-positive and -negative FACS sorted endothelial cells demonstrating vascular expression of the oxytocin receptor (*oxtlr*).

CaDI, caudal division of internal carotid; CrDI, cranial division of the internal carotid artery; MO, morpholino antisense oligonucleotide; OA, optic artery; PICA, primitive internal carotid artery; PLA, palatocerebral artery; PLV, palatocerebral vein. The asterisk (*) demarcates the location of the neurohypophysis. See also Figure S4.

a developmental cue that induces angiogenesis of neurohypophyseal vessels during embryonic development.

We went on to test whether specific disruptions of oxytocin signaling cause a hypophyseal vascular phenotype. We injected 1 cell stage embryos with splice-blocking morpholino oligonucliotides targeted against either the oxytocin-like (*oxtl*) gene or its receptor (*oxtlr*). These genetic perturbations caused aberrant *oxtlr* splicing and a dramatic reduction in Oxytocin protein levels (Figures S4A–S4D). Targeted knockdown of either *oxtl* or *oxtl*-receptor led to malformation of neurohypophyseal vessels ranging from mild to severe hypoplasia and vessel dysmorphism, but, importantly, did not disrupt nearby internal carotid arteries (Figures 6A–6E). This vascular phenotype appeared to be mediated by oxytocinergic neurons as knockdown of the

gene encoding the other neurohypophyseal hormone, arginine-vasopressin (*avpl*), did not result in any visible vascular phenotype (data not shown). We went on to quantify this effect using double-transgenic embryos that express distinct fluorescent markers in both nuclei and the plasma membranes of vascular endothelial cells (*fli1*:nuc-EGFP;*vegfr2*:ras-mCherry) (Figures 6D and 6E). This allowed us to readily identify and count the individual endothelial cells. We found that targeted knockdown of the *oxtl*-receptor, which affected the neurohypophyseal vasculature, led to marked reduction in the number of endothelial cells that make up the hypophyseal vessel but did not affect the number of cells in the nearby internal carotid arteries (Figure 6F).

Our findings suggest that the neuropeptide oxytocin serves as a developmental angiogenic cue regulating the morphogenesis of neurohypophyseal vessels during embryonic development.

Oxytocin signaling may affect vascular endothelial cells directly or it may do so by regulating a secondary angiogenic cue that is received by the forming hypophyseal vasculature. For example, blocking oxytocin signaling may interfere with autocrine activation of the oxytocin receptor that could in turn regulate the secretion of a proangiogenic cue, thus affecting hypophyseal vascular morphogenesis. Alternatively, the oxytocin receptor might be autonomously affecting hypophyseal vascular morphogenesis as was shown in the case of cultured human endothelial cells (Cassoni et al., 2006; Cattaneo et al., 2008, 2009; Thibonnier et al., 1999). In agreement with these studies, RT-PCR expression analysis of *oxtlr* mRNA in FACS-sorted endothelial cells derived from *vegfr2:mCherry* transgenic embryos clearly shows that the zebrafish oxytocin receptor is expressed in vascular endothelia (Figure 6G and Figure S4E).

To directly address whether oxytocin receptor autonomously affects hypophyseal vascular morphogenesis, we performed a tissue-specific rescue of *oxtlr* deficient embryos (Figure 7). To this end, we knocked down the *oxtlr* gene in the entire embryo and simultaneously re-expressed Oxtlr in discrete endothelial clones. We used a *fli1*:Gal4;UAS:Kaede transgenic line (Zygmunt et al., 2011) to drive endothelial-specific expression of oxytocin receptor. *fli*:Gal4;UAS:Kaede embryos were microinjected with a transgenic vector harboring the oxytocin receptor cDNA under the control of multiple Gal4 upstream activation sequences (10xUAS), resulting in mosaic vascular clones expressing the oxytocin receptor. To identify these clones, we made use of a multicistronic gene expression cassette in which the viral 2A peptide sequence (Provost et al., 2007) was placed between the oxytocin receptor and EGFP, causing simultaneous expression of EGFP+ oxytocin receptor in discrete clones throughout the Kaede-positive blood vessels (Figures 7A–7C). We analyzed hypophyseal vasculature by scoring two parameters: (1) integrity of the hypophyseal vascular structure, and (2) presence of clones expressing the Oxtlr-2A-EGFP cassette in the hypophyseal vessels. We found that the existence of Oxtlr-expressing clones in the hypophyseal vasculature is significantly associated with a rescued hypophyseal vascular structure (Figure 7C; $n = 20/22$, $p < 0.0001$). These results suggest that oxytocin receptor mediates a proangiogenic signal by acting autonomously in vascular endothelial cells.

Taken together, this study demonstrates that the formation of the neurovascular interface of the neurohypophysis is regulated during development by the neuropeptide oxytocin and its receptor. Oxytocin secreted from developing NH nerve termini signals to nearby endothelial cells at the site of the neurohypophyseal primordium. Other vascular endothelial cells may also express the receptor but the ligand is not available to them. This axovasal cell communication event is essential for the establishment of a tight interface between HN neurons and blood vessels of the HNS (Figure 7D).

DISCUSSION

The HNS is a main conduit by which the brain exerts control over peripheral organs. The activities of the HNS are conserved in all vertebrates and its main anatomical hallmark is the tight interface between hypothalamic nerve termini and neurohypophyseal blood vessels. In the present study, we have characterized the structure and morphogenesis of the zebrafish HNS and showed that HN axons secrete a localized proangiogenic cue (oxytocin) that is received by endothelial cells leading to the formation of a specialized neurovascular interface.

Morphogenesis of the HN System

The embryonic development of the neurohypophysis has been previously described in other model organisms and in human (Eurenius, 1977; Fink and Smith, 1971; Galabov and Schiebler, 1983; Okado and Yokota, 1980). However, the elaborate three-dimensional structure of the neurohypophysis makes it difficult to study its developmental dynamics. Moreover, the above studies were based on electron microscopy and immunohistological methods, which are useful to study fine structure of the neurovascular interface, but are limited in their ability to resolve the spatiotemporal cellular processes that shape the developing organ. To overcome these limitations, we have utilized a unique transgenic reporter system, in which zebrafish HN cell bodies and neurovascular contacts are labeled. Using this vertebrate model system we were able to monitor the spatiotemporal morphogenesis of neurohypophyseal axons and blood vessels in an intact developing brain. Based these results, we can now conclude that the anatomy of the HNS is largely conserved between fish and mammals.

We show that the zebrafish neurohypophysis is a discernable area, which develops within a concave-shaped indentation formed by the adenohypophysis. The identity of the zebrafish hypophyseal blood vessels has not been reported before (Isogai et al., 2001). Our study provides a structural and functional description of this unique vascular formation. Using real-time imaging, we showed that the hypophyseal artery develops before the veins and separately from them. As the vascular network of the brain is predominantly formed by angiogenesis, it is likely that the hypophyseal vessels we identified sprout from existing vascular network of the head. Future identification of the exact origins of the hypophyseal artery and veins may contribute to elucidation of the factors regulating these vascular identities. Interestingly, HN axons begin to innervate the neurohypophysis 24 hr prior to the appearance of endothelial neurohypophyseal precursors and approximately 48 hr before the establishment of the tight neurovascular contacts between the axon termini and the hypophyseal blood vessels suggesting that the final morphogenesis of these axons and vessels is regulated by temporally distinct pathway(s).

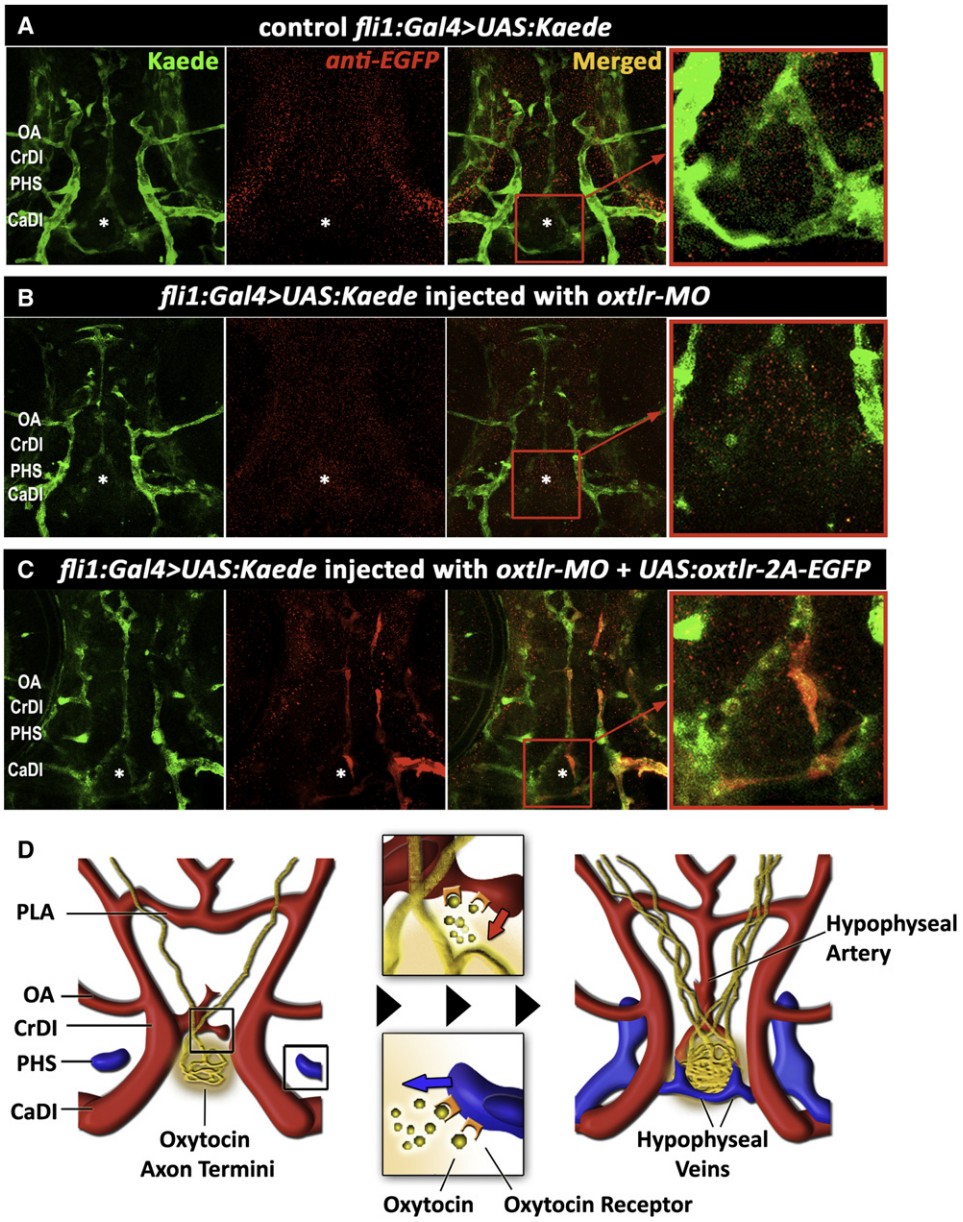

Figure 7. Cell-Autonomous Effect of the Oxytocin Receptor on the Pituitary Vasculature

(A–C) Genetic complementation of oxytocin receptor in the vascular endothelia of *oxtlr*-deficient embryos. Double transgenic embryos expressing an endothelial Gal4 driver (*fli1*:Gal4) and a fluorescent reporter protein (*UAS*:Kaede; green) were injected with transposon-based transgenic vector containing a multicistronic gene expression cassette (UAS:*oxtlr*-2A-EGFP) allowing simultaneous mosaic coexpression of the oxytocin receptor and EGFP in discrete vascular clones (red). These clones were detected by immunostaining with an anti-EGFP antibody that does not react with the Kaede protein followed by a secondary cy3-conjugated antibody. The asterisk (*) demarcates the location of the neurohypophysis.

(D) Schematic model describing the hypothalamohypophyseal neurovascular connection by local secretion of oxytocin (see text).

CaDI, caudal division of internal carotid; CrDI, cranial division of the internal carotid artery; OA, optic artery; PHS, primary head sinus; PLA, palatocerebral artery.

Mechanisms of Neurovascular Connection

The elaborate networks of vertebrate vascular and neuronal systems display striking anatomic similarities. Nerve fibers and blood vessels often follow parallel routes in the body. Furthermore, attraction and repulsion of axons and vascular endothelial cells to/from target tissues were found, in some instances, to be regulated by common guidance molecules (Adams and Eichmann, 2010; Carmeliet and Tessier-Lavigne, 2005). The question we addressed here is: how do hypothalamic axons contact neuroendocrine blood capillaries? The formation of this vital neurovascular interface could potentially be regulated in different ways: neurohypophyseal blood vessels may attract HN neurons to the site of the neurohypophysis similar to the reported guidance of a subset of developing sympathetic axons by

vascular-derived endothelins (Makita et al., 2008). We have ruled out this possibility in the present case by showing that oxytocinergic axons display normal hypophyseal innervation and axonal branching in the avascular zebrafish mutant *cloche*. On the other hand, tissue-specific genetic ablation of HN neurons and knockdown of the HN neuropeptide oxytocin specifically impaired the formation of neurohypophyseal vasculature. These results indicate that neurohypophyseal morphogenesis is regulated by the local release of the neuropeptide oxytocin from the developing nerve termini. A similar type of mechanism, in which axons affect endothelial cells, was shown in the case of peripheral sensory nerves that regulate the pattern of arterial branching via local secretion of VEGF-A (Mukouyama et al., 2002, 2005) and more recently, in the case of motor neurons-derived Netrin-1a that mediates lymphangiogenesis (Lim et al., 2011). A third, nonexclusive possibility is that blood vessels and nerve fibers of the HNS respond to a common attractant that is expressed in the ventral diencephalic midline.

Notably, our data indicate that blocking oxytocinegic signaling does not prevent the guidance of blood vessels to the area of the neurohypophysis. Therefore, it is likely that oxytocin signaling cooperates with other guidance cues to orchestrate vascular morphogenesis in the neurohypophysis, leading to the formation of a tight neurovascular interface.

Role of Oxytocin in Angiogenesis

It has been known for some time that when the HN tract is transected, many of the axons regenerate and re-establish functional neurovascular connections with blood capillaries (Harris, 1948b, 1955). Regenerated areas are characterized by a marked increase in angiogenesis, which was found to occur near large deposits of neurosecretory material derived from the regenerated axon fibers (Moll, 1958). A possible interpretation of these studies is that neurohypophyseal angiogenesis may be regulated by the release of a proangiogenic factor from the developing nerve termini.

Our present finding that the neuropeptide oxytocin has a proangiogenic role during the embryonic development of the HNS receives reinforcement from many studies. Human vascular endothelial cells derived from several organs express the oxytocin but not the arginine-vasopressin receptor (Thibonnier et al., 1999). Oxytocin induces differentiation of embryonic stem cells and adult Sca-1-positive cells to cardiomyocytes (Matsuura et al., 2004; Paquin et al., 2002). Remodeling of uterine blood during human pregnancy involves increased oxytocin receptor expression in vessel walls (Wakasa et al., 2009). Oxytocin and its receptor have been implicated in developmental formation of the coronary vessels and in angiogenic remodeling following myocardial infarction (Jankowski et al., 2004; Kobayashi et al., 2009). Finally, oxytocin stimulates migration and sprouting of cultured human vascular endothelial cells and this angiogenic effect is dependent on oxytocin receptor signaling events (Cassoni et al., 2006; Cattaneo et al., 2008, 2009). Several studies have reported metabolic abnormalities in mice deficient in either oxytocin or its receptor (Kasahara et al., 2007; Takayanagi et al., 2008). As none of these studies have analyzed the integrity of the hypophyseal neurovascular interface it remains to be determined whether the metabolic abnormalities observed in these mice are caused by compromised neurohypophyseal development. Finally, loss of functional Otp disrupts the development of oxytocinergic neurons as well as the neurohypophysis (Acampora et al., 1999; Wang and Lufkin, 2000).

The question of why hypophyseal vasculature responds to oxytocin while other vessels do not remains open. The simplest explanation is that the local secretion of the oxytocin protein by HN termini is a focal attractant that affects the sprouting morphogenesis of only nearby endothelial cells, as shown in our model (Figure 7D) Another nonexclusive possibility is that hypophyseal vascular precursors have a unique molecular composition that renders them responsive to oxytocin signal.

Mechanism of Action of Oxytocin during Neurohypophyseal Morphogenesis

Given that the primary function of the HNS is the mass secretion of oxytocin into the neurovascular interface, we favor the possibility that localized developmental secretion of oxytocin is important for the integrity of neurovascular contacts at the site of the neurohypophysis. We show that endothelial-specific re-expression of the oxytocin receptor rescues the vascular phenotype of in *oxtlr*-deficient embryos suggesting that this receptor mediates a proangiogenic signal by acting in vascular endothelial cells that receive oxytocin signal from HN neurons. However, we still cannot rule out the possibility that, in addition to the oxytocin-oxytocin receptor-mediated neurovascular signaling event we found here, autocrine activation of the oxytocin receptor regulates another, yet undiscovered, angiogenic cue released by HN axons. So far, we have examined the expression of various isoforms of vegf, semaphorin, and tgfβ/Bmp that could conceivably be involved in HN neurovascular development and found none of them is expressed in HN neurons (data not shown).

Oxytocin receptor belongs to the rhodopsin-type (class I) G protein-coupled receptor family and is coupled to phospholipase C through Gαq11 (Gimpl and Fahrenholz, 2001). Recent reports show that oxytocin stimulates migration and sprouting of human umbilical vein endothelial cells (HUVEC) through a 3D angiogenesis assay, via Gq coupling of the oxytocin receptor leading to phospholipase C activation and phosphorylation of the Pyk2 Src kinase proteins and that knockdown of Pyk2 impaired this effect (Cattaneo et al., 2008, 2009). As these proteins are known to be involved in Semaphorin and/or VEGF signaling in the vascular system, the signal transduction cascade underlying the effect of oxytocin on hypophyseal vascular morphogenesis may feed into known intracellular pathways used for branching morphogenesis of endothelial cells (Gelfand et al., 2009).

Finally, oxytocin-mediated vascular angiogenesis might prove relevant to adult regenerative processes. The regeneration of the HNS following hypophysectomy has been extensively studied in many vertebrate species including fish and humans (Billenstien and Leveque, 1955; Daniel and Prichard, 1972; Harris, 1955; Moll, 1957; Sathyanesan and Gorbman, 1965; Stutinsky, 1951). A strong association has been found between deposition of neurosecretory material and high vascularity in HNS regeneration models (Moll, 1958). The communication between the oxytocinergic neurons and the vasculature reported herein may play a role in this well-documented regeneration of the HNS following local lesion.

In summary, we present a genetic system to study the developmental assembly of the vertebrate HNS. Using this system, we have identified key cellular and biochemical processes required for formation of the neurohypophyseal neurovascular interface, a vital intersection that allows neuropeptidergic hormones from the central nervous system to be transferred directly into the blood and regulate the body's homeostasis.

EXPERIMENTAL PROCEDURES

Antibodies and Transgenesis Plasmids and Lines

Guinea pig polyclonal antibody directed to the Oxytocin peptide was purchased from Bachem (Bachem California, Torrance, CA, Cat. T-5021.0050). Antibodies made in rabbit and mouse (Molecular Probes, Eugene, OR) were used to detect the transgenic EGFP expression. For all plasmid DNA constructs we used the Tol2kit transposon-based transgenic vectors system for site-specific recombination-based cloning (Kwan et al., 2007). cDNA encoding to the *oxtlr* (gene locus FJ556870) was cloned downstream of the Gal4 responsive 10xUAS element and basal promoter. We used a multicistronic gene expression cassette in which the viral 2A peptide sequence was placed between the gene of interest and EGFP fluorescent protein, which reports the expression of the transgene (Provost et al., 2007). Genotypes of transgenic lines used in this study are as follows: Tg(oxtl:EGFP); Tg(vegfr2:EGFP) [a.k.a. Tg(kdrl:EGFP)s843]; Tg(vegfr2:mCherry) [a.k.a. Tg(kdrl:HsHRAS-mCherry)s896]; Tg(prl:RFP); Tg(pomc:EGFP) [a.k.a. Tg(-1.0pomca:GFP)zf44]; Tg(gata1:dsRed)sd2; Tg(otpb:caax-EGFP) [a.k.a. = Tg(otpb:1EGFP)zc49]; Tg(fli1:dsRed) [a.k.a. Tg(fli1a.ep:DsRedEx)um13]; Tg(otpb:Gal4) [a.k.a Tg(otpb.A:Gal4, myl7:EGFP)zc67]; Tg(UAS:NTR-Cherry) [a.k.a. Tg(UAS-E1b:NfsB-mCherry)c264]; Tg(fli1:nuc-EGFP) [a.k.a. Tg(fli1a:nEGFP)y7]; Tg(fli1:Gal4) [a.k.a. Tg(fliep:gal4ff)ubs4].

Microinjection of Transgenic DNA and Oligonucleotides

Gene knockdowns were performed using synthetic antisense morpholino oligonucleotides (MO; Gene Tools, LLC, Corvallis, OR) targeted to an RNA-splicing sites (Figure S2) of *oxtl,* (CACTGCAGATGGTAAGGGAAACCTA) and *oxtlr* (CATCGCTTTGGAGGAGAAGAAAACA). MOs were microinjected (each at 1.5 ng per 1.7 nl) into 1 cell stage embryos as we previously described (Blechman et al., 2007). The *oxtlr* cDNA sequence (gene locus FJ556870) used for the rescue experiment lacked the respective MO binding site and was therefore resistant to its effect.

Tissue Preparation and Immunohistochemistry

Immunofluorescent staining of transgenic embryos was performed as we previously described (Russek-Blum et al., 2008). The skulls of Juvenile and adult fish were exposed using sharp forceps and fixed at 4°C overnight in 2%–4% paraformaldehyde/0.1 M phosphate buffer (pH 7.5). Samples were washed twice with phosphate buffer and transferred into 20% sucrose/20% EDTA in 0.1M PB (pH 7.5) for decalcification and cryoprotection. Brains were frozen in 7.5% gelatine/20% sucrose and cut at 14 μm. Sections were stored at −20°C. Primary and secondary antibodies were incubated in PBS with 0.3% Triton X-100 (PBS TX). Primary antibodies were incubated overnight at 4 C° and secondary antibodies for 1 hr at room temperature. The slides were then washed in PBS TX followed by washes in PBS and mounted in PBS:Glycerol (1:1).

Tissue-Specific Cell Ablation

For the nitroreductase-mediated tissue-specific cell ablation we used the analytical-grade metronidazole drug, Vetranal (Sigma-Adridch, Rehovot, Israel Cat. #46461), which was dissolved in E3 medium (1.74 mM NaCl, 0.21 mM KCl, 0.12 mM $MgSO_4$, 0.18 mM Ca[NO_3], 0.15 mM HEPES [pH 7.4]). Embryos were manually dechorionated at 22 hpf and treated with 5 mM Vetranal from 24–48 hpf, and then switched into 10 mM Vetranal for additional 30 hr.

FACS and RNA Extraction

Three-day-old *vegfr2:mCherry* embryos were dissociated by Liberase blendzyme 3 (Roche, Basel, Switzerland) in combination with GIBCO-trypsin (Invitrogen, Carlsbad, CA), each for 15 min at 28°C, with occasional pipetting. Reaction was stopped by three washes of 1% bovine serum. Cells were suspended in L15 medium, and filtered by nylon mesh. Fluorescence activated cell sorting (FACS) was performed using a SORP FACSAriaII cell sorter. RNA was extracted from approximately 50,000 cells and RT-PCR with specific primer pairs (see Supplemental Experimental Methods) were performed as described (Blechman et al., 2007).

Live Imaging and Image Analysis

Embryos growing in E3 solution were embedded in drops of warm 1% Ultra Pure LMP agarose (Invitrogen, Carlsbad, CA) and imaged on a Zeiss 710 inverted confocal microscope with 488 and 561 nm lasers. Data sets were analyzed using Imagej and ZEN (Zeiss). 3D reconstructions were generated and analyzed with Volocity (Improvision, Covington, UK).

Statistical Analyses

Statistical significance between average cell counts was determined using Student's t test (two-tailed, $\alpha = 0.05$) on Excel (Microsoft Corp., Redmond, WA). All error bars indicate the standard error of the mean. Correlation between the occurrence of *oxtlr*-positive clones in ventral head vessels and phenotypic rescue of hypophyseal vasculature was determined by calculating the Phi coefficient of association, then performing a chi-square test of association ($p < 0.0001$) using the statistical web tool VassarStats.

SUPPLEMENTAL INFORMATION

Supplemental Information includes Supplemental Experimental Procedures, four figures, and six movies and can be found with this article online at doi:10.1016/j.devcel.2011.09.004.

ACKNOWLEDGMENTS

Thanks are due to Helit Nabel-Rosen for her initial observation of HN projections; Shifra Ben Dor for phylogenetic and genomic analyses; Genia Brodsky for help with figure graphics; Yossy Machluf and Liron Gibbs for FACS technical advice. Chi-Bin Chien for the Tol2kit plasmid vectors; Didier Stainier, Wiebke Herzog, Nathan Lawson, Michael Parsons, and Shlomo Melmed for transgenic lines. The research in the Levkowitz lab is supported by the Israel Science Foundation; Minerva Foundation; Kirk Center for Childhood Cancer and Immunological Disorders; Irvin Green Alzheimer's Research Fund. G.L. is an incumbent of the Tauro Career Development Chair in Biomedical Research. We declare that we have no conflicting interests. A.G. and J.B. designed and performed most of the experiments and collected and analyzed the data. J.K. performed the colocalization experiment of oxytocin and EGFP in adult fish. J.L.B. generated the otpb:Gal4 line and performed the analysis of Otp+ HN projections. L.H., H.-G.B., and M.A. generated the *fli1:Gal4;UAS:Kaede* line. G.L. initiated and headed the project and helped with data interpretation. G.L. and A.G. prepared the manuscript and figures.

Received: May 31, 2011
Revised: September 2, 2011
Accepted: September 12, 2011
Published online: October 17, 2011

REFERENCES

Acampora, D., Postiglione, M.P., Avantaggiato, V., Di Bonito, M., Vaccarino, F.M., Michaud, J., and Simeone, A. (1999). Progressive impairment of developing neuroendocrine cell lineages in the hypothalamus of mice lacking the Orthopedia gene. Genes Dev. *13*, 2787–2800.

Adams, R.H., and Eichmann, A. (2010). Axon guidance molecules in vascular patterning. Cold Spring Harb. Perspect. Biol. *2*, a001875.

Amer, S., and Brown, J.A. (1995). Glomerular actions of arginine vasotocin in the in situ perfused trout kidney. Am. J. Physiol. *269*, R775–R780.

Bargmann, W. (1949). J. Mol. Med. *27*, 617–622.

Billenstien, D.C., and Leveque, T.F. (1955). The reorganization of the neurohypophyseal stalk following hypophysectomy in the rat. Endocrinology *56*, 704–717.

Blechman, J., Borodovsky, N., Eisenberg, M., Nabel-Rosen, H., Grimm, J., and Levkowitz, G. (2007). Specification of hypothalamic neurons by dual regulation of the homeodomain protein Orthopedia. Development *134*, 4417–4426.

Blechman, J., Amir-Zimberstein, L., Gutnick, A., Ben-Dor, S., and Levkowitz, G. (2011). The metabolic regulator PGC-1α directly controls the expression of the hypothalamic neuropeptide oxytocin. J. Neurosci., in press.

Brownstein, M.J., Russell, J.T., and Gainer, H. (1980). Synthesis, transport, and release of posterior pituitary hormones. Science *207*, 373–378.

Burbach, J.P., Luckman, S.M., Murphy, D., and Gainer, H. (2001). Gene regulation in the magnocellular hypothalamo-neurohypophysial system. Physiol. Rev. *81*, 1197–1267.

Cajal, S.R. (1911). Histologie du Systeme Neurveux de L'Homme et de Vertebres (Paris: A. Maloine).

Carmeliet, P., and Tessier-Lavigne, M. (2005). Common mechanisms of nerve and blood vessel wiring. Nature *436*, 193–200.

Cassoni, P., Marrocco, T., Bussolati, B., Allia, E., Munaron, L., Sapino, A., and Bussolati, G. (2006). Oxytocin induces proliferation and migration in immortalized human dermal microvascular endothelial cells and human breast tumor-derived endothelial cells. Mol. Cancer Res. *4*, 351–359.

Cattaneo, M.G., Chini, B., and Vicentini, L.M. (2008). Oxytocin stimulates migration and invasion in human endothelial cells. Br. J. Pharmacol. *153*, 728–736.

Cattaneo, M.G., Lucci, G., and Vicentini, L.M. (2009). Oxytocin stimulates in vitro angiogenesis via a Pyk-2/Src-dependent mechanism. Exp. Cell Res. *315*, 3210–3219.

Chan, D.K.O. (1977). Comparative physiology of the vasomotor effects of neurohypophysial peptides in the vertebrates. Am. Zool. *17*, 751–761.

Chi, N.C., Shaw, R.M., De Val, S., Kang, G., Jan, L.Y., Black, B.L., and Stainier, D.Y. (2008). Foxn4 directly regulates tbx2b expression and atrioventricular canal formation. Genes Dev. *22*, 734–739.

Curado, S., Stainier, D.Y., and Anderson, R.M. (2008). Nitroreductase-mediated cell/tissue ablation in zebrafish: a spatially and temporally controlled ablation method with applications in developmental and regeneration studies. Nat. Protoc. *3*, 948–954.

Daniel, P.M., and Prichard, M.M. (1972). The human hypothalamus and pituitary stalk after hypophysectomy or pituitary stalk section. Brain *95*, 813–824.

Davison, J.M., Akitake, C.M., Goll, M.G., Rhee, J.M., Gosse, N., Baier, H., Halpern, M.E., Leach, S.D., and Parsons, M.J. (2007). Transactivation from Gal4-VP16 transgenic insertions for tissue-specific cell labeling and ablation in zebrafish. Dev. Biol. *304*, 811–824.

Eurenius, L. (1977). An electron microscope study of the differentiating capillaries of the mouse neurohypophysis. Anat. Embryol. (Berl.) *152*, 89–108.

Fink, G., and Smith, G.C. (1971). Ultrastructural features of the developing hypothalamo-hypophysial axis in the rat. A correlative study. Z. Zellforsch. Mikrosk. Anat. *119*, 208–226.

Fujimoto, E., Stevenson, T.J., Chien, C.B., and Bonkowsky, J.L. (2011). Identification of a dopaminergic enhancer indicates complexity in vertebrate dopamine neuron phenotype specification. Dev. Biol. *352*, 393–404.

Galabov, P.G., and Schiebler, T.H. (1983). Development of the capillary system in the neurohypophysis of the rat. Cell Tissue Res. *228*, 685–696.

Gelfand, M.V., Hong, S., and Gu, C. (2009). Guidance from above: common cues direct distinct signaling outcomes in vascular and neural patterning. Trends Cell Biol. *19*, 99–110.

Gimpl, G., and Fahrenholz, F. (2001). The oxytocin receptor system: structure, function, and regulation. Physiol. Rev. *81*, 629–683.

Harris, G.W. (1948a). Further evidence regarding the endocrine status of the neurohypophysis. J. Physiol. *107*, 436–448.

Harris, G.W. (1948b). Neural control of the pituitary gland. Physiol. Rev. *28*, 139–179.

Harris, G.W. (1955). Neural Control of the Pituitary Gland, *Vol No. 3* (London: Edward Arnold & Co.).

Isogai, S., Horiguchi, M., and Weinstein, B.M. (2001). The vascular anatomy of the developing zebrafish: an atlas of embryonic and early larval development. Dev. Biol. *230*, 278–301.

Jankowski, M., Danalache, B., Wang, D., Bhat, P., Hajjar, F., Marcinkiewicz, M., Paquin, J., McCann, S.M., and Gutkowska, J. (2004). Oxytocin in cardiac ontogeny. Proc. Natl. Acad. Sci. USA *101*, 13074–13079.

Jin, S.W., Beis, D., Mitchell, T., Chen, J.N., and Stainier, D.Y. (2005). Cellular and molecular analyses of vascular tube and lumen formation in zebrafish. Development *132*, 5199–5209.

Kasahara, Y., Takayanagi, Y., Kawada, T., Itoi, K., and Nishimori, K. (2007). Impaired thermoregulatory ability of oxytocin-deficient mice during cold-exposure. Biosci. Biotechnol. Biochem. *71*, 3122–3126.

Kobayashi, H., Yasuda, S., Bao, N., Iwasa, M., Kawamura, I., Yamada, Y., Yamaki, T., Sumi, S., Ushikoshi, H., Nishigaki, K., et al. (2009). Postinfarct treatment with oxytocin improves cardiac function and remodeling via activating cell-survival signals and angiogenesis. J. Cardiovasc. Pharmacol. *54*, 510–519.

Kulczykowska, E. (1998). Effects of arginine vasotocin, isotocin and melatonin on blood pressure in the conscious atlantic cod (Gadus morhua): hormonal interactions? Exp. Physiol. *83*, 809–820.

Kwan, K.M., Fujimoto, E., Grabher, C., Mangum, B.D., Hardy, M.E., Campbell, D.S., Parant, J.M., Yost, H.J., Kanki, J.P., and Chien, C.B. (2007). The Tol2kit: a multisite gateway-based construction kit for Tol2 transposon transgenesis constructs. Dev. Dyn. *236*, 3088–3099.

La Pointe, J.L. (1977). Comparative physiology of neurohypophysial hormone action on vertebrate oviduct uterus. Am. Zool. *17*, 763–773.

Le Mevel, J.C., Pamantung, T.F., Mabin, D., and Vaudry, H. (1993). Effects of central and peripheral administration of arginine vasotocin and related neuropeptides on blood pressure and heart rate in the conscious trout. Brain Res. *610*, 82–89.

Lim, A.H., Suli, A., Yaniv, K., Weinstein, B., Li, D.Y., and Chien, C.B. (2011). Motoneurons are essential for vascular pathfinding. Development *138*, 3847–3857.

Liu, N.A., Huang, H., Yang, Z., Herzog, W., Hammerschmidt, M., Lin, S., and Melmed, S. (2003). Pituitary corticotroph ontogeny and regulation in transgenic zebrafish. Mol. Endocrinol. *17*, 959–966.

Liu, N.A., Liu, Q., Wawrowsky, K., Yang, Z., Lin, S., and Melmed, S. (2006). Prolactin receptor signaling mediates the osmotic response of embryonic zebrafish lactotrophs. Mol. Endocrinol. *20*, 871–880.

Macfarlane, N.A., and Maetz, J. (1974). Effects of hypophysectomy on sodium and water exchanges in the euryhaline flounder, Platichthys flesus (L). Gen. Comp. Endocrinol. *22*, 77–89.

Machluf, Y., Gutnick, A., and Levkowitz, G. (2011). Development of the zebrafish hypothalamus. Ann. N Y Acad. Sci. *1220*, 93–105.

Makita, T., Sucov, H.M., Gariepy, C.E., Yanagisawa, M., and Ginty, D.D. (2008). Endothelins are vascular-derived axonal guidance cues for developing sympathetic neurons. Nature *452*, 759–763.

Matsuura, K., Nagai, T., Nishigaki, N., Oyama, T., Nishi, J., Wada, H., Sano, M., Toko, H., Akazawa, H., Sato, T., et al. (2004). Adult cardiac Sca-1-positive cells differentiate into beating cardiomyocytes. J. Biol. Chem. *279*, 11384–11391.

Moll, J. (1957). Regeneration of the supraoptico-hypophyseal and paraventriculo-hypophyseal tracts in the hypophysectomized rat. Z. Zellforsch. Mikrosk. Anat. *46*, 686–709.

Moll, J. (1958). The effect of hypophysectomy on the pituitary vascular system of the rat. J. Morphol. *102*, 1–21.

Mukouyama, Y.S., Gerber, H.P., Ferrara, N., Gu, C., and Anderson, D.J. (2005). Peripheral nerve-derived VEGF promotes arterial differentiation via neuropilin 1-mediated positive feedback. Development *132*, 941–952.

Mukouyama, Y.S., Shin, D., Britsch, S., Taniguchi, M., and Anderson, D.J. (2002). Sensory nerves determine the pattern of arterial differentiation and blood vessel branching in the skin. Cell *109*, 693–705.

Okado, N., and Yokota, N. (1980). An electron microscopic study on the structural development of the neural lobe in the human fetus. Am. J. Anat. *159*, 261–273.

Paquin, J., Danalache, B.A., Jankowski, M., McCann, S.M., and Gutkowska, J. (2002). Oxytocin induces differentiation of P19 embryonic stem cells to cardiomyocytes. Proc. Natl. Acad. Sci. USA *99*, 9550–9555.

Peter, R.E., and Fryer, J.N. (1983). Endocrine Functions of the Hypothalamus of Actinopterygians, *Volume 2* (Ann Arbor, MI: University of Michigan Press).

Provost, E., Rhee, J., and Leach, S.D. (2007). Viral 2A peptides allow expression of multiple proteins from a single ORF in transgenic zebrafish embryos. Genesis *45*, 625–629.

Russek-Blum, N., Gutnick, A., Nabel-Rosen, H., Blechman, J., Staudt, N., Dorsky, R.I., Houart, C., and Levkowitz, G. (2008). Dopaminergic neuronal cluster size is determined during early forebrain patterning. Development *135*, 3401–3413.

Sathyanesan, A.G., and Gorbman, A. (1965). Typical and atypical regeneration and overgrowth of hypothalamo-hypophysial neurosecretory tract after partial or complete hypophysectomy in the goldfish. Gen. Comp. Endocrinol. *5*, 456–463.

Scharrer, E. (1928). [The light sensitivity of blind minnows (Investigations About the diencephalon of the fish I)]. Journal of Comparative Physiology A. Neuroethology *7*, 1–38.

Stainier, D.Y., Weinstein, B.M., Detrich, H.W., 3rd, Zon, L.I., and Fishman, M.C. (1995). Cloche, an early acting zebrafish gene, is required by both the endothelial and hematopoietic lineages. Development *121*, 3141–3150.

Stutinsky, F. (1951). [Origin of the Gomori-positive substance of the hypothalamo-hypophyseal complex]. C. R. Seances Soc. Biol. Fil. *145*, 367–370.

Takayanagi, Y., Kasahara, Y., Onaka, T., Takahashi, N., Kawada, T., and Nishimori, K. (2008). Oxytocin receptor-deficient mice developed late-onset obesity. Neuroreport *19*, 951–955.

Thibonnier, M., Conarty, D.M., Preston, J.A., Plesnicher, C.L., Dweik, R.A., and Erzurum, S.C. (1999). Human vascular endothelial cells express oxytocin receptors. Endocrinology *140*, 1301–1309.

Unger, J.L., and Glasgow, E. (2003). Expression of isotocin-neurophysin mRNA in developing zebrafish. Gene Expr. Patterns *3*, 105–108.

Verbalis, J.G. (2007). How does the brain sense osmolality? J. Am. Soc. Nephrol. *18*, 3056–3059.

Wakasa, T., Wakasa, K., Nakayama, M., Kuwae, Y., Matsuoka, K., Takeuchi, M., Suehara, N., and Kimura, T. (2009). Change in morphology and oxytocin receptor expression in the uterine blood vessels during the involution process. Gynecol. Obstet. Invest. *67*, 137–144.

Wang, W., and Lufkin, T. (2000). The murine Otp homeobox gene plays an essential role in the specification of neuronal cell lineages in the developing hypothalamus. Dev. Biol. *227*, 432–449.

Zygmunt, T., Gay, C.M., Blondelle, J., Singh, M.K., Flaherty, K.M., Means, P.C., Herwig, L., Krudewig, A., Belting, H.G., Affolter, M., et al. (2011). Semaphorin-PlexinD1 Signaling Limits Angiogenic Potential via the VEGF Decoy Receptor sFlt1. Dev. Cell *21*, 301–314.

EDITED BY KRISTEN MUELLER AND JAKE YESTON

ASTROPHYSICS

A Test to See in the Dark

According to current models of structure formation in the universe, large galaxies, like our Milky Way, formed from the merging of many smaller systems. The models predict that a large number of small satellite galaxies should exist in our galaxy's vicinity, but this prediction does not match the observations. However, some of these small galaxies may be too difficult to detect, because they may be dominated by dark matter, a mysterious type of matter that does not emit or absorb light but does exert a gravitational pull. The Tidal Analysis method, developed to derive the locations and masses of satellite galaxies from the gravitational perturbations the satellites induce in the gas disk of the primary galaxy, has the potential to reveal satellite galaxies dominated by or composed entirely of dark matter. To demonstrate its validity, Chakrabarti *et al.* applied the Tidal Analysis method to two nearby spiral galaxies, M51 and NGC 1512, which each interact with a known visible companion. The method successfully recovered the masses and locations of the smaller companions; their masses ranging from one-third to one-hundredth of the mass of the primary galaxy. — MJC

Astrophys. J. **743**, 35 (2011).

BIOMEDICINE

Young at Heart

Cell-mediated repair of heart damage is one of the most exciting areas of cardiovascular research but is also one of the most challenging and controversial. One key point of disagreement is which cell type is optimal for such therapy. Among the list of candidates being actively explored are resident cardiac stem cells, embryonic stem cells, induced pluripotent stem cells, and bone marrow–derived cells.

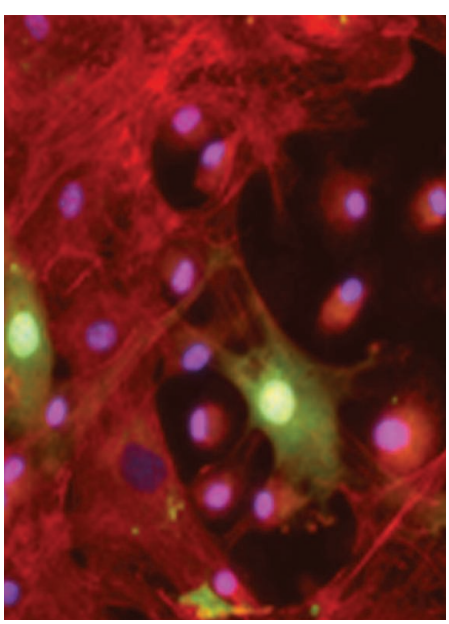

A new candidate cell has emerged from a study of peripartum cardiomyopathy, a form of heart failure that affects a small percentage of pregnant women and is associated with an unusually high rate of spontaneous recovery. Kara *et al*. speculated that fetal or placental cells might contribute to this high recovery rate. Consistent with their hypothesis, they found that when the heart of a pregnant mouse is subjected to acute injury, fetal cells migrate through the blood to the injury site in the maternal heart, where they differentiate into three distinct cell types required for heart repair: endothelial cells, smooth muscle cells, and cardiomyocytes. About 40% of these fetal cells express a marker gene (*Cdx2*) associated with trophoblast stem cells, which form the placenta. This raises the intriguing possibility that readily accessible cells in the placenta might be capable of heart repair. — PAK

Circ. Res. 10.1161/circresaha.111.249037 (2011).

EDUCATION

Calendar Effects

Does the organization of the school calendar affect student learning? Year-round schooling, which distributes school days with short, frequent breaks, is becoming more popular because it is thought to prevent the summer learning loss that occurs under a more traditional school calendar. Using longitudinal data from California public schools over a 9-year period, Graves examined the effect of year-round school calendars on nationally standardized test performance of traditionally disadvantaged students. Analysis showed that year-round calendars, especially multitrack year-round calendars in which the student body is never all in attendance at the same time, have a larger negative impact on the lower end of the distribution of scores, with Hispanics/Latinos and low–socioeconomic status students experiencing a larger fall in performance than the overall population. African American students are more negatively affected than the overall student population with respect to reading. Policy-makers take note: These results present an additional cost of implementing year-round calendars. — MM

Econ. Educ. Rev. **30**, 1281 (2011).

GENETICS

Evolution Illuminates Function

Long noncoding RNAs (lncRNAs) are enigmatic transcripts of the genome defined as noncoding RNAs over 200 bp in length. Although function has been ascribed to some lncRNAs, most are expressed at low levels, and their function, or even whether they have a specific function, is unknown. By examining the transcription of mammalian lncRNAs, focusing on comparisons between lncRNAs found in mice and humans, Managadze *et al.* set out to determine how

Published by AAAS

lncRNAs evolve. Calculation of the degree of evolution of these lncRNAs and examination of their relative expression levels revealed a negative correlation between evolutionary rate and expression level. This is similar to what has been observed with protein-coding genes, and like protein-coding genes, nonsynonymous mutations were observed in lncRNAs; that is, mutations predicted to change the amino acid encoded by the codon. No significant correlation was observed between the evolutionary rate of lncRNAs and their predicted secondary structure. On the basis of these findings, the authors conclude that lncRNAs are subject to weak purifying selection and thus are probably functional. — LMZ

Genome Biol. Evol. 10.1093/gbe/evr116 (2011).

CHEMISTRY

Colloidal Construction Kit

Total-synthesis approaches have made an art form of building complex organic molecules from much simpler and smaller pieces, using established rules of reactivity to selectively form specific products at each step. Colloidal particles are often described as "artificial atoms," and hooking them together can produce "artificial molecules" that manifest combinations of useful optical, magnetic, catalytic, and electronic properties. However, synthetic strategies at this scale have largely been limited to fusing two particles together or growing a second particle on the surface of an existing one. Buck *et al.* have now developed a rational and stepwise approach for constructing hybrid nanoparticle oligomers. They started with Fe_3O_4 grown on Pt seed particles. The addition of a gold precursor surprisingly yielded Au-Pt-Fe_3O_4 as the exclusive trimetallic product. Using the same reaction method, the authors produced trimers in which the Au could be replaced by Ag, Ni, or Pd. A fourth component (PbS or mixed-valence Cu_xS) could also be added selectively, and the Au-Pt-Fe_3O_4 trimers could be fused into superdimers or higher-ordered branched nanostructures by heating in the presence of a trace quantity of sulfur. — MSL

Nat. Chem. 10.1038/NCHEM.1195 (2011).

CHEMISTRY

Electrifying Peroxide Synthesis

Traditionally, the purpose of a fuel cell has been to channel chemical energy into electrical energy, and research has focused on optimizing the design to maximize the efficiency of this transformation. In this context, reducing oxygen all the way to water, rather than stopping halfway at hydrogen peroxide, is a central feature. On the other hand, there's a market for hydrogen peroxide, and the current production route is frustratingly indirect (featuring the intermediacy of an organic quinone compound). Jirkovsky *et al.* consider the prospect of using polymer electrolyte fuel cells to cogenerate electricity and hydrogen peroxide. Beginning with the knowledge that certain gold surfaces manifest relatively high selectivity toward the partial reduction reaction, they performed density functional theory calculations to guide optimization. The calculations suggested that isolated Pd or Pt sites on the gold surface should enhance O_2 binding while suppressing scission of the O-O bond, but that adjacent centers of the second metal would promote further reduction to water. These predictions were then borne out in rotating ring-disc electrode measurements: Peroxide selectivity peaked near 95% at a Pd alloying concentration of 8%, but then plummeted as the Pd abundance passed 15% (the threshold for aggregation). — JSY

J. Am. Chem. Soc. **133**, 10.1021/ja206477z (2011).

DEVELOPMENT

Network Development

The circulatory system is made up of complex vascular networks that originate from the association of numerous angiogenic sprouts with motile tip cells and trailing stalk cells. Tip cells contact each other, fuse, and subsequently form an interconnected lumen. Herwig *et al.* now visualize the behavior of single zebrafish endothelial cells during blood vessel fusion (anastomosis) and lumen formation. They used transgenic zebrafish whose endothelial cell junctions of dorsal longitudinal anastomotic vessels were fluorescently labeled to monitor cell movements and cell shape. Anastomosis is seen to result from different morphogenetic mechanisms—one involving cell rearrangement for a process of cord hollowing to generate a multicellular tube or through cell shape changes involving membrane invagination for a unicellular tube. These processes are associated with lumen formation at the position of vessel fusion. In addition, the luminal membrane compartments are polarized apically. With the elegant complexity of the vascular network, perhaps it is not surprising that multiple mechanisms are used to establish blood vessel morphology. — BAP

Curr. Biol. **21**, 1942 (2011).

CREDIT: ALAMY.COM

Published by AAAS

Curiculum Vitae - Lebenslauf

Persönliche Daten

Name:	Herwig
Vorname:	Lukas Walter
Adresse:	Peter Rot-Strasse 68, 4058 Basel
Telefon Mobil:	078 835 90 19
Geburtsdatum:	03.04.1983
Geburtsort:	Basel (BS)
Staatsangehörigkeit:	Schweiz
Bürgerort:	Basel BS
Familienstand:	ledig

Ausbildung

1999-2002 Gymnasium Münchenstein, Matur, Typus B (Latein)
2003-2006 Bachelor of Science in Biology (Major in Molecular Biology) an der Universität Basel
2006-2007 Master of Science in Molecular Biology (betreut von Prof. Markus Affolter), Titel der Arbeit: “Cellular characterization of the intersegmental vessels in the zebrafish embryo by different tools”
2008-2012 Doktorarbeit Biozentrum Universität Basel (betreut von Prof. Markus Affolter), Titel der Arbeit: Morphogenetic mechanisms of blood vessel fusion in the zebrafish embryo

Publikationen

Blum, Y., Belting, H.-G., Ellertsdottir, E., Herwig, L., Lüders, F., and Affolter, M.. Complex cell rearrangements during intersegmental vessel sprouting and vessel fusion in the zebrafish embryo. *Developmental biology* 316 (2008) 312-22.

Elín Ellertsdóttir, Anna Lenard, Yannick Blum, Alice Krudewig, Lukas Herwig, Markus Affolter, Heinz-Georg Belting Vascular morphogenesis in the zebrafish embryo *Developmental Biology* 341 (2010) 56–65

Tomasz Zygmunt, Carl Michael Gay, Jordan Blondelle, Manvendra K. Singh, Kathleen McCrone Flaherty, Paula Casey Means, Lukas Herwig, Alice Krudewig, Heinz-Georg Belting, Markus Affolter, Jonathan A. Epstein and

Jesus Torres-Vazquez Semaphorin-PlexinD1 Signaling Limits Angiogenic Potential via the VEGF Decoy Receptor sFlt1 *Developmental Cell* 21 (2011) 1-14

Roland Totong, Thomas Schell, Fabienne Lescroart, Lucile Ryckebüsch, Yi-Fan Lin, Tomas Zygmunt, Lukas Herwig, Alice Krudewig, Dafna Gershoony, Heinz-Georg Belting, Markus Affolter, Jesus Torres-Vazquez and Deborah Yelon The novel transmembrane protein Tmem2 is essential for coordination of myocardial and endocardial morphogenesis *Development* 138 (2011) 4199-4205

Gutnick A, Blechman J, Kaslin J, Herwig L, Belting HG, Affolter M, Bonkowsky JL, Levkowitz G. The hypothalamic neuropeptide oxytocin is required for formation of the neurovascular interface of the pituitary. *Developmental Cell* 21 (2011) 642–654

Lukas Herwig*, Yannick Blum*, Alice Krudewig, Elin Ellertsdóttir, Anna Lenard, Heinz-Georg Belting and Markus Affolter *these authors contributed equally to this work Distinct Cellular Mechanisms of Blood Vessel Fusion in the Zebrafish Embryo *Current Biology* 21 (2011) 1942–1948

Besondere Weiterbildung, Kenntnisse und Kurse

Meetings:
First Swiss Zebrafish Meeting in Ovronaz, 2008
8th International Conference on Zebrafish Development and Genetics, Madison (USA), 2008
9th International Conference on Zebrafish Development and Genetics, Madison (USA), 2008
6th European Zebrafish Genetics and Development Meeting, Rome (Italy) 2009
USGEB 2011, IMAGING Meeting at University of Zürich 2011
Gordon Research Conference on Vascular Cell Biology, Ventura (CA, USA), 2011

Kurse:
Labortierkunde Kurs Modul 20E, Universität Zürich (Irchel), 2008
Venture Challenge Kurs Herbstsemester 2011, Kommission für Technologie und Innovation KTI (Switzerland)

Hobbies

Musik: Oboe und E-Gitarre
Sport: MountainBike, Schwimmen, Joggen, Wandern, Outdoor-aktivitäten, Reisen
Literatur: Sachbücher, Romane mit geschichtlichem Hintergrund, Science Fiction
Kochen